Dual Component Estimation; a probabilistic approach to estimate undiscovered oil and gas in an underexplored basin, Taranaki Basin, New Zealand

by

Beatrice Jones

A thesis
submitted to Victoria University of Wellington
in fulfillment of the
requirements for the degree of
Doctor of Philosophy
in Geology

Victoria University of Wellington
2015

Abstract

New Zealand has relied on the supply of oil and gas from the Maui Field in the Taranaki Basin for 40 years. As this field nears depletion, there is considerable governmental encouragement for increased investment in exploration to ensure continued oil and gas production for domestic use and the export market.

The Taranaki Basin covers a 100,000 km^2 area and has a 10 km-thick Cretaceous to Holocene sediment fill, which hosts only 200 exploration wells with 33 oil and gas discoveries $\geq$ 1 million barrels of oil equivalent (mmboe). Discoveries have been made throughout Paleocene to Holocene sequences in multiple reservoirs within onshore and offshore parts of the basin. A review of the hydrocarbon potential of the Taranaki Basin suggests that more than one working petroleum system operates in the basin, based on the distribution of oil and gas-condensate. As part of this study the most productive and prospective reservoir intervals have been studied to ascertain the working petroleum systems. The reservoir intervals are grouped into four plays and are referred to as the Cretaceous, Paleocene, Eocene and Miocene plays.

The Dual Component Estimation (DCE) is a novel way of combining a modified, existing, size distribution-based discovery-sequence sampling method with a Geographical Information Systems (GIS)-based spatial method to estimate the amount and likely location of undiscovered oil and gas in an underexplored basin. In particular, the DCE uses an inverse sampling method to ensure the total number of all accumulations in the basin is not constrained by the size distributions of discoveries, which typically represent a very small proportion of accumulations in an underexplored basin. Furthermore, it is a probabilistic approach that captures ranges in uncertainties that result from using regional scale data and assumptions used to simplify the process of generating and trapping hydrocarbons. Given the underexplored character of the Taranaki Basin, this study has included potential discoveries to define the size distribution of the original population of all accumulations in a basin, which is used to derive the undiscovered volume.

Potential discoveries are based on basin modelling and mapped structural traps. This approach increases the dataset of accumulations (discovered and modelled) from 33 to 338 and generates an original parent population that includes petroleum systems information from explored and unexplored areas of the basin.

DCE modelling results suggest that the basin has an undiscovered oil and gas resource potential of ~1500 oil and gas accumulations totalling 8210–10800 mmboe. The mean discovery size is 328.7 mmboe; however the next discovery could be as large as 550–900 mmboe (with a 10% probability). More likely, the next discovery is estimated to be at least 50 mmboe (with a 90% probability) which is a commercially significant size in the Taranaki Basin. New discoveries in the Palaeocene play have been modelled in the Manaia anticline area, Western Platform and onshore eastern margin of the basin. It is most likely that a discovery in this play will be at least 40 mmboe, with a 90% probability; however it may be closer to 470 mmboe, with a 10% probability. The Eocene play is the most prospective and future discoveries will most likely be located along the eastern margin of the basin, nearshore and onshore of the western peninsula, and offshore, east of the Maui Field. There is a 10% probability that a new discovery in this play may be as big as 200–500 mmboe. More likely, with a 90% probability, a new discovery may be at least 35 mmboe. Discoveries in the Miocene play are most likely in the onshore peninsular area and in the offshore Northern Graben. There is a 90% probability that the next discovery may be at least 55 mmboe and a 10% probability that it may be much larger (310–800 mmboe). A discovery is yet to be made in the Cretaceous play. This study indicates that a new discovery in this play is most likely to be at least 50 mmboe (with a 90% probability) but may be greater and be at least 500 mmboe (with 10% probability).

The strength of the DCE is in the use of additional geological data to include unexplored areas of the underexplored Taranaki Basin in the estimation. This estimation should also be applicable to other geologically similar, underexplored, sedimentary basins of New Zealand.

Acknowledgements

I am sincerely grateful to my head of school: Dr. Mike Hannah (VUW), my supervisors: Dr. John Collen (VUW), Rob Funnell (GNS), Dr. Peter King (GNS) and Dr. Euan Smith (VUW), the Associate Dean of Science, Shona de Sain (VUW) and Dr. Annette George, University of Western Australia. They are thanked for their guidance, shared scientific knowledge and wisdom, support, patience, and humour.

This project received financial assistance via: an Institute of Geological and Nuclear Sciences Limited PhD Scholarship; a New Zealand Association of Graduate Women award; an AAPG grant, International Science and Technology award; a VUW Science Faculty grant; and a Victoria University PhD finishing scholarship.

This project involved technical discussions by a number of people, whom I thank, including:

- Statistical grandmasters: Dr. Euan Smith, Dr. David Rhodes (GNS), Dr. Colleen Kelly (VUW), Dr. Shirley Pledge (VUW) and Dr. Peter Thompson.
- Arc(GIS) angels: David Heron; Ray Wood, Biljana Lukovic and Craig Jones (GNS), Greg Partington (Kenex Information Systems) and Christopher Brookes (VUW).
- Software wizards: Dr. Wolfe Rottke (IES), Drs. Matt Gerstenberger and William Powell (GNS),
- Earth scientists: Dr. Richard Sykes, Dr. Andy Nicol, Dr. Brad Ilg, Dr. Malcolm Arnott, Dr. Chris Uruski, Dr. Rosalie Pollack, Dr. Karen Higgs, Dr. Kim Manzano-Kareah;
- Oil and gas assessors Ron Charpentier (USGS), Pierre Laharerre, Peter Rose and David Cook, Kristian Bjarnoe (NTNU) and Andrew Barrett (Geoscience Australia).
- USGS Oil and Assessment team for hosting me in their Denver office for three weeks.
- Dr. Greg Partington for introducing me to spatial data modelling.
- Everyone at GNS Science for creating an inspiring work environment. Special thanks to Dr. Mike Issac for his many words of wisdom, and Dr. Dave Darby and Dr. Greg Brown.
- VUW Awhina group members Liz Richardson, Adele Whyte, and Dawn Reynolds for their support and friendship.

With all my heart I thank my husband, Andrew, for his total support and belief in me. Thanks to Andrew and my canine friend, Mont, for all the fun. My family are thanked for their support and encouragement and the many things they did to help smooth the bumps. To my many friends, thank you for the extra-curriculum activities: Andrea and Leslie for unscientific discussions; bikers, Andrew, Kate, Fraser, Nick, April and Nick; runners, Ray, Dan, Matt, Jeff, and Vanessa; and disc players team Frenzy and the NZ women's team. Special thanks to Kate for her inspiring ability to keep things real and get things done. Thank you to all field geologists and explorers who provided data I used. Thank you also to those who have made these data well documented and accessible.

Contents

List of figures

List of tables

This doctoral thesis consists of three authored papers intended for submission to the journal *Natural Resources Research* and forming chapters 4 to 6:

1. Paper 1: **Dual Component Estimation; theoretical framework of a probabilistic approach to estimate undiscovered oil and gas in an underexplored basin**, *Jones B.*

2. Paper II: **Using the Dual Component Estimation to assess the undiscovered oil and gas resource potential of the Taranaki Basin, New Zealand,** *Jones B.*

3. Paper III: **Key uncertainties associated with estimating undiscovered oil and gas in the Taranaki Basin, New Zealand; using the Dual Component Estimation**, *Jones B.*

Chapter 1

Introduction

1.1 Significance of study

This study focuses on making an assessment of the amount and likely location of undiscovered oil and gas in the Taranaki Basin, which is located on the west coast of the North Island of New Zealand (Figure 1.1). Although there are a number of other sedimentary basins within the New Zealand sub-continent, the Taranaki Basin is the only hydrocarbon-producing one.

The basin covers ~100,000 km^2 and contains 10 km of Late Cretaceous to Holocene sediment fill. The basin has proven petroleum systems and 36 discoveries have been made at multiple stratigraphic levels from the Paleocene to the Plio-Pleistocene (Figure 1.2). Estimated total recoverable reserves for the basin are 560 millions of barrels of oil (mmbbl) of oil/condensate and 6657 billion cubic feet (bcf) of gas (Crown Minerals, 2006). There are 19 producing fields however most of these reserves are held within the three largest fields (Figure 1.3 & Table 1.1). Maui contains 44% of the reserves within three main accumulations (Maui A (C sandstone) Maui B (C sandstone) and Maui B (F and D sandstone) Kapuni contains 17% and Pohokura contains 10%.

The basin is covered in variable vintages of mostly widely-spaced 2D seismic and ~200 exploration wells have been drilled (Figure 1.4). However, most of these wells are onshore and a large part of the basin remains undrilled, therefore it is considered underexplored. The basin has modelled potential to yield further oil and gas discoveries based on knowledge of its petroleum systems (King & Thrasher, 1996; Funnell et al., 2002) and ongoing discovery success and the continuing addition of reserves (Figure 1.5). Present-day Taranaki Basin is an active-margin basin. Such basins elsewhere have produced significant oil and gas reserves, such as the North Tejon oil fields, California (Namsen & Davis, 1988) and deepwater North-West Borneo fields (Ingram et al., 2004).

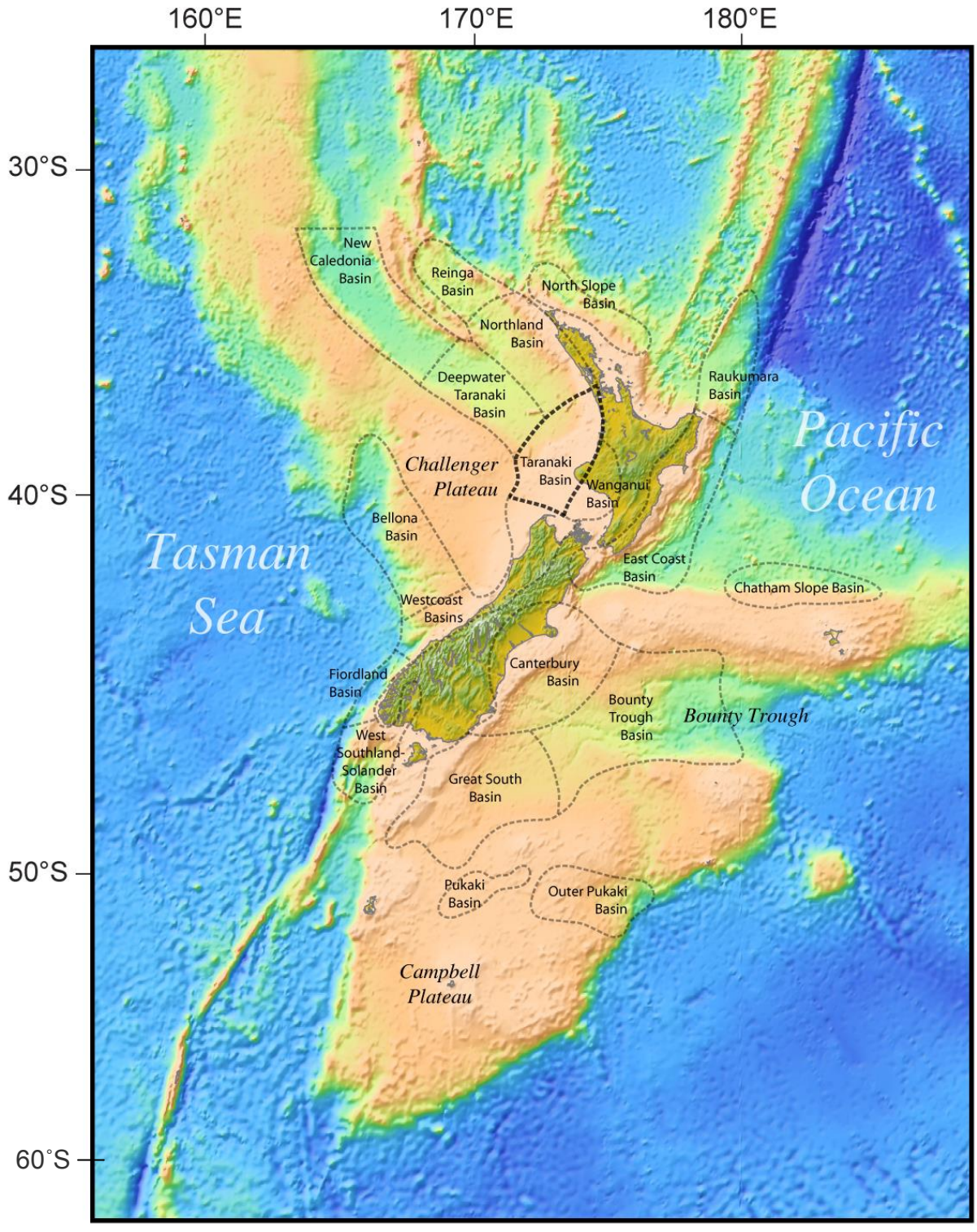

Figure 1.1: Cretaceous to Cenozoic sedimentary basins within the greater New Zealand sub-continent. Modified from Uruski et al. (2002).

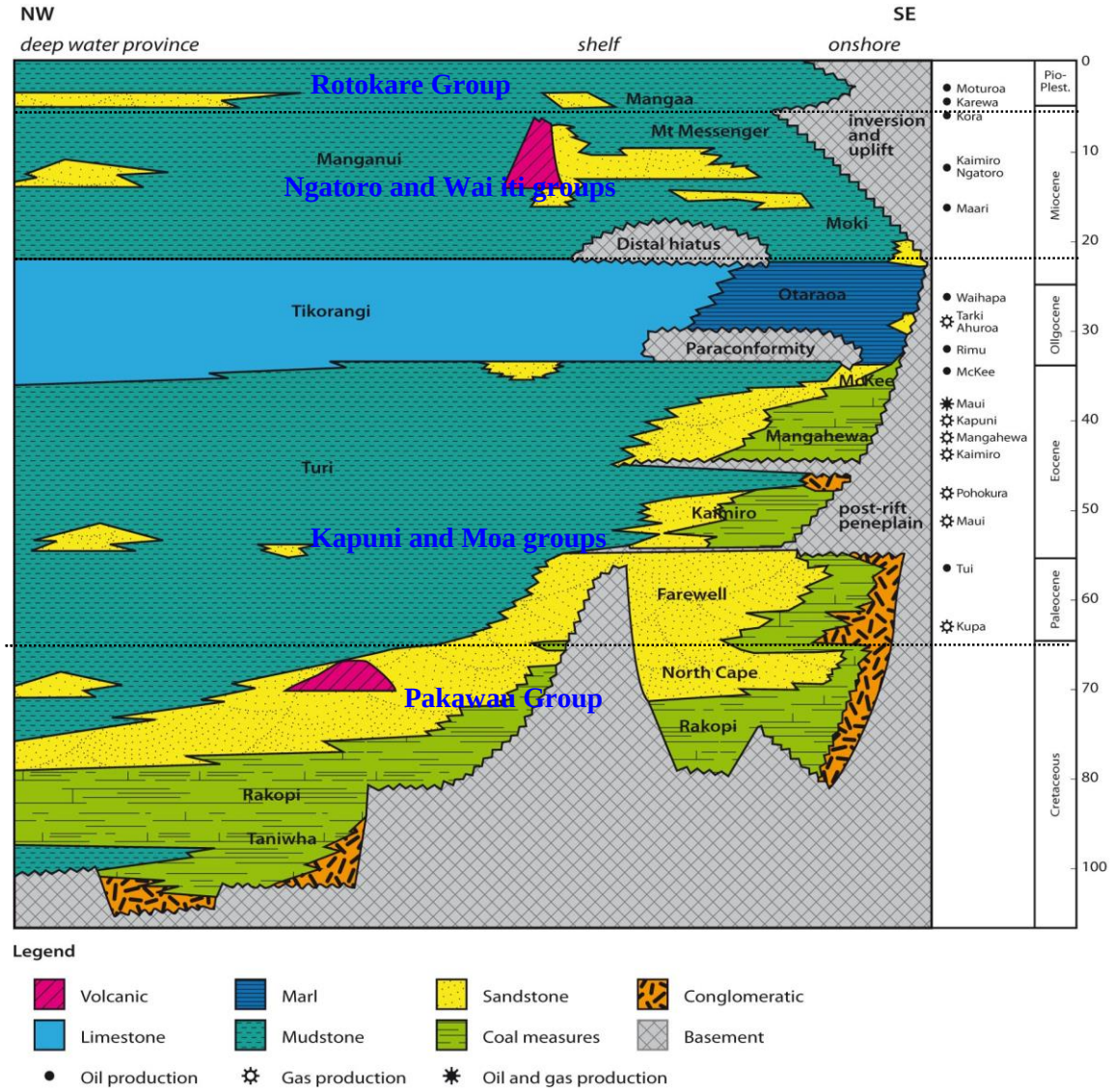

Figure 1.2: Cretaceous to Cenozoic stratigraphic record of the Taranaki Basin, showing relative stratigraphic levels for producing fields in the basin. Source, MED, 2005. NW is northwest, SE is southeast.

The Maui Field has provided 80% of New Zealand's domestic oil and gas (MED, 2005). The imminent depletion of this field and a predicted shortfall in replacement reserves (Figure 1.6) has resulted in growing awareness of a continuing hydrocarbon supply for both domestic and export markets (MED, 2008). Fifty percent of New Zealand's electricity is generated from natural gas and 50% of oil consumption is used in the transport sector (MED, 2005). The demand for electricity and oil for the transport section have been increasing continuously for ~20 years (MED, 2009). A large amount of natural gas is also consumed by petrochemical and industrial sectors and a smaller amount is used by the commercial and residential sectors (MED, 2009).

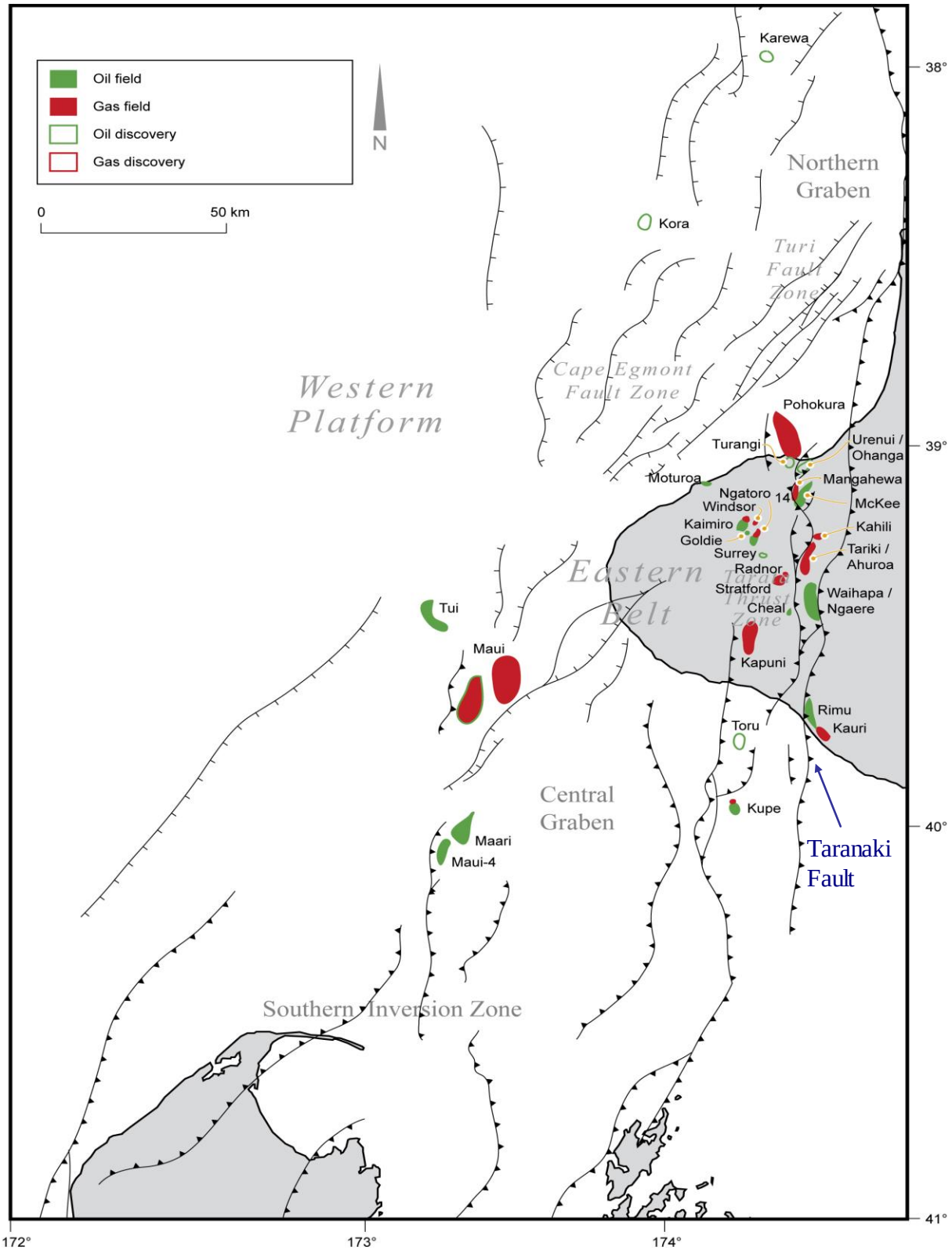

Figure 1.3: Oil and gas fields and undeveloped discoveries in the Taranaki Basin (Table 1). The study area is denoted by the map border. Subsurface faults are shown at the top-Eocene surface. Faults with triangular marks are thrust faults and the triangles mark the upthrown side. Faults with tick marks are normal faults and the ticks mark the upthrown side. Filled red polygons = oil field, green filled polygons = gas field, green unfilled polygons = gas discovery. Green outline with red filled polygon = oil, gas-condensate field.

					Original P50 Reserves				Cumulative Reserves					
					Oil/cond				Oil/cond and gas					
Accumulation	Field	Reservoir play	Status	Location	Gas bcf	mmbbl	bcf to boe	mmboe	Gas BCF	Oil mmbbl	bcf	mmbbl	mmbbl	Discovery date
Maui A	Maui	Paleocene/Eocene	P	Offshore	2097	134	399.49	533	2097.34	133.51	533	3496	381	1969
Maui B	Maui	Paleocene/Eocene	P	Offshore	1341	85	255.52	340.91	3438.83	267.02	874	5731	763	1979
Kapuni	Kapuni	Paleocene/Eocene	P	Onshore	1366	66	260.15	326.15	4804.63	352.41	1200	8008	1007	1959
Pohohura	Pohohura	Eocene	UD	Offshore	700	43	133.33	176.13	5504.63	418.41	1376	9174	1195	2000
McKee	McKee	Eocene	P	Onshore	183	47	34.8	82.2	5687.33	461.21	1458	9479	1318	1979
Kupe	Kupe	Paleocene/Eocene	UD	Offshore	264	16	50.29	66.59	5951.33	508.61	1525	9919	1453	1986
Maari/Moki	Maari	Paleocene/Eocene	UD	Offshore	0	49	9	49	5951.33	524.91	1574	9919	1500	1989
Turangi-1	Turangi	Paleocene/Eocene	P	Onshore	144	5	27.43	32.23	6095.33	573.91	1606	10159	1640	2006
Waihapa/Ngaere	TAWN	Paleocene/Eocene	P	Onshore	29	23	5.49	29.59	6124.13	578.71	1636	10207	1653	1993
Tariki/Ahuroa	TAWN	Eocene	P	Onshore	115	6	22	28.3	6239.61	602.81	1664	10399	1722	1986
Tui* (Amokura/Pateke)	Tui	Paleocene/Eocene	UD	Offshore	0	28	0	27.9	6239.61	609.11	1692	10399	1740	2003
Maui B (F&D sandstone)	Maui	Paleocene/Eocene	P	Offshore	0	20	0	20	6239.61	637.01	1712	10399	1820	1993
Karewa-1		Paleocene/Eocene	D	Offshore	105	0	20	20	6344.61	657.01	1732	10574	1877	2002
Mangahewa	Mangahewa	Eocene	P	Onshore	73	1	13.81	14.51	6417.11	657.01	1747	10695	1877	1997
Kauri	Kauri	Miocene	P	Onshore	42	6	8.05	13.75	6459.39	657.71	1760	10766	1879	2001
Rimu	Rimu	Eocene	P	Onshore	22	5	4.19	8.89	6481.38	663.41	1769	10802	1895	1999
Ngatoro	Ngatoro	Miocene	P	Onshore	9	6	1.66	8.06	6490.08	668.11	1777	10817	1909	1992
Kaimiro (shallow)	Kaimiro	Miocene	P	Onshore	15	3	2.78	6.08	6604.68	674.51	1783	10841	1927	1988
Urenui		Paleocene/Eocene	D	Onshore	30	0	5.71	5.71	6634.68	677.81	1789	10891	1937	1972
Cardiff	Cheal/Cardiff	Paleocene/Eocene	UD	Onshore	30	0	5.71	5.71	6664.68	677.81	1795	10941	1937	2006
Radnor	Radnor	Paleocene/Eocene	UD	Onshore	20	1	3.81	5.23	6684.68	677.81	1800	10974	1937	2004
Cheal	Cheal/Cardiff	Paleocene/Eocene	UD	Onshore	0	5	0	5.01	6684.68	679.23	1805	10974	1941	1995/2005
Stratford		Eocene	D	Onshore	23	1	4.38	4.98	6607.68	684.24	1810	11013	1955	1992
Waihapa/Ngaere	TAWN	Miocene	P	Onshore	17	0	3.24	3.64	6624.68	684.84	1814	11041	1957	1987
Toru		Eocene	D	Offshore	10	1	1.9	2.8	6634.68	685.24	1816	11058	1958	1990
Kauimiro (deep)	Kaimiro	Paleocene/Eocene	UD	Onshore	10	0	1.9	2.3	6644.67	686.14	1819	11074	1960	1982
Moki	Maari	Paleocene/Eocene	UD	Offshore	0	2	0	2	6644.68	686.54	1821	11074	1962	1983
Goldie	Ngatoro	Miocene	P	Onshore	1	2	0.1	1.76	6645.18	688.54	1822	11075	1967	2001
Piakau North A1		Eocene	D	Onshore	1	1	0.19	1.19	6646.18	690.2	1824	11077	1972	2005
Kora		Paleocene/Eocene	D	Offshore	0	1	0	1	6646.18	691.2	1825	11077	1975	1987
Maui-4	Maui-4	Paleocene/Eocene	UD	Offshore	0	1	0	1	6646.18	692.2	1826	11077	1978	1970
Windsor	Windsor	Miocene	P	Onshore	4	0	0.76	0.76	6650.18	693.2	1826	11084	1981	2000
Surrey		Eocene	D	Onshore	4	0	0.76	0.76	6654.18	693.2	1827	11090	1981	2002
Moturoa	Moturoa	Miocene	D	Onshore	2	0	0.4	0.4	6656.28	693.2	1828	11094	1981	1906
Kahili	Kahili	Eocene	P	Onshore	1	0	0.23	0.23	6657.48	693.2	1828	11096	1981	2002
Supplejack-1		Eocene	D	Onshore	0	0	0	0	6657.48	693.2	1828	11096	1981	2005

Table 1.1: Oil and gas discoveries in the Taranaki Basin. P = production, UD = under development, D = discovery awaiting further appraisal. Bcf = billions of cubic feet, mmbbl = millions of barrels of oil, boe = barrels of oil equivalent. Reserve values are sourced from the Crown Minerals website, as at January 2007 (Crown Minerals, 2007).

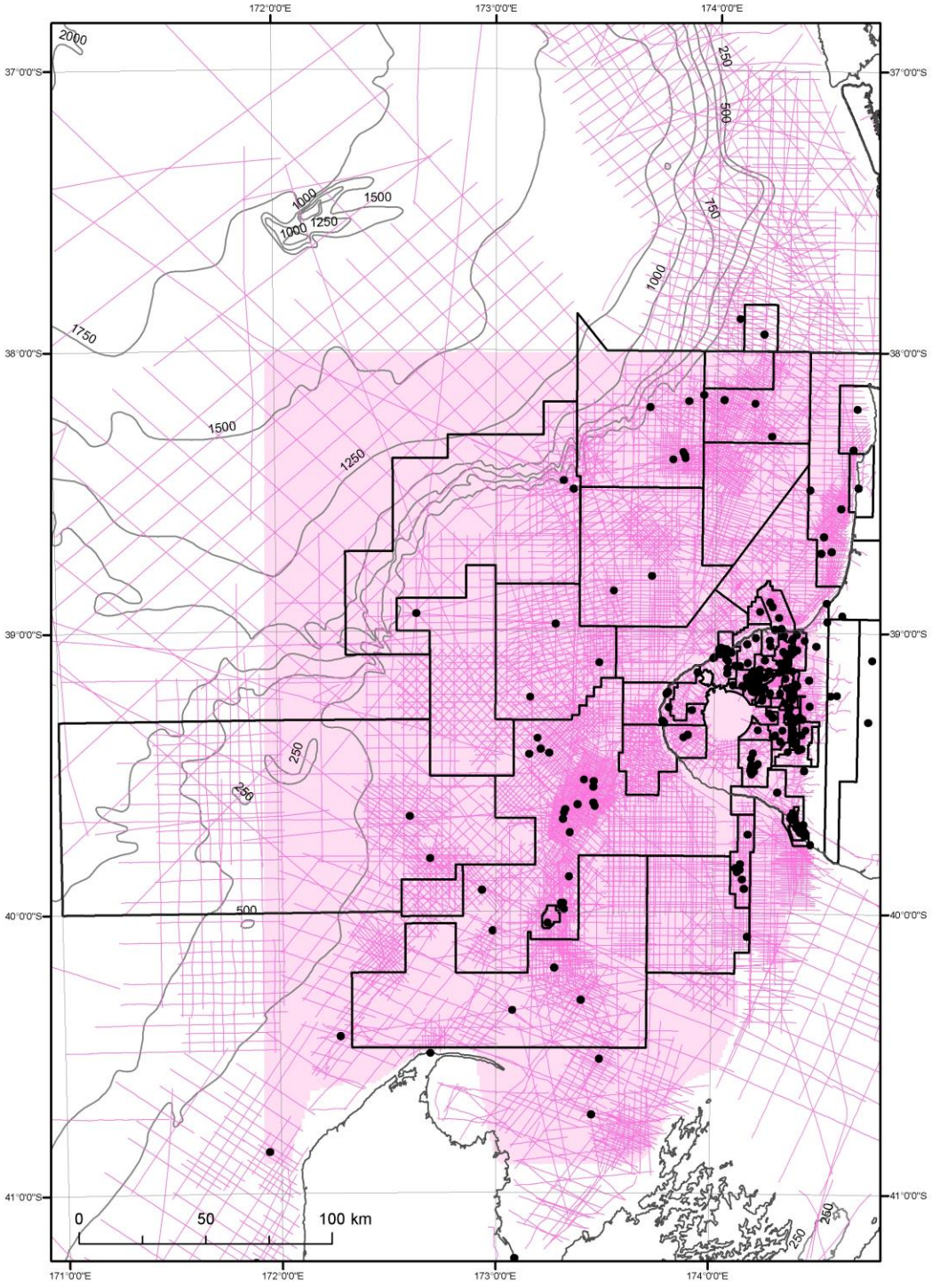

Figure 1.4 Exploration activities in the Taranaki Basin, as at January 2007. Areas under permit are shown as black polygons, seismic data acquisition is shown by the pink lines and wells that have been drilled in the basin are shown as black dots. The study area is shown in solid pink. Bathymetry = units are meters.

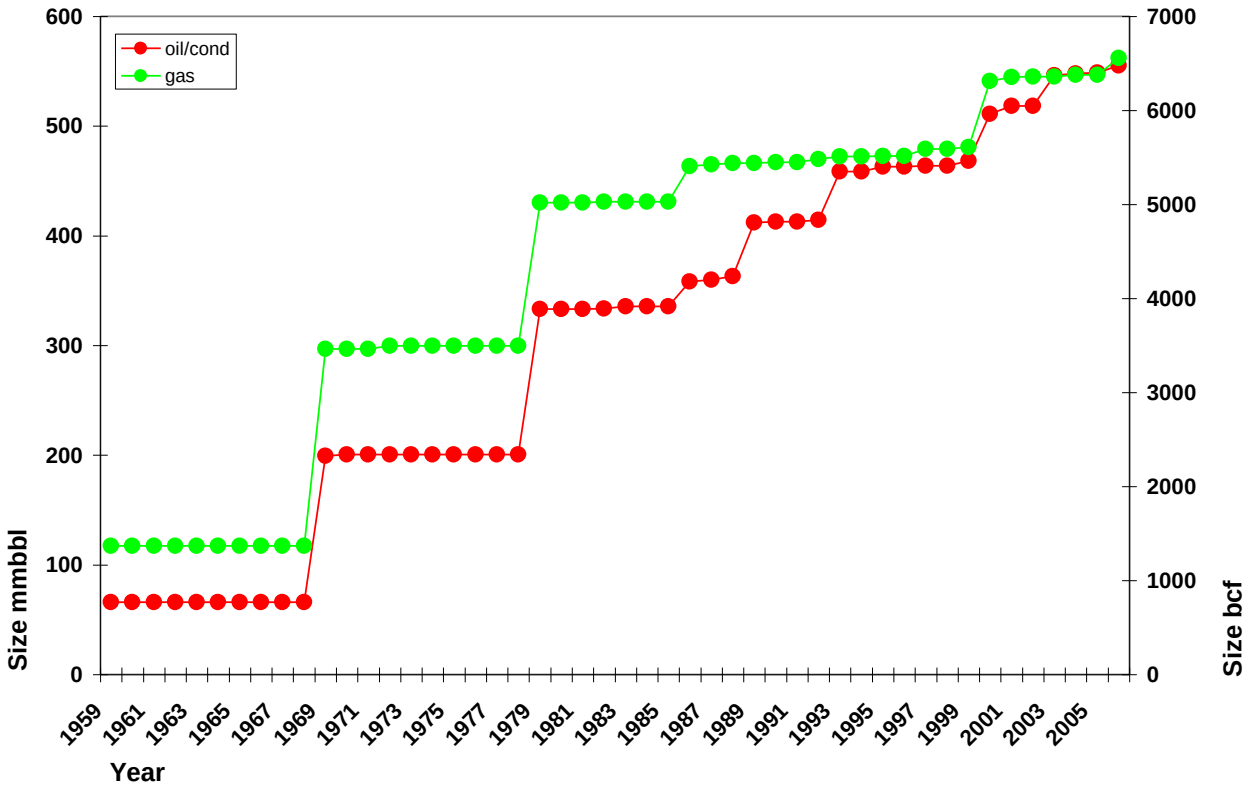

Figure 1.5: Cumulative reserves discovered in Taranaki Basin from 1959 to 2007. mmbbl = millions of barrel of oil. bcf = billions of cubic feet. This plot shows how reserves continue to be added with continued discovery success.

Gas is produced from 16 fields however; the bulk of the gas comes from the Maui and Pohokura fields. Production from the Maui Field is predicted to last until 2020 and based on a growing demand for gas, especially as methanol production increases, the supply is expected to be significantly short unless major new discoveries are made (MED, 2005). Another alternative is to import liquefied natural gas (LNG), however this option may be contentious because of the impact on local electricity prices, energy security, domestic exploration and New Zealand's balance of payments (MED, 2008). Oil is produced from 10 fields although most is extracted from the Maui, Pohokura and Tui fields (Table 1.1). Most domestically produced crude oil is exported because it is chemically lighter than what is required to produce 70% of petrol and diesel, however (MED, 2005). Petroleum production is New Zealand's third largest export earner and continues to be a key economic contributor, with ~NZ$1.7 billion of high-quality oil exported annually (MED, 2010).

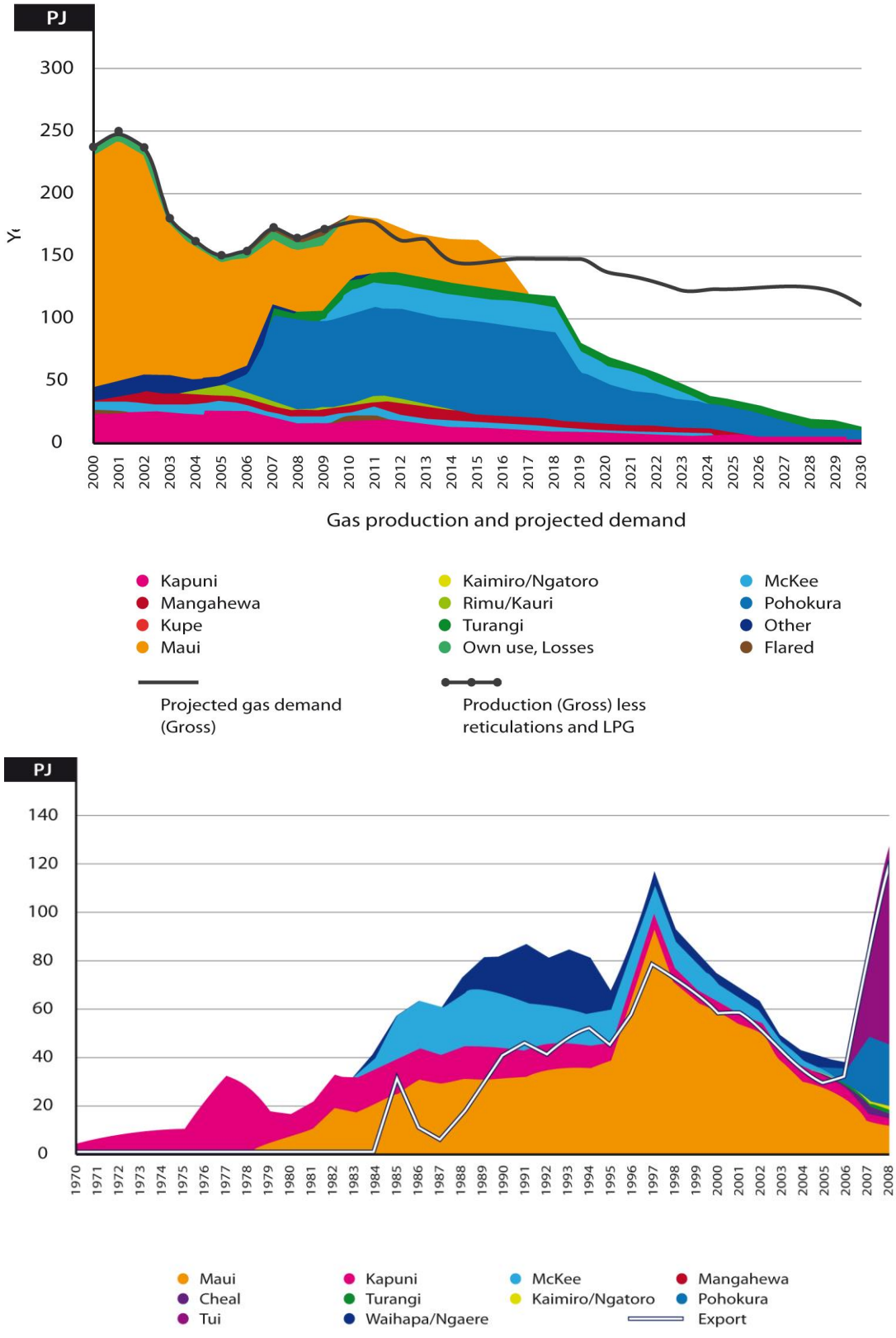

Figure 1.6: (a) New Zealand gas production from 2000 and projected production out to 2030 based on the known reserves of each producing field. "Other" includes production from the Kaimiro Deep and Radnor fields. PJ = petajoules. LPG = liquid petroleum gas. (b) New Zealand oil production by field from 1970 to 2008. Data sourced from the Ministry of Economic Development (MED, 2010).

Author	Method	Total volume mmboe	Size distribution predicted	Scope	Success
Cook (1985)	Size-distribution analysis with a gap analysis approach.# (Perrodon 1983)	57-142	7 accumulations sized 7–18 mmboe and 4 accumulations sized 2–4 mmboe	Includes very few and some non-Taranaki Basin discoveries	Did not predict the 18 discoveries >18 mmboe made since 1985 including the largest one, Pohokura (2000) with reserves of 176 mmboe
Cook and Beggs (1993)	Size-distribution analysis #(Crovelli 1986)	79	Not disclosed	Kapuni Group reservoirs only. Predates Mangahewa, Ngatoro, Rimu, Kauri, Pohokura, Windsor and Goldie discoveries	Did not predict Pohokura Field of 176 mmboe. Predicted 3 20–30 mmboe discoveries made in Kapuni Group (Mangahewa, Maui-F, Tui)
O'Connor (2003)	Size-distribution analysis using a gap analysis approach. # (Perrodon 1983)	340	1 accumulation 125–250 mmboe and 82% of all accumulations <4 mmboe	Onshore only	6 discoveries have been made since 2002 in the 1–32 mmboe range and totaling 77.26 mmboe. All are onshore except a 27.9 mmboe one (Table 1.1).
Mare-Jones (2004)*	Size-distribution analysis using a gap analysis approach.# (Perrodon 1983)	997	1 327 mmboe accumulation, 7 82 mmboe accumulations and 6 onshore accumulation of 16 mmboe.	Assumes Maui is the largest accumulation in the basin. Gas only modelled	6 discoveries have been made since 2002 in the 1–32 mmboe range and totaling 77.26 mmboe. All are onshore except a 27.9 mmboe one (Table 1.1).
Mare-Jones (2004)*	Modified Delphi, expert opinion	834	8 onshore accumulation totaling 250 mmboe (mean size of ~31 mmboe) and 7 offshore accumulations totalling 584 mmboe (mean size of ~84 mmboe)	Gas only modelled	6 discoveries have been made since 2002 in the 1–32 mmboe range and totalling 77.26 mmboe. All are onshore except a 27.9 mmboe one (Table 1.1).
Mare-Jones (2004)*	Creaming curve analysis	341-390	163 mmboe in offshore Eocene play, 81 mmboe in Northern Graben play, 81–130 mmboe in thrust belt play and 16 mmboe in onshore Eocene play	In the Eocene, Northern Graben, deep Cretaceous, and eastern margin thrust belt plays. Gas only modelled	6 discoveries have been made since 2002 in the 1–32 mmboe range and totalling 77.26 mmboe. All are onshore except a 27.9 mmboe one (Table 1.1).

Table 1.2: Previous estimations of undiscovered oil and gas for the Taranaki Basin, * Means this is not the original author but references the table where the work was published. The original work was presented in Funnell et al. (2002), a Geological and Nuclear Sciences Limited unpublished report and permission was given to publish the above results in Mare-Jones 2004. # demotes the use of a lognormal probability distribution function in the size-distribution method used. mmboe is millions of barrels of oil equivalent.

The New Zealand government has invested NZ$25 million into the petroleum industry to acquire exploration data in frontier areas with a view to increasing the value of this sector to the overall economy (MED, 2010).

1.2 Objective and aims of study

The objective of this project is to estimate undiscovered oil and gas in the Taranaki Basin. Very little work has been published about how much undiscovered oil and gas may exist in the basin (Cook, 1985; Beggs & Cook, 1993; O'Conner, 2002; Mare-Jones, 2004) (Table 1.2). The most recent estimates (O'Connor, 2002; Mare-Jones, 2004) suggest ~1000 millions of barrels of oil equivalent (mmboe) remains undiscovered (Table 1.2).

However, previous estimates are of limited use because they relate to confined areas of the basin, for example onshore only (Cook, 1985; O'Connor, 2002), offshore only (Mare-Jones, 2004) and selected reservoir sequences (Beggs & Cook, 1993; Mare-Jones, 2004). Previous estimates are purely volumetric and do not include maps showing where undiscovered accumulations may be located. To better assess the hydrocarbon potential of the Taranaki Basin this project aims to:

1. establish an estimation methodology that is suitable for the basin, given a large part of the basin is underexplored and geologically prospective;

2. present probabilistic volumes of the amount of undiscovered oil and gas; and

3. present maps showing the most likely locations of undiscovered oil and gas.

In order to achieve these aims this project will apply:

1. a novel estimation approach, which combines a modified, existing volumetric method with a geographical information systems (GIS)-based spatial model; and

2. datasets of potential oil and gas discoveries in addition to known oil and gas discoveries to include a measure of the geologic potential of the basin, especially in unexplored areas.

1.3 Outcomes of study

The main outcome of this study is present a comprehensive and useful assessment of undiscovered oil and gas for the Taranaki Basin. Exploration activity is expected to move further into underexplored areas of the basin (MED, 2007) and these relatively frontier areas will be included in the assessment. It is anticipated that the results will be useful in providing information about the resource potential of the basin and guiding exploration risk profiles. This will be the first time the combined volumetric and spatial models will be applied and the undiscovered resource potential maps will be the first publicly available.

1.4 Thesis Organisation

This thesis is presented as seven chapters. Chapters 1–3 are introductory and the core work of this study is presented in Chapters 4–6. Chapter 2 describes the geology and petroleum systems of the Taranaki Basin. Chapter 3 describes the various methods and approaches that have been applied in this study. Firstly it describes the basin modelling tools and inputs, and the approach used to identify structural traps. The assessment is made for four of the basin's main reservoir intervals and this chapter describes how they are classified as plays. Background information is provided about size distribution models that are used to estimate the volume of undiscovered oil and gas in this study. The limitations of the size distribution method are discussed to explain the modification that has been made in this study. A gap analysis size distribution approach is also described in order to examine the results of previous estimates for the basin. The concept of spatial modelling is introduced in this chapter. Chapter 4 describes the Dual Component Estimation and in particular demonstrates how datasets of discovered and modelled oil and gas accumulations are applied in the volumetric and spatial components. Chapter 5 considers the key uncertainties that are likely to impact on the estimates. Chapter 6 presents the estimation results, which are made for the basin and each of the reservoir plays. Chapter 7 highlights the main conclusions of the study and makes recommendations for future work.

Chapter 2

Regional geology and petroleum systems

2.1 Introduction

The main aim of this chapter is to describe the geology and petroleum systems of the Taranaki Basin in order to highlight the hydrocarbon potential of the basin and provide background information about geological concepts and assumptions that have been used to describe how the reservoirs been grouped into plays, build a basin model and generate datasets of potential discoveries.

2.2 General geology

2.2.1 Geological setting

Present-day Taranaki Basin is an active-margin basin associated with the modern-day converging Australia-Pacific plate boundary and sits ~200 km above the subducting Pacific Plate, within the plate boundary zone of deformation (King & Thrasher, 1996) (Figure 2.1). The current relative plate motion vector is ~40-45 mm/yr (De Mets et al., 1990, 1994). The basin is bounded to the east by the Taranaki Fault and the associated north-south trending basement fault block, the Patea-Tongaporutu High (Figure 2.1). It is mostly a subsurface feature offshore and continues onshore across the Taranaki Peninsula and north along the western coast.

2.2.2 Basin evolution

The Taranaki Basin has a composite morphology of superimposed half-graben and sub-basins, which record changing plate boundary kinematics associated with relative motion between the Pacific, Australian and Antarctic plates (Figure 2.2) (King and Thrasher, 1996; Uruski and Baillie, 2002). The evolution of the basin is described by three distinct time periods of tectonic development: Late Cretaceous to Paleocene; Paleocene to Oligocene, and Neogene (Figure 2.3).

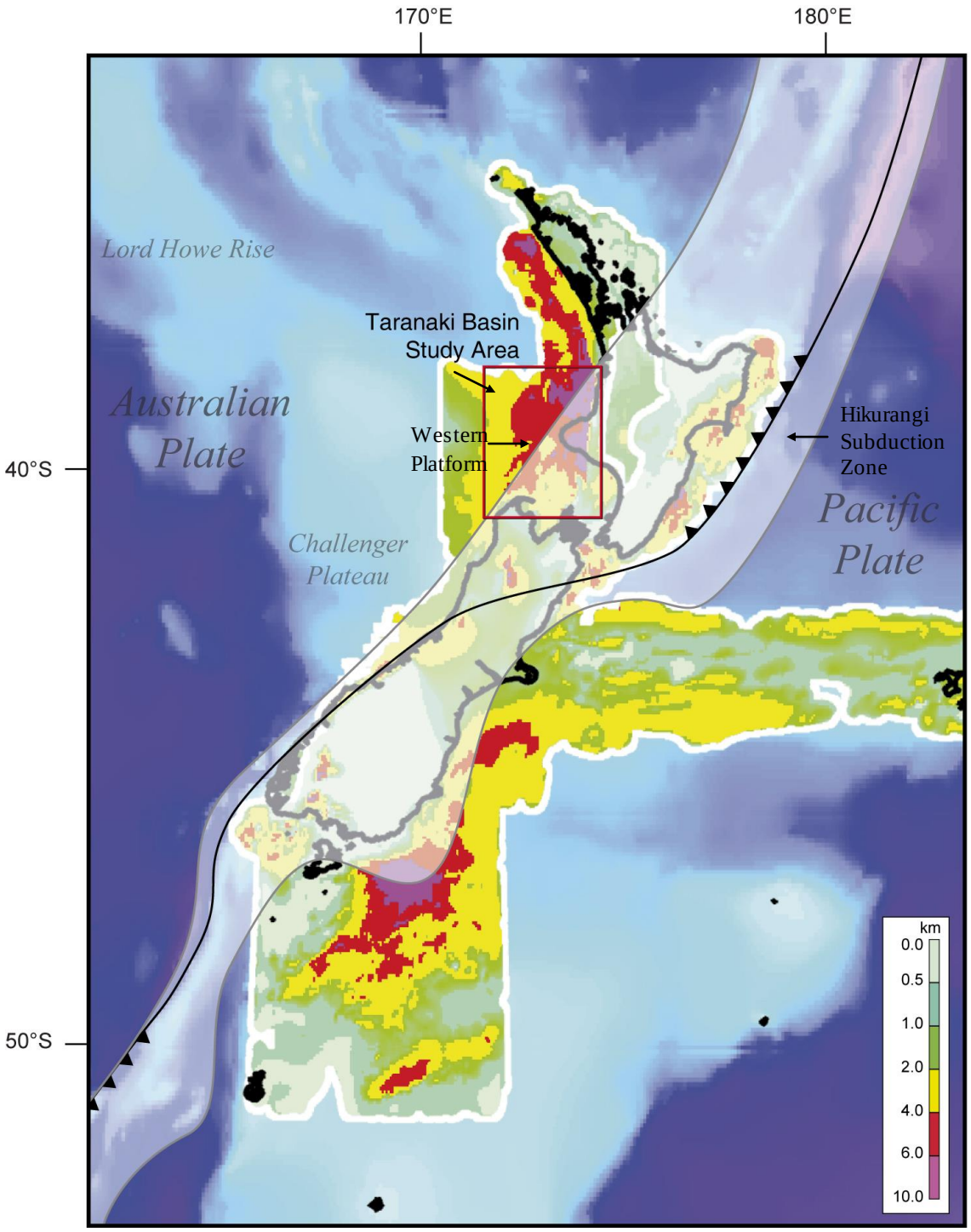

Figure 2.1: Geologic setting of the Taranaki Basin study area (red rectangle) showing its proximity to the Australian-Pacific plate boundary and location within the plate boundary zone of deformation (translucent white band). Sediment thickness is shown in the key on the lower right. Bathymetry shown shallow depths <2000 m (light blue) and depths >2000 m (purple). Modified from Uruski & Baillie (2002).

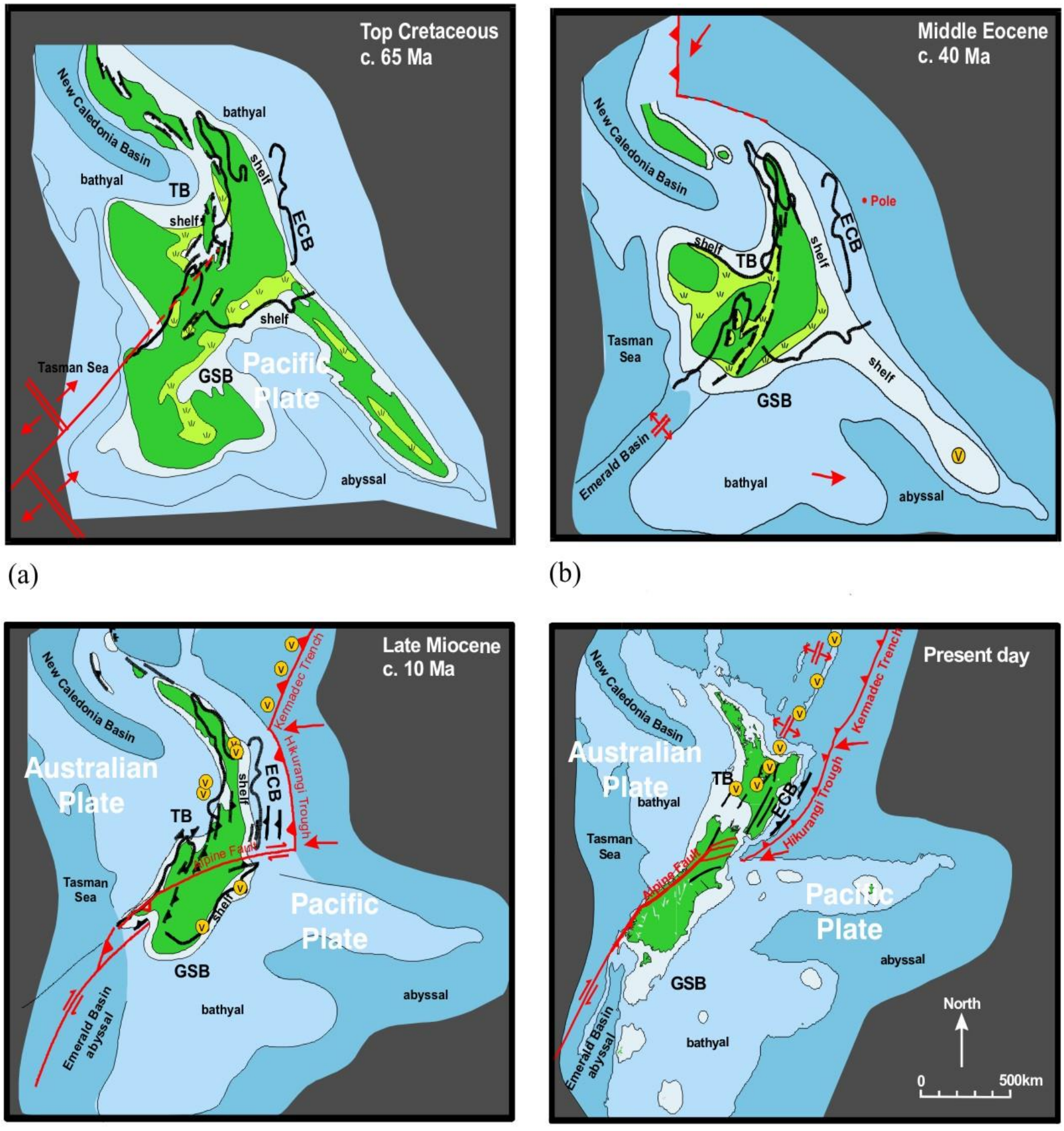

Figure 2.2: Schematic diagrams showing the re-construction of the Australia-Pacific plate boundary through New Zealand and the development of the distribution Cretaceous to Cenozoic sedimentary basins (shown here as light blue) over the last ~65 million years. (a) = 65 Ma, (b) = 40 Ma, (c) = 10 Ma and (d) = the present day tectonic regime. TB = Taranaki Basin. ECB = East Coast Basin. GSB = Great South Basin. Red arrows show plate motion and spreading ridges. Modified from King (2000).

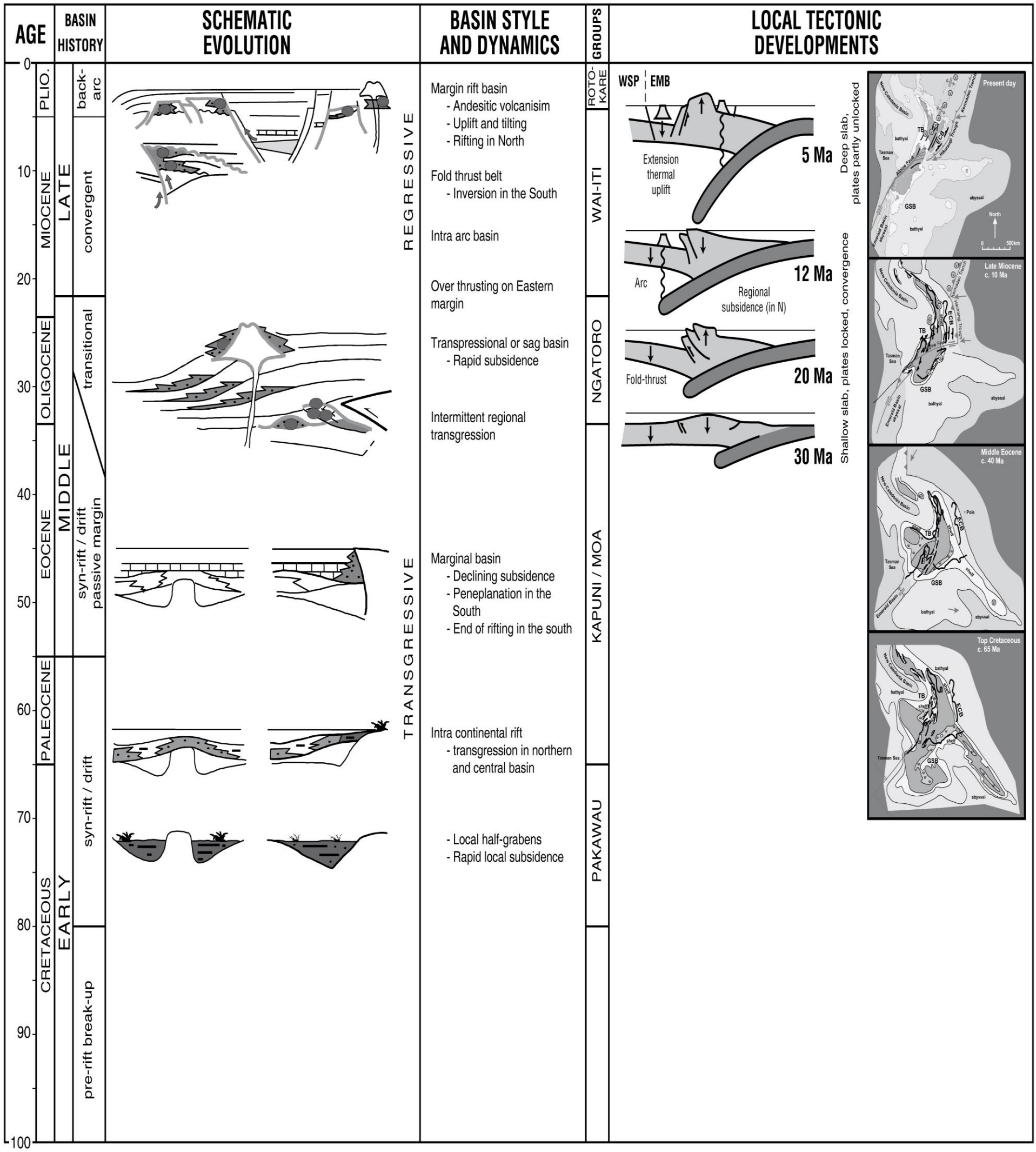

Figure 2.3: Taranaki Basin evolution showing the timing of events, basin dynamics, main depositional groups and tectonic developments. Ma = million years ago, ECB = East Coast Basin, GSB = Great South Basin, TB = Taranaki Basin. Modified from King & Thrasher (1996).

During the Late Cretaceous to Paleocene the basin was part of the New Caledonian Basin, along a rift-transform passive margin sub-parallel to the Tasman Sea Rift that developed with the initial break-up of Gondwana (~80 Ma) and seafloor spreading in the Tasman Sea. A series of interconnected rift sub-basins formed and filled rapidly with sediment as basement subsided (Hayward and Wood, 1989; King and Thrasher, 1996). By the end of the Late Cretaceous the sea had flooded coastal plains and fault-controlled alluvial valleys.

By the Paleocene rifting had stopped as spreading in the Tasman Sea came to an end and regional subsidence and marine inundation dominated forming a large embayment within a passive margin. Peneplanation of the adjacent hinterland provided sediments forming the youngest source rocks and key reservoir lithologies in the basin. By the Late Eocene the tectonic regime had begun to change, in response to the propagating Australia-Pacific plate boundary through New Zealand and by the Early Oligocene the sediment supply had declined (King and Thrasher, 1996). This was followed by a renewed phase of rapid subsidence began (Hayward, 1987; Hayward and Wood, 1989; Hayward, 1990) affecting the entire basin. Thick sedimentary sequences accumulated and a rise in relative sea-level culminated in a maximum marine inundation and carbonate deposition by the Late Oligocene.

By the Neogene an active plate boundary margin had developed through New Zealand resulting in the development of fold-thrust belts, a foreland basin, an intra-arc and back-arc basin, and extrusive volcanism in the Taranaki Basin (King and Thrasher, 1996). The basin hinterland and southern margin uplifted with the onset of Miocene regression and the two most significant uplift and erosion events occurred in the Middle Miocene and Plio-Pleistocene. The entire basin was affected and in some areas, especially in the south of the basin, seabed was raised from slope to shelf depths. Compressional tectonics ceased ~12 Ma, (Walcott, 1984, 1987) and the basin began to subside rapidly.

2.2.3 Tectonic elements

The Taranaki Basin is characterised by a set of diverse structures including normal faults, low-angle thrust faults, high-angle reverse faults resulting from the

polyphase tectonic history. The basin has two distinct structural domains known as the Western Platform and the Eastern Belt (King & Thrasher, 1996) (Figure 2.1). The Western Platform is located offshore beneath the western continental shelf and is ~150 km wide and 5000 m thick. It is composed of Cretaceous to Paleocene half graben overlain by progradational basin strata of Eocene to Holocene age. It was affected by Late Cretaceous to Eocene block faulting and except for its south-eastern margin it is relatively undeformed and has remained relatively stable throughout the Cenozoic (Palmer & Bulte, 1991). Structurally it is characterised by broad, anticlinal structures typical of low-level tectonic deformation.

The Eastern Belt is ~140 km wide and shows evidence of Miocene to recent thrust faulting and structural inversion, folding, uplift and exhumation, rapid sedimentation, and volcanism. It formed as the result of both compressional and extensional tectonics; however is mainly characterised by intense Neogene convergent-margin deformation, which has overprinted the basin's earlier extensional and passive-margin history. Late Cretaceous half graben have been everted and folded, and extensional faults have been re-activated as reverse faults. The structural deformation is greatest in the Eastern Belt because of its closer proximity to the active plate boundary. As a result of this there are five structurally distinctive domains, which are known as the Northern Graben, Mohakatino Volcanic Complex, Central Graben, Tarata Thrust Zone, and Southern Inversion Zone (Figure 2.4).

The major fault systems are northeast- or north-trending (Figure 1.3). The northeast-trending sets form two distinct clusters, one in the southwest and the other in the north. In the southwest faults are related to Early Cretaceous rifting. North-trending faults relate to tectonic movement in the Late Cretaceous and are parallel to terrane boundaries in basement. During the Cenozoic these faults were reactivated. In the north faults are related to Late Cenozoic movement (King & Thrasher, 1996). Fault offsets are predominantly dip-slip, with some showing minor strike-slip movement (Voggenreiter, 1993; Bussell, 1994).

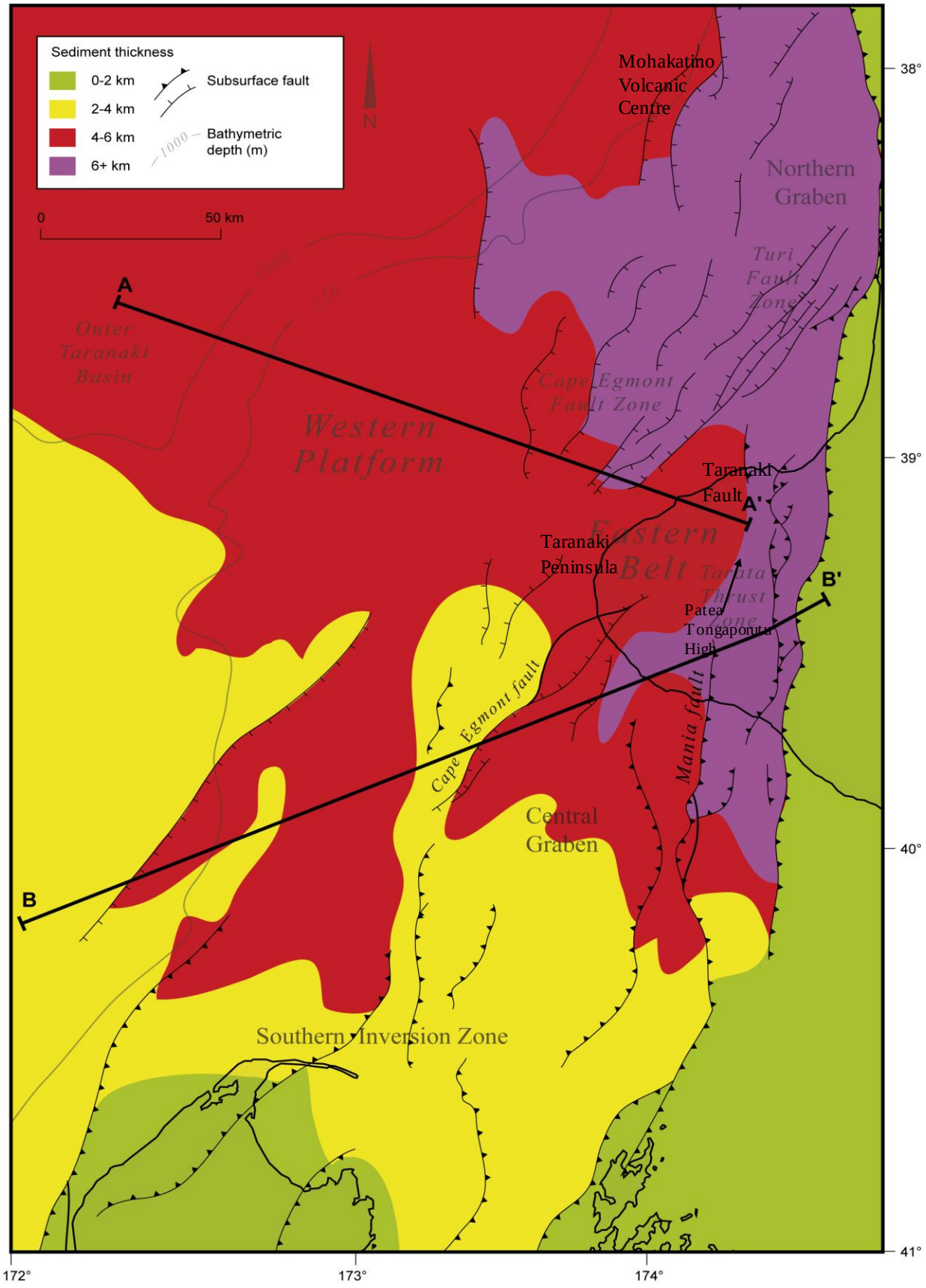

Figure 2.4: Key tectonic elements of present-day Taranaki Basin, and, in particular, Western Platform, Eastern Belt, Northern Graben, Central Graben and Southern Inversion Zone. Source, Crown Minerals (2004).

2.2.4 Stratigraphy

The Taranaki Basin contains Cretaceous to Cenozoic strata that record a major depositional cycle containing an early transgressive phase, followed by a regressive phase that continues today. Within the strata are four seismic-stratigraphic units (Figure 1.3) which are based on the interpretation of basin-wide seismic reflectors at top basement, top Cretaceous, top Eocene and top Miocene horizons (King & Thrasher, 1996). They are referred to as the Pakawau, Kapuni and Moa, Ngatoro and Wai-iti, and Rotokare groups (King & Thrasher, 1996).

The Pakawau Group (~100–65 ma) is a thick (1–3 km) Late Cretaceous terrestrial syn-rift sequence of fluvial-deltaic strata and comprises the Rakopi and North Cape formations. The Rakopi Formation consists of terrestrial sandstone cyclically interbedded with carbonaceous siltstone and mudstone, thin coal seams and rare conglomerate. The overlying North Cape Formation is dominated by shallow-marine, paralic and terrestrial lithofacies. The contact between these two formations marks a significant basin-wide marine transgression. The Rakopi Formation sediments form the basin's primary coaly source rocks, which are mapped discontinuously within a 150 x 400 km northeast-trending swath of individual sub-basins, as shown in Figure A1, Appendix 1 (King and Thrasher, 1996). North Cape Formation sediments form the second most important source rocks, which are also mapped discontinuously across the basin, but less extensively, as shown in Figure A2, Appendix 1 (King and Thrasher, 1996).

The Kapuni and Moa groups (~65–35 ma) comprise a thick (up to 4 km) Paleocene to Eocene late-rift and post-rift transgressive sequence of fluvial-deltaic sediments. The Kapuni Group is mainly characterised by low energy deposition typical of a long lived marine transgression. The Moa Group is a lateral equivalent of the Kapuni Group however it is entirely marine. The Kapuni and Moa groups are subdivided into six formations: Farewell; Kaimiro; Mangahewa; McKee; Turi; and Tangaroa (King and Thrasher, 1996).

The Farewell Formation is lithologically similar to the underlying Pakawau Group and has interbedded coarse to medium-grained sandstones and mudstones containing conglomerates, siltstones and coals (King and Thrasher, 1996). The Kaimiro Formation comprises Early Eocene lower alluvial plain, inner delta or

coastal plain and transgressive shoreline sandstones (King & Thrasher, 1996). Lithologies are primarily non-fossiliferous sandstone, siltstone and mudstone with minor coal, and show evidence of several depositional cycles. The Mangahewa Formation comprises Middle Eocene lower coastal-plain and estuary and transgressive shoreline complex sandstones. This formation is characterised by terrestrial and marginal marine lithofacies consisting of interbedded alternating cycles of sandstone, coal, carbonaceous sediments, siltstone and mudstone, as seen in Kapuni Field (King & Thrasher, 1996). The McKee Formation is characterised by shallow-marine, sandstone-dominated lithologies that were deposited as a transgressive shoreface or barrier bar complex with significant sediment reworking. The Tangaroa Formation consists of fine- to coarse-grained basin floor sandstones.

The Ngatoro and Wai-iti groups (~20–5 ma) are thick (up to 4 km) carbonate and clastic dominated marine sequences. The Ngatoro Group is an Oligocene to Miocene foredeep and distal shelf and slope carbonate dominated sequence and has three formations. The Otaraoa Formation is the youngest and is an outer shelf to upper bathyal deposit, which includes the Tariki and Matapo Sandstone members. Overlying this formation is the Tariki Sandstone Member, which is a submarine fan deposit that comprises interbeds of fine to coarse-grained sandstone, calcareous mudstone and limestone. The Matapo Sandstone member is glauconitic sandstone. The Tikorangi Formation is an outer shelf to upper slope carbonate deposit mapped in eastern parts of the basin. It is tightly cemented and has very low matrix porosity and permeability. The Taimana Formation is a fine grained sandy siltstone which marks the influx of clastics into the foredeep ending the deposition of carbonate.

The Wai-iti Group is a clastic-dominated marine regressive sequence and has six formations: Manganui; Moki; Mohakatino; Mount Messenger; Urenui; and Ariki. The Mount Messenger and Moki formations comprise deep-water basin-floor sandstones.

2.3 Petroleum systems

Discoveries in the basin are predominantly oil and gas-condensate, reflecting the mix of terrestrial and marine source rocks in the basin (Killops et al., 1998; Suggate, 2002; Sykes, et al 2004) the variable maturation of source rock organic matter (Sykes et al., 1991) and post-accumulation preservation conditions, which led to the displacement of oil and loss of gas in some traps (Wood et al., 1998).

A revised version of the Magoon & Dow (1984) petroleum systems event chart (Figure 2.5) is used in this study to systematically describe oil and gas generation, charge and entrapment in the Taranaki Basin. The chart describes the timing of source, reservoir, and seal rock deposition, and hydrocarbon charge, entrapment and preservation. It highlights the critical moment when the timing of each essential element and process for the accumulation of oil and gas was met, which was in the latest part of the Miocene (King & Thrasher, 1996).

2.3.1 Source

There are five primary source rock intervals in the Taranaki Basin: Late Cretaceous Rakopi Formation; Late Cretaceous North Cape Formation; Paleocene Farewell Formation; Early Eocene Kaimiro Formation; and Middle to Late Eocene Mangahewa Formation (Figure 2.5) (Cook, 1987; Sykes et al., 1991; Killops et al., 1998). Source rocks are typically Type III kerogen coals with interbedded carbonaceous shales, which have a minor contribution of marginal marine material (Killops et al., 1994; Armstrong et al., 1996; Wood et al., 1998; Sykes et al., 2004). The oils are paraffinic and waxy in nature and have high API gravity values, from 32˚–48˚, and low sulphur content typical of a terrestrial Type III kerogen source (Killops et al., 1994).

Biomarker studies have not confirmed a genetic link between source rocks and oil and gas accumulations in the Taranaki Basin. This may be because generation and expulsion conditions have varied within the basin and with time, and the hydrocarbons may have originated from source rock mixing (Manzano-Kareah, 2004). Therefore, hydrocarbons in the basin are assumed to originate from more than one working petroleum systems and any of the five lithologies above.

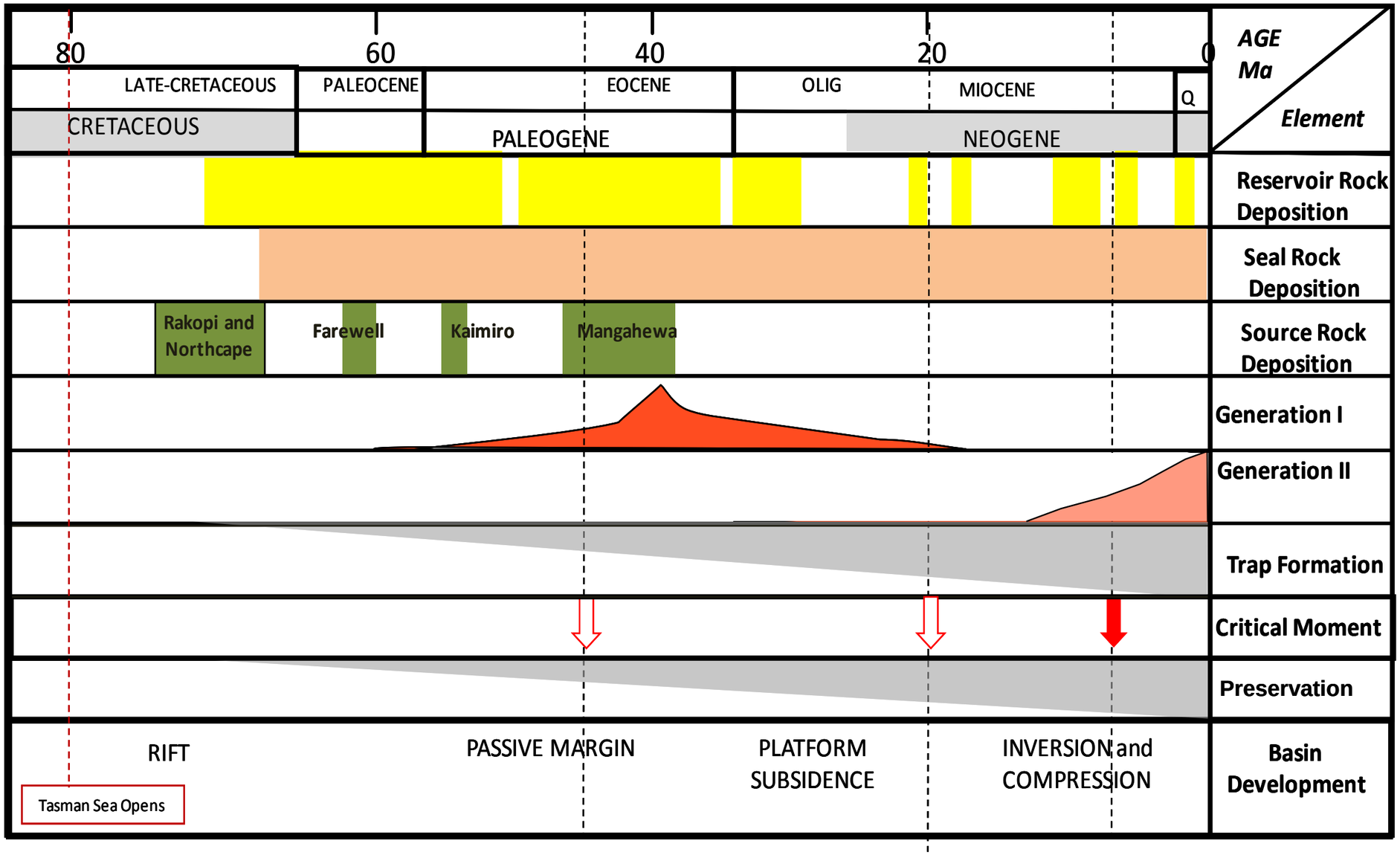

Figure 2.5: Petroleum systems event chart. Source rock deposition shows formation names. Solid red arrow marks the time of the critical moment, when all requisite conditions of a working petroleum system were met. The critical moment is based on Wood et al. (1998). Red-outlined arrows indicate early expulsion (Generation I) which is based on basin modelling; however this charge was not preserved primarily due to insufficient trap development, as shown by the light-grey shading in the Trap Formation section. Generation II is hydrocarbon charge from 10 ma to present-day.

2.3.2 Reservoir

The most productive reservoirs are the Paleocene shoreline and Eocene coastal plain sandstones of the Farewell, Kaimiro, Mangahewa and McKee formations. These reservoirs are found in the Maui, Kapuni, Kupe, Pohokura, Mangahewa and Tui fields (Table 1.1). Neogene reservoirs, which include the Mt Messenger and Moki formations submarine fan sandstones (Section 2.2.4) have produced reserves in smaller sized fields (Table 1.1). Pakawau Group fluvio-deltaic sandstones remain unproven as a reservoir. Reservoir is discussed in more detailed in Section 3.4 where the reservoirs included in this study are classified into four play levels.

2.3.3 Seal

Marine mudstones are the dominant seals across the Taranaki Basin (Figure 2.5) and although these occur throughout Cretaceous and Paleogene stratigraphy, it is the fine-grained siltstones and mudstones of the Turi Formation that form the most effective regional top seals (King & Thrasher, 1996). The fine grained sediments within all siliciclastic reservoir sequences (e.g. Kaimiro and Mangahewa formations) also produce effective intra-formational seals in stacked reservoirs typical of the Maui, Kaimiro and Mangahewa fields. Carbonate rocks, such as the Tikorangi Formation, have low porosity and permeability and where they are not fractured they also form seals.

2.3.4 Traps

All hydrocarbon accumulations in the Taranaki Basin have been found within structural traps and most of them are fault bounded (Nicol et al., 2004). They are include four-way dip closures, three-way dip and fault closures, drape folds over basement horsts, thrust-controlled anticlines, and overthrusts. All formed as a result of Neogene tectonic deformation. Older trapping structures related to Cretaceous normal faulting may exist, however Neogene reverse faulting and fault reactivation makes it difficult to separate the two stages of structural development (King & Thrasher, 1996). Consequently, there is potential for hydrocarbons from earlier charge events (Figure 2.5) to be trapped in older structures. However, their

preservation is unlikely given the impact of Neogene deformation on seal and trap integrity (Darby & Ellis, 2002).

2.3.5 Charge and accumulation

Mature source rocks exist throughout the basin but are thicker and most mature in the Eastern Belt to the north where superimposed sequences of Cretaceous to Plio-Pleistocene strata are thickest and Neogene subsidence and local heatflow has favoured source rock maturation conditions.

Present-day hydrocarbons in the basin have been generated and expelled in the last five to 10 million years based on the chemical compositions of oil (Armstrong et al., 1994; Killops et al., 1994; Armstrong et al. 1996), basin modelling investigations (Funnell et al. 2001; Funnell et al. 2004) and recent charging of post-Miocene reservoirs (Armstrong et al., 1994; and earlier references therein). Although there may have been earlier expulsion (Figure 2.5) it is unlikely to contribute to present-day accumulations because of the timing of traps (King & Thrasher, 1996).

Hydrocarbon discoveries in the basin confirm effective secondary migration in the basin including in areas of continuing tectonic deformation, such as those that are undergoing or have recently undergone active faulting and volcanic intrusion (Funnell et al., 2004). Migration flowpaths are inferred to be mostly vertical and short, along bedding and fault planes (Wood et al., 1991).

2.3.6 Preservation

Seal integrity in some parts of the basin may be compromised due to hydraulic fracturing and extreme overpressures and ongoing Neogene tectonic deformation (Darby & Ellis, 2002). In support of this theory, most column heights in the basin are <200 m based on well data (McAlpine, 2005) and the maximum burial depth of topseal (Figure 2.6) suggests the Taranaki Basin seal rocks are incapable of holding back actual hydrocarbon column heights >200 m. Seal rocks in the Taranaki Basin have to be buried to at least 2500 m to uphold a minimum column of 100 m, and at least 1400 m to uphold a minimum column of 35 m, based on a plot of trapped hydrocarbon column height versus maximum burial depth of seal

rock (Figure 2.6). Without a greater number of hydrocarbon column heights available, a minimum burial depth for seal rock in the basin is unknown.

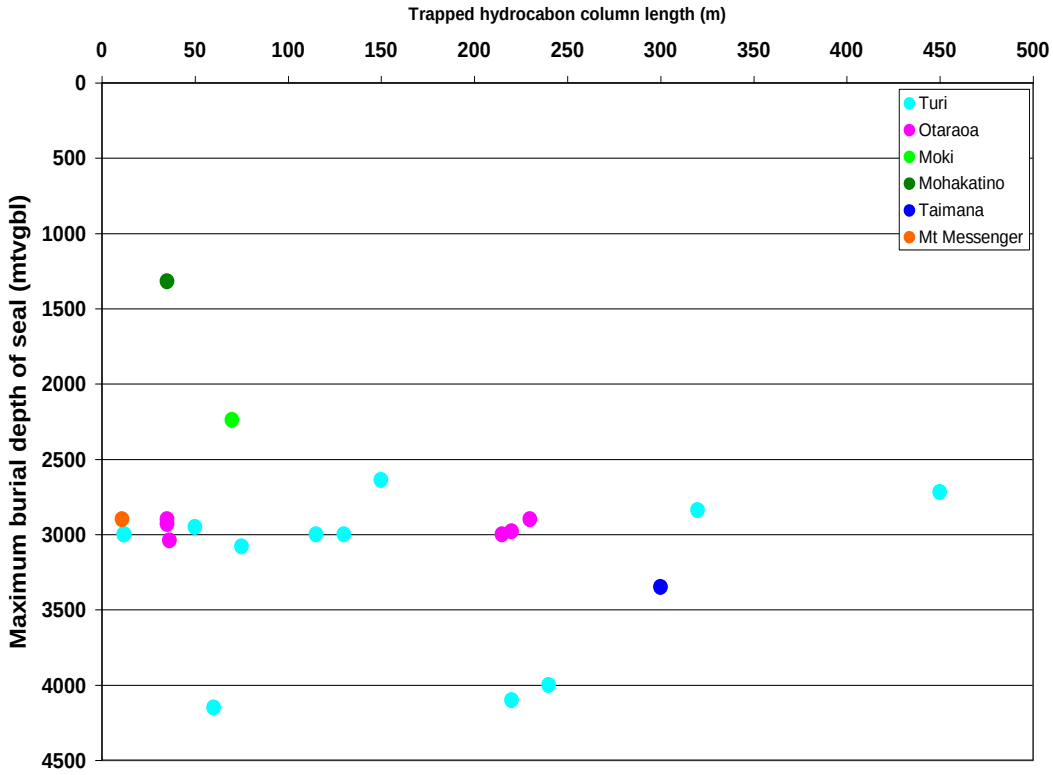

Figure 2.6: Hydrocarbon column heights in the Taranaki Basin. The different coloured dots show the different formations that have lithologies, which have seal rock properties (McAlpine, 2005). Mtvgbl = meters total vertical ground below.

Seal integrity is most likely to be compromised where there is a lack of grain size contrast between reservoir and seal sediment, limited burial or breaching caused by compaction-generated overpressures (Darby & Ellis, 2002). These three factors are more pronounced in Miocene reservoirs (McAlpine & O'Connor, 1998). Capillary entry pressure measurements indicate that seal capacity is highly variable in the Taranaki Basin due to depositional composition and subsequent diagenetic modification (Darby & Ellis, 2002). The lack of seal integrity may also explain why some traps are not filled to their structural spill-point (Haskell, 1991; McAlpine, 2005, Darby and Ellis, 2002). Such seal risk may mean a trapping structure is not full to its maximum trap capacity. However because of present day hydrocarbon charge traps are likely to be full.

2.4 Conclusion

The petroleum geology of the Taranaki Basin suggests the basin has good resource potential. In particular, there is a number of working petroleum systems in the basin based on the distribution of discoveries across the basin and throughout the thick Cretaceous to Cenozoic sedimentary sequence.

The petroleum system chart highlights the favourable conditions for hydrocarbon accumulation. In particular, the basin has a variety of mature terrestrial and marine source rocks; multiple reservoir sequences; regional and intraformational seals, a variety of trapping configurations and oil and gas charge. Although Neogene deformation may have detrimentally affected some petroleum systems elements, such as topseal integrity, present day charge means traps (that receive charge) should retain hydrocarbons.

Chapter 3

Background to methods and models

3.1 Introduction

The purpose of this chapter is to provide background information about the techniques that have been used to prepare input data and the methods and models that have been used to estimate undiscovered oil and gas in this study.

A challenge of this study is to represent the hydrocarbon potential of the entire basin, including the undrilled parts. Hydrocarbon potential is the postulation that oil and gas exist based on our understanding of the petroleum systems of a basin (Drew, 1997; Charpentier, 2005). Down-hole well data provides the most convincing information about the hydrocarbon potential of a basin, however these data are often concentrated in easily accessible areas and widely spaced in more offshore and deeper-water areas. As a result prospective areas of a basin can be overlooked.

Traditionally a probabilistic size distribution function is used to approximate a parent population of oil and gas accumulations (Howarth et al., 1980; Harbaugh & Ducastaing, 1981; Klemme, 1983; Houghton, 1988). The parent population is the original population of all accumulations in an area, such as a play or basin, and represents the maximum number of accumulations in an area. All previous estimations of undiscovered oil and gas for the Taranaki Basin (Table 1.1) are based on this approach and the size distribution of the parent population has been estimated using the size and number of discoveries in the basin. The earliest assessments (Cook, 1985, Beggs & Cook, 1993) are underestimates because more discoveries have been made than these assessments predicted. Recent estimates (Beggs, 1998; O'Connor, 2002; Mare-Jones, 2004) are expected to be underestimates also because they too are based solely on discovery data.

The Taranaki Basin has excellent potential to yield further discoveries given the coverage of working petroleum systems (King & Thrasher, 1996) and variety of

proven and prospective plays (Thrasher et al., 1995a–e). Most drilling is onshore which probably reflects the preference of explorers to target accessible, shallow structures and not the prospectivity of the basin. Approximately 70% of the basin, which covers an offshore area of ~70,000 km^2 (Figure 1.2) is relatively undrilled.

In an attempt to capture the hydrocarbon potential of the Taranaki Basin this study uses three datasets of oil and gas accumulations to represent actual and potential discovers.

1. S_1, is the sampled population of discovery-based accumulations comprising 33 oil and gas discoveries >1 mmboe in the Taranaki Basin. The discovery volumes are P50 recoverable reserves, which means they have a 50% certainty of being extracted to the surface and produced (Crown Minerals, 2004) (Table 1.1).

2. S_2, is the sampled population of basin-modelled accumulations. It is one of the semi-synthetic datasets and is based on the results of the two basin models, Bassim® and PetroCharge Express® (PCE).

3. S_3, is the sampled population of structural trap accumulations and is based on structural traps identified on structure contour depth maps. This dataset is further divided into S_{3i}, which includes all identified traps and S_{3ii}, which includes only charged traps, based on discoveries and basin-modelling results.

The datasets are used in the volumes component to define the size distribution of the parent population and to represent locations of hydrocarbon-charged traps in the spatial model. The semi-synthetic datasets, S_2 and S_3, represent potential discoveries and are used to represent unexplored areas of the basin that are geologically prospective, based on the petroleum systems of the Taranaki Basin (King and Thrasher, 1996).

3.2 Basin-modelled oil and gas accumulations

3.2.1 Introduction

Bassim® is a deterministic finite element generation and expulsion model (Armstrong et al., 1994; Armstrong et al., 1996; Wood et al., 1996; Wood et al., 1998; Funnell et al., 2004) and was used to estimate the amount of oil and gas generated and expelled in the Taranaki Basin. PCE® is a volumetric migration flowpath model and was used to migrate the expelled volumes of oil and gas through a reservoir and estimate the volume of modelled oil and gas accumulations (Figure 3.1) (IES, 2000).

Bassim® and PCE® were used because of their availability and access, which was granted as part of the primary research scholarship conditions. No other industry standard basin modelling tools were available to enable a critical evaluation of the software used.

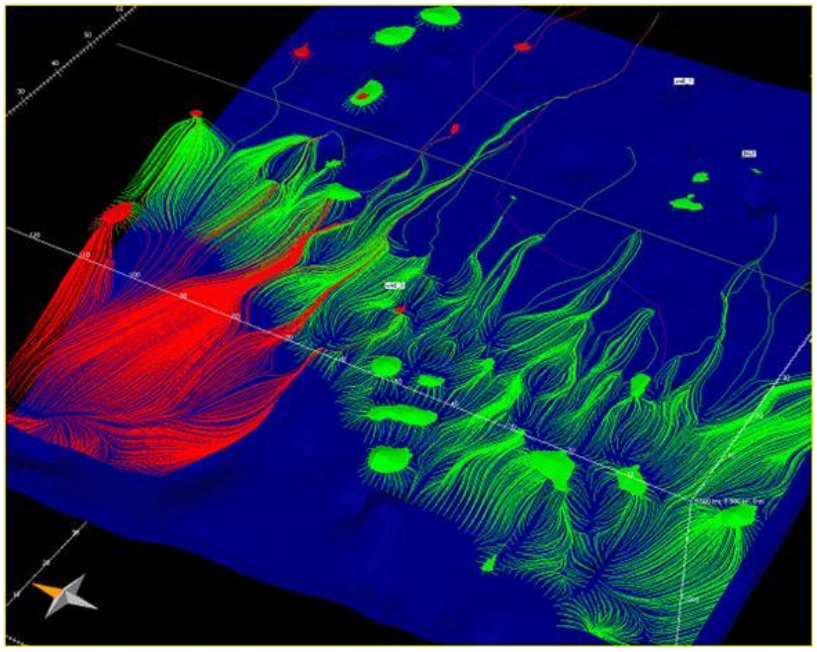

Figure 3.1: A visual display from the PCE® flowpath model showing the trapped hydrocarbons and the migration flowpaths which move from mature source rock areas and up-gradient of a surface toward topographical highs. Red is liquids (oil and condensate), green is gas.

3.2.2 Modelling generation and expulsion

Primary migration and the generation of hydrocarbons from source rock and expulsion into reservoir rock is dependent on kerogen conversion, which is controlled by temperature and time dependent kinetic processes (Tissot & Welte, 1984). These processes are largely driven by sediment compaction and subsurface heat flow (North, 1985) and the volumes and types of hydrocarbons that are produced are primarily dependent on source rock type and the timing of expulsion (Pepper, 1995).

Bassim® models primary migration by reconstructing deposition through time based on burial history and source rock maturity profiles throughout a sedimentary sequence (Wood et al., 1998). Structural contour depth maps and paleo-water depth maps are used to model the evolution of the basin, based on time-stratigraphic interval backstripping and decompaction as described in Wood et al. (1998). The sediment fill of the basin is represented by isopach maps and each source, reservoir and seal rock interval is assigned an age and lithology to model the burial history through time. Lateral variations in sediment type are controlled by paleogeographic maps which illustrate the variation of depositional environment.

Maps of source rock distribution and thickness are used to define the source rock intervals. Source rock maturity is modelled as a function of burial depth and source rock richness is represented by percent total organic carbon (%TOC). Source rock hydrocarbon potential is represented by hydrocarbon index (HI) and hydrocarbon saturation threshold (S_r). The thermal regime and organic matter transformation kinetics used are described by Wood et al. (1998).

Two significant Neogene uplift and erosion events (Section 2.2) are included in the Bassim® model because of the significant effect on basin heatflow and source rock maturation and expulsion (Funnell et al., 1996). Maps showing the age and thicknesses of the eroded strata are used to determine the maximum burial depth of source rock. The thicknesses were modelled as described by Wood et al., 1998). The first amount of uplifted and eroded strata was modelled by decompacting the Plio-Pleistocene strata on the present-day distribution of Miocene sediments and then subtracting the resulting strata thickness from the

pre-erosional pattern, as described. The second amount of uplifted and eroded strata was modelled using empirical porosity-depth trends.

The amounts of hydrocarbons generated and expelled were calculated using Equation 3.1, described by Funnell et al (2001):

$$HC_{vol} = \frac{TOC}{100}\left[TR.HI - S_r\right].\rho_{rock}.vol_{source} / \rho_{HC} \qquad (3.1)$$

HC_{vol} is the volume of hydrocarbons expelled in millions of barrels per square kilometre ($mmbbls/km^2$) for oil, and billion cubic feet per square kilometre bcf/km^2 for gas; TOC is in $(\%)$; TR is the transformation ratio, which is a measure of the effectiveness of the conversion of organic matter into kerogen and petroleum, HI is in kilograms per tonne of total organic carbon (kg/tC_{org}), S_r for oil expulsion, is the amount of hydrocarbons retained in the coal and is in kilograms per tonne (kg/t); ρ_{rock} is the dry rock density and is in kilograms per cubic metre (kg/m^3); vol_{source} is the volume of source rock associated with a particular transformation ratio and is in cubic metres (m^3); and ρ_{HC} is hydrocarbon density and is also in kilograms per cubic metre (kg/m^3).

3.2.3 Modelling migration and entrapment

PCE® models secondary migration based on a ray-trace modelling technique, which means oil and gas move up-dip under the influence of buoyancy with no significant hydrodynamic component of flow (Schroeder & Sylta, 1991). This means the hydrocarbons flow through the reservoir along a single migration surface which is based on present-day gradients at the top of the reservoir. The dip gradients of the surface create drainage areas which control the direction and speed of flow until the migrating hydrocarbons culminate at a trap or flow out of the basin. The hydrocarbons are trapped by anticlinal and fault-bounded structural traps and/or facies-bounded stratigraphic traps beneath a regional seal.

The volumetric capacity of a trap is based on the hydrocarbon pore volume between the crest and spill-point of a trap. If the volume of oil and free gas reaching a trap exceeds the trap capacity oil and then free gas will spill. Hydrocarbons will also leak through topseal when the buoyancy of long hydrocarbon columns override seal capillary entry pressure (CEP). In the PCE® model, in a two-phase scenario of gas and oil gas will displace liquid if an accumulation is filled to its maximum capacity and additional liquid is injected. Excess liquid will spill into an adjacent drainage area. Consequently, traps that are fill-to-spill with some proportion of oil may contain a higher proportion of gas than liquid compared to what occurs in reality because spilt gas may displace the liquid.

Seven input maps were used in PCE® to represent the main petroleum systems elements and processes described in Section 2.3.2 and shown in Figure 2.6, including:

- structure contour surface of top reservoir;
- reservoir porosity;
- reservoir thickness;
- amounts of oil and condensate generated and expelled;
- amounts of gas generated and expelled;
- top seal capillary entry pressure; and
- regional fault traces.

All input maps except the amounts of oil, condensate and gas, were prepared directly from four basin-wide structure contour depth maps including: Basement (Figure A1) (Thrasher and Cahill, 1990); top Cretaceous (Figure A2) (Thrasher and Cahill, 1990); top Eocene (Figure A3) (Thrasher et al., 1995); and top Miocene (Figure A4) (Thrasher et al., 1995) (Appendix 2). These surfaces are seismically mapped and depth converted, as described in Thrasher (1992), and presented as depth below the ground-surface/sea-floor. Each surface was converted into an ArcMAP® coverage shapefile of contoured depth then converted to a pixelated raster surface by gridding the contours to a map surface

of numerical cells using the ArcINFO 7® GRID command. The datagrids are presented in Appendix 3.

The maps of the amounts of oil, condensate and gas that are available for migration (Appendix 4) were output from the Bassim® model. They are input into PCE® for each source rock interval (Section 3.2.2). The inputs used to create them in Bassim® are also based on the regional structure contour depth maps.

3.2.3.1 Reservoir

The top Cretaceous (Thrasher and Cah ill, 1990) and top Eocene (Thrasher et al., 1995) structure contour depth maps discussed above were used to define present-day migration surfaces at the top of the Cretaceous and Eocene reservoir sequences. The top horizons of the Paleocene and mid-Miocene reservoir plays are based on proxy depth maps because there were no available regional depth maps at these reservoir levels and time did not allow for them to be interpreted from seismic data.

Most of the pre-Neogene structural traps in the Taranaki Basin are large (Thrasher & Cahill, 1990a & b; Thrasher et al., 1995a–e) and contain a sequence of progressive reservoir ages, made up of sediments deposited during the Late Cretaceous to Oligocene transgression (King & Thrasher, 1998). Consequently, the structure contour depth surfaces at the top of each reservoir from the Cretaceous to the Oligocene are assumed to be structurally similar. Because of this assumption, the top Paleocene proxy surface was derived by producing an isopach thickness between the top Cretaceous and top Eocene depth surfaces and creating a surface within that interval at the required depth.

The intra-Miocene surface, which is used to represent the reservoirs sequences of the Mt Messenger and Moki formations, is more problematic to model from proxy data because of the significant structural difference at this level compared to older horizons due to Neogene tectonic deformation. Because of this and since the base of the Oligocene to early-Miocene Ngatoro Group corresponds to a major unconformity that has different origins in different parts of the basin (King & Thrasher, 1996) the top Eocene structure contour depth surface could not be used

to derive the intra-Miocene surface. Instead the top Miocene structure contour depth was used to represent the top of the intra-Miocene surface. However, the top Miocene surface is not an ideal structural representation for the Mt Messenger and Moki reservoir surfaces and to minimise the uncertainty associated with the preparation of this surface the area of potential reservoir was constrained by including a facies map of the Moki and Mt Messenger formation lithologies.

Reservoir facies maps showing the distribution and quality of reservoir were prepared using an iterative approach. Firstly, regional-scale paleogeographic maps (King & Thrasher, 1996) and local-scale maps (from petroleum well reports) were used to create reservoir distribution maps based on paleoenvironments of periods when reservoir was deposited. Well data, namely lithological observations based on stratigraphic interpretations and composite and well completion logs and petrophysical data, were then used to define areas of effective reservoir. For example the good reservoir characteristics of the Eocene sandstones encountered in the Hochstetter-1 (Mills, 2000) and Tui-1 wells (NZOG, 1995) were used to revise the Eocene shoreline complex sandstones previously mapped by King & Thrasher (1996). Also although the Oligocene to early-Miocene paleogeographic map (King and Thrasher (1996) shows carbonate rock mapped over most of the basin oil and gas has only been produced from carbonate rock (e.g. Tikorangi Formation, see Section 2.2) in a very small area.

Maps showing reservoir thickness and porosity were created using well data. Reservoir depths and net-sandstone thickness recorded at well locations are shown in Enclosures 1 and 2. Net-sandstone thickness and reservoir porosity were interpolated between well locations using the ArcMAP® GIS inverse-distance-weighted interpolation tool. Structural cross-sections were used to evaluate the interpolated thicknesses and finalise the reservoir-facies maps. Three different ranges in reservoir thickness were defined to show areas of probable productive, possible productive and unproductive reservoir using thicknesses of 100 m, 25 m, and 0 m respectively. The thickness ranges were initially determined by examining the relationship of reservoir thickness and trap filling dynamics, such as the spillage of hydrocarbons from one structure into one another, using PCE®. They were also constrained by a dataset of hydrocarbon column heights (Figure

2.7) and carrier-bed thickness is at least the height of the hydrocarbon column at each well location within each reservoir interval. Unproductive reservoir includes lithologies with little or no reservoir potential and areas were reservoir was not deposited or was eroded.

Reservoir porosity was predicted as a function of compaction based on maximum burial depth (Athy, 1930; Hamilton, 1976; Magara, 1976) using equation 3.2:

$$\iota = 45\% * \exp (R_{cd} / 3000) \qquad (3.2)$$

where ι is porosity, 45% is the depositional porosity and R_{cd} is reservoir compaction depth, which is measured as maximum burial depth (Figure 3.2).

Maximum burial depth was estimated using the present-day depth at the top of a reservoir and subtracting water-depth in offshore areas and adding topographic height in onshore areas. An empirical regression curve through well-based porosity data (Figure 3.3) was not used instead because of the limited availability of wells with porosity data. The predicted porosity trend was, however, compared to the dataset of well-based porosity (Figure 3.3) and the best-case (P50) predicted porosity trend falls well within the depth-related empirical porosity range.

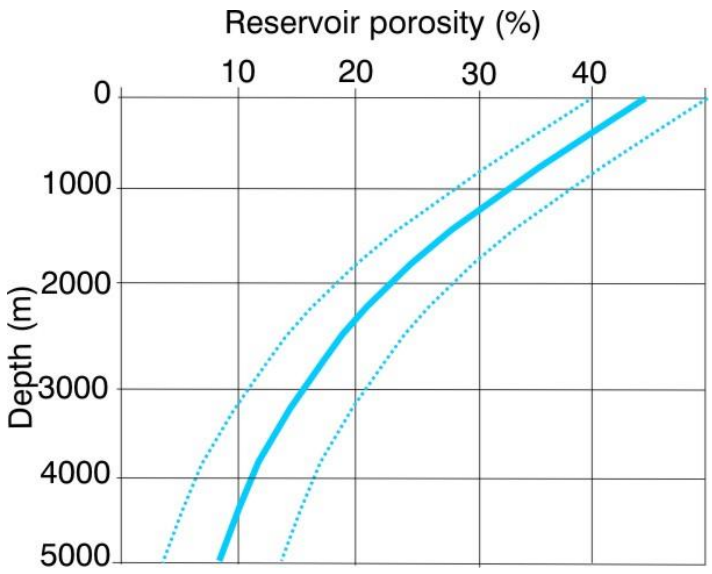

Figure 3.2: Reservoir porosity predicted as a function of depth. The dotted lines represent a range in porosity based on the uncertainty associated with the depositional porosity. The solid blue line is the best-case (P50) porosity depth curve for this range, where the depositional porosity ranges from 40–50%.

3.2.3.2 Entrapment

In PCE® structural traps are created by topographic highs and faulting. The regional fault traces relating to each structure contour surface at the top of each reservoir interval were input as a fault trace surfaces, which intersect the top surface of each reservoir level. Faults are treated as an infinitely thin line in, which means where a fault subdivides two neighbouring cells it acts only as a boundary without taking up any volumetric space within the cell. Faults are assigned as either permeable or impermeable to flow based on a conceptualisation of their impact on migration.

Stratigraphic traps form when a contrasting and relatively impermeable facies boundary, such as top seal within a regional topographic high or a lateral seal rock pinching out along an anticlinal flank, prevents the flow of hydrocarbons. Top seal maps were created using paleogeographic maps (King and Thrasher, 1996) to define the effective seal rock lithologies, such as mudstone and limestone, and used to represent regional seal rock above the reservoir intervals. Maps of seal rock efficacy were created based on the CEP acting on the topseal. CEP is the capillary pressure at which the non-wetting phase first displaces the wetting phase and is expressed in mega Pascals (MPa). CEP is dependent on many variables and, in particular, sediment porosity, tortuosity, grain size and sorting (Bear, 1972).

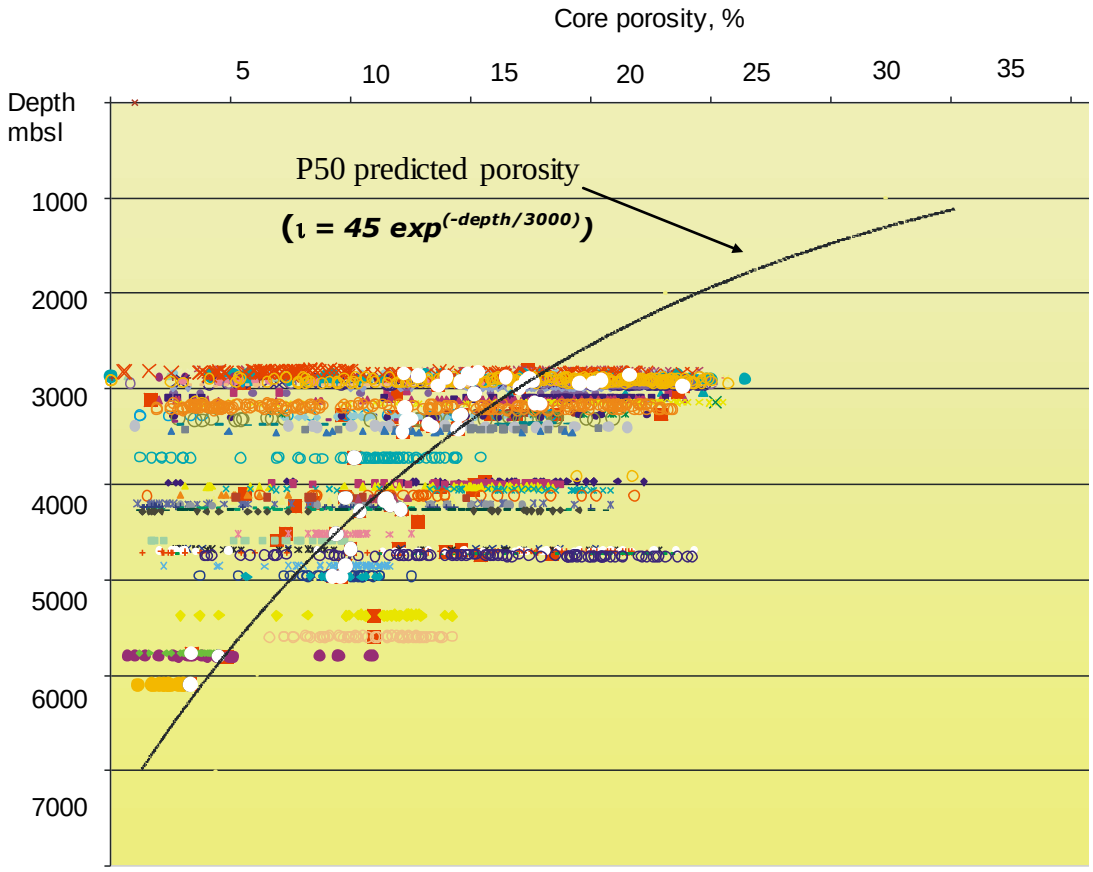

Figure 3.3: Comparison of the predicted porosity trend shown in Figure 3.2 with empirical porosity values from 75 core intervals in 14 Taranaki Basin wells from the following fields, Maui (Maui-6) Kapuni, McKee, Maari, Tariki/Ahuroa, Waihapa/Ngaere (Waihapa-1), Rimu, Kaimiro, Ngatoro, Waihapa/Ngaere. The coloured symbols represent different fields; however, at this scale not all coloured symbols are visible and, therefore, are not labelled. mbsl = metres below seal level. θ = porosity.

CEP increases with depth and seal rock effectiveness is predicted in PCE® as a function of maximum burial depth determined porosity using Equation 3.3:

$$\text{CEP} = 2: \text{ for } \iota < 20; \text{ and CEP} = 3.6 - 0.08 * \iota: \text{ for } \iota \geq 20 \qquad (3.3)$$

where ι is porosity. With increased maximum burial depth, porosity is reduced and with decreasing porosity, CEP increases. The higher the CEP the less likely the hydrocarbons will breach the seal rock. CEP values for the Taranaki Basin seal rocks are not known and a sensitivity study using a range of CEP values (from 1–4 MPa) showed that an increase from 2–4 MPa more than doubles the volume of hydrocarbons (mostly gas) accumulating. A seal rock with a CEP as high as 4 MPa is impermeable to hydrocarbon flow.

3.2.3.3 PCE® migration model

PCE® was run in a UNIX-based operating system. Each petroleum systems map is input as an ArcMAP® GIS datagrid where, x and y are the map coordinates and z is the datum point that numerically represents the mapped parameter. Then the flowpath model parameter settings and calculation options which control the input map sensitivities, map borders, flowpath density and resolution, and the precision of the volume calculations, are selected. For example, study area borders can be assigned as open or closed to control the flow of hydrocarbons within and out of the study area and individual input maps can be turned on and off for scenario testing. The model is run for both gas and liquids and the modelled accumulations are calibrated against known hydrocarbon accumulations, well data and petroleum systems information. Simulated accumulations are expected where discoveries have been made and not expected where dry holes have been drilled. In cases where accumulations were simulated in areas where a structure was deemed dry of hydrocarbons drilling reports were examined to determine if the well was a valid test of the structure.

Each simulation produces a set of accumulations that contain a proportion of gas, oil and condensate. Maps of accumulations are output and trap volume is calculated in million cubic metres (mcm). Other hydrocarbon volume information, including volumes accumulated, spilt and leaked, drainage area, trap closure pore volume, hydrocarbon phase density and trap fill are output in table form.

3.2.3.4 Trap volumes

PCE® simulates trap volumes were converted to industry standard units. Liquids were recalculated to millions of barrels of oil (mmbbl) by multiplying mcm by 6.289. Gas volumes were recalculated at standard temperature and pressure to billion cubic feet (bcf) by multiplying mcm by 0.035314.

Liquid (oil and condensate) and gaseous hydrocarbons are reported in different units of volumetric measure because they have different physical properties (USGS, 2000). However, these volumes are typically combined to calculate the total hydrocarbon volume of a trap, field or basin. To combine them a volume of gas is recalculated as an equivalent volume of oil which is known as millions of

barrels of oil equivalent (mmboe). The equivalence value is based on the relative energy content of the gas which is related to its chemical composition and may vary slightly from field to field. For example, one barrel of Taranaki Basin oil has the same approximate equivalent energy content as 5250 scf of gas (King & Thrasher, 1996). The original inplace P50 gas volume (which is the original reserves volume with 50% certainty of being produced) for the Maui Field is 3444 bcf (Table 1.1) which is equivalent to 655 mmboe.

The volume of PCE®-modelled accumulations are based on trap geometry and migration dynamics and hydrocarbon phase separation, and to compare them with accumulations in the S_1 and S_2 datasets they are standardised, to reflect recoverable volumes at surface temperature and pressure conditions, using the following calculation:

$$V_{cal} = V_{PCE}(A, h, \phi, NG) * FVF * FTS * S_{hc} * R_{hc} * C_{mcm} \quad (3.4)$$

where V_{cal} is the calibrated volume, $V_{PCE®}$ is the migration model volume, A is area, h is carrier-bed thickness/crest height, ι is carrier-bed porosity, NG is net-to-gross sandstone, C_{mcm} is a units conversion factor (Section 3.2.2), FTS is fill-to-spill correction factor, FVF is formation volume factor, S_{hc} is hydrocarbon saturation factor and R_{hc} is hydrocarbon recovery factor.

The fullness of a hydrocarbon trap is related primarily to the volume of hydrocarbons available during migration and access to trap charge, tectonic tilting of a structure and seal rock capacity and integrity (Schowalter, 1979). PCE® typically models all traps as filled to their structural spill-points (IES, 2000) and because of this a FTS correction factor is used in this study to express the uncertainty related to the fullness of a charged trap. The spill-point of a structural trap is the elevation marked by the lowest contour value where the volume of hydrocarbons exceeds the available trap space and spills out (North, 1985).

All of the known fields in the Taranaki Basin were simulated in PCE® as 100% full because PCE® is unable to sufficiently model any variability in seal rock integrity. However, traps may not be filled to their structural spill point (Funnell et al., 2004; Funnell, 2005) due to topseal integrity (McAlpine & O'Connor, 1998;

Darby & Ellis, 2002). Tectonic tilting may have also impacted the volume of hydrocarbons in some structural traps, such as the Maui Field structure which shows evidence of progressive trap formation during hydrocarbon charge (Funnell et al., 2005). Tectonic tilting is not accounted for in this study and as a consequence the trapped volumes may be overestimated. It was not possible to assess the impact of tectonic titling in the basin without a 3D basin model to look at the evolution of each field and structure and the timing of charge.

FTS correction factors were determined for the Taranaki Basin by quantifying seal rock integrity based on known hydrocarbon column lengths in the basin. The maximum hydrocarbon column length is used as a proxy measurement to infer the ability of the seal rock to hold back a column of hydrocarbons. Firstly, a dataset of hydrocarbon column lengths was used to show the relationship between column length and the maximum burial depth of seal rock (Figure 2.7) to infer representative column lengths for each reservoir interval at a given depth. Secondly, average column lengths were compared to net-sandstone intervals representative of the same reservoir interval. The ratio of the column length to the net-sandstone thickness was used as the FTS factor to correct the simulated volumes. Minimum, medium and maximum FTS correction factors were used to express the uncertainty associated with estimating trap FTS conditions.

PCE® calculates volume at reservoir depth and a FVF was used to convert the volume of an accumulation to surface temperature and pressure (STP) conditions. Only a gas compressibility factor was used in this study because gas expansion is volumetrically significant, whereas liquid shrinkage is not (Franchi, 2006). FVFs for gas increase with depth and range from ~180–300 (Franchi, 2006). Minimum, medium and maximum formation volume factors for varying reservoir depths were used to express the uncertainty associated with the range in FVF values.

PCE® volumes were multiplied by a saturation factor (S_{hc}) to reflect the proportion of hydrocarbons in each volume because the mechanics of migration in PCE® is solely buoyancy driven and hydrocarbon saturation is not accounted for, as it would be in a Darcy-flow migration model (IES, 2000). Hydrocarbon saturation is the fraction of pore space occupied by hydrocarbons, which is 1- S_w,

where S_w is water saturation (Franchi, 2000). The hydrocarbon saturation factors used to recalculate the volumes for the Taranaki Basin accumulations are based on well data. Values available for each reservoir interval were summed and averaged to determine a mean factor for each interval. Minimum, medium and maximum mean saturation factors were calculated to account for the uncertainty associated with the range in saturation values.

To compare PCE®-simulated accumulation volumes to known field reserves a hydrocarbon recovery factor was used to calculate reserves-equivalent volumes. The recovery factors used in this study were taken from Taranaki Basin well reports and range from 50–80% for gas and 25–60% for oil. A recovery factor reflects the efficiency of the reservoir to allow hydrocarbons to flow to the surface, which is also known as the reservoir drive mechanism (Sills, 1992). Recovery factors are variable and based on the natural drive mechanism of a reservoir. They are affected by a number of factors including: physical properties of the fluids, such as viscosity and specific gravity; reservoir lithology heterogeneity, including gross volume, porosity, relative permeability and connectivity; formation dip angle; aquifer volume; gas cap volume; and the development programme used to bring the hydrocarbons to surface (Sustakoski & Morton-Thompson, 1992). The uncertainty associated with the well-based ranges is recognised by using minimum, medium and maximum values for each reservoir.

3.3 Structural trap-based oil and gas accumulations

3.3.1 Introduction

Three different sets of structural contour maps were used to identify structural traps for the four plays including:

1. The regional structure contour depth surfaces of the top Cretaceous, top Eocene and top Miocene horizons cited in Section 3.2.3 (Appendix 2);

2. Two regional structural contour depth surfaces for the top Cretaceous and top Rakopi Formation, northern Western Platform (Uruski et al., 2002) (Appendix 5); and

3. Local-scale high-resolution structural contour depth maps, obtained from petroleum well reports and exploration company reports and websites. These maps include an assortment of top horizon, top formational and -intra-formation structural contour time and depth surfaces.

3.3.2 Calculating volumes

Firstly each structural trap was digitised into an ArcMAP GIS project and a bulk rock volume, which is a measure of the maximum volume of a trap, was calculated using ArcMAP® GIS 3D analyst tools.

Bulk rock volume was calculated using Equation 3.5:

$$VBR = AI*h \tag{3.5}$$

Where VBR is an integrated bulk rock volume, AI is an integrated area (m^2) and h is height. VBR is calculated using the ArcMAP® triangulated integration net (TIN) tool, which is a vector data model used to calculate elevation, area and volume. For traps with only one contour value, volume was calculated using a specified crest height of 50 m. This height was based on the average crest height of high-resolution structures of similar areal size in the Taranaki Basin.

The bulk rock trap volumes were calibrated to reflect extractable volumes at surface temperature and pressure conditions that are comparable with reserves volumes as explained in the basin modelling section, using Equation 3.6:

$$Vtrap=AI*h*Gf*\theta*S_{hc}*NG*FVF*R_{hc} \tag{3.6}$$

where Gf is a geometric correction factor, θ is porosity, S_{hc} is hydrocarbon saturation, NG is the net-to-gross percentage of the reservoir, FVF is formation volume factor and R_{hc} is hydrocarbon recovery factor.

A difference with these volumes compared to the basin-modelled volumes is the inclusion of a geometric correction factor which is used to define the proportion of the trap that is occupied by reservoir lithology by taking into account the shape and amplitude of the structure, and the relative thickness of reservoir within the

structural closure. The factor reduces closure height or reservoir thickness to the effective average for the whole area of closure. It varies for different trap styles and is typically around 0.6. Three different geometric correction factors were defined based on the geometry of the traps in the area and the variation was expressed as a minimum, medium and maximum.

As with the recalculated basin-modelled volumes porosity and net-to-gross values are based on well data.

3.4 Plays

A play describes a group of oil and gas accumulations in a region that are related by geological characteristics (Allen, 1990). Four plays are assessed in this study, Cretaceous, Paleocene, Eocene and Miocene. They are based on four seismic-stratigraphic units which are used to define the distribution of key reservoir sequences (Section 2.2.4). This approach enables the accumulations to be treated as homogeneous populations based on the first-order depositional environments of the reservoir they are found within, which is important for the statistical analyses used in this study.

3.4.1 Cretaceous

The distribution of the Cretaceous reservoir play is based on the deposition of the terrestrial syn-rift Pakawau Group, which comprises the Rakopi and North Cape formations (Section 2.2.4) (Figures A1 & A2, Appendix 1). Structural traps that have been identified at this level and the wells that have encountered this age reservoir rock are shown in Figure 6.8 and Enclosures 1 and 2.

The Rakopi Formation is the lowest stratigraphic unit with widespread distribution in the basin. Six wells have drilled this formation (Enclosures 1 & 2) and it ranges in thickness from ~380 m (Tahi-1) to ~3000 m (Fresne-1). In sandstone units porosities are up to 20%, and permeabilities are up to 16 mD. The formation is well bedded and contains numerous shale beds, which could provide good intra-formational seals. The North Cape Formation has been encountered by 25 wells (Enclosure 2). It is less widespread than the Rakopi Formation and ranges in thickness from <100 m (Wainui-1 and Te Ranga-1) to ~2050 m (North

Cape-1 and Kapuni-7). Sandstone units have porosities of up to 26% and permeabilities of >500 mD.

This reservoir play is yet to be proven and porosities may be significantly reduced where Cretaceous lithologies are at depths of 4.5 to >6.5 km. However, exact burial-porosity relationships of Late Cretaceous lithologies have not been established and good porosity may be preserved (King & Thrasher, 1996).

3.4.2 Paleocene

The distribution of the Paleocene reservoir play is based on the deposition of the fluvio-deltaic shoreline sandstones of the Farewell Formation (Section 2.2.4) (Figure A3, Appendix 1). Structural traps that have been identified at this level and the wells that have encountered this age reservoir rock are shown in Figure 6.9 and Enclosure 2. The Farewell Formation ranges in thickness from 1200 m (Kupe-1) to 1670 m (Kapuni Deep-1). The coastal plain and fluvial-estuarine sandstones have core porosities >20% and permeabilities up to several hundred mD (Maui-F sands) (Shell BP & Todd Oil Services Ltd, 1973; Mathews & Bennet, 1987). The Farewell Formation is a gas-condensate reservoir in the offshore Kupe Field and an oil reservoir in the Maui (F-Sands) and Tui fields (Table 1.1).

3.4.3 Eocene

The distribution of the Eocene reservoir play is based on the deposition of the fluvio-deltaic shoreline sandstones of the Kaimiro, Mangahewa and McKee formations and the Oligocene to Early Miocene Otaraoa and Tikorangi formations (Section 2.2.4) (Figures A4–A8, Appendix 1). This play has produced the most oil and gas in the basin (Table 1.1).

The reservoirs of the Otaraoa and Tikorangi formations are included in this play because there is insufficient discovery data to treat them as a separate play. They are geologically more similar to the Eocene play reservoirs than the Miocene play reservoirs based on changes in depositional environment controls with the onset of Neogene tectonics. Structural traps that have been identified at this level and

the wells that have encountered this age reservoir rock are shown in Figure 6.10 and Enclosure 2.

In the Maui Field the Kaimiro Formation consists mainly of stacked (10-15 m thick) tidal inlet channel and tidal-creek sandstones with interbedded mudstones and has core porosities of up to 20% and permeabilities of up to 100 mD (Flores et al., 1993). The Mangahewa Formation is thickest (~400-830 m) in the Taranaki Peninsula region. In the Maui Field at the C-Sands level, the formation shows an increasingly up-sequence marine influence and porosities in channel sandstones are up to 27% with permeabilities ranging from 460 to 2000 mD. The McKee Formation is relatively thin and ranges from <100 m (Cardiff-1 and Waihapa-1) to ~170 m (Kaimiro-1). Average porosities are ~17% with permeabilities of 20–50 mD. The Tangaroa Formation is mapped in the Northern Graben and porosities can be >20%, typical of a turbidite deposit (Geotechnical Services Pty Ltd, 2005). These sandstones may extend further north into the Western Platform area where Eocene slope and basin-floor fans have been interpreted in the northwestern section of the Taranaki Basin (Figures A1 & A2, Appendix 5) (Baillie & Uruski, 2004).

The Otaraoa Formation is distributed along the eastern flank of the basin from Awakino-1 to Kupe-1. The Tariki Sandstone Member is ~200 m thick with porosities of up to 23% (Tariki/Ahuroa Field). The Matapo Sandstone is distributed across the northern peninsula and is typically 20–50 m thick. Thick sequences of the Tikorangi Limestone are recorded along the northeastern margin of the basin in the Tarata Thrust Zone. It reaches its maximum thickness of ~200 m in the Waihapa/Ngaere Field where oil production comes from natural fractures in the rock (Hood et al., 2003). It is also a reservoir further south in the Rimu Field and hydrocarbons in this interval were encountered in the Toko-1, Piakau-1 and Kupara-1 wells. Fracturing occurred after dolomitisation and is associated with compressional deformation along the eastern edge of the basin including along the Taranaki Fault (Hood et al., 2003).

3.4.4 Miocene

The distribution of the Miocene reservoir play is based on the Neogene shelf, foredeep, slope, and submarine fan deposits of the Mt Messenger and Moki formations (Section 2.2.4) (Figures A9 & A10, Appendix 1). Neogene reservoirs exist predominantly onshore and at relatively shallow depths, and have produced oil, condensate and gas. The structural traps that have been identified at this stratigraphic level and wells that have encountered this reservoir play are shown in Figure 6.11 and Enclosure 2. This reservoir play is also proven (Table 1.1) and in thrust faulted and folded complexes reservoirs typically form stacked zones (e.g. Tariki Field).

The Moki Formation is a Middle Miocene sandstone-rich submarine fan succession, which is best developed in the southern and central areas of the basin. Sandstone dominated sequences are ~250 to 350 m thick (e.g. Maui, Kapuni and Kaimiro fields) (Shell BP & Todd Oil Services Ltd, 1979). Core porosities are ~15-26% with a mean permeability of ~98 mD (Halliburton Australia Pty Ltd, 1999). The Mt Messenger Formation is a system of Late Miocene bathyal fan deposits that cover a broad area of the Taranaki Basin in a northeast-southwest trend across the middle of the basin. The formation is typically 1 km wide and 40 m thick, but can be thicker (~300 m) where it has been deposited in channel complexes (e.g. Maui Field). Porosities range from 14-25% and permeabilities range from 20 to 800 mD. It is best developed beneath the northern Taranaki Peninsula and decreases in thickness and sand content towards the south.

Sub-plays have been defined for each reservoir play, based on trapping configurations. They are used in conjunction with the results of the spatial model to describe the areas of undiscovered oil and gas. Details of these sub-plays, including maps showing proven and potential traps are presented in Appendix 6.

3.5 Size-distribution models

3.5.1 Introduction

A size-distribution model uses a scaling invariance of naturally occurring populations of oil and gas accumulations, where many small accumulations coexists with very few large accumulations, to estimate the parent population of

oil and gas accumulations in a basin (Howarth et al., 1980; Harbaugh & Ducastaing, 1981; Klemme, 1983; Houghton, 1988).

A statistical probability distribution function is used to mathematically express this relationship between the size of an accumulation and its frequency and approximate the parent population (Arps & Roberts, 1958; Kaufman, 1963; Capen, 1984. The size distribution of the parent population can be described by three distribution shape factors, mean (μ) standard deviation (σ) and exponential (γ) as shown in Figure 3.4, (Kaufman, 1993; Drew, 1997; Charpentier et al., 2000).

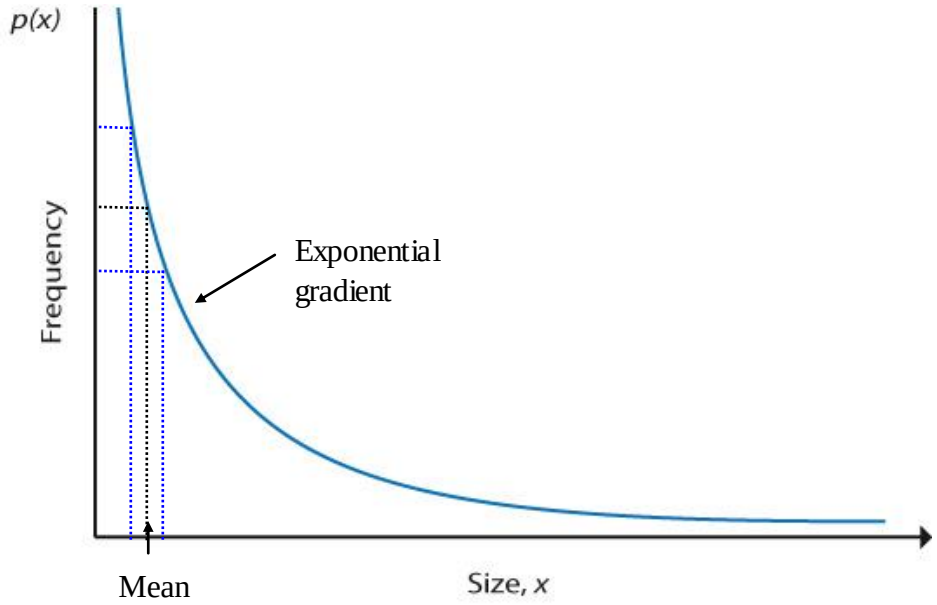

Figure 3.4: Graphical representation of the continuous Pareto probability density function. The horizontal axis represents accumulation size and the vertical axis represents frequency. p(x) is the probability of x, and the solid blue line shows that x has a greater probability of being a smaller sized accumulation and a lesser probability of being a large sized accumulation. The area under the curve is the probability space, which includes all the possible outcomes of size and frequency x can be. The standard deviation of the mean is marked by the blue dotted lines either side of the mean.

Size distributions of oil and gas accumulations are traditionally presented as size-frequency histograms in order to demonstrate the number of accumulations in a distribution by bin size (Drew, 1997). In a well-sampled basin with many discoveries the size-frequency histogram shows an exponential form with decreasing frequency as accumulation size increases, as shown in Figure 3.5 (Drew et al. 1995; Drew, 1997). The bottom histogram in Figure 3.5 shows the progressive left hand shift of the modal accumulation size with time and as a

greater number of smaller sized fields were discovered. These time-based discovery increments form an exponential size boundary on the right hand side of the histogram, which represents the emerging edge of the size distribution of the parent population of all oil and gas fields in this play, as shown in Figure 3.5.

Such a well-sampled dataset provides a good understanding of the order in which discoveries are made; in general, the largest accumulations are found first and with further exploration smaller accumulations are found (Drew, 1997; Charpentier et al., 2000).

In contrast, an underexplored basin is typically characterised by a more random size-frequency pattern (Figure 3.7) because accumulations of various sizes are yet to be discovered (Drew, 1997). The bin size can have an impact on the histogram shape however, it is typical to increase bin sizes of oil and gas accumulations by an exponent which reflects the fractal relationship between size and frequency, such as 1-2, 2-4, 4-8, 8-16 mmboe and such a sequence in bin size is unlikely to change the difference seen between well-sampled and undersampled populations

In this study both a lognormal and a power-law probability distribution function are used to represent the size distribution of the original population of all oil and gas accumulations in a basin.

3.5.2 Lognormal probability distribution function

A lognormal probability distribution function was the first and is the most commonly used distribution function that has been used to describe the size invariance seen in populations of oil and gas accumulations (Kaufman, 1963; Klemme, 1971; Harbaugh & Ducastaing, 1981; Capen, 1984; Forman & Hinde, 1985; Rose, 2001).

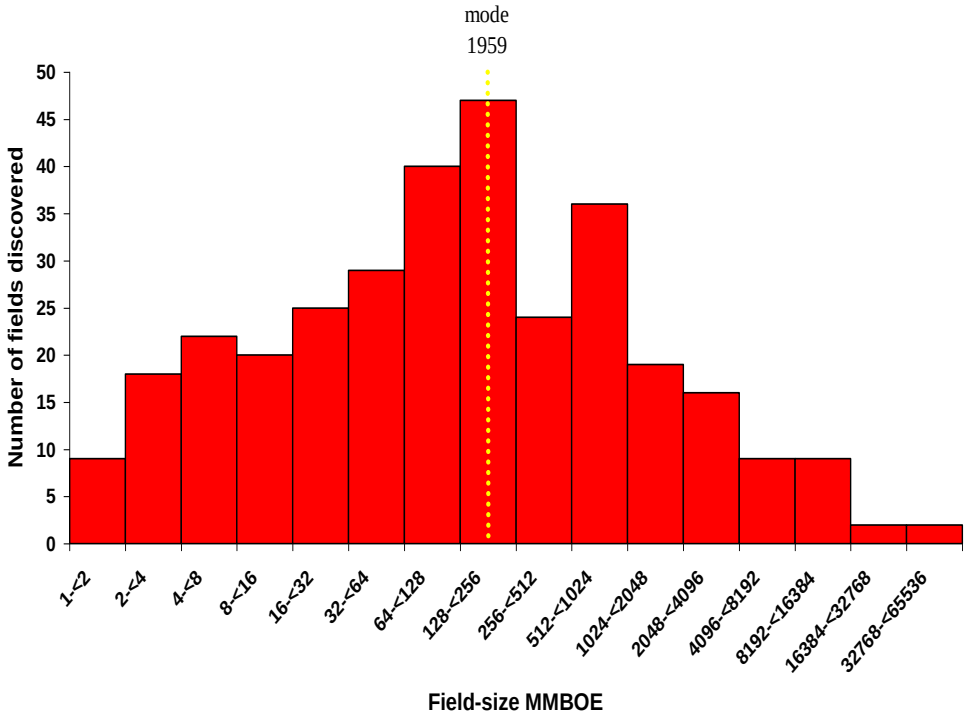

a.

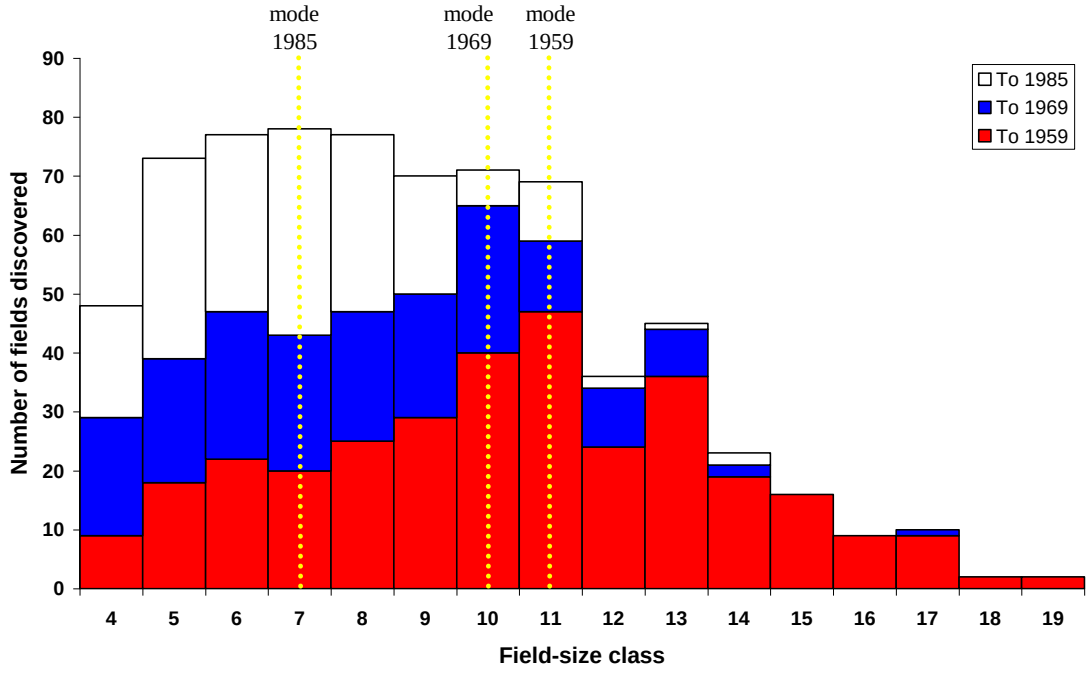

b.

Figure 3.5: An example of size frequency histograms of oil and gas accumulations for a well explored basin. This data are from 756 fields in the Frio Strandplain play, Texas. Figure a. shows the discoveries to 1959. Figure b. shows discoveries to 1985. Field size class 11 equates to fields sized 128–256 mmboe. Source: Drew (1997).

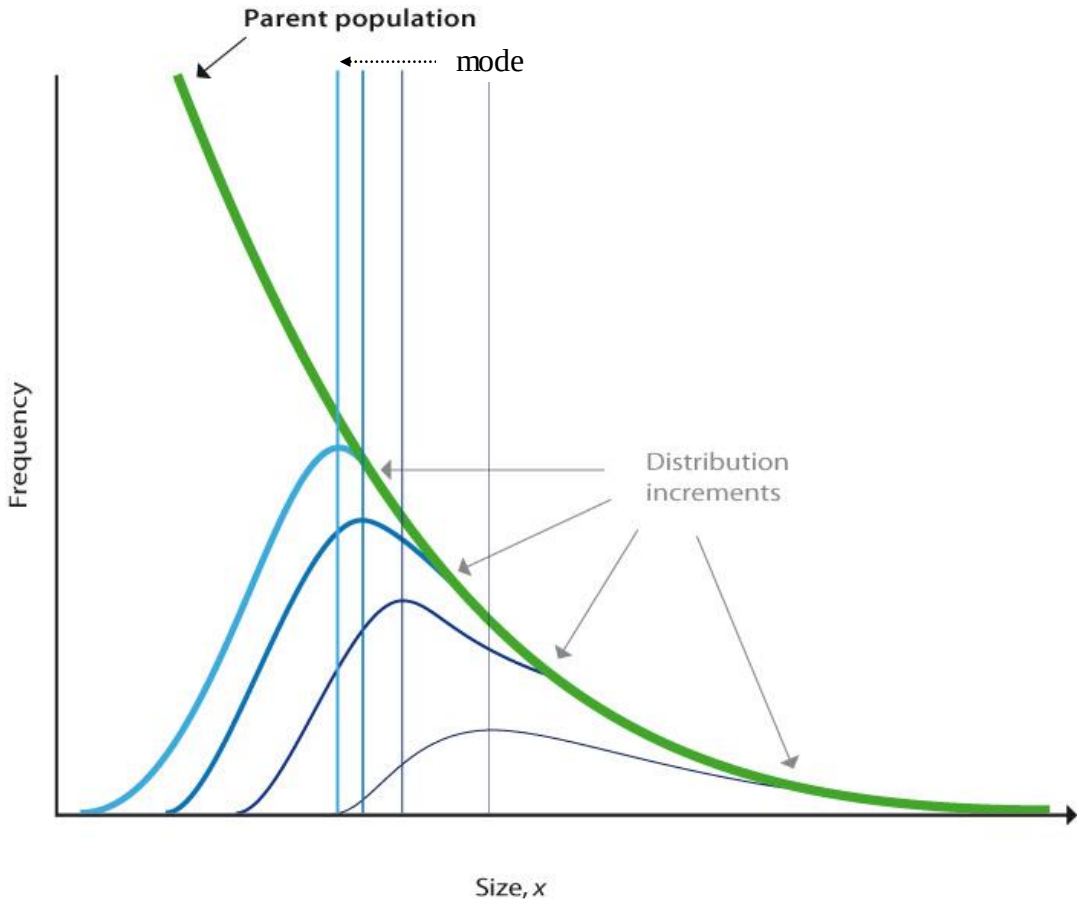

Figure 3.6: Graphical representation of the trace of the emerging parent population based on the progressive exhaustion of an oil and gas size distribution. x = oil and gas accumulations and frequency measures the number of accumulations. This graphic is a schematic drawing of the size-frequency data shown in figure 3.5, which shows distribution of 756 discovered fields of the Frio Strandplain play, Texas, from 1959 to 1985. The histograms of each set of fields are replaced with distribution traces (blue curves) which are referred to here as distribution increments. With time and the progressive discovery of smaller and smaller fields the modal size of each increment gets smaller, shifting the distribution curve towards the left and ultimately forming the right hand edge of the parent population distribution (green curve). The modal size is drawn here as vertical lines through the peak of each distribution increment.

.

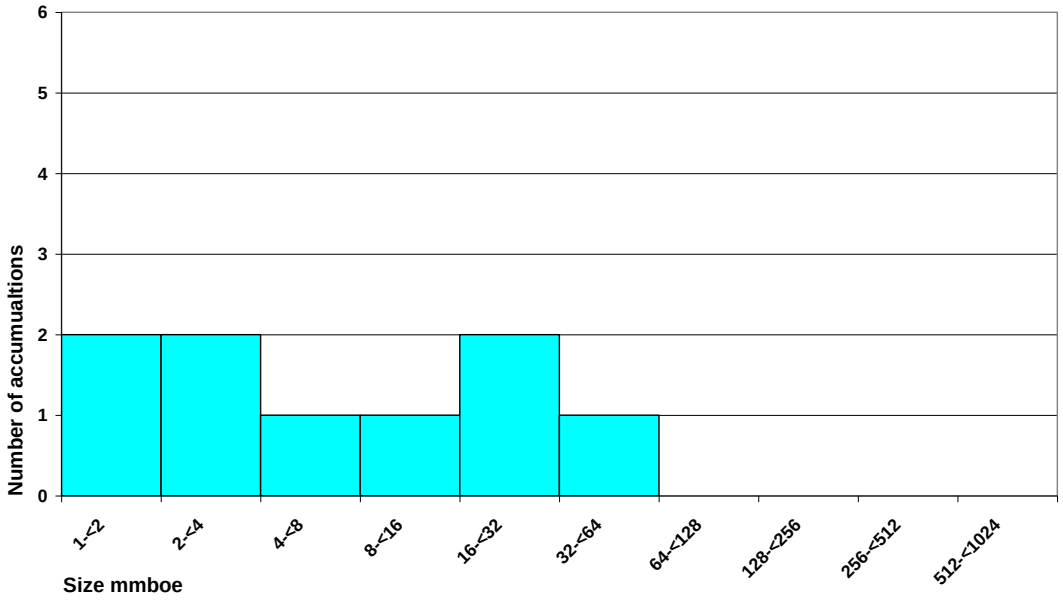

Figure 3.7: An example of a size-frequency histogram of a population of oil and gas accumulations in an underexplored basin. These discovery data are for the Miocene reservoir play in the Taranaki Basin.

A lognormal distribution (Aitchison & Brown, 1957) is the probability distribution of any random variable whose logarithm (to any base) forms a normal or Gaussian distribution. If x is a random variable with a normal distribution, then $\exp(x)$ has a lognormal distribution. A probability density function of a lognormal distribution is expressed as:

$$f(x) = \frac{\exp\left[-\frac{1}{2}\left[\frac{\ln(x)-\mu}{\sigma}\right]^2\right]}{\sqrt{2\pi\sigma^2 x^2}} \qquad (3.7)$$

for $x>0$, where μ is the mean and σ the standard deviation of the log-transformed variable. The graphical form of a lognormal model illustrates the unimodal and right-skewed relative frequency of size (Figure 3.8). Like the Pareto distribution, the lognormal distribution expresses a similar relationship of few large and many small accumulations. However, unlike the Pareto distribution, the lognormal distribution exhibits a modal size where the number of smaller accumulations declines rapidly.

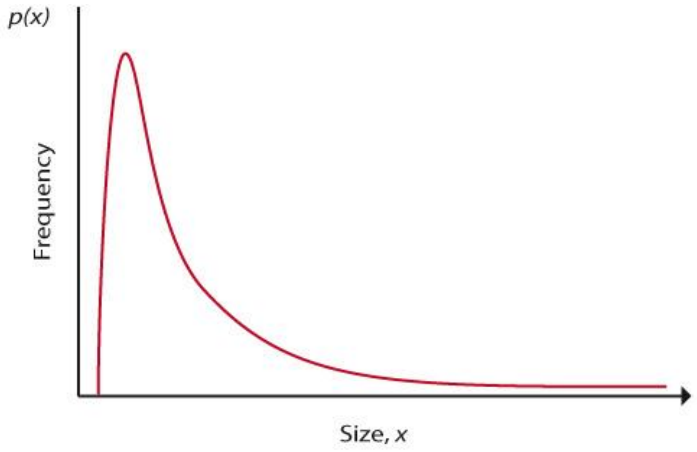

Figure 3.8: Graphical representation of a probability density function for a continuous lognormal distribution showing the relative frequencies p(x) of size x, where the area below the curve represents the distribution of the population. The curve is strongly right-skewed and shows the single mode close to the origin typical of a lognormal distribution. The long tail to the right hand side shows the infinite trend of the greatest sized accumulations.

3.5.3 Power-law probability distribution function

More recently power-law distributions, such as the Pareto distribution function, have become more common (Drew et al., 1995; Laherrere & Sornette, 1998; Attanasi and Charpentier, 2002; Laherrere, 2003,).

Mathematically, a power-law expresses the relationship between two quantities where the number or frequency of an object or event, such as the number of oil and gas accumulations, varies as a power of some attribute of that object, such as the size of an accumulation (Laherrere & Sornette, 1998), as shown in Figure 3.4. The probability density function is used to define a size distribution for a relationship between two scalar quantities x and, and is written as:

$$y = ax^k \tag{3.8}$$

where a is a constant of proportionality and k is a constant exponent of the power-law (Moore & McCabe, 2003).

For oil and gas accumulations, y is the number of accumulations and x is accumulation size.

3.5.4 Truncating a probability distribution function

The mathematical expression of both distributions (Equations 3.7 & 3.8) has limits from zero to plus infinity and must be truncated to describe the finite and economically constrained nature of oil and gas populations. The distribution is truncated by defining the largest accumulation possible, x_1, based on the geology of the area, and the smallest accumulation possible, x_0, at which it is not economical to explore for anything smaller (Figures 3.9 & 3.10). An x is used to define these two parameters in this chapter because they are on the x-axis, however in the following chapters a_0 and a_1 are used to represent the minimum and maximum accumulation size. The main statistical effect of truncating a distribution is the mean size is lowered to a value that is more representative of accumulations in a basin. Even though only a small portion (~0.001%) of the probability is truncated, very large accumulations, larger than what is geologically possible, are excluded from the parent population.

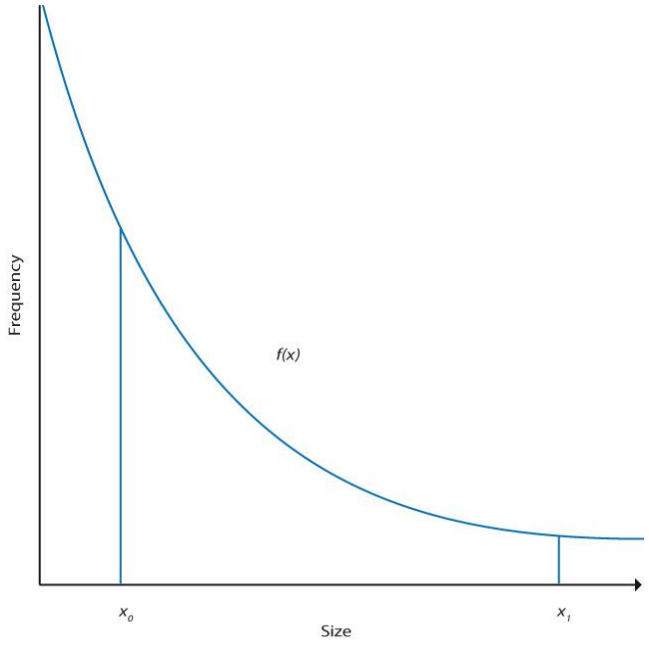

Figure 3.9: Graphical representation of a truncated Pareto probability density function showing the part of the distribution that is modelled in this study, where x_0 is the smallest accumulation and x_1 is the largest accumulation possible. Although the long right-hand side tail of this distribution function increases to infinity we know that accumulation size is not infinite and the distribution is truncated by the largest accumulation possible. Similarly, infinitely small accumulations are not targeted in exploration and they too are truncated.

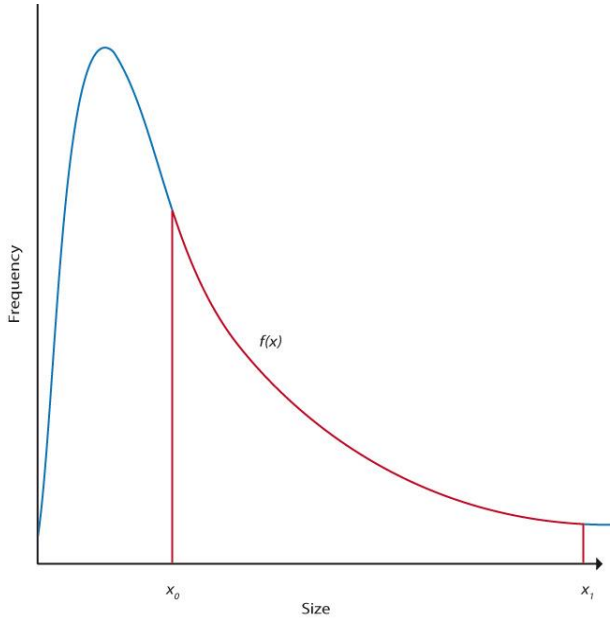

Figure 3.10: Graphical representation of the double-truncated, lognormal probability density function, showing the part of the distribution that is modelled in this study, where x_0, is the smallest accumulation possible and x_1, is the largest accumulation possible. Although the long right-hand side tail of the lognormal probability distribution function increases to infinity we know that accumulation size is not infinite and the truncation is used to represent the largest accumulation possible in a basin. Similarly, we know that infinitely small accumulations will not be targeted in exploration and the truncation at the small accumulation end is used to ensure the accumulations simulated in the discovery-sequence sampling programme are no smaller than the economically viable size for the Taranaki Basin.

The probability space of a truncated distribution is a finite proportion of an originally infinite distribution (Attanasi & Charpentier, 2002) and because of this the correct parameters must be used to define the truncated probability space. Once a distribution is truncated the shape parameters of the original infinite distribution (μ, σ, γ) are changed because the truncated distribution is now defined by a new set of shape parameters. To ensure the correct area of the distribution is being used in the estimation the shape parameters must represent the correct probability space of the original distribution being used.

Traditionally, to estimate the volume of undiscovered oil and gas in a basin, using a size distribution model, the shape factors (μ, σ, γ) of the distribution of the parent population of accumulations have been based on an empirical sample of discoveries (Attanasi & Charpentier, 2002). However, it is debatable whether a representative parent population can be derived from such a random sample with a small amount of discoveries (Drew, 1990 & 1997) because discoveries produce a non-truncated dataset that typically displays sampling bias. Such a dataset is

unlikely to produce a size-distribution that is representative of a truncated parent population.

A non-truncated distribution represents a different probability space to a truncated distribution, as shown in figures 3.4, 3.8–3.10, which means it most likely includes a different number and range in sizes of oil and gas accumulations. Furthermore, if the mean value of a non-truncated dataset of discoveries is used to define the mean of a truncated distribution then the resulting distribution density function may be in error (Attanasi & Charpentier, 2002). The mistake of using the incorrect untruncated distribution parameters (μ, σ, γ) to describe a truncated size-distribution of accumulations is often not recognised (Attanasi & Charpentier, 2002).

The significance of this error will depend on the sensitivity of the size-distribution to the mean value used to define it. For example, if the mean value from a non-truncated dataset is close to the truncated maximum size of the dataset then the resulting size distribution would be associated with a significant error. This mean value would assume that the mean accumulation size in the parent population is a similar size to the largest accumulation discovered and such a distribution would predict very large (and probably geologically impossible) accumulations toward the right hand-side tail of the distribution. In contrast, if the mean value from a non-truncated dataset is a long way from the truncated maximum value than the error is likely to be negligible (Attanasi & Charpentier, 2002).

3.5.5 Cumulative size-probability plot

The amount of undiscovered oil and gas is plotted as a cumulative probability distribution on a size-probability plot in order to predict the probability of the size of a new discovery (Figure 3.11). A cumulative probability distribution is expressed on a size-probability plot by plotting each data point of accumulation size as a fraction of the total dataset, known as a fractile (Megill, 1992). The fractiles are converted to size-probability Z-values using the Microsoft Excel norminverse function (Rose & Cook, 2006). Details of this approach and the calculation of fractiles are shown in Appendix 7. Size (mmboe) is plotted on the x

axis using a logarithmic scale and cumulative probability is plotted on the y axis using a normal probability scale.

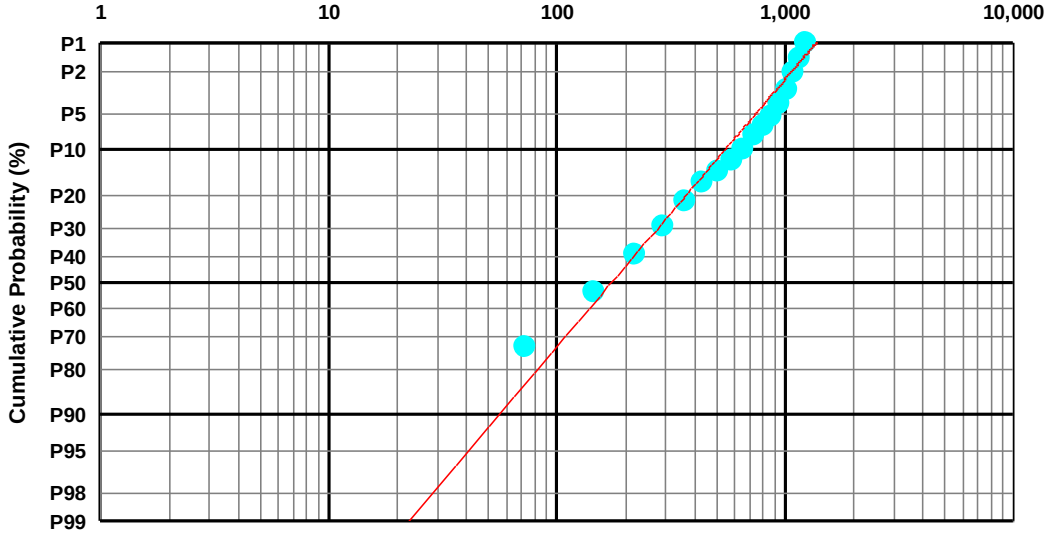

Figure 3.11: Cumulative size-probability plot used to determine the probability that the next discovery in an area will be a certain size. The x-axis is accumulation size (mmboe) and is a logarithmic scale. The y-axis is cumulative probability and is a normal probability scale. This plot shows there is a 90% probability that the next discovery from this population will be equal to or greater than 55 mmboe, a 10% probability that the next discovery will be equal to or greater than 510 mmboe. The mean accumulation size from this population is 245.5 mmboe, based on a Swanson's mean calculation.

A best-fit regression line is fitted through the data of undiscovered accumulations (Figure 3.11) and because the plot shows cumulative probability, any point on the line is interpreted as having y probability that the corresponding accumulation is equal to or greater than x mmboe. For example in Figure 3.11 x = 180 mmboe and y = P50, which means there is a 50% probability that the next discovery from this distribution is equal to greater than 180 mmboe.

The mean accumulation size is based on a Swanson's mean which calculated using Equation 3.9 (Rose & Cook, 2006):

$$P10 * 0.3 + P50 * 0.4 + P90 * 0.3 \qquad (3.9)$$

Swanson's mean is used instead of the median P50 value because it better represents the average value for a skewed distribution such as a lognormal or Pareto probability distribution (Rose & Cook, 2006). The greater the mean is above the medium the more skewed the distribution.

3.5.6 Analysis

There are two controversial aspects associated with estimating undiscovered oil and gas using a size-distribution model (Drew et al., 1995). The first one concerns the choice of probability distribution function to approximate the parent population of oil and gas accumulations (Drew et al., 1995). Both a lognormal and a Pareto power-law probability distribution function are used in this study and the volumetric estimates of undiscovered oil and gas that have been calculated using each of them are compared.

The second one concerns the use of discoveries to directly derive the size distribution of a parent population of oil and gas (Drew et al., 1995) as discussed earlier in this section. In this study an empirical sample of discoveries is not used to define the distribution shape of the parent population of all oil and gas accumulations in a basin and instead the shape parameters are defined by numerical integration, in Chapter 4.

3.6 Previous estimations

Previous estimations of undiscovered oil and gas in the Taranaki Basin are discussed in this chapter to demonstrate the limitations and sensitivities of a size distribution method, known as a gap analysis (Perrodon, 1983; Crovelli, 1986). The earliest assessments of undiscovered oil and gas for the Taranaki Basin by Cook (1985) and Beggs & Cook (1993) (Table 1.2) are underestimates. They are based on discovery data, which means the parent population has been defined by extrapolating the size of each discovery as shown in Section 3.5.1.

Volumes have increased with each consecutive assessment and the most recent estimates suggest ~1000 mmboe of oil and gas remains to be found and any new single discovery is predicted to have a mean size of ~100 mmboe (O'Connor, 2003; Mare-Jones, 2004). The most recent estimates (O'Conner, 2003; Mare-Jones, 2004) are based on discovery data only. They also treat the Maui Field as a single accumulation even though it comprises three separate oil and gas accumulations (Figure 3.12). Because of this treatment, the method choice and use of discovery data only these estimates are also likely to be underestimates.

The gap analysis approach utilises the scalar relationship between size and rank (Section 3.5.1) which can be mathematically described by a power-law probability function (Laherrere, 2000; Attanasi & Charpentier, 2002). Power-law probability functions become linear when a logarithmic transformation is applied to the data and a simple way of transforming the data is to plot them on a graph with the vertical and horizontal axes as logarithmic scale (e.g. Figure 3.13). Each accumulation is plotted according to its size (x-axis) and relative rank (y-axis); the largest accumulation is ranked as number 1, the second largest as number 2, and so on. A best-fit regression line, which is defined by a slope equal to one and a y-intercept equal to the size of the largest accumulation, is used to represent the size distribution of the parent population. The undiscovered accumulations are then estimated by identifying gaps between the plotted accumulations along the parent population line.

For example, in Figure 3.13a it is estimated that there is an undiscovered accumulation in the 400–800 mmboe range, 5–10 in the 80–100 mmboe range and five in the 32–40 mmboe range, totalling 1120–1700 mmboe.

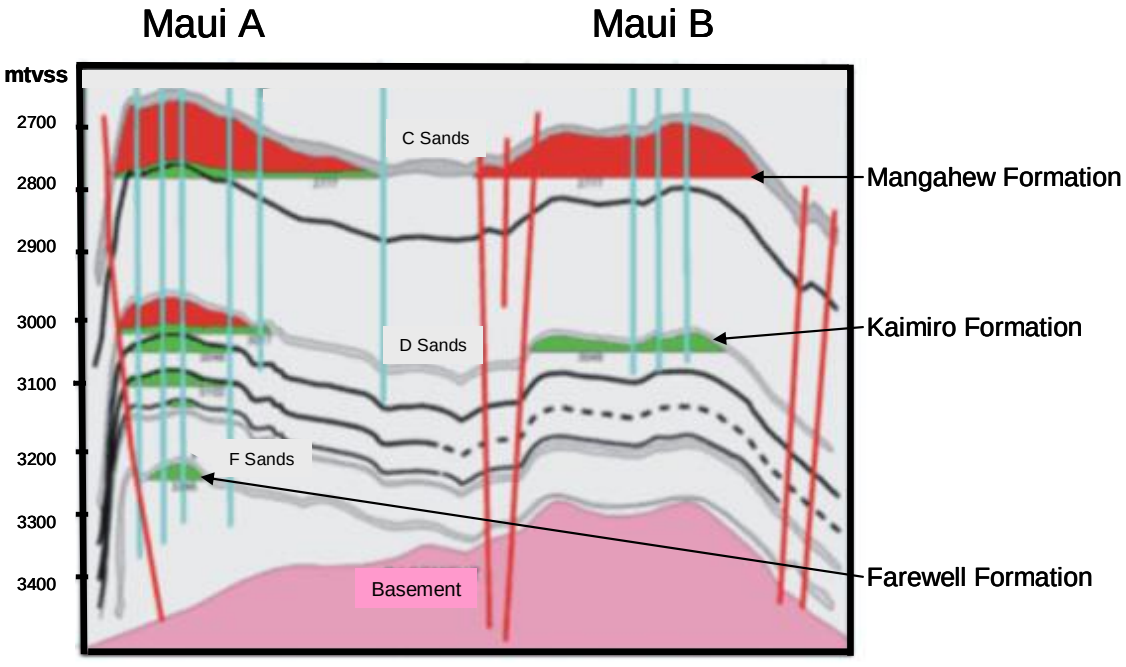

Figure 3.12: Graphical representation of a cross-section through the Maui Field showing a low relief anticline which has a combination of dip-closure and faulting or two broad anticlinal closures separated by a saddle The Maui Field has a number of stacked reservoirs. Maui C Sands include Mangahewa Formation sandstone, Maui D Sands include Kaimiro Formation sandstone and Maui F Sands include Farewell Formation sandstone. Red = gas, green = oil. mtvss = meters, total vertical subsea. Source, Crown Minerals (2006).

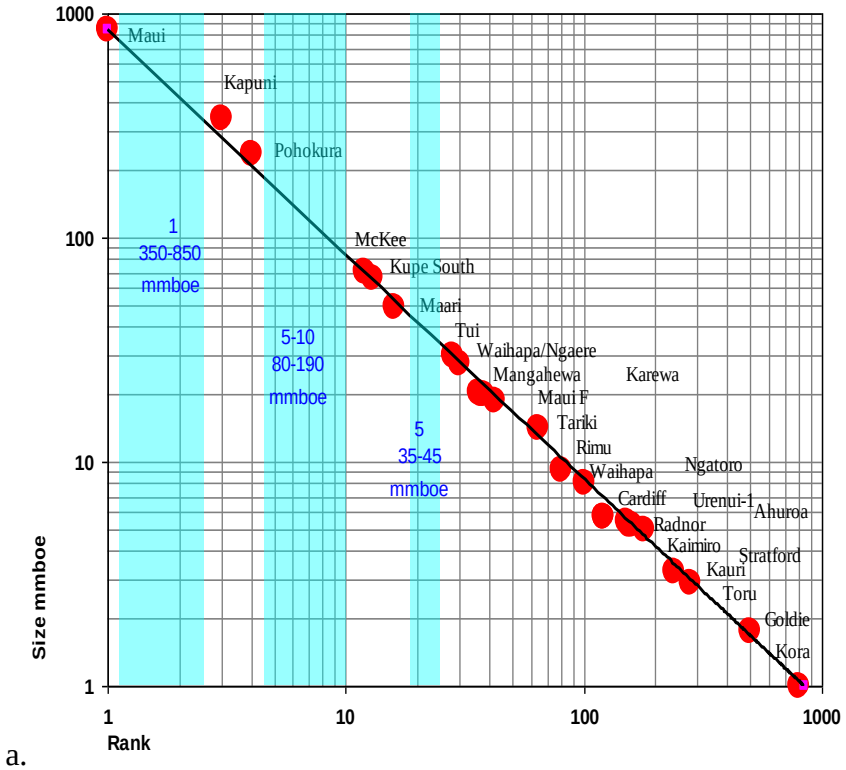

a.

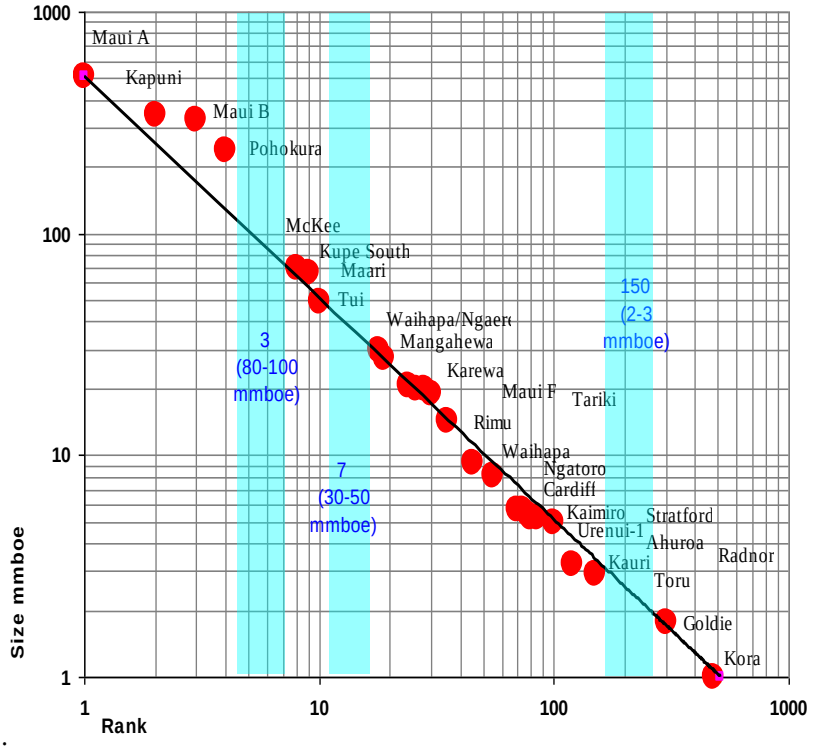

b.

Figure 3.13: Size-rank log-log plot used in the gap analysis approach. The red points are the discovered accumulations from Table 1.1. The black line is the best-fit regression curve of the data points, the regression correlation value = 0.8982. This line represents the parent population of all accumulations in the Taranaki Basin. The bright-blue vertical bands highlight the gaps between the ranked accumulations. These represent the number and size of accumulations that are yet to be discovered. a. The Maui Field reserves are modelled as a single accumulation by combining the reserves of Maui A and Maui B. b. The Maui Field A and B reserves are modelled as two separate accumulations. mmboe = millions of barrels of oil equivalent.

The assumptions and sensitivities of the gap analysis approach may result in limited estimates. Firstly, this approach assumes the parent population can be approximated using the relative rank of few discoveries and the largest discovery is the largest accumulation possible in a basin. A parent population that is based on a small number of discoveries cannot represent the geological potential of a basin, especially if the largest discovery is used to truncate the size distribution. In many basins around the world it is not uncommon for large discoveries to be made after a significant amount of exploration and many discoveries. For example in the Taranaki Basin the Pohokura Field, which is the fourth largest accumulation in the basin (Maui is treated as two accumulations) was discovered in 2000, 50 years and 21 discoveries after the first discovery. The discovery of other large fields later on in a basin's exploration life, such as Prudhoe Bay in Alaska, Widuri in Indonesia and Cusiana in Colombia, are also a reminder that the inclusion of geological knowledge in an assessment is acceptable and widely accepted statistical beliefs, such as the largest fields in an area tend to be found early on in exploration operations, does not always hold true (Beggs, 1996).

Secondly, the size distribution of a gap analysis-derived parent population is sensitive to the largest discovery in the distribution. For example estimation results for the Taranaki Basin based on a gap analysis method will be different if the Maui Field is plotted as one or two accumulations. In Figure 3.13a the Maui Field is plotted as a single accumulation (of 873.91 mmboe) and is rank number one. However, if the Maui Field is plotted as two separate accumulations, to recognise the two structurally-defined accumulations within this field (Figure 3.13b) (Maui A = 533 and Maui B = 340.91 mmboe) than it is estimated that there is three undiscovered accumulations in the 80 to 300 mmboe range, seven in the 30 to 50 mmboe range and 150 in the 2 to 3 mmboe range, totalling 750 to 1700 mmboe.

Thirdly, the method assumes the gaps between discoveries on the parent population curve equate to the number and sizes of the undiscovered accumulations. There is no theoretical basis that supports the theory that a gap between discoveries on a size-rank logarithmic-logarithmic plot represents the deterministic number of discoveries that are yet to be found. The line between

discoveries can be used to represent an apparent population, but the statistical representation of the parent can only be used to estimate the relative size or rank of missing accumulations in this population, not the exact number of missing or yet to find accumulations (Attanasi and Charpentier, 2002.

3.7 Discovery-sequence sampling models

3.7.1 Introduction

Discovery-sequence sampling models use assumptions about the exploration process to predict undiscovered volumes by forward modelling an extrapolated time-series trend of discovery (Meisner & Demirmen, 1981; Forman & Hinde, 1986; Drew, et al., 1995). Initially exploration performance or behaviouristic data were used to relate a sequential order of discovery or some measure of exploratory effort to the future discovery of oil and gas. The discovery data, such as predrill areas of a field (Klemme, 1971; Ivanhoe 1986; Barrett et al. 2003) were ranked against the order of discovery and the correlation trend was extrapolated to predict future discoveries (Meisner & Demirmen, 1981; Forman & Hinde, 1986).

The gradient of the extrapolated trend was used to show that the effectiveness of exploration effort diminished with advancing exploration as discovery size and success rate decreased (Forman & Hinde, 1986). This is why these early models were called creaming methods (Meisner & Demirmen, 1981) because with time the exploration process takes the cream off the top.

Arps & Roberts (1958) and Attanasi (1980) showed that the number of discoveries was frequently two times more, than predicted using a discovery-sequence sampling model that was based on discovery being proportional to size and discoveries larger than predicted were being made later in a discovery sequence. This unexpected pattern of discovery success was attributed to geologic and technological advances (USGS, 1995 & 2000) and economic influences (Attanasi & Root, 1988) and to account for it a discovery coefficient, γ, which is based on the exponential of the data series, was included in discovery-sequence models. The probability of discovery was revised and proportionality of size was raised to a constant exponential power, γ, (Arps & Roberts, 1958; Attanasi, 1980; Power, 1990).

More complex discovery-sequence sampling methods use an underlying probability distribution function to model the parent population (Arps & Roberts, 1958; Barouch & Kaufman, 1977) or fit historic exploration data into logistic or growth curves in order to extrapolate the discovery data to make future predictions (Lee & Wang, 1983; Schuenemeyer & Drew, 1983; Lee & Wang, 1985). More recent probabilistic discovery-sequence sampling models use computer simulations to model the biased behaviour of the exploration process and the order of discovery in order to predict new discoveries (Attanasi and Charpentier, 2002: Sinding-Larsen & Brandsegg, 2005).

3.7.2 Analysis

There are a number of limitations of using a traditional discovery-sequence sampling model to estimate undiscovered oil and gas in an underexplored basin are. Firstly, large datasets of discoveries are required and exploration process constraints such as the probability of discovery need to be well understood (Charpentier et al., 2000). Secondly, typically it is assumed that discoveries represent all the petroleum systems in a basin and are, therefore, likely to underestimate future discoveries (Charpentier et al., 2000; Charpentier, 2005). Thirdly, typically a constant gradient exponential is used to model the slope of future discoveries which has been shown to vary with time (Charpentier, 2005). This means the extrapolated exponential does not account for significant changes with time, such as the discovery of a new play or improved seismic data.

Traditional discovery-sequence sampling models forward simulate discovery data and cannot forecast discoveries out of size sequence. In an underexplored basin, with few data, such a model would produce a very constrained assessment of undiscovered oil and gas. Even in more mature basins large fields can be found after a long duration of exploration, such as Prudhoe Bay in Alaska, Widuri in Indonesia and Cusiana in Colombia (Beggs, 1996). These discoveries are a reminder that widely accepted statistical beliefs, such as the largest fields in an area are found early on in exploration, may not always hold true.

3.8 Spatial models

Geographical information systems (GIS)-based spatial models have become increasingly popular to quantify and examine geological data. They were first used to assess hard-rock minerals (Bonham-Carter et al., 1988; Watson et al., 1989; Agterberg et al., 1993; Bonham-Carter, 1994) and more recently they have been applied to hydrocarbons (Chen et al., 2000 & 2001; Chen et al., 2002; Osadetz et al., 2003; Rostirolla et al., 2003; Sinding-Larsen & Brandsegg, 2005).

GIS-based models have been applied in a number of different ways to quantify undiscovered oil and gas. Some are deterministic and model hydrocarbon generation and accumulation based on the theoretical specification of geologic processes (Wood et al., 1998) and others are predictive and are based on Fourier algorithms (Chen et al., 2002), favourability mapping (Rostirolla et al., 2003), or characteristic analysis methods (Gao et al., 2000; Chen et al., 2000a; Sinding-Larsen & Brandsegg, 2005).

The simplest GIS-based spatial models combine a set of input maps with a mathematical function to produce an output map. For example, three petroleum systems maps showing reservoir, mature source rock and structural traps in a basin are graded from 1–3 to represent good to poor reservoir, mature source rock and density of structural traps in a basin. These three maps are then combined into one to evaluate the hydrocarbon potential of this basin by using mathematical addition to. Areas with a value of 9 are the most prospective and areas with a value of 3 are the least prospective.

This deterministic approach does not weight each variable, according to its relative significance, relate the petroleum systems maps to discoveries, or consider the uncertainty associated with mapping petroleum systems elements such as reservoir. These aspects however, are included in predictive probabilistic spatial models (Rattenbury & Partington, 2003; Rostirolla et al., 2003) which use spatial correlations between petroleum systems maps and locations of hydrocarbon accumulation to predict the preferential location of oil and gas in a basin.

3.9 Conclusions

A number of different methods are used in this study to ensure the parent populations that are used to estimate undiscovered oil and gas represent the hydrocarbon potential of the four reservoir plays studied.

The dataset of accumulations that are based on structural traps are based on mapped structural traps and provides a maximum number of accumulations for input into the volumes and spatial models. The basin-modelled dataset of accumulations are based on the petroleum systems of the Taranaki Basin and provides a maximum number of charged accumulations for input into the volumes and spatial models. They are generated by modelling primary and secondary migration. The amounts of oil and gas that have been generated and expelled are based primarily on source rock richness and type and changing thermal conditions due to sediment loading and uplift and erosion that have resulted in kerogen conversion to oil and gas. Maps used in the reservoir migration model represent key petroleum systems elements and account for regional flow paths, structural and stratigraphic traps, and reservoir and seal rock quality. The simulated accumulations are validated by calibrating them with known discoveries and well results.

A traditional size distribution-based discovery-sequence sampling method has a number of limitations, which are likely to be exacerbated in an underexplored basin. A dataset comprising a small number of discoveries is unlikely to be suitable to extrapolate as a time-series in order to predict future discoveries because it cannot sufficiently represent the hydrocarbon potential of a basin, as shown in figure 3.5 and 3.6. Such a dataset is likely to underestimate the size distribution of the parent population, resulting in an underestimation of future discoveries. Traditional discovery-sequence sampling models also forward simulate discovery data and therefore cannot forecast discoveries out of size sequence, because it is not possible to model a new discovery that is greater than a previous discovery. However, in an underexplored basin with a small amount of data such a model would produce a very constrained assessment of the amount of undiscovered oil and gas.

GIS-based spatial models are useful to integrate map data in order to establish a relationship between geological data and the accumulation of oil and gas in order to predict areas of hydrocarbon favourability.

Chapter 4

Dual Component Estimation; theoretical framework of a probabilistic approach to estimate undiscovered oil and gas in an underexplored basin

Abstract

The Dual Component Estimation combines a modified, existing size distribution-based volumetric discovery-sequence sampling method with a geographical information systems (GIS)-based spatial model to estimate the amount and likely locations of undiscovered oil and gas in an underexplored basin.

An inverse discovery-sequence simulation has been constructed as part of this study by modifying a traditional discovery-sequence method. The simulation uses exploration process-based assumptions typical of traditional discovery sequence methods; however, the size distribution of the parent population is defined first and is not based on a direct extrapolation of discoveries, which is characteristic of forward models. The advantage of this approach is that the size distribution of the derived parent population is not constrained by size distribution limitations, which occur if there are few discoveries to model.

Two probability distribution functions, a truncated Pareto and double-truncated lognormal, are used in this study to approximate the parent population in order to derive an independent comparison of results. Using these functions, the parent population is defined initially numerically and then redefined using potential and actual discoveries. This approach minimises the constraints caused by using a small number of discoveries, which is important in an underexplored basin.

The spatial method calculates spatial correlations between mapped parameters indicative of hydrocarbon generation, charge and entrapment and

locations of oil and gas accumulation in order to predict areas favourable for hydrocarbon accumulation. The maps include amounts of oil and gas generated and expelled, reservoir distribution and quality, maximum burial depth of source and reservoir rock, structural traps, seal rock quality, migration flowpaths and regional fault traces. The locations of oil and gas accumulation are represented by known and potential discoveries. Known discoveries include producing fields and non-commercial encounters of hydrocarbons such as shows and surface tests. Potential discoveries are based on basin modelling results and structural traps that have been identified in structure contour maps. These semi-synthetic data are used in addition to discovery data to represent petroleum systems in relatively unexplored areas and to boost the number of accumulations in the estimation in order to increase the confidence of the data.

Spatial correlations are calculated using Bayesian weights-of-evidence (WoE) conditional statistics. An initial prior probability is calculated for a given mapped parameter, such as reservoir porosity, and then updated to a posterior probability given a second mapped parameter, such as the maximum burial depth of seal rock. The conditional posterior probability is further updated with additional parameter maps. A rolled-up integrated map, of all maps, highlights areas with a low, medium and high probability of hydrocarbon accumulation.

4.1 Introduction

The aim of this chapter is to describe the theory and methodology of the Dual Component Estimation (DCE) which is constructed as part of this study and used to estimate undiscovered oil and gas. The DCE is applied in Chapter 6 to estimate undiscovered oil and gas in the Taranaki Basin. It comprises a volumetric and spatial component (Figure 4.1) which share key data inputs: petroleum systems-based maps (Section 3.2.2); and datasets of semi-synthetic oil and gas accumulations (Section 3.1).

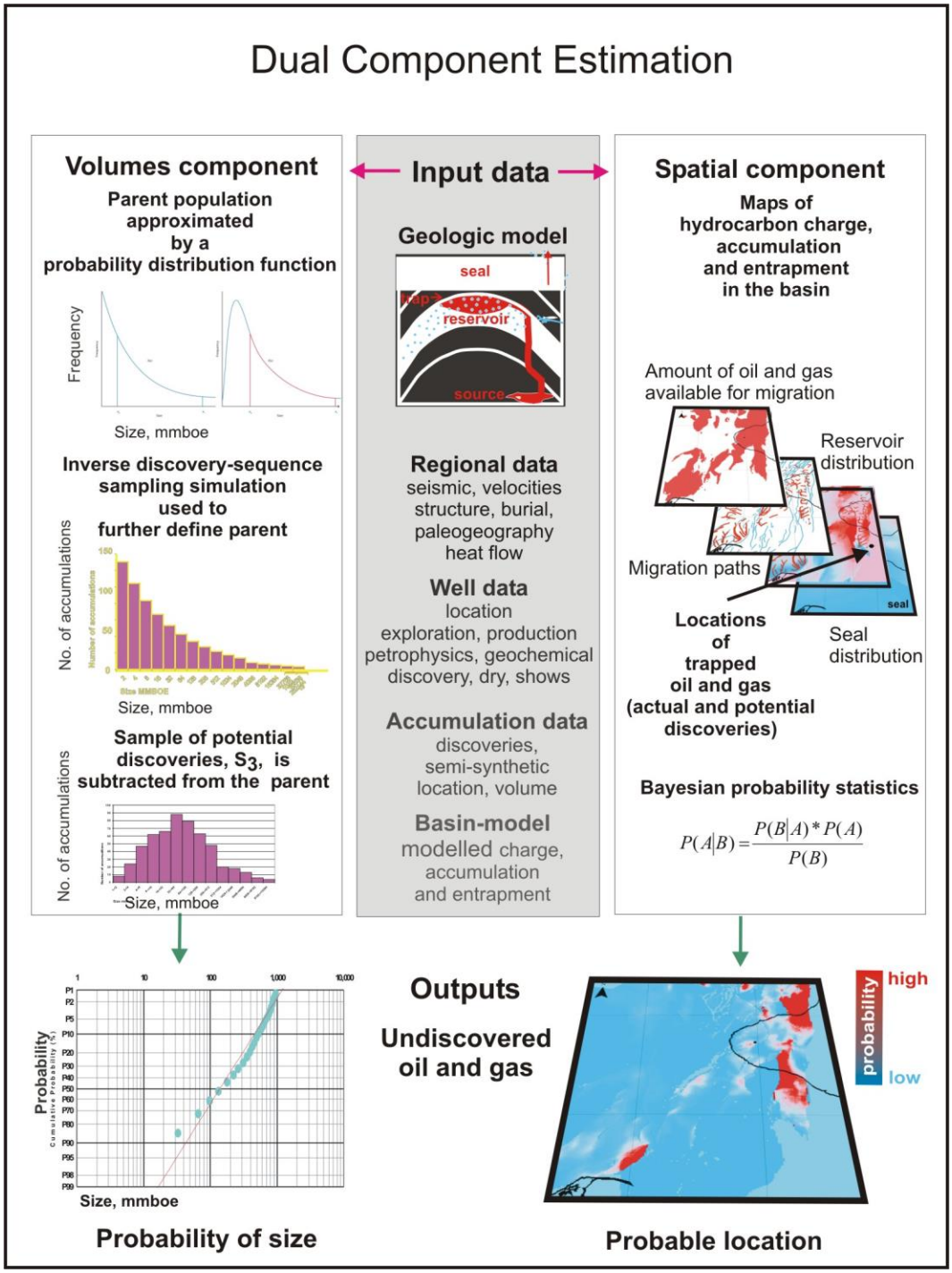

Figure 4.1: Fundamental elements of the DCE. The volumes component defines a parent population based on a probability distribution function, an inverse, modified, discovery-sequence sampling simulation and geologic and exploration data. The spatial component uses datagrids of petroleum systems maps, location of oil and gas accumulations and Bayesian conditional probability theory to identify areas of likely oil and gas accumulation. The maps of hydrocarbon charge, accumulation and entrapment are used in a basin model to generate the semi synthetic dataset of potential discoveries, S_2 and in the spatial component to predict areas of undiscovered oil and gas.

4.2 Volumes component

4.2.1 Introduction

The volumes component uses a discovery-sequence sampling simulation to estimate a parent population of oil and gas accumulations in a basin to calculate its undiscovered oil and gas potential. In this study the size distribution of the parent is approximated using a lognormal and a power-law probability distribution function (Section 3.5) and the undiscovered portion is estimated by subtracting a sample of discoveries, such as S_1, S_2 or S_3, from the parent population.

4.2.2 Discovery-sequence sampling simulation

4.2.2.1 Theory

The objective of the discovery-sequence simulation is to estimate the most likely parent population from which the sample of discoveries has originated. To achieve this, this study applies an inverse discovery-sequence sampling simulation, which aims to minimise the impacts of the data limitations of traditional discovery-sequence models that depend solely on discoveries (e.g. Meisner & Demirmen, 1981; Forman & Hinde, 1986; Macdonald et al., 1994) as summarised in Section 3.5.

The inverse discovery-sequence simulation (Figure 4.2) defines the size distribution of the parent population first, numerically, and then redefines it by simulating many series of drawn discoveries in order to match the mean drawn sample of discoveries with potential or actual discoveries (S_1, S_2 or S_3). This approach ensures the parent population is not based on a direct extrapolation of a time-series of known discoveries and therefore is not constrained by the size distribution of the discoveries. The simulation comprises two consecutively run computer programmes, A and B (Appendix 8).

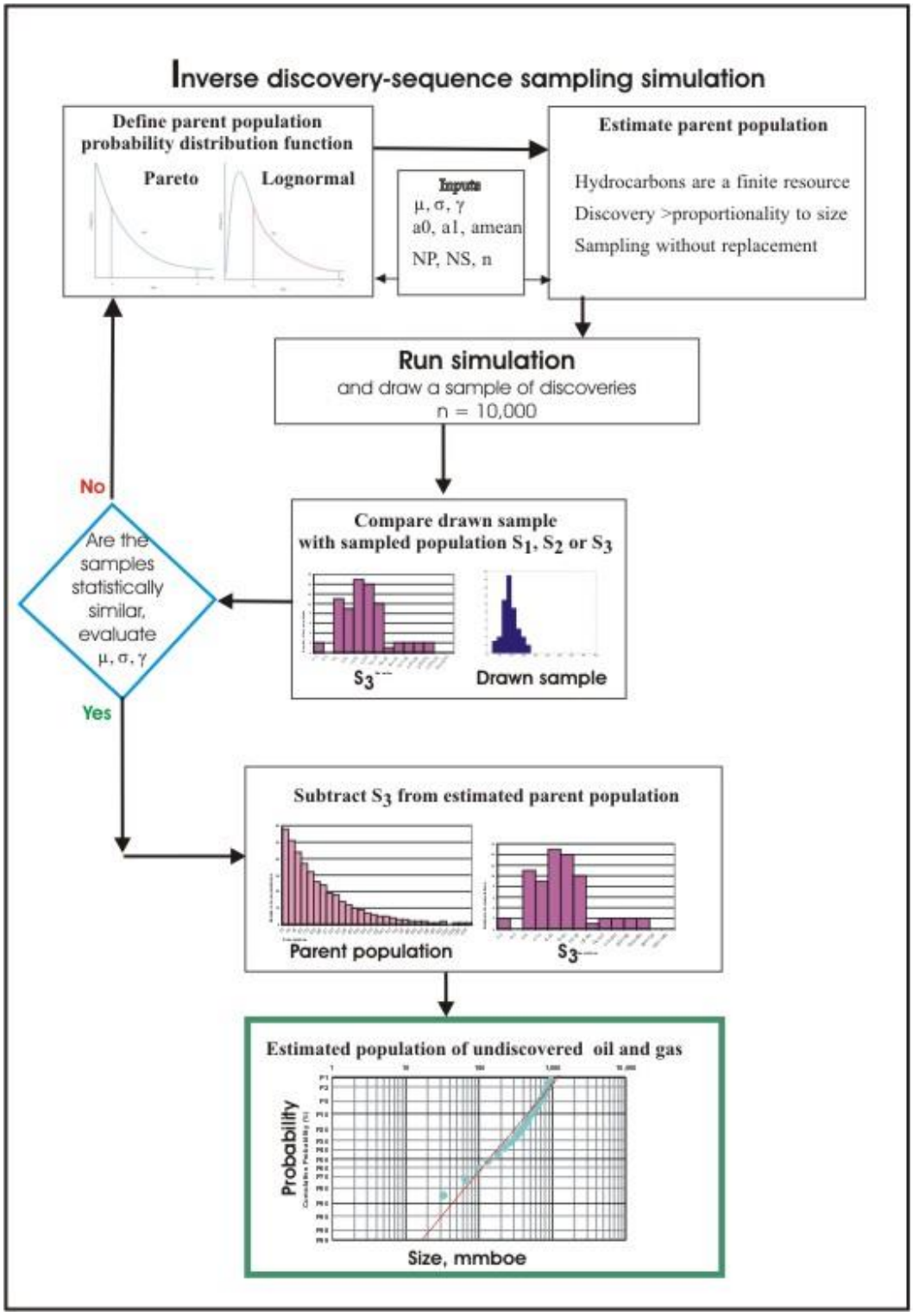

Figure 4.2: Workflow diagram showing the main parts of the volumes component of the DCE. a_0 is minimum accumulation size, a_1 is maximum accumulation size, NP is total number of accumulations and n is the maximum number of simulations per run, NS is the sample of oil and gas accumulations that is drawn in the simulation. The probability of a certain-sized discovery being made from the estimated population of undiscovered oil and gas is shown on a size-probability plot.

4.2.2.3 Programme A

Programme A computes a mathematical expression of a probability distribution function to numerically define a size distribution for a mean parent population, as described by Attanasi and Charpentier (2002). The statistical shape parameters of the distribution, including the mean, μ, standard deviation, σ, and gradient exponential, γ, that are calculated at this stage, are used in Programme B to represent an approximation for a parent.

Key inputs in Programme A (a_0, a_1, NP) are used to describe the truncated probability distribution of the parent population. a_0 represents the smallest accumulation and a_1 represents the largest accumulation geologically possible in the basin. NP is the maximum number of accumulations in a parent population

a_0, a_1, are used to truncate the distribution (Attanasi and Charpentier, 2002) consistent with the finite nature of hydrocarbons (Capen, 1984; Long, 1988) and commercial cut-offs (Barrett, et al., 2003). a_1 is based on the largest valid trap in the basin and a_0 is based on extraction economics, which may differ from basin to basin and from year to year.

Values for a_0 and a_1 are input into the simulation as square kilometers because the range in accumulation trap area is more stable than the range in accumulation volume (Chungcharoen, 1994). Range in volume can span several orders of magnitude, which is very unlikely for area (Chungcharoen, 1994). For example, in the Taranaki Basin the area measurements for known oil and gas accumulations range from ~1–800 km^2, whereas volume ranges from ~1–11,000 mmboe (Figure 4.3). Statistically, a large range in volume is associated with a greater standard deviation and thus volume data typically have a greater associated uncertainty (Chungcharoen, 1994). There is a strong correlation between area and volume (e.g. Figure 4.3) and area is converted back to volume for presentation of results, using a correlation plot of area versus volume such as the one shown in Figure 4.3.

NP is initially based on geological and exploration data, such as, discoveries, basin-modelled accumulations and the number of structural traps identified

through mapping. NP is the most sensitive input parameter because it controls the number and sizes of accumulations from which the simulated discoveries are drawn and the undiscovered oil and gas accumulations are estimated.

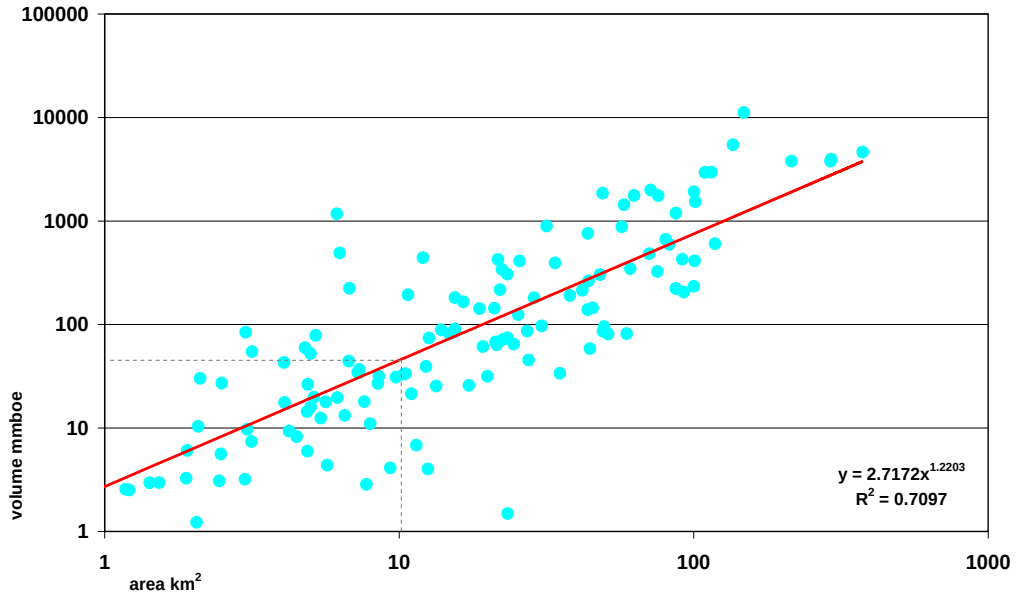

Figure 4.3: Structural trap area versus structural trap volume. The blue data points represent 359 structural traps in the Taranaki Basin. This plot shows the much greater range in trap volume, compared to trap area. The best-fit regression line, in red, characterises this positive correlation which is used to determine the volume of an accumulation given its area. For example, an accumulation with a trap area of 10 km^2 has an equivalent extrapolated volume of 75 mmboe (million barrels of oil equivalent).

4.2.2.4 Probability distribution functions

The equations for the truncated Pareto and double-truncated lognormal probability distribution functions that are used to derive an independent comparison of estimation results (Attanasi & Charpentier, 2002) are presented in Appendix 9.

The distribution shape factors (Section 3.5.4) that are used to mathematically describe the Pareto and double-truncated lognormal probability distribution functions in this study are calculated mathematically. The mean of the truncated lognormal distribution, μ, is derived using the methodology described by Feller (1966). The mean of the truncated Pareto distribution, μ, is derived using the methodology described by Attanasi & Charpentier (2002). Deriving the shape factors numerically, instead of approximating them using a sample of discoveries, means they are directly related to the mathematical equations that are used to describe the truncated distribution functions and are not constrained by the

statistical parameters of a sample of discoveries (e.g. Attanasi & Charpentier, 2002). This is important because a sample of discoveries is a non-truncated dataset and the mean value of such a dataset is unlikely to be representative enough of the size distribution of a parent population to determine its mean (see Section 3.5.4 for further explanation).

4.2.2.5 Programme B

Programme B, which is a multi-run simulation that mimics the exploration process of discovery, uses the numerical approximation of the parent population that was derived in Programme A to generate potential discoveries (Section 3.7). The simulation forward models many series of potential discoveries depending on assumptions such as the number of oil and gas accumulations in a parent or the number of accumulations in a sample.

The key inputs in Programme B are NP, NS, and γ. NS is the maximum number of accumulations in a drawn sample and γ is a exponential gradient. NS is initially based on the number of accumulations in one of the sampled populations such as, S_1, S_2 or S_3. NS is the second most sensitive input parameter because the total number of accumulations simulated in the drawn sample has a direct impact on the size distribution of the undiscovered portion of oil and gas accumulations.

The exponential gradient, γ, is used to express the discovery coefficient (Chapter 3) in the simulation. It is used to assist with making more useful discovery predictions because the probability of discovery is often twice that predicted using accumulation size proportionality (Arps & Roberts, 1958; Attanasi, 1980; Power, 1990) and explain larger than predicted discoveries being made later in a discovery-sequence (Schuenemeyer & Drew, 1983; Power, 1990; Mandelbrot, 1995; Sinding-Larsen & Brandsegg, 2005). It is typically between 1 and 4, based on global datasets of oil and gas discoveries from mature basins (Attanasi & Charpentier, 2002).

NP and NS are redefined during the discovery-sequence simulation and it is important to run many simulations to test the sensitivity of the final parent

population with these parameters. Each series of potential discoveries is based on 10,000 iterations, and from these a mean sample of discoveries is calculated.

4.2.2.6 Probability of discovery

The probability that a certain-sized accumulation is drawn in the discovery-sequence simulation presented here is initially based on the size of the accumulation (Meisner & Demirmen, 1981; Forman & Hinde, 1986). In the simulation a range of pseudo probabilities are used to determine the likelihood of an accumulation being drawn (Appendix 8). The pseudo probabilities are based on the sorting of the individual sizes of each accumulation in the specified parent population distribution, in descending order and are normalised using a scale from 0 to just less than 1 by dividing each value by a number larger than the maximum size. The likelihood of an accumulation being drawn is then weighted using a constant discovery coefficient, γ, to recognise that the probability of discovery is also dependent on other factors such as geological knowledge or economic impacts (Section 3.5.1).

4.2.2.7 Sampling without replacement

Once an accumulation has been drawn or sampled from the parent population it cannot be sampled or drawn again. To achieve sampling without replacement J is used to represent each individual accumulation that is drawn. All individual accumulations in the sample are assigned from J_1 to J_{NS}. Each J drawn is evaluated individually to determine if it has been sampled before. If a J has not yet been drawn, it is held in a storage vector of possible accumulations. If the accumulation has been drawn previously it is not included in the storage vector. Sampling continues until the specified sample size, NS is reached.

4.2.2.8 Defining the most suitable parent population

To estimate the most likely parent population from which a sampled population of discoveries (S_1, S_2 or S_3) has originated the size distribution of the simulated discoveries (drawn from the defined parent population) is statistically compared to the sampled populations S_1, S_2 or S_3. These three populations represent the discovered and potential hydrocarbons of a basin and if these and the drawn

sample are statistically similar, then the parent population of the drawn sample can be used to represent the parent of the sampled population.

Typically the sampled population with the greatest number of accumulations is chosen for comparison because it represents the greatest range in accumulation size and to increase the confidence of the data. For example, the S_{3ii} sample of evaluated traps is used to estimate the parent population of the Taranaki Basin because it has the greatest number of hydrocarbon accumulations.

The sample of simulated discoveries is a mean sample that results from a minimum of 10,000 replicates. This many replicates are necessary to ensure the variation of the standard deviation of the estimated parameters is reduced to an insignificant quantity (Power, 1990; Ninpong, 1992; Chungcharoen, 1994).

The comparison compares the shape and statistical skewness of the distribution. The skewness of a probability distribution looks at how far left the mode has moved from the center toward the right or left hand extremes of probability of the plot. The central area of the distribution is most important to compare because it includes the accumulations which have the greatest probability of existing. The shape is evaluated by comparing the mean, mode and standard deviation (μ, σ, γ) of the distribution. Skewed datasets create a distribution that is said to have a tail (Moore & McCabe, 2003) and for a distribution of hydrocarbon accumulations the tail typically represents a low number of large accumulations. The statistical comparison is an iterative process and input parameters are redefined and the simulation rerun, as shown in Figure 4.2, until a suitable parent is found. The number and sizes of discoveries in the basin are then subtracted from the most suitable parent population, leaving the undiscovered portion of oil and gas accumulations.

4.2.2.9 Workflow steps

The discovery-sequence simulation has the following workflow steps.

Part 1: Programme A, define parent population

1: Input the equation used to approximate a truncated Pareto or truncated lognormal distribution probability distribution function (Appendix 9).

2: Input shape parameters, μ, σ, γ. For the truncated Pareto distribution μ is calculated using the parent distribution equation shown in Appendix 9. For the truncated lognormal distribution μ is calculated using the parent distribution equation shown in Appendix 9.

3: Input values for a_0, a_1 and a_{mean}, using units of area.

4: Run Programme A and evaluate the shape factors, μ, σ and γ by examining the shape of the size-distribution of the parent population.

Part 2: Programme B, estimate parent population

5: Input the truncated Pareto or truncated lognormal probability distribution function derived in Programme A.

6: Input the shape parameters, (μ, σ) that were calculated in Programme A.

7: Input NP and NS.

8: Input γ, to represent a discovery coefficient.

9: Input n, the number of simulations for a single run, for example 10,000.

10: Run the simulation and evaluate the mean drawn sample of oil and gas accumulations and its associated standard deviation.

11: Examine each of the sampled populations, S_1, S_2, and S_3, and decide which one is most suited to estimate the parent population.

12: Compare the statistical shape factors of the mean drawn sample with the selected sampled population, S_1, S_2, or S_3.

13: Determine the probability of drawing such a sampled population, and, if necessary, redefine NP, NS, and γ. Define appropriate ranges of values. For example, define a range of NP to represent a spectrum of parent-population distributions capable of generating a sample that is statistically similar to the sampled population of discovered or basin-modelled accumulations. Continue this process until the drawn sample and sampled population is statistically similar and a representative parent population of oil and gas accumulations is identified.

4.2.2.10 Output plots

The discovery-sequence simulation outputs:

1. A graph showing the probability density function of the parent population of all oil and gas accumulations in a basin that was derived using computer programme A. This graph is used to check that the parent population simulation is running as it is programmed to and this graph should show a probability density function curve representative of either the lognormal or Pareto probability function.

2. A size-frequency histogram of the estimated parent population of all oil and gas accumulations in a basin, as shown in Figure 4.4. Each individual accumulation in the parent and undiscovered populations cannot be shown in a table because there are too many and instead numerous histograms are generated.

3. Two frequency histograms of the mean drawn sample of oil and gas accumulations showing two different bin-size intervals to test the vulnerability of the distribution shape to bin-size (Figure 4.5).

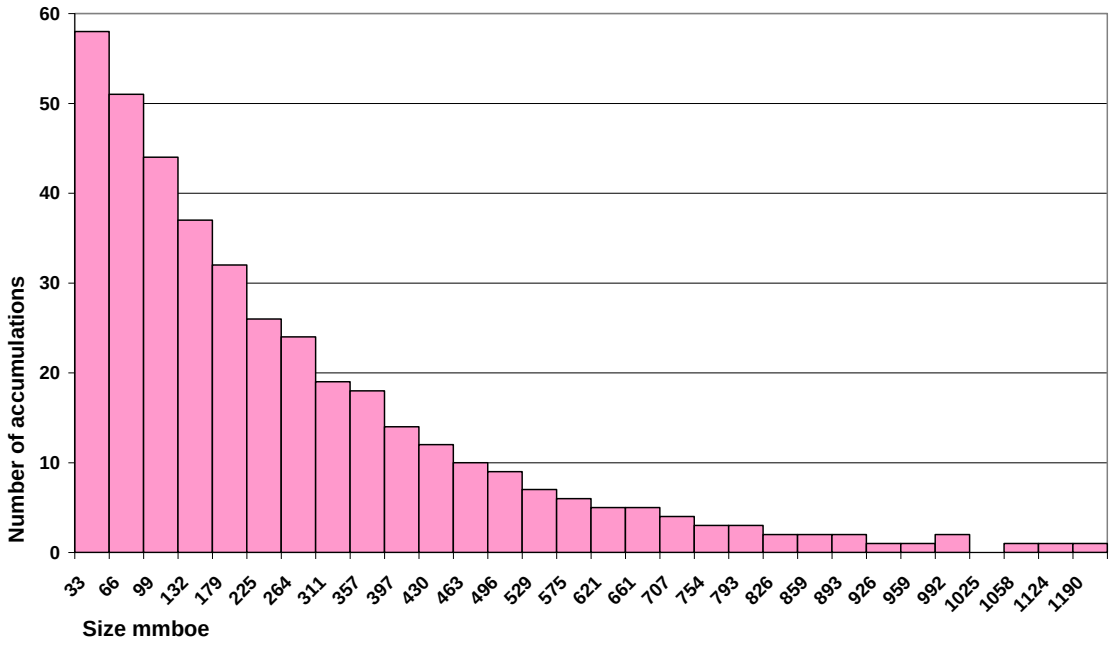

Figure 4.4: An example of a size-frequency histogram of an estimated parent population of oil and gas accumulations. The volume size for a bin denotes the maximum accumulation size in a bin, for example 33 is bin size 0–33 mmboe.

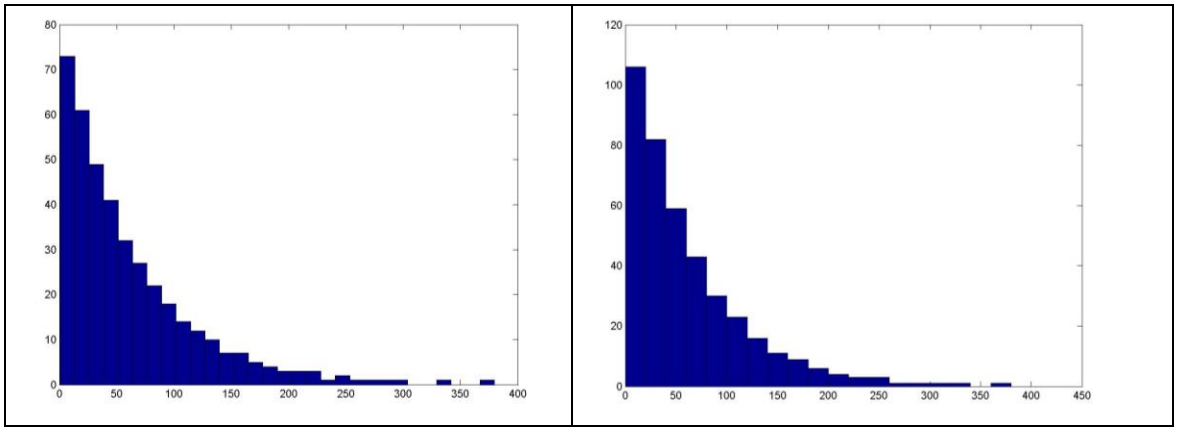

Figure 4.5: An example of the two size-frequency histograms of a mean drawn sample of simulated oil and gas accumulation that were generated by the discovery-sequence simulation. The horizontal axis is size, mmboe and the vertical axis is number of accumulations. Note different bin size for these two histograms.

Histogram bin-size can be varied in the simulation programme and depends primarily on how many accumulations are modelled in the parent population. Smaller sized bin intervals provide more detail about the number of accumulations for a greater number of sizes of accumulations. For example, a bin-size from 1–100 mmboe cannot provide as much information as a bin-size of 1–10 mmboe and the sizes used in this study were chosen following repeated sensitivity trials.

4.2.3 Calculate the undiscovered population of oil and gas

The undiscovered oil and gas is estimated by subtracting the mean sample of simulated oil and gas accumulations from the parent population that is estimated in Programme B. The calculated volumes are plotted on a cumulative probability plot (Figure 3.11) using the calculations described by Rose (2006) and provided in Appendix 7. On the horizontal axis is accumulation size, using a logarithmic scale, and on the vertical axis is the probability of size, using a normal probability scale. The plot shows the probability that the next discovery from this population will be equal to or greater than the corresponding accumulation size (Section 3.5.5).

4.3 Spatial component

4.3.1 Theory

The spatial component assumes that undiscovered oil and gas is most likely to exist in areas where petroleum systems elements and processes, such as reservoir quality, are proven. Furthermore, areas of a basin where these data are mapped have a greater probability of yielding a new discovery compared to areas where the data are not mapped. The aim of the spatial model is to establish a spatial relationship between these areas and locations of trapped oil and gas to predict where undiscovered oil and gas may be located, following the work of Rostirolla et al. (2003) and Sinding-Larsen & Brandsegg (2005).

The spatial component uses the ESRI Spatial Data Modeler® (SDM) software (Bonham-Carter, 1994; Kemp, et al., 2001) to predict where undiscovered oil and gas may be located in a basin. The petroleum systems maps, that are used in the spatial model include:

- amounts of oil generated and expelled;
- amounts of gas generated and expelled
- reservoir thickness;
- reservoir porosity;
- regional fault traces;
- seal rock distribution;
- structural traps;
- migration flowpaths;
- maximum burial depth of seal rock; and
- structural domains.

The oil and gas maps were output from Bassim® (Section 3.2.2). The reservoir, faults and seal rock maps were originally prepared for the PCE® model (Section 3.2.3 & Appendix 4). The traps and flowpath maps were output from PCE®. The burial depth map was originally prepared for the Bassim® model (Section 3.2.2). The structural domains map was prepared for the spatial model. Each map is referred to herein as an evidential theme map and the mapped data produces an

evidential theme pattern (Bonham-Carter, 1994). The 10 evidential theme maps are presented in Appendix 10.

The locations of trapped oil and gas are based on the sampled populations, S_1, S_2, and S_3 introduced in Section 3.1 and referred herein as points of success (Bonham-Carter, 1994). They are superimposed onto an evidential theme map in order to calculate a spatial correlation between them and the mapped data (Kemp et al., 2001). The different datasets are used to run a probable and a possible scenario in the spatial model. The probable scenario uses the S_1 dataset of discoveries and well locations where significant hydrocarbon shows were reported. This scenario results in a most likely prediction given the correlations are based on proven hydrocarbon accumulations. The possible scenario uses discovery and hydrocarbon show data plus the semi-synthetic accumulations in datasets S_2 and S_3 and results in a prediction that includes unexplored areas of a basin that may have hydrocarbon potential.

Strong spatial correlations result if many or most of the locations of oil and gas are located where the evidential theme pattern is mapped. A relatively weak spatial correlation results if no or not many accumulations are located where the evidential theme pattern is mapped (Bonham-Carter et al., 1994, Sawatzky et al., 2004). Correlations are calculated for each individual map in a series of up to 10 maps (Kemp et al., 2001) and are then integrated into a single map to reveal an overall spatial pattern between mapped working petroleum systems and trapped oil and gas in a basin.

The ESRI® spatial model is used in this study because it is capable of making complex spatial correlations between many different maps for a large variety of regional-scale data. No other publicly available model with this capability was available and, because of this, the ESRI® software was not evaluated against another spatial model.

4.3.2 Datagrids

The evidential theme maps are converted into numerical datagrids and GIS point files of the points of success are created using the ESRI® GIS packages

ArcInfo7®, ArcMAP9® and ArcView3.3®. All grids are modelled in a common projection, are defined by spatial coordinates and have a suitable cell resolution, such as 1000 m x 1000 m. In areas of the datagrid where data are missing, for example, where source or reservoir rock has not been deposited or has been eroded, each cell is assigned a NoData value and is not included in any of the analyses. Areas where data are missing due to the absence of data are modelled with a value to reflect this and are not assigned with a NoData value, because the area may have potential that is yet unmapped.

4.3.3 Calculating spatial correlations

In this study, the ESRI SDM® WoE quantitative tool is used to calculate the spatial correlations using Bayesian probability statistics (Kemp et al., 2001; Sawatzky et al., 2004; Carranza, 2004). The mathematical algorithms and probability equations are described in Bonham-Carter (1994). Bayesian probability statistics follows the axioms of Bayes theorem, which expresses the plausibility of an event as:

$$P(A|B) = \frac{P(B|A) * P(A)}{P(B)} \tag{4.1}$$

where P(A) is the prior probability of A, P(A|B) is the conditional posterior probability of A given B and depends on the specified value of B, P(B|A) is the conditional posterior probability of B given A and P(B) is the prior probability of B (Moore & McCabe, 2003).

The probabilities are used to weight the number of points of success that are located where the geological data are mapped versus where the geological data are not mapped (Rostirolla, et al., 2003). A spatial pattern based on this weighted relationship, of these two datasets, emerges for each map. Prior probabilities are initially calculated for each evidential theme map and are then updated into conditional posterior probabilities with the addition of new information (Rostirolla, et al., 2003).

4.3.4 Area-based spatial correlations

The spatial correlations are calculated relative to area, based on the probability that a point of success will be located in a cell of the modelled grid. Model cells in this study are 1000 m x 1000 m. The size of a point of success is based on an average physical size of a single oil and gas accumulation in a basin.

A prior probability is an initial probability of an event occurring, based on some set conditions and its plausibility. The prior probability that a unit cell contains an accumulation is the number of points of success divided by the area of the datagrid in unit cells. For example, in an area of 10,000 km^2, which has 50 hydrocarbon accumulations, each with an areal coverage of 1 km^2, the total area, T, = 10,000, the number of points of success = 50 and the density of accumulations = 50/10,000 = 0.005. With no other information available, this fraction is used to define the prior probability P(A) of a hydrocarbon accumulation existing in an area.

With additional information about an area, the probability is recalculated as a conditional probability (Moore & McCabe, 2003; Rostirolla et al., 2003). For example, a factor that affects the likelihood of a discovery is information about the distribution of good-quality reservoir. If 45 of the 50 points of success are located where good-quality reservoir is mapped then the probability of an accumulation existing is greater where the reservoir is mapped than where it is not mapped. The potential for finding an accumulation given the presence of a reservoir is, therefore, expressed as a conditional posterior probability (Bonham-Carter, 1994).

The conditional probability is the proportion of the binary pattern B taken up by the points of success where A and B intersect. The spatial relationship between the binary pattern of the evidential theme and the points of success is summarised in a Venn diagram (Figure 4.6). The top square shows the binary pattern, where yellow represents the presence of reservoir, grey represents the total study area, T, and the blue dots represent the points of success. The bottom square shows the probability expressions for the relationships between the binary pattern and the points of success. Of the 50 points of success, 45 of the them reside in area B, an area of 3000 km^2; therefore the conditional probability of an accumulation given

the mapped reservoir binary pattern map is 45/3000 = 0.015, which is three times greater than the initial prior probability of 0.005. With further additional information, the posterior probability, and hence the spatial model are further updated (Bonham-Carter, 1994; Sawatzky et al., 2004).

4.3.5 Likelihood ratios

The WoE method uses logits to express the probability statistics (Sawatzky, et al., 2004). Logits are the natural logarithm of odds and is used to define likelihood ratios (Moore & McCabe, 2003). Odds are the ratio of the probability that an event will occur to the probability that it will not occur (Singer & Kouda, 1999). The likelihood ratios are referred to as weights, which are represented by W (Bonham-Carter, 1994; Sawatzky, et al., 2004). This means that anywhere on the map where the evidential theme such as reservoir is mapped a positive weight, W^+, is assigned (Bonham-Carter, 1994). The odds of an accumulation given the evidential theme is absent is used to determine its negative weight, W^-. This means that anywhere on the map where the evidential theme, such as reservoir, is absent a negative weight is assigned. Weights are used instead of posterior probabilities because they are straight forward to calculate using a single equation, which is particularly important when multiple maps are integrated and multiple likelihood ratios are calculated (Bonham-Carter, 1994; Sawatzky, et al., 2004).

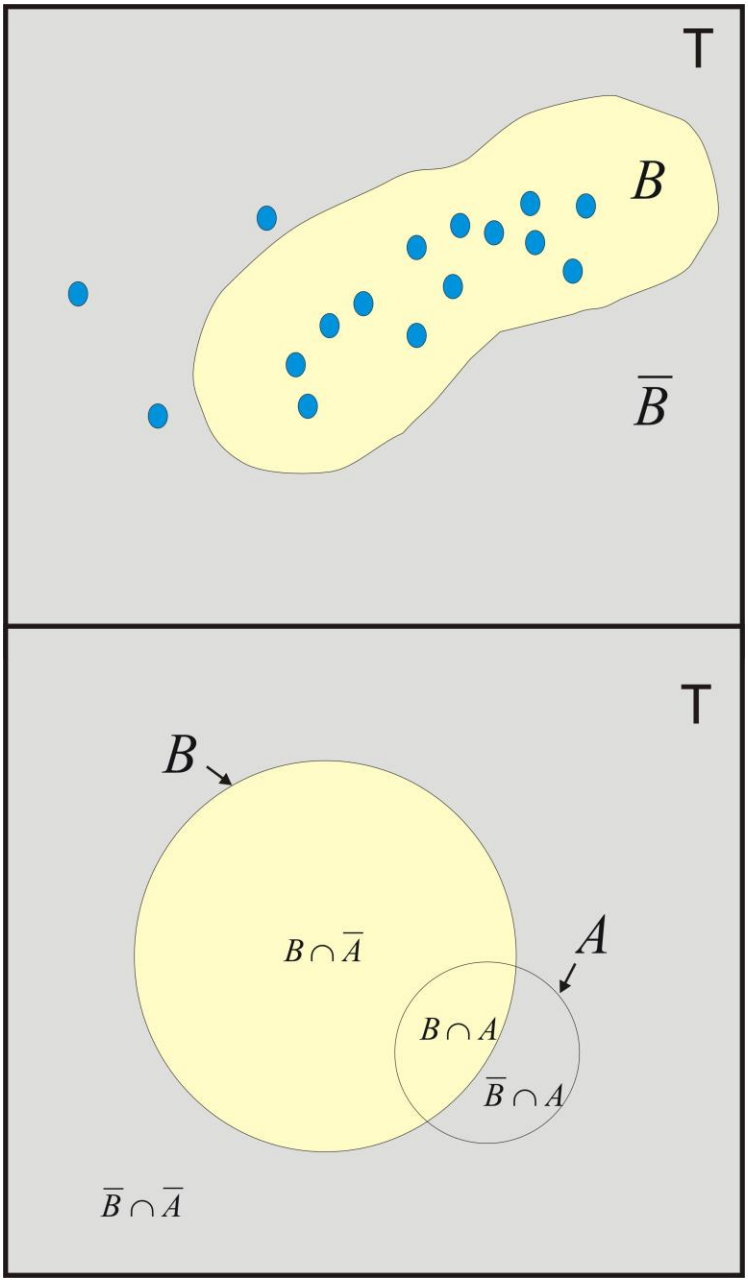

Figure 4.6: Venn diagram used to explain the spatial relationship between the binary pattern of an evidential theme map and the points of success used in the WoE calculations. The top square shows the binary pattern, where yellow represents the presence of reservoir, grey represents the total study area, and the blue dots represent the location of points of success, such as known oil and gas accumulations. T = total study area, B = binary pattern present, $\overline{B}$ = binary pattern absent, A = the presence of the points of success (location of the accumulations), Ā = the absence of points of success, and ∩ = the statistical intersection. B∩A is where areas of reservoir coincide with locations of the accumulations. $\overline{B}$ ∩A is where areas with no reservoir coincide with locations of the accumulations. $\overline{B}$ ∩ Ā is the intersection where areas of no reservoir coincide with no locations of the accumulations. B∩ Ā is where areas of reservoir coincide with no locations of the accumulations.

4.3.6 Reclassification

Evidential theme maps are reclassified into ranked categorical and ordered classes of variables as part of the WoE method (Bonham-Carter, 1994; Sawatzky, et al., 2004). A categorical map shows categories of data such as a reservoir thickness. An ordinal map shows ordered or scaled data such as a map of fault traces that have a 5 km-wide buffer zone, made up of 1 km intervals (Sinding-Larsen & Brandsegg, 2005).

Data are reclassified into classes to optimise the weighted spatial correlations (Bonham-Carter et al., 1994). For a reclassified categorical map, a spatial analysis is determined for each category of data. For a reclassified ordinal map, a spatial analysis is determined for each increment of order or scale. The reclassification process creates a derivative theme map of derived weights for each evidential theme map (Sawatzky, et al., 2004).

The objective of reclassification is to produce a derivative map with as few classes as possible without compromising the categorical relevance of the variable being represented to maximise the likelihood ratio calculations and integration of all maps (Bonham-Carter et al., 1994). The number of classes selected should reveal a useful pattern. If there are too many classes, the points of success are so spread that the weight estimates become weak and of little use. If there are too few classes, the spatial patterns are so generalised that important correlations between the point data and mapped data are not shown.

For example, a reservoir map showing two different sedimentary facies, such as a marginal-marine sandy-siltstone and coastal-plain sandstone, will show areas with different ranges in porosity, such as 4–18% and 15–45% respectively. If only two classes were used, such as <4% and >4%, the resulting binary spatial pattern of the map would show where reservoir was mapped and where it was not mapped. However, such a pattern would not highlight the two different facies. A multi-class spatial pattern that was based on a porosity classification of 0–45% at intervals of every 2% would also be unhelpful because it is unlikely to reveal a pattern that is based on a depositional feature. However, a multi-class pattern which was based on a porosity classification of 0–4 %, 4–18 %, and 18–45 %

would reveal a useful spatial pattern highlighting different depositional environments.

The optimal number of classes is guided by derivative correlation values including, a contrast value, C, standard deviation of a weight s(W) and Studentised confidence contrast s(C). They are based on logit weights, W^+ or W^-, and used to measure correlation strength (Sawatzky, et al., 2004). C determines how strong a correlation is between an evidential theme map and the points of success and is calculated as the number of points of success where the evidential theme is mapped versus where it is not mapped per unit area. For example, if 23 out of 29 points of success coincide with the mapped data then C, would be very high, with the actual value depending on the areal extent of the pattern. Correlation strength and C are sensitive to the size of an area (Bonham-Carter et al., 1994) and because of this the basin is best modelled using a number of geological domains.

A standard deviation of a weight s(C), is a measure of the uncertainty with which the contrast is known and is calculated as C / s(W). s(C) is used as an informal test for the hypothesis that C = 0, which means there is no contrast (Bonham-Carter, 1994). A large ratio implies the contrast is much greater than the standard deviation suggesting the contrast is likely to be real. A s(C) value >1.5 is preferable (Bonham-Carter et al., 1994). The correlation derivative s(C) is used as a relative test, because of the assumptions required for a formal statistical test and s(C) values can be dependent on the units of measurement (Bonham-Carter, 1994).

To reclassify a map with categorical data, each evidential theme class is examined against all other classes as if it were binary. For example, a reservoir thickness map may be reclassified into three classes, to represent variable thicknesses relating to known hydrocarbon column heights in a basin, such as <50 m = small volume accumulations, 50–200 m = large volume accumulations and >200 m = no volumes, based on potential seal breach. Each class is examined against the other two to establish any spatial relationships between the points of success and specific reservoir thickness.

To reclassify a map with ordinal data, weights are generated for either cumulatively increasing or decreasing class values. For example to reclassify an evidential theme map of buffered regional-scale faults, spatial correlations between the distance from a fault and the points of known oil and gas accumulation are calculated for each interval. Derivative maps are generated from the spatial correlation calculations and these are used to determine the optimum distance from the fault for the optimum spatial correlation. The derivative correlation values are used to decide the buffer distance that shows the strongest spatial correlation. For example, Figure 4.7a shows a top-Eocene fault-trace map for the Taranaki Basin. Superimposed on this map are the points of success of known hydrocarbon accumulation, which are located relatively close to the regional-scale fault traces. If there is a relationship between an oil and gas accumulation and its proximity to a fault, it may be useful for predicting undiscovered oil and gas accumulations. To determine a spatial correlation, the distance of an accumulation from a fault is optimised by calculating the weights and contrast values for each interval of distance from the fault.

Using a categorical analysis, five buffer zones are spaced at 1 km intervals either side of the fault-trace (Figure 4.7b). If the buffer zone is too narrow, many of the known hydrocarbon accumulations are excluded. If the buffer is too wide, the usefulness of the association between the faults and the hydrocarbon accumulations is reduced. The variation in contrast with distance is determined by calculating the weights and contrast values for each interval of distance. The greatest contrast is represented by the largest C value, which is 1 km from the fault (Figure 4.8a and Table 4.1a) and C = 1.768, W^+ = 0.91, and s(C) = 4.60. However, a problem with this approach is that some intervals have few or no points of success, making the results noisy (Figure 4.8b and Table 4.1b).

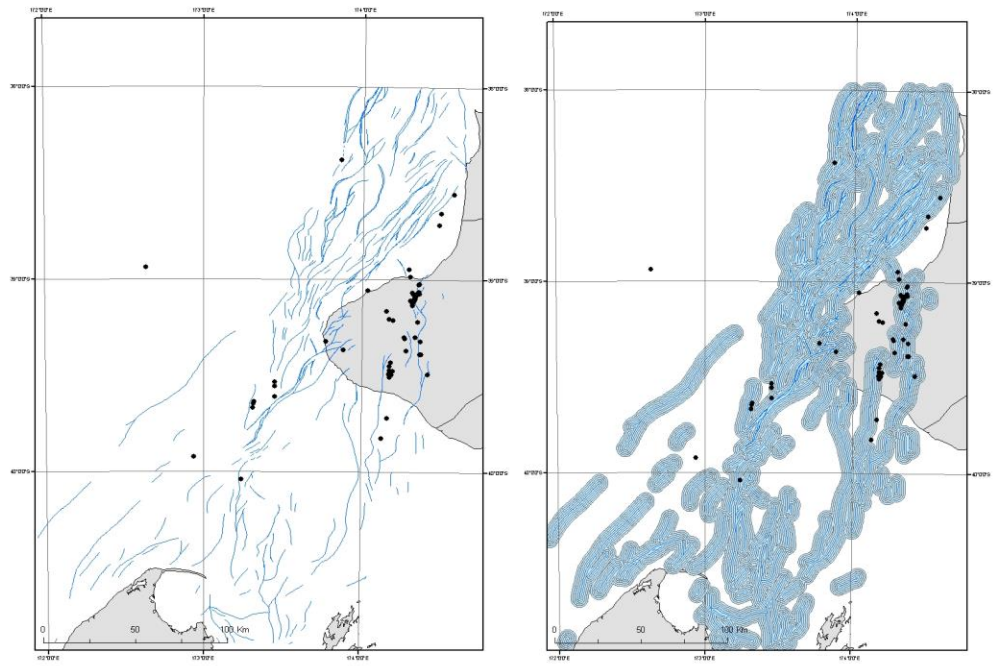

(a) (b)

Figure 4.7: a. Example of an evidential theme map showing fault traces of major top-Eocene surface faults in Taranaki Basin and training points (black dots), which represent known oil and gas accumulations. b. an example of a derivative theme map of map (a) showing the derived buffered fault traces.

To address this issue, cumulative distances are examined from the fault and out to 1, 2, 3, 4 and 5 km. The weights and contrast values are calculated for the cumulative intervals (Table 4.1b). C is now maximised at a cumulative distance out to 4 km and is 2.886, compared to 1.768, for the spatial correlation out to 1 km. The strongest correlation between the faults and accumulation is within a 4 km buffer zone of a fault; therefore, spatial correlations should be calculated for this area, to relate the accumulation of oil and gas with proximity to faults.

Fault buffer class	Area: km^2	Area: unit cell	W+	W-	C	S(C)
1	11296	2259.2	1.228	-0.540	1.768	10.825
2	22592	4518.4	0.910	-0.110	1.020	4.614
3	33888	6777.6	0.096	-0.007	0.103	0.326
4	45184	9036.8	1.252	-0.125	1.377	6.098
5	56480	11296	-1.867	1.109	-2.886	-10.899

(a)

Fault buffer class	Area: km^2	Area: unit cell	W+	W-	C	S(C)
1	11296	2259.2	1.228	-0.540	1.768	10.825
2	33888	6777.6	1.140	-0.859	1.999	11.578
3	67776	1355.2	0.975	-1.015	1.990	10.765
4	112960	22592	1.010	-1.867	2.886	10.899
5	169440	33888				

(b)

Table 4.1: (a) Derivative weights used to determine the optimal distance from each fault-trace for each separate class, that results in the strongest spatial correlation between the location of an oil and gas accumulation and its proximity to a fault-trace. Fault class is each of the areas that are 1, 2, 3, 4, and 5 km from the fault-trace. The derivative values are given for each 1 km distance from the fault, out to a total distance of 5 km. C is the contrast value, W+ is the positive weight, W- is the negative weight and S(C) is the Studentised contrast value. (b) Cumulative ascending class-derivative weights for the spatial analysis identifying the optimal distance from the fault-trace for the evidential theme and derivative evidential theme maps in Figure 4.8, to maximise the spatial correlation between the fault-trace buffer pattern and the points of success.

4.3.7 Predictive strength of a map

Correlation values are also used to determine the predictive strength of an individual map before it is integrated into the spatial model. Predictive strength is a measure of how useful the map data, such as reservoir quality, is at predicting the probability of an oil and gas accumulation. Maps with the strongest correlation values are selected for the spatial data model. The WoE spatial tool is the only quantitative tool within ESRI's modelling tool suite that allows evidential theme maps to be optimised. Predictive strength optimisation is also useful to get a better understanding of which maps are likely to be useful for predicting where hydrocarbons may be located in a basin.

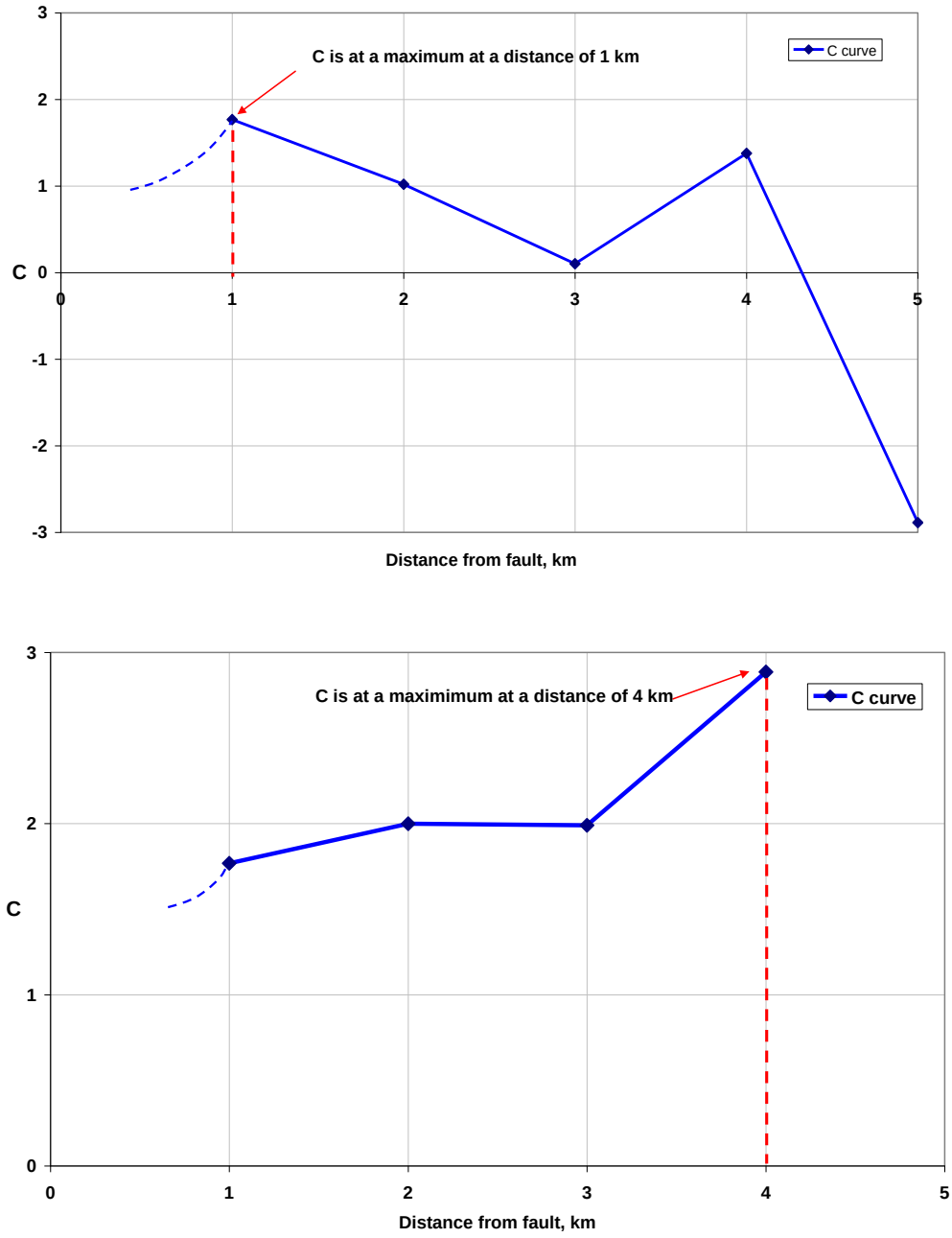

Figure 4.8: (a) Variation of contrast with buffer zone distance from a fault for the evidential theme and derivative evidential theme maps used in Figure 4.7 and data in Table 4.1. The strongest contrast, where C = 1.768, resulted for the buffer zone distance of 1 km from a fault-trace, which suggests that most of the oil and gas accumulations plotted are located within 1 km from a major Eocene level fault-trace. There is also a relatively strong contrast out to 4 km from a fault, with C = 1.020. (b) Variation of contrast with distance for cumulative distance from a fault-trace, using the cumulative ascending reclassification data in Table 1b. C is the contrast value. This is a derivative correlation value used to measure the strength of a spatial correlation between an evidential theme and the points of success, and in this case it measures the spatial correlation between the locations of known oil and gas accumulations and their proximity to a set of related faults. Here the greatest spatial correlation is out to 4 km, which means most of the oil and gas accumulations are located within a 4 km distance from the regional-scale top-Eocene fault traces in Figure 4.7.

4.3.8 Conditional independence (CI)

The integration of all the maps into a single map assumes each map is conditionally independent (Bonham-Carter, 1994). This means that the data on a map stand alone and are not directly related to another map. However, for some geologic data this assumption is violated to some degree because they are directly related, such as reservoir porosity and permeability. In this case, it may be more correct to only use a porosity or a permeability map and not both to prevent an artificially inflated spatial correlation being calculated.

CI is checked by applying a pair-wise CI examination using a Chi-square, χ^2, statistical test (Moore & McCabe, 2004). A Chi-square, χ^2, statistical test is a test of statistical independence that uses a Chi-square distribution to assess whether paired observations for two variables are independent of each other. In this study, the spatial correlations calculated for two different evidential theme maps are paired up and tested to see if the actual evidential theme is related to the calculated correlations. χ^2 values are calculated and a value greater than that specified for the specific degrees of freedom (as presented in the Eton Statistical and Math Tables, 1980) is an indication of a CI violation. Maps that violate CI cause the calculated posterior probability to be overestimated. This does not mean the predictive map is incorrect, but rather that the analysis should consider which datasets are likely to cause a violation of independence and results should be interpreted relative to this consideration.

4.3.9 Workflow steps

In this study the following workflow steps were followed to estimate the likely locations of undiscovered oil and gas in a basin using the spatial component.

1: A base map of the area of interest is created and is used to define the area for each evidential theme map.

2: A geologic model is defined to describe charge, accumulation and entrapment elements and mechanisms for a basin.

3: Up to 10 evidential theme maps are prepared.

4: Prepare a point-set file identifying the locations of accumulations in datasets S_1, S_2 and S_3.

5: Convert all maps to datagrids using the specifications described in Section 4.3.1.

6: Following the input prompts of the ESRI ArcGIS® Spatial Data Modelling software, define the spatial coordinates of the basin being assessed and input the evidential theme maps.

7: Reclassify the evidential theme maps and generate corresponding derivative maps. Compare the tables of derivative values and decide which of the maps will remain in the spatial model, based on the correlation strength and conditional independence.

8: Run the spatial model using the derivative maps for the selected evidential theme maps and output the normalised posterior probability and associated uncertainty maps.

4.3.10 Output map

The estimate of where undiscovered oil and gas is likely to be located is presented as a map of relative, normalised, posterior probability. The values of posterior probabilities are normalised and reclassified into three classes to show areas of high, medium and low posterior probability. The probabilities are normalised into relative probabilities, to ensure any overinflated calculated posterior probabilities, which may result if two evidential theme maps have a similar spatial pattern, are interpreted correctly (Bonham-Carter, 1994). Areas of high-posterior probability are coloured red, areas of medium-posterior probability are coloured yellow and areas of low-posterior probability are coloured blue. Uncoloured areas have a zero-posterior probability of oil and gas accumulation. A zero-probability results in areas where the evidential theme is not present because the area is not expected to yield hydrocarbons. However, where data are unavailable hydrocarbon potential may exist and these areas require further research and exploration to update their likelihood of yielding hydrocarbons.

4.4 Conclusions

The volumetric component of the DCE uses a probability size-distribution function to estimate the maximum number of oil and gas accumulations in a basin. Discoveries are draw from this parent, using an inverse discovery-sequence simulation, until a sample of drawn discoveries statistically matches a sample of

known or semi-synthetic discoveries (S_1, S_2 or S_3). Once a match has been found S_1, S_2 or S_3 is subtracted from the estimated parent leaving the undiscovered portion. The advantage of the inverse discovery-sequence approach is the size distribution of the estimate parent is not constrained by a sample of few discoveries, which is typical of forward discovery-sequence methods used in an underexplored basin. Instead, an estimated parent presented here has the potential to predict new discoveries greater in size than known discoveries and includes explored and unexplored areas of a basin.

The spatial component of the DCE uses 10 maps to represent hydrocarbon charge, accumulation and entrapment and locations of known and potential discoveries (S_1, S_2 or S_3) to calculate spatial correlations between areas of oil and gas accumulation and mapped petroleum systems elements in order to predict areas of new discoveries. The WoE tool uses probability statistics to establish the relative importance of each variable, such as reservoir quality, and weights its importance accordingly. As a result of the weighting procedure the strongest geological parameters are given the highest weighting and have the greatest impact on the estimation results.

Chapter 5

Key uncertainties associated with estimating undiscovered oil and gas in the Taranaki Basin, New Zealand; using the Dual Component Estimation

Abstract

There are two main sources of uncertainty that impact on the estimates of undiscovered oil and gas for the Taranaki Basin, using the Dual Component Estimation. These are data quality and availability, and software assumptions and limitations.

Regional maps and well data were used to prepare inputs used in the volumetric and spatial models. The structure contour and paleogeographic maps used in the study are based predominantly on 5–10 km line-spaced, 2D seismic data and the datasets of potential discoveries, used to constrain parent population, are based on basin modelling and structural traps. The data limitations have a direct impact on the size distribution of the parent that is used to estimate the undiscovered oil and gas. For example, accumulations below a certain size may not have been modelled and may be underrepresented in the parent.

Four software programmes were used; a primary migration basin model, Bassim®, a secondary migration model, PetroCharge Express®, an inverse discovery-sequence sampling simulation, which was written as part of this study, and a spatial model, ESRI Spatial Data Modeller®. The assumptions of each of these software may mean specific details, such as primary migration, which is specified in Bassim®, or the probability of discovery, which is modelled in the discovery-sequence simulation, may not be fully represented. The discovery-sequence simulation has the greatest direct impact on the size distribution of the parent population, affecting the number of accumulations and the maximum, mean and minimum accumulation sizes in the distribution.

5.1 Introduction

The aim of this chapter is to outline the uncertainty associated with the petroleum systems maps (Sections 4.3.1 & Appendix 3) and S_1, S_2, and S_3 datasets (Sections 3.1–3.3, Table 1.1, Appendix 13) that are input into the volumetric and spatial models, and the software used in the estimation method.

The datasets and software are interconnected, as shown in Figure 5.1. In the figure, grey-coloured boxes highlight the data inputs; including the geologic model, regional maps and well data, and petroleum systems maps and discovered and modelled accumulations. The green-coloured boxes highlight the software which is used to: model hydrocarbon generation and expulsion (Bassim®, Section 3.2.2); migrate hydrocarbons through reservoir and into traps (PetroCharge Express® (PCE) Section 3.2.3); derive a parent population to estimate the amount of undiscovered oil and gas (inverse discovery-sequence simulation, Section 4.2.2); and estimate likely locations of the undiscovered resource (ESRI® spatial model, Section 4.3).

The calculation method used to determine the P50 recoverable reserves volumes (Table 1.1) of the discovered accumulation in the S_1 dataset is not included in Crown Minerals (2004). However, these volumes would have been calculated using a method similar to the volume calculations for the S_2 and S_3 datasets (Section 3.2.3) and the uncertainties associated with this method also apply to the S_1 dataset.

A significant amount of data extrapolation and inference have been used in this study to describe the geology of areas where there is limited data. In particular, proxy and analogue data, mathematical equations, basin modelling and interpolation software have been used. The impact of these techniques on the confidence of the input data is discussed qualitatively. In most cases there were too few data to assign standard random errors (Moore and McCabe, 2003) to the estimation results to account for the uncertainty associated with interpretation and inference. Similarly, there were too few data to prepare multiple scenarios and input maps to represent geological inputs such reservoir distribution.

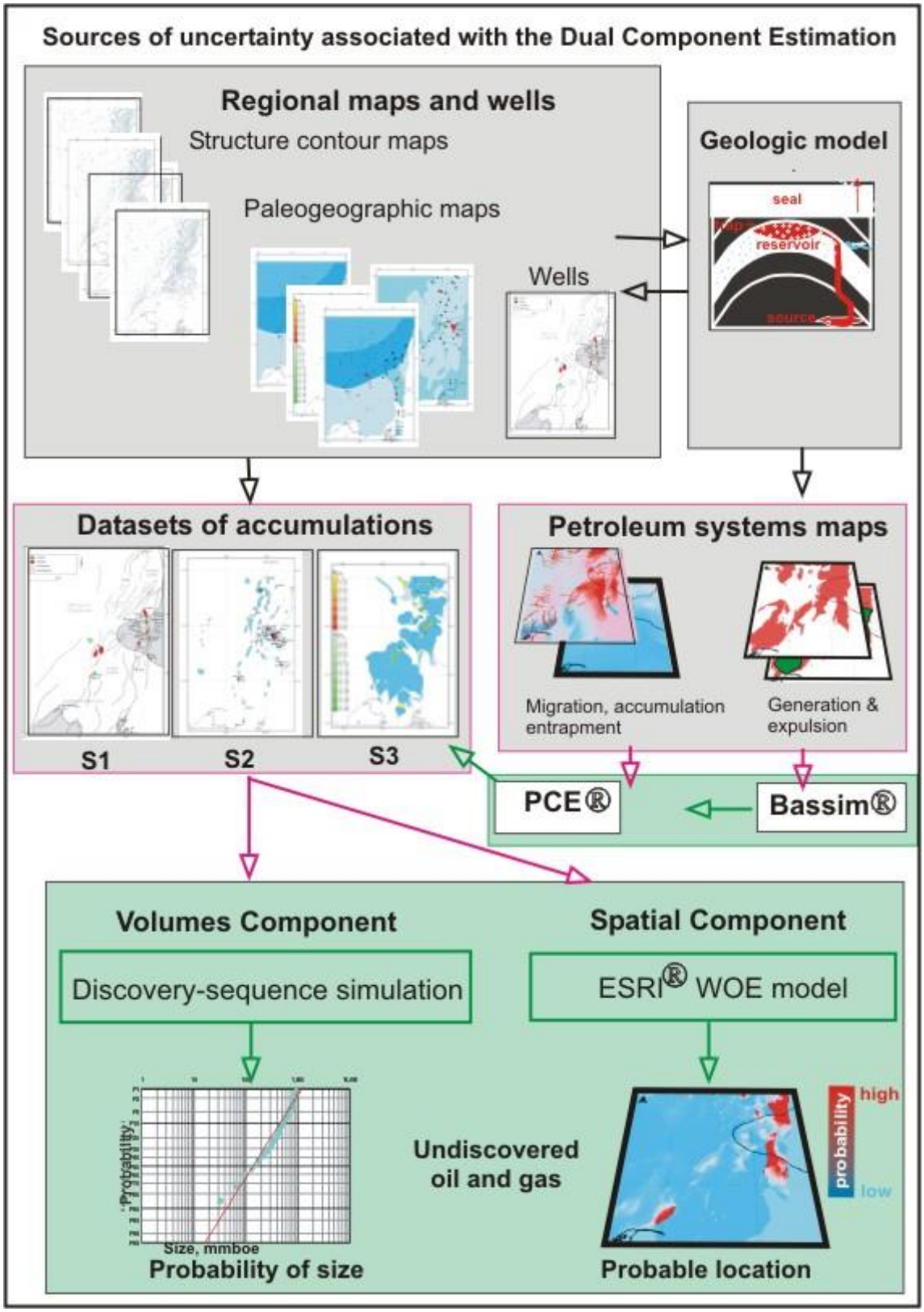

Figure 5.1: Main sources of uncertainty associated with the Dual Component Estimation (DCE) approach. The grey boxes highlight data inputs. The black arrows show the flow of information from regional data to the datasets of accumulations and petroleum systems maps. The green boxes highlight the software programmes used in the DCE. The pink arrows show the flow of data inputs into the four models and the green arrows show the flow of software generated outputs.

A number of practises have been used here to consider alternative outcomes given a different set of data, input parameters or modelling specifications. For example, probability distribution functions are used to represent the probability space of variables such as the number and size of accumulations in a population (Roadifer, 1975 & Attanasi and Charpentier, 2002). Mean values or ranges in values are used for inputs such as reservoir porosity (Moore and McCabe, 2004). Sensitivity studies, random sampling, and multiple-scenario runs were used in the discovery-sequence sampling simulation to determine input parameters such as NP, which is the number of accumulations in a simulated parent population. Cumulative uncertainties and ranges of possible outcomes have been captured in the estimation results by presenting undiscovered volumes on cumulative probability plots (Section 3.5.5) and areas of favourable hydrocarbon accumulation are based on probable and possible conditional probabilities (Kemp, et al., 2001) (Section 4.3.3).

5.2 Basin-modelled oil and gas accumulations

5.2.1 Introduction

The basin models described in Section 3.2 are used to create the S_2 dataset of modelled oil and gas accumulations. One of the advantages of using a basin model is the simulated accumulations are based on geological inputs which account for hydrocarbon charge, accumulation and entrapment. The other advantage is volumetric parameters, such as reservoir thickness and porosity, are represented by numerical grids which capture regional trends across a basin. This means the trap volumes (that are therefore based on the regional trends) can be calculated more accurately when compared to more manual approaches that use single location regional depth trends to represent porosity over an a basin, for example.

The main sources of uncertainty, which impact on the number and sizes of modelled accumulations in the Taranaki Basin are associated with modelling primary and secondary migration. These processes are still not fully understood in general (Lerche, 1991; Hermanrud, 1993) including in the Taranaki Basin (King & Thrasher, 1996; Funnell, 2005) and are a challenge to express and model numerically (Schroeder & Sylta, 1991; Wood et al., 1998). The extent of the

modelling limitations is minimised in this study using repeatable model runs and identifying inputs with the greatest impact on the number and sizes of modelled accumulations.

5.2.2 Primary migration

The amounts of oil and gas generated and expelled using Bassim® and used to migrate through the Taranaki Basin in PCE® are greater than the volumetric capacity of the trapping structures modelled for the basin in PCE®. They are based on a total potential oil productivity of 0.11 barrels per cubic metre (bbl/m^3) and gas productivity of 319 standard cubic feet per cubic metre (scf/m^3) for a source rock with a total organic carbon (TOC) content of 4% (Wood et al., 1998). A sensitivity study that used various proportions of these volumes showed that even 10% of the generated volumes sufficiently filled all structural traps at each reservoir level in the basin. Therefore, the uncertainty associated with generating these volumes does not appear to have a first-order impact on the location, number and size of accumulations simulated in PCE®.

Source rock type and abundance, however, do have a first-order impact on the types of hydrocarbons (gas, oil and condensate) that are generated and expelled in Bassim®. This is important because the mix of oil and gas that is migrating through a reservoir will control the proportional amounts of oil and gas that become trapped and the volumes that are calculated for the S_2 dataset.

Taranaki Basin hydrocarbons are sourced predominantly from hydrogen-rich coals (Killops et al., 1994) which present a significant amount of uncertainty to model hydrocarbon generation and expulsion, especially compared to more common marine or lacustrine organofacies (Suggate & Boudou, 1993; Sykes, 2001; Sykes et al., 2004). Firstly, the amount of hydrocarbons generated in Bassim® is directly dependent on the distribution and thickness of coaly source in the model (Wood et al., 1998). Coaly source rocks of the Taranaki Basin, such as the Rakopi Formation, consists of a series of thin and discontinuous coal seams (Sykes et al., 2004) making them a challenge to map. Although this is the major source rock in the Taranaki Basin (Thrasher, 1992; Sykes et al., 2004) only 15 wells have encountered this formation. The discontinuous nature of these coals

may mean that this formation is below seismic resolution in parts of the basin and as a consequence a map showing the distribution and quality of the Rakopi Formation relies heavily on a paleogeographic model.

Secondly, Taranaki Basin coals are lithologically heterogeneous making it difficult to define source rock quality. They also exhibit a deposition-related coastal plain to marginal marine variation in kerogen type (King & Thrasher, 1996) resulting in mixed oil and gas potential in the basin (Sykes et al., 2001). Different types of kerogens will influence the kinetic transformation to oil and gas, which controls the timing and extent of source rock maturation and expulsion (Tissot & Welte, 1984). Different kerogen types within the Rakopi Formation source rocks are represented in the model by a range in hydrogen index (HI). A variation in HI alters the proportions of oil and gas that are produced and makes phase prediction difficult (Sykes et al., 2001; Sykes et al., 2004). Furthermore, HI is determined by Rock-Eval™ analysis (Baskin, 1997) which can overestimate HI results in coal (Killops et al., 1998). This is important because the HI value controls expulsion timing. High-HI source rocks expel oil earlier and more efficiently, whereas low-HI source rocks expel oil later causing oil to crack more readily to gas (Pepper & Corvi, 1995) thereby affecting the types of hydrocarbons that are available for migration in PCE®.

Lastly, oil-generation models for coaly source rocks and type III kerogens are still not as well developed compared to models for type I and II kerogens associated with more common marine and lacustrine source rocks (Funnell, 2005). Historically, Type III kerogens are expected to produce more gas than Type I and Type II (Tissot and Welte, 1984) even though research in some basins, including the Taranaki Basin, confirms the major source of oil is generated from type III kerogens (Sykes et al., 2001).

Kerogen transformation is controlled by a number of kinetic parameters based on different types of kerogen and is determined as a function of depth and temperature (Wood et al., 1998). A comparison of different industry-standard kinetic parameters on a maturity with depth or temperature profile is shown in Figure 5.2. Sensitivity trials of these different kinetic parameters showed that the

volumes generated and expelled in Bassim® can change markedly, depending on which kinetic parameters are used. But, for a given set of kinetics parameters the volumes are less than 90% reduced (Wood et al., 1998).

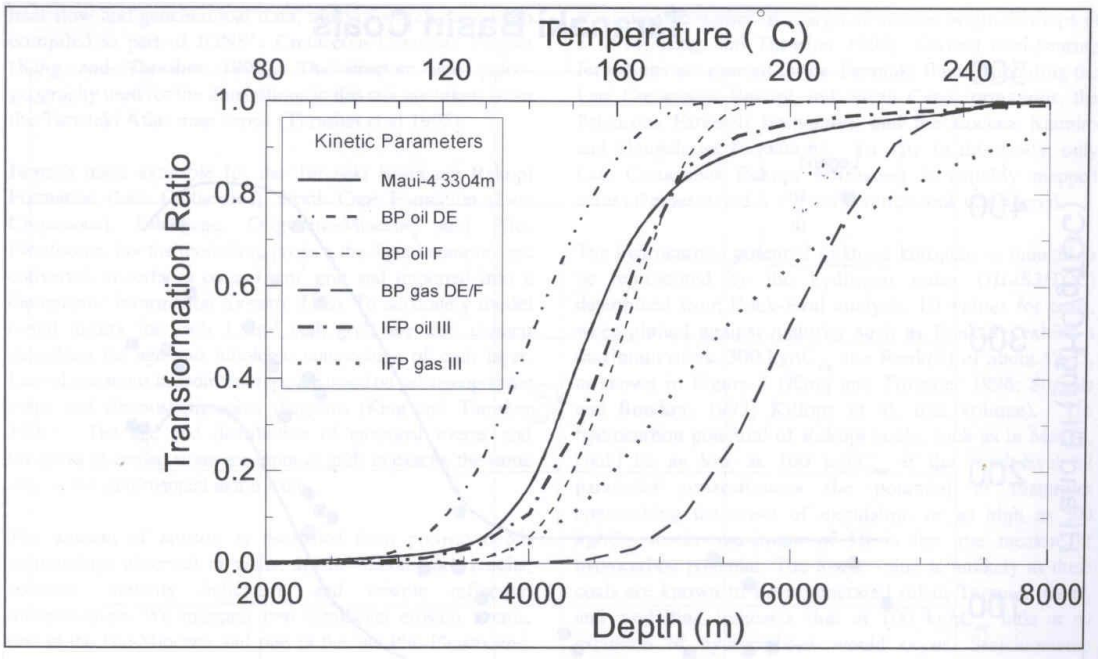

Figure 5.2: Comparison of different kinetic parameters on a maturity with depth or temperature profile. The different kinetic parameters are for (1) bulk hydrogens from a sample of Rakopi Formation, (2) standard Institut Francais de Pondichery (IFP) type III data for oil and gas generation (Tissot et al., 1987) and (3) BP type III data for oil and gas generation from organofacies DE and F (Pepper & Corvi, 1995). Source is Wood et al. (1998).

5.2.3 Secondary migration

Secondary migration is primarily controlled by a number of Petrophysical (e.g. porosity and permeability) and fluid properties (e.g. specific gravity and gas-oil-ratio (GOR)) together with pressure conditions within the reservoir (BP Research, 1995). PCE® is unable to fully account for these and as a result there are a number of uncertainties associated with the PCE®-modelled accumulations.

During secondary migration there is significant loss of hydrocarbons; as much as 90% of generated and expelled oil and gas may not have become trapped, or was trapped but not preserved (England & Fleet, 1998; Sylta, 1987). As a result, only 10% of the volumes generated and expelled in Bassim® are used in PCE® to recognise the uncertainty associated with migration-process loss based on the work of England & Fleet (1998). A sensitivity study, using different amounts of oil and gas in the PCE® model, showed no change in the number of simulated oil and gas accumulations when only 10% of the volumes were migrated through the basin.

The migration of oil and gas in PCE® is particularly sensitive to reservoir porosity and permeability. These two parameters are included in the basin model as deterministic reservoir facies maps (Appendix 12). In reality, the variation in the distribution and quality of the reservoir is much more complex, introducing uncertainty associated with defining effective reservoir. Reduction in porosity and permeability may be caused by compaction, cementation, spatial variation in lithology and tectonic stresses as the basin evolves. These geologic processes are not modelled in PCE® but may have an impact in reality. To minimise any impact the reservoir quality values, such as porosity, were based on empirical porosity data in the basin.

Secondary migration is modelled in PCE® on a single surface and vertical migration from the source rock to this surface is assumed; such that no inter-surface fluid flow is modelled. Migration is effective where reservoir coincides with up-dip flow, based on the structure contour surface at the top of each reservoir interval. However, because a reservoir interval is limited to a single level in the model multi-stacked reservoirs typical of some of the Taranaki Basin Fields (e.g. Kapuni, Maui, Kaimiro, and Ngatoro fields) were not modelled using separate reservoir-seal pairs because of the deficiency

of basin-wide intraformation surfaces. Instead the total reservoir thickness, which is based on reservoirs in known fields, accounts for multiple reservoir-seal pairs.

5.2.4 PCE® correction factors

We saw in Section 3.2.3 that PCE® trap volumes must be recalculated using four correction factors to recognise uncertainties associated with the fullness of a trap and converting reservoir volumes to surface and recoverable volumes.

The uncertainty associated with determining trap fullness is significant because all trapping structures in the Taranaki Basin may not be full to their structural spill-point due to seal integrity (McAlpine & O'Connor, 1998; Darby & Ellis, 2002) and tectonic tilting (Funnell et al., 2005). PCE® is unable to sufficiently model any variability in either seal rock integrity or tectonic tilting (IES, 2000) and a correction factor is used to account for these processes, which vary across the basin (King and Thrasher, 1996). To minimise this uncertainty a fill-to-spill (FTS) correction factor was determined using a dataset of Taranaki Basin column heights to determine seal integrity (shown in Section 3.2.3). Minimum, medium and maximum values were used to represent the range in FTS corrected volumes calculated.

The other three correction factors, which are used to express a PCE® volume at surface conditions, including a formation volume factor, hydrocarbon saturation factor and hydrocarbon recovery factor are based on well data (Section 3.2.3) and minimum, medium and maximum values were used to represent a range in corrected volumes.

5.2.5 Neogene deformation

Neogene tectonic deformation has had a significant impact on hydrocarbon charge and entrapment (King and Thrasher, 1996) as shown in the petroleum systems event chart in Figure 2.6. Most importantly, all proven structural traps have been formed by compressional tectonics and the youngest source rocks reached optimal burial depths to generate and expel hydrocarbons in the last five million years.

However, not all Neogene events were favourable for hydrocarbon accumulation. Compressional tectonics resulted in processes such as seal fracturing and overpressured

reservoir conditions that may be detrimental to preserving trapped hydrocarbons (Darby & Ellis, 2002). PCE® is not capable of forward-modelling tectonic fracturing of topseal or reservoir overpressures, which are potentially important for predicting the accumulation of oil and gas in the Taranaki Basin. Although good topseal and intra-formational seals exist across most of the basin (King and Thrasher, 1996) it is possible that Neogene deformation has reduced seal integrity. However discoveries prove how effective seal is in the basin and suggest present day charge means oil and gas is preserved in traps throughout the basin. To consider the impact of seal integrity, the maximum burial depth of sealing lithologies was used as a control on the distribution of effective seal in the basin, given all hydrocarbon columns within individual reservoirs are <200 m in height (Figure 2.7).

During migration the behaviour and role of faults in the Taranaki Basin are not fully understood (Nicol et al., 2004) and all faults were modelled as impermeable in PCE®. This is based on the observation that all known accumulations in the basin are fault-bounded. PCE® cannot model thrust faults; therefore, any uncertainty associated with the accumulation of oil and gas in thrust zones may mean there are a number of missing accumulations because they were not modelled. This uncertainty impacts the Miocene reservoir play the most because most Miocene reservoirs exist in thrust faulted and folded complexes and form multiple-stacked reservoir zones, as shown in Figure 5.3 (Section 2.3.4). The impact of this uncertainty was minimised by preparing a reservoir map for each reservoir-seal pair.

The thicknesses of missing strata that were calculated for the two significant Neogene uplift and exhumation events (Section 3.2.3, Figure A1, Appendix 15) and input into Bassim® were approximated using the methods described in Section 3.2.3. Because the missing sections impact on the maximum burial depth of source rock they influence the depths at which hydrocarbons were generated and expelled and therefore the amount of mature source rock and amounts generated. As mentioned above, the amounts of hydrocarbons generated and expelled and used in PCE® are greater than the trap capacity, therefore do impact on the number and sizes of accumulations that are modelled.

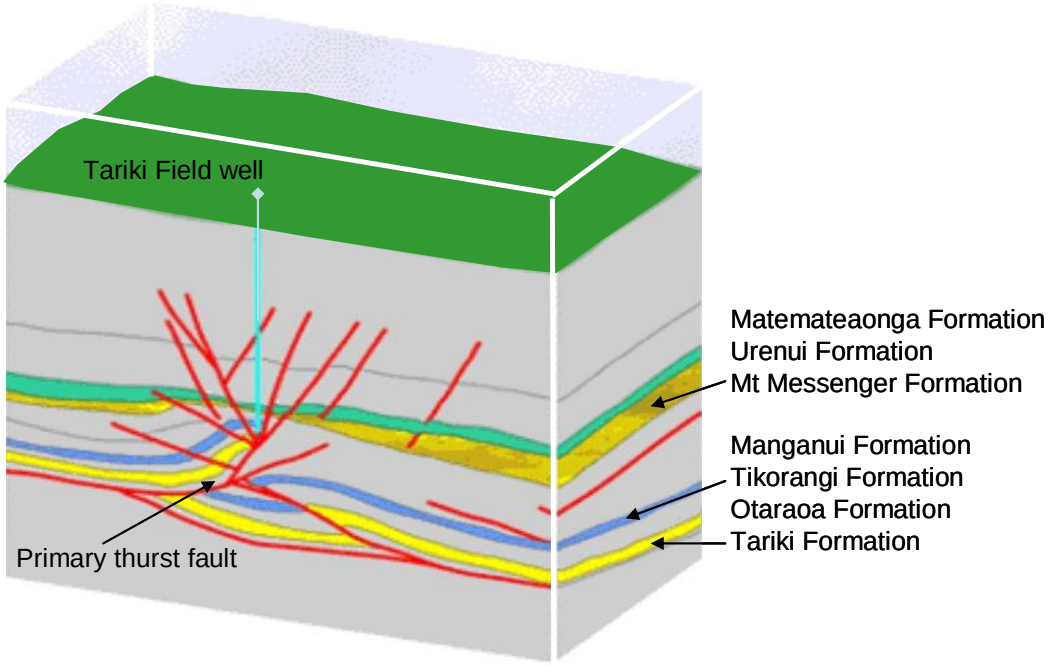

Figure 5.3: Thrust zone within the Tariki Field showing the multiple reservoir horizons as a result of thrust fault compartmentalisation. The trap forms a typical structure found in the Taranaki Basin controlled by a primary thrust fault within a series of splaying faults. The Tariki Formation is the main reservoir in this field and is thickened by over thrusting. Source: Crown Minerals, 2006.

5.3 Structural trap-based oil and gas accumulations

5.3.1 Identifying traps

The S_3 dataset of oil and gas accumulations is based on structural traps (Section 3.3). The quality of this dataset relies on the identification of a structural trap and the calculation of its volume. Structural traps were identified on regional and high-resolution structure contour depth surfaces interpreted from 2D and 3D seismic data. The regional surfaces are expected to reveal the largest anticlinal structural traps, especially in areas of relatively dense seismic data acquisition (Figure 1.3).

The number of structural traps that are identified is considered a minimum because of data resolution and amount of thrust faulting in the basin (Nicol, 2005). A number of high-resolution structure depth maps were compared to a regional structure depth map (Appendix 2) over the same area, such as the Huiroa Bore in Petroleum Report PR1039. Only traps greater than the contour interval of a structure depth map (which was

typically 80-100 m for regional scale maps and 15-20 m for higher resolution maps) could be identified highlighting the limitation of the regional maps. The impact of this undersampling is not known; and although it may be moderately significant based on the comparison of regional and high-resolution maps the largest accumulations were identified.

Known and many undrilled thrust fault-controlled traps were identified on high-resolution maps. However, small structural traps associated with thrust faults may not have been identified because thrust faults are a challenge to image, even with good resolution data (Percher et al., 2004). A number of fields in the Taranaki Basin involve thrust faults, such as the Tariki Field (Figure 5.3). Specific processing can improve the imaging of thrust faults, for example, by using post-stack depth migration (PSDM) (Percher et al., 2004) however these seismic data were not available for this study.

5.3.2 Calculating volumes

The volume of hydrocarbons in a structural trap was calculated using:

$$V_{OHIP} = A * h * \phi * NG * S_{hc} \quad (5.1)$$

where V is volume, A is trap area, h is height or thickness of the reservoir and ϕ is reservoir porosity (in the trap) NG is the net-to-gross percentage of the reservoir and S_{hc} is the hydrocarbon saturation of the reservoir (Sustakoski & Morton-Thompson, 1992) (Chapter 3). Area and height have the greatest impact on the uncertainty of the calculated trap volume.

Each structural trap was digitised into an ArcMap® GIS project and trap area and height were calculated using the triangulated irregular network (TIN) and 3D Analysts tools (Chapter 3). The volumetric uncertainty of each trap is recognised by using a range in values for area and height which are based on a random error of one and two standard deviations associated with digitising the trap and measuring these parameters.

The calculated volume is for a trap filled with hydrocarbons to the structure spill point. Although traps may be underfilled in the Taranaki Basin (Funnell et al., 2001; Funnell

et al., 2004) they are modelled here as full because (as mentioned earlier) there is sufficient present-day hydrocarbon charge in the basin (King & Thrasher 1996; Wood et al., 1998).

5.4 Petroleum systems datagrids

The 10 maps that were prepared to represent hydrocarbon generation, charge and entrapment in the Taranaki Basin and used in the basin model (Chapter 3) and spatial model (Chapter 4) are based on a variety of datasets including 2D and 3D seismic data, structure-contour maps, paleogeographic reconstructions (King & Thrasher, 1996) and down-hole well data and basin modelling results. The main sources of uncertainty associated with their preparation are related to:

- regional-scale data;
- sparse seismic and well data;
- representing variables deterministically;
- proxy data and mathematical approximations; and
- extrapolating analogous data and interpolating where data is absent.

5.4.1 Regional data

The regional structure contour depth maps (Thrasher & Cahill, 1990a & b; Thrasher et al., 1995a, b & c) and paleogeographic maps (King & Thrasher, 1996) used in this study were selected because they are basin-wide and created using a single-velocity model to convert time-based surfaces to depth (Thrasher, 1992). Although these sets of maps have been used in conjunction with well data the petroleum systems maps that are prepared from the regional data, such as source rock quality and reservoir distribution, are general approximations and more detailed data may produce different estimation results.

For example, the Eocene reservoir facies map is based on a regional top Eocene, structure contour depth map, ~300 wells and paleogeographic reconstructions for this time. The resulting facies map (Appendix 10) highlights the Mangahewa Formation coastal sand system, which is represented by a large polygon to indicate where the

reservoir has been deposited. However, any depositional details such as intersecting or amalgamating fluvial channels and channel bars are not represented. As a result, the area of effective reservoir modelled may be too large.

This type of overestimation of reservoir may be even more significant for the Miocene Mt Messenger and Moki submarine fan systems. Well results confirm the presence of submarine fans at the bottom of the slope (de Bock et al., 1991); however, with a small number of wells and limited 2D seismic data, it is difficult to map the turbidite channels, which cut the slope, using the regional data. Consequently, the presence and quality of Miocene reservoir may have a greater level of uncertainty when compared to other depositional systems, such as the Eocene transgressive sandstone. For example, in 2002 four wells drilled the Middle to Late Miocene Mt Messenger, Moki and Mangaa formation levels resulting in hydrocarbon shows in the Hihi-1 and Honeysuckle-1 wells but no hydrocarbons in the Karariki-1 and Karaka-1 wells (Crown Minerals, 2006. Although, hydrocarbons were discovered at the Hihi-1 and Honeysuckle-1 wells they were abandoned as non-commercial mainly due to the insufficient thickness of the sandstones. Similarly the Maketawa-1 seismic amplitude anomalies in upper Mt Messenger sandstone units, and AVO analysis indicated the likely presence of hydrocarbons. However, this well was not a successful discovery because the high quality reservoir sandstone filled channel that was predicted was mud filled and only poor reservoir was encountered (Crown Minerals, 2006).

5.4.2 Well data

The quality of the datagrids is constrained by the paucity of well data. Only ~ 500 wells have been drilled over the 100,000 km^2 study area and in some areas there is very little or no well data available (Enclosure 1 & Figure 1.2). For example, only eight wells have penetrated Late Cretaceous rock intervals (Enclosures 1 & 2); therefore, the thickness of this potential reservoir across the basin is essentially unknown and is primarily based on seismic interpretation and paleogeographic models.

5.4.3 Proxy data

Proxy depth maps were used to represent the depth at the top of the Paleocene and Miocene reservoir plays. The methods used to create these two surfaces are described

in Section 3.2.3. The maps were used to define present day gradients for secondary migration and calculate reservoir porosity and maximum burial.

The Paleocene play surface has less uncertainty associated with it than the Miocene play surface because it is structurally similar to the Eocene and Cretaceous surfaces and was created using an isopach interval between these two. Due to a change in tectonic regime and Neogene deformation (Section 2.2) the Miocene play surface could not be prepared using this approach.

In contrast, the intra Miocene surface is based on the top Miocene structure contour map which is not structurally representative of the intra Miocene and covers the offshore area only. Even though facies maps of the Mt Messenger and Moki formations were used to constrain the proxy depth map for the top intra Miocene surface it may carry a greater level of uncertainty than the Paleocene proxy surface. Neogene reservoirs are formed in complex depositional environments which typically include intersecting and amalgamating channels (Walcott, 1984: Thrasher et al., 1995e). Within the channels pockets of sandstones are found stacked within and between formations. These reservoirs subsequently have a greater lateral and vertical variability, especially compared to other depositional systems such as a delta top system.

5.4.4 Numerical approximations

The reservoir porosity datagrid is calculated as a function of compaction (Figure 3.2) using equation 3.2 and an initial depositional porosity of 45% (Figure 3.2, Section 3.2.3)

An empirical regression curve, using well porosity data, was not used instead of the predicted porosity surface because of the lack of wells with porosity data across the basin. However, the predicted porosity trend was compared to well porosity data (mostly core porosity) from a number of wells in the basin and falls within two standard deviations of measured ranges. The uncertainty associated with this reservoir porosity is expressed by using medium porosity values relating to the reservoir depth. As can be seen in Figure 3.3, porosity values have a large range in values for most of the Taranaki Basin wells, and the best-case (P50) predicted porosity trend falls well within most of the porosity ranges.

5.4.5 Deterministic datagrids

This study used only one interpretation of each input map. Although the use of a range of possible outcomes is a systematic way to account for uncertainty (Moore & McCabe, 2003) this practice is not always a better way of minimising uncertainty. For example, a map showing the distribution of reservoir which has been interpreted using down-hole well and seismic data and paleogeographic reconstructions represents only one scenario of many other interpretation possibilities, especially if the data are sparse. However, without further data the fabrication of multiple reservoir distribution maps to represent other possible interpretations may not be any more objective, especially if the constraints of the data you have cannot be used to produce further high confidence possibilities.

The petrophysical parameters that are used to create the reservoir porosity, topseal capillary entry pressure and reservoir thickness, are best-case or mean values based on empirical data and theoretical relationships. The variability of these input parameters across the basin for each reservoir interval is essentially unknown; therefore, it is unlikely that high- and low-case model runs of these parameters would have provided a better evaluation for a basin-wide study. For example, reservoir porosity values from core samples (mentioned above) were used to evaluate the predicted reservoir porosity datagrids and high and low initial depositional porosities of 35% and 55% did not represent the range in empirical reservoir porosity values any better.

5.5 Discovery-sequence simulation

The main sources of uncertainty associated with the inverse discovery-sequence sampling simulation relate to:

- the use of a probability distribution function to approximate the size distribution of a parent population of all oil and gas accumulations in a basin;
- discovery process assumptions discussed in Section 3.7;
- using basin-modelled and structural trap-based accumulations to represent potential discoveries of the unexplored areas of a basin ; and
- deterministic inputs.

This study uses both a lognormal and a power-law probability distribution function to approximate the size distribution of a parent population of oil and gas accumulations to examine the uncertainty related to the choice of statistical approximation. The use of a lognormal probability distribution function is more common than a power-law function such as the Pareto probability distribution function (Laherrere, 1997) and although both are acceptable (Attanasi & Charpentier, 2002) they do produce different results (as shown in Appendix 11). In particular, the lognormal distribution has a tendency to generate a greater number of large oil and gas accumulations than the Pareto distribution and as a result the Pareto distribution is preferred in this study.

The values used for a_1 (largest accumulation) and a_0 (smallest accumulation) to truncate the parent population (Section 3.5.4) are represented by deterministic values. Therefore, as part of the simulation workflow ranges in values were trialled in multiple runs to determine the impact of ranges in values on the size distribution of the simulated discoveries (Chapter 4). For example, a_1 should be larger than the largest discovery but no larger than the largest trapping structure identified in a basin. However a_1 may be > than the largest identified trap, therefore a range in a_1 values should be examined.

5.6 Spatial component

The main sources of uncertainty associated with the spatial component are related to the preparation of the 10 map-based datagrids and the assumptions and limitations of the ESRI Spatial Data Modeller® software. This software uses uncertainty statistics and maps to account for both of these sources of uncertainty.

As we saw in Chapter 4, the spatial model estimates the likely location of undiscovered oil and gas using a weights-of-evidence (WoE) method. The main criticisms of this approach (Kemp et al., 2001) is that predictions of hydrocarbon favourability are underestimated in areas where there are low levels of data (Bonham-Carter, 1994). This problem is also common in other data-driven models (Ganguli & Dandopadhyay, 2003). In this study the effects of data paucity was minimised by populating areas of fewer discoveries with potential discoveries based on basin modelling and mapping structural traps (Section 3.1). This approach of combining actual and modelled discoveries together boosts the number of locations of hydrocarbon accumulations being modelled,

which increases the statistical confidence of the spatial calculations especially in areas where there would otherwise be very few or no data.

5.6.1 Weights of Evidence (WoE) statistics

As part of the Bayesian WoE calculations in the spatial model, two different uncertainty statistics are generated: the standard deviation (SD) of a weight, s(W) and a Studentised confidence contrast, s(C) (Bonham-Carter, 1994). s(C) is a measure of the uncertainty with which the contrast (between an evidential theme map pattern and locations of oil and gas accumulation) is known and is calculated as C/s(W) where C is the contrast strength and W is a weight (Chapter 4). s(C) is used as an informal test for the hypothesis that C = 0, which means there is no contrast between the map pattern and the locations of oil and gas accumulation (Bonham-Carter, 1994) (Chapter 4). A large ratio for s(C) typically >1.5, implies the contrast is much greater than the SD, suggesting the contrast is likely to be real (Bonham-Carter, 1994). However, the s(C) value is best used as a relative test because of the assumptions required for a formal statistical test. In particular, s(C) values can be dependent on the units of measurement (Bonham-Carter, 1994). If the weights vary significantly, an associated uncertainty map can be calculated to see where the impact of the variation occurs.

The WoE tool calculates the uncertainty associated with the weights assigned for each spatial correlation relating to input data quality such as a variation in the amount of data across an area (Sawatzky et al., 2004). The calculated uncertainties are shown in a table and as an uncertainty map, which shows where the results of hydrocarbon favourability have greater or lesser certainty.

5.6.2 Conditional independence (CI)

CI is a statistical test, using the Chi-squared (χ^2) test statistic, to determine the independence of each input, such as source rock thickness, used in the spatial model. The test is important because maps that are dependent on each other and subsequently violate CI cause the calculated posterior probability to be overestimated (Section 4.3.8). This does not mean the resulting predictive map (that is based on each input map) is incorrect, but rather the results should be interpreted relative to this knowledge. In this study, three evidential theme maps, including amounts of oil and gas generated and

expelled and migration flowpaths, displayed high Chi-squared (χ^2) values. They were all, however, included in the spatial analyses because although the distribution maps of these three themes are spatially similar their geological significance warrants their individual inclusion.

5.7 Conclusions

The methodology used to estimate undiscovered oil and gas in this study is specifically adapted to the Taranaki Basin by including potential discoveries (S_2 and S_3 datasets discussed within) in addition to actual discoveries (S_1 dataset) in order to primarily represent unexplored and geologically prospective areas. Potential discoveries are also included to minimise the statistical effects of limited discovery data and ensure the size distribution of the parent population leads to an insightful estimate of the resource potential.

The main sources of uncertainty associated with generating the potential discoveries are due to techniques used to identify those using regional datasets, proxy data, and geological inference, and basin modelling software.

To recognise and minimise the impact of the uncertainty associated with regional data a non-deterministic approach has been used and cumulative uncertainties and ranges of possible outcomes have been captured in the results by presenting the undiscovered volumes on cumulative probability plots. Similarly, maps showing areas of favourable hydrocarbon accumulation are presented using probabilistic techniques.

The use of regional structure contour maps may mean that a number of small traps have not been identified and included in the potential accumulations datasets. For example, it is assumed that the largest accumulations were identified. However, a large structural trap may have a smaller closure or be compartmentalised into two or more discrete structural traps, which may not be obvious at the scale of the maps that were used. As such, there may be a greater number of smaller accumulations in the basin than have been estimated.

A reduced number of small accumulations may statistically affect the mean of the parent used in the discovery sequence sampling simulation, depending on how many small accumulations have not been included (as discussed in Section 4.2.2) Any effect on the parent will have a direct impact on the estimated size distribution of the undiscovered population and in this case would

The limitations of the assumptions made to model hydrocarbon charge, accumulation and entrapment in a geologically complex basin have been evaluated by calibration using known discoveries. The basin modelling results are geologically constrained by the petroleum systems maps that are used in the hydrocarbon generation, accumulation and entrapment model. To minimise other areas of uncertainty during the basin modelling, such as those associated with input parameters like the quality of source rock, different input ranges were trialled and multiple simulations were carried out to understand the sensitivity of the modelled accumulations to the input parameters.

The S_2 and S_3 datasets have the greatest influence on the size distribution of the parent population, which is defined in the discovery-sequence sampling simulation and used to estimate the undiscovered portion. To understand how the S_2 and S_3 datasets and sampling mechanics affect the size distribution of the parent population at least 10,000 simulations were run for each set of input parameters and a mean parent population was used to calculate the undiscovered portion.

Some sources of uncertainty do not have a first-order effect on the number and sizes of accumulations in the parent and undiscovered populations. For example The total trap volume represented in PCE® is less than the Bassim® volumes that were migrated through the Taranaki Basin model, therefore the uncertainties associated with Bassim® are not expected to have a direct effect on the number and sizes of PCE® modelled accumulations.

Chapter 6

Using the Dual Component Estimation to assess the undiscovered oil and gas resource potential of the Taranaki Basin, New Zealand

Abstract

Estimation results indicate there is ~1500 oil and gas accumulations that remain undiscovered in the Taranaki Basin study area of 100,000 km^2 (Figure 1.3) totalling a resource potential of 8210–10800 mmboe. The next discovery could be as large as or greater than the Maui A accumulation (with a 10% probability) which is the largest discovery in the basin, containing 533 million barrels of oil equivalent. The most likely size of the next discovery is equal to or greater than 50 mmboe (with a 90% probability) which is a commercially-significant size for this basin.

Undiscovered oil and gas is estimated throughout a large part of the basin; onshore and offshore and within all four major, Late Cretaceous to Miocene reservoir intervals. The Eocene reservoir play is estimated to be the most prospective. New discoveries in this play are most likely to be located along the eastern margin of the basin from nearshore in the south and up to an offshore area within the Northern Graben, in the nearshore and onshore margin of the western peninsula area, and in two offshore areas immediately east of the Maui Field and where the Toru-1 well was drilled. The next discovery in this play may be as large as 350 mmboe (with a 10% probability) but more likely, it will be equal to or greater than 35 mmboe (with a 90% probability).

New discoveries in the Paleocene reservoir play are likely in the Manaia anticline and Western Platform areas and onshore eastern margin of the basin. In this play there is a 10% probability a discovery will be equal to or greater than 470 mmboe; more likely it will be equal to or greater than 40 mmboe (with a 90% probability). A discovery in the Miocene reservoir play is most likely in the onshore peninsular area,

offshore in the Northern Graben and immediately west of the Taranaki Peninsula. A discovery in this play has a 10% probability of being at least 550 mmboe but has a much greater chance, with a 90% probability, of being equal to or greater than 55 mmboe. The estimation suggests there is a good chance, with a 90% probability, that the first discovery in the Cretaceous play may be at least 50 mmboe. It could also be much larger because this play has a 10% probability of a new discovery being at least 500 mmboe.

The estimated undiscovered resource potential presented here is greater than previously reported because the assessment methodology is specifically modified for the basin, given a large part of it is underexplored and geologically prospective. Basin-wide petroleum systems data and modelled accumulations have been included in the analyses resulting in an estimated original population of all oil and gas accumulations in the basin that has a significant geological basis, as well as a statistical one.

6.1 Introduction

This chapter presents an estimation of the amount and the most likely location of undiscovered oil and gas for the Taranaki Basin as assessed by the Dual Component Estimation (DCE).

As we saw in Chapter 2 the basin has excellent geological potential to contain additional oil and gas because there are multiple reservoirs, more than one working petroleum system, a variety of traps and sufficient present day charge. The following section recaps the key geological aspects from Chapter 2 to emphasise the main assumptions that have influenced the estimates.

1. All hydrocarbons are located within the four reservoir plays identified in this study, which include reservoirs of the Late Cretaceous Pakawau Group fluvio-deltaic sandstones and coal measures (Thrasher et al., 1995a,b) the Paleocene shoreline Farewell Formation (Thrasher et al., 1995c) the Eocene coastal plain Kaimiro, Mangahewa and McKee formations (Thrasher et al., 1995d) and the Middle to Late Miocene Mt Messenger and Moki formations (Thrasher et al., 1995f);

2. All hydrocarbons have originated from one or more of five identified Late Cretaceous to Late Eocene source rock formations (Cook, 1987; Johnston et al., 1990, Killops et al., 1994; Manzano-Kareah, 2004) and source rocks are located in close proximity to each other and trapped hydrocarbons (Wood et al., 1998);

3. All hydrocarbons are predominantly trapped structurally (King & Thrasher, 1996);

4. Effectual expulsion occurred in the last 5–10 million years (Wood et al., 1998); and

5. All hydrocarbon accumulations in the basin are considered to be part of a homogeneous original population based on source rock origin and the timing of charge.

The basin results are presented first. They were modelled by amalgamating the petroleum systems maps and S_1, S_2 and S_3 datasets for each play and running the discovery-sequence simulation and spatial model for the basin. The results for each reservoir play follow in separate sections.

Only the volumetric estimations that are based on a Pareto parent population are presented in this chapter. As we saw in Section 3.5 lognormal and power-law probability distribution functions are typically used to estimate undiscovered oil and gas. However, the Pareto function is preferred in this study, to approximate the parent of the undiscovered portion, because it generates a more realistic number of large accumulations. The lognormal function generated a significant number of large accumulations that were geologically unfeasible leading to excessive total undiscovered volumes. A comparison of the two distributions is shown in Appendix 11.

In this study, the parent and undiscovered populations are modelled using the sampled population of evaluated structural traps, S_{3ii} (Section 4.2.2). This involves using the size distribution shape factors of the S_{3ii} sample to constrain the size distribution of the parent. For example the largest trap-based accumulation in S_{3ii} is used to constrain the largest accumulation in the parent. The following section presents histograms of S_{3ii} and the other three sampled populations that were examined as part of this study (S_1, S_2 and S_{3i}) to demonstrate why S_{3ii} is used. The number of accumulations in each sampled population is shown in Table 6.1.

Number of accumulations in a sampled population				
	S_1	S_2	S_{3i}	S_{3ii}
Cretaceous	0	23	86	53
Paleocene	3	15	78	62
Eocene	21	23	204	122
Miocene	9	25	171	101
Basin	33	86	539	338

Table 6.1: Number of oil and gas accumulations in each sampled population for the Taranaki Basin and each reservoir play. S_1 is the sample of discoveries > 1mmboe, S_2 is the sample of basin-modelled accumulations, S_{3i} is the sample of all identified structural traps and S_{3ii} is the sample of charged structural traps.

The S_1 dataset of 33 discoveries in the basin is undersampled as shown by the frequency histogram in Figure 6.1a suggesting a number of accumulations <512 mmboe remain undiscovered. A well-sampled population for the basin would include more discoveries in all bin sizes especially around the modal size as illustrated in Figure 3.5. A time-increment histogram (Section 3.4.1) for the basin shows how extreme the undersampling is (Figure 6.2). Compared to Figure 3.5b, the Taranaki Basin shows an erratic histogram pattern and undersampling occurs mostly in bin sizes 8–256 mmboe.

The S_2 dataset for the basin includes 86 basin-modelled accumulations (Figures 6.3–6.6). Input maps that were used in PCE® (Section 3.2.3) to generate these accumulations are presented in Appendix 12 and the associated volumes are shown in Table A1, Appendix 13. The frequency histogram for the basin shows a strong, bell-shaped curve around a central mode of 64–128 mmboe (Figure 6.7e). Histograms of S_2 for each of the plays show a variety of statistical forms and modal sizes vary from 8–16 mmboe for the Cretaceous play, 16–32 mmboe for the Paleocene play, 64–128 for the Eocene play and 32–64 and 128–256 mmboe for the Miocene play (Figures 6.3a–d). Undersampling exists for all bin sizes <64 mmboe, suggesting many small accumulations were not simulated by the PCE® basin model.

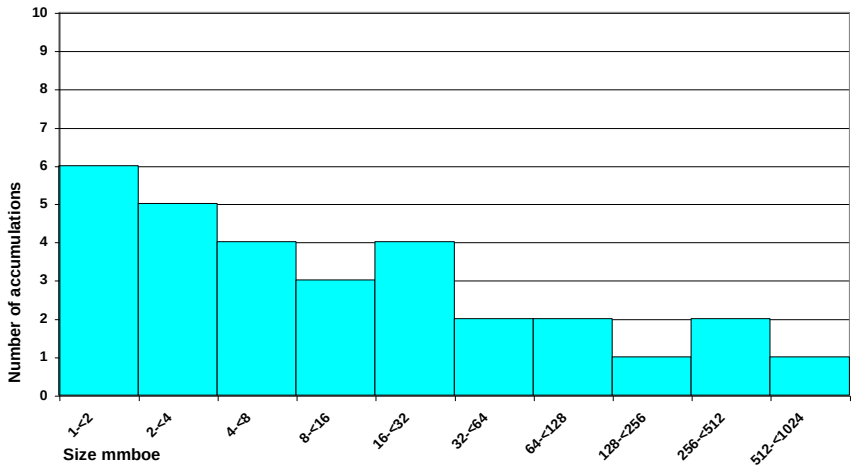

(a)

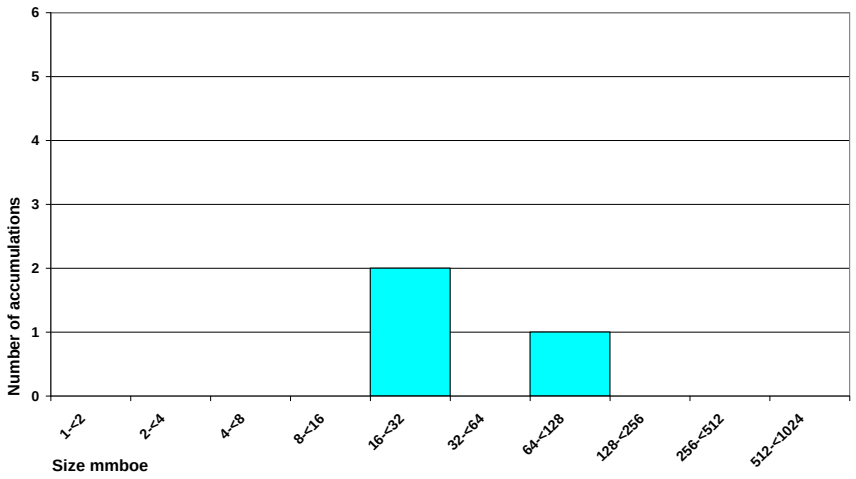

(b)

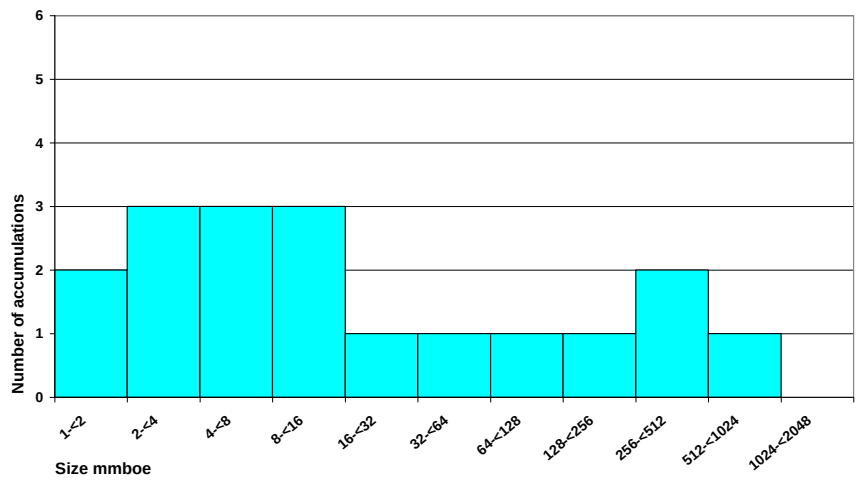

(c)

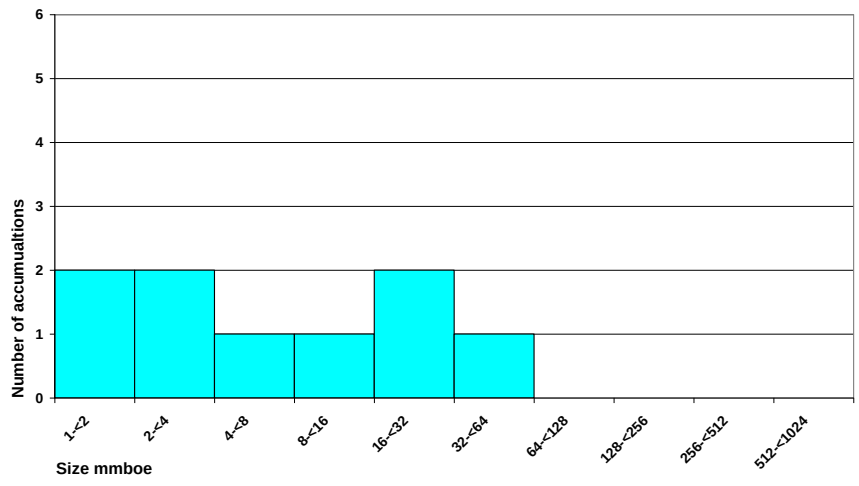

(d)

Figure 6.1: Size-frequency histograms of S_1, of known oil and gas accumulations with reserves >1 mmboe for (a) the Taranaki Basin, (b) the Paleocene play; (c) the Eocene play; and (d) the Miocene play. Maui is treated as two separate accumulations: the Maui A reserves; and the Maui B and F and D sands reserves.

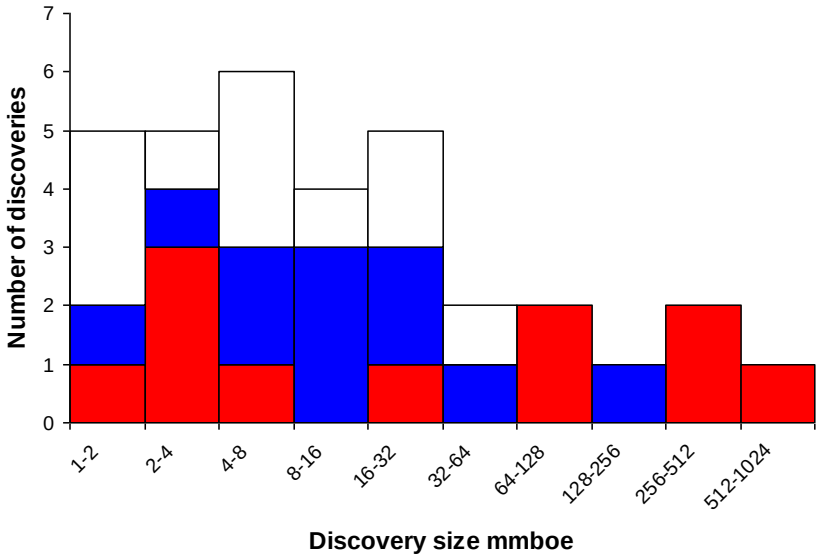

(a)

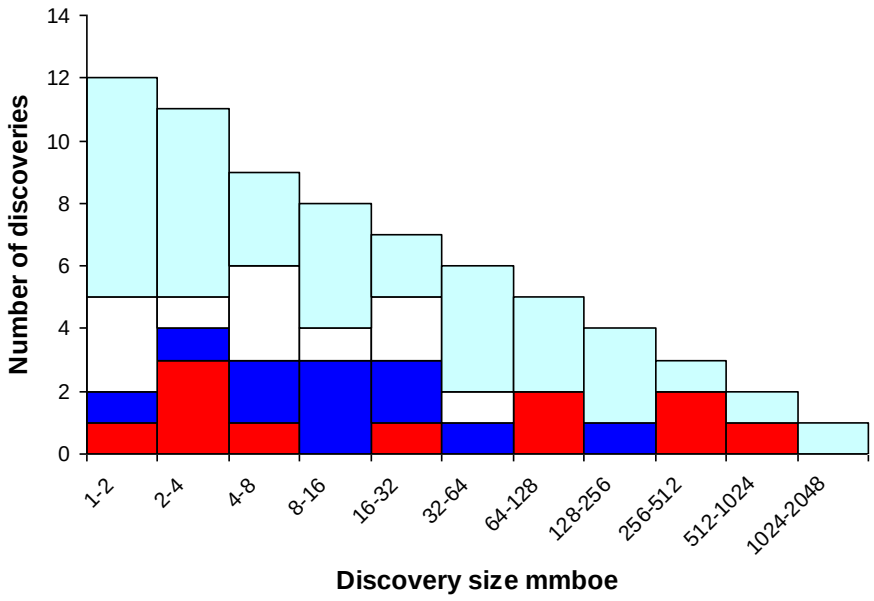

(b)

Figure 6.2: a. Time-increment size-frequency histogram of discoveries made in the Taranaki Basin, using the S_1 population. The red coloured discoveries date from 1959–1987, the blue coloured discoveries date from 1987-2000 and the white coloured discoveries date from 2000 to 2006. b. Light-blue discoveries are theoretical based on the log-geometric methods used to calculate the number of missing discoveries in a basin and a discovery greater than the Maui accumulation of ~874 mmboe.

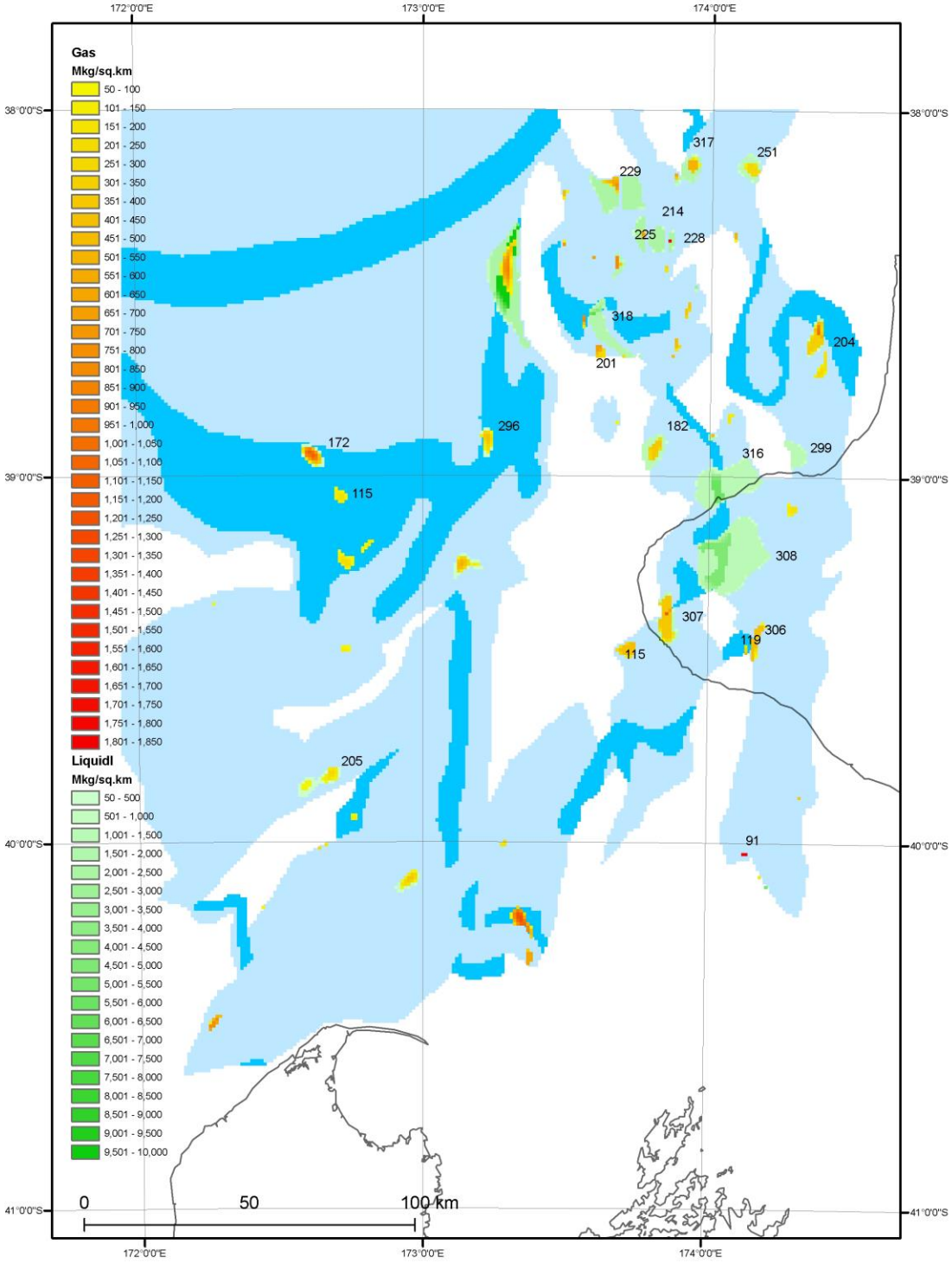

Figure 6.3: Map showing the locations of the basin-modelled oil and gas accumulations for the Late Cretaceous play. The numbered accumulations are the evaluated accumulations and accumulation volume is Mkg/km2 (Appendix 13, Table A1). The dark blue shows the distribution of Late Cretaceous transgressive shoreline sandstones and the light blue shows the distribution of Late Cretaceous lower coastal plain sandstones.

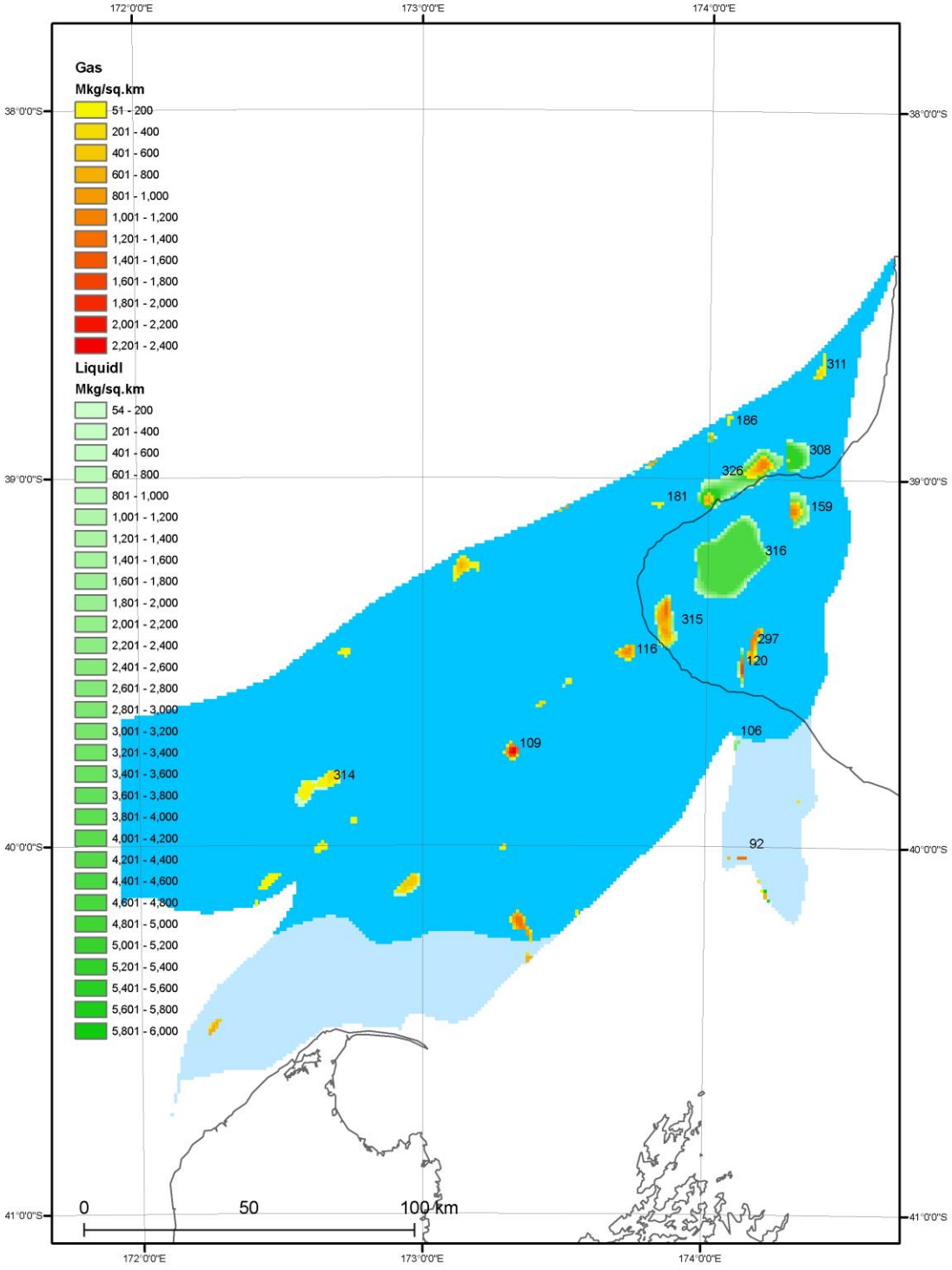

Figure 6.4: Map showing the locations of the basin-modelled oil and gas accumulations for the Paleocene play. The numbered accumulations are the evaluated accumulations and accumulation volume is Mkg/km^2 (Appendix 13, Table A1). The dark blue shows the distribution of Paleocene transgressive shoreline sandstones and the light blue shows the distribution of Paleocene fluvial sandstones.

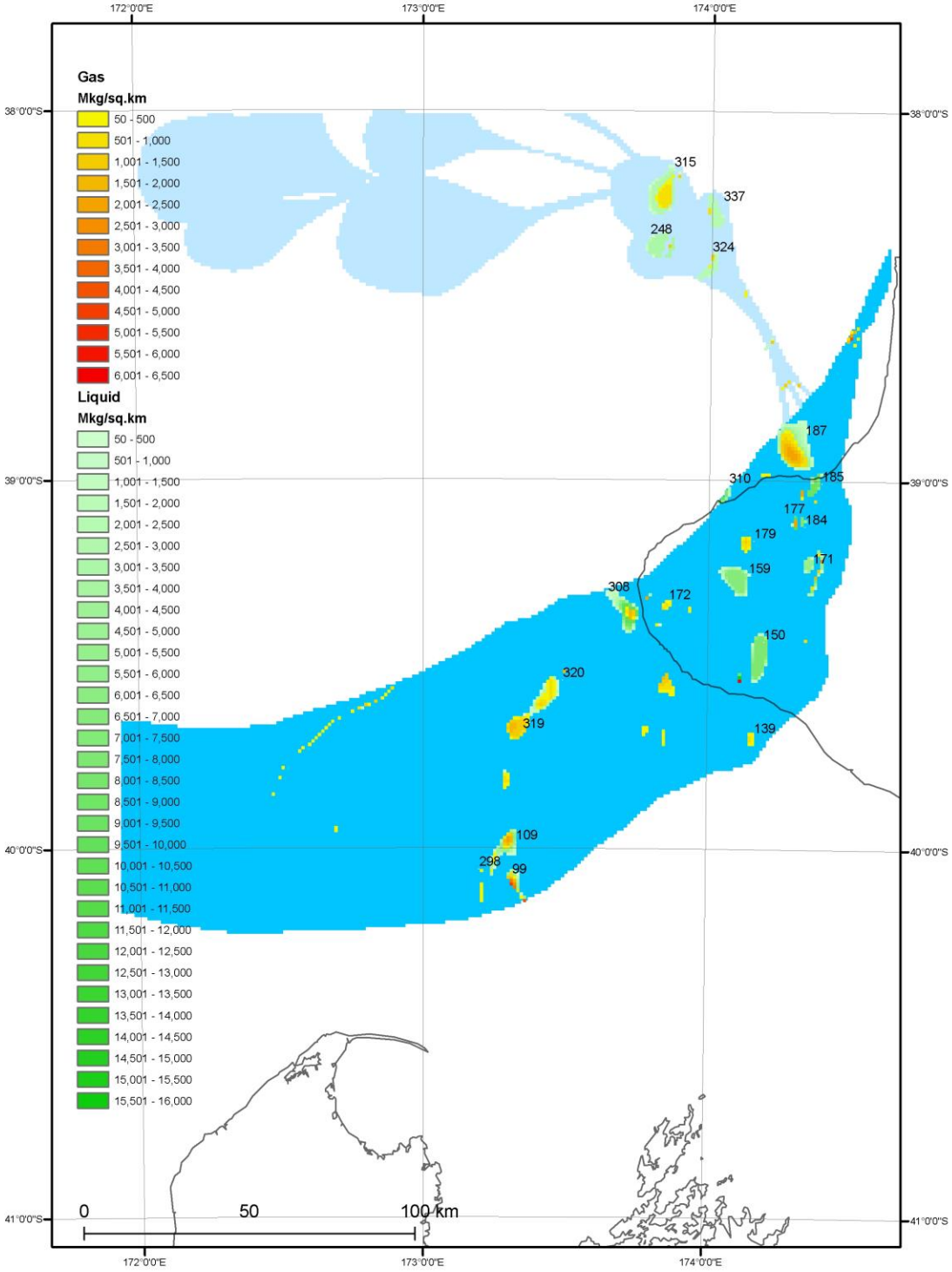

Figure 6.5: Map showing the locations of the basin-modelled oil and gas accumulations for the Late Eocene play. The numbered accumulations are the evaluated accumulations and accumulation volume is Mkg/km^2 (Appendix 13, Table A1). The dark blue shows the distribution of Eocene coastal plain and transgressive shoreline sandstones and the light blue shows the distribution of Eocene submarine turbidite sandstones.

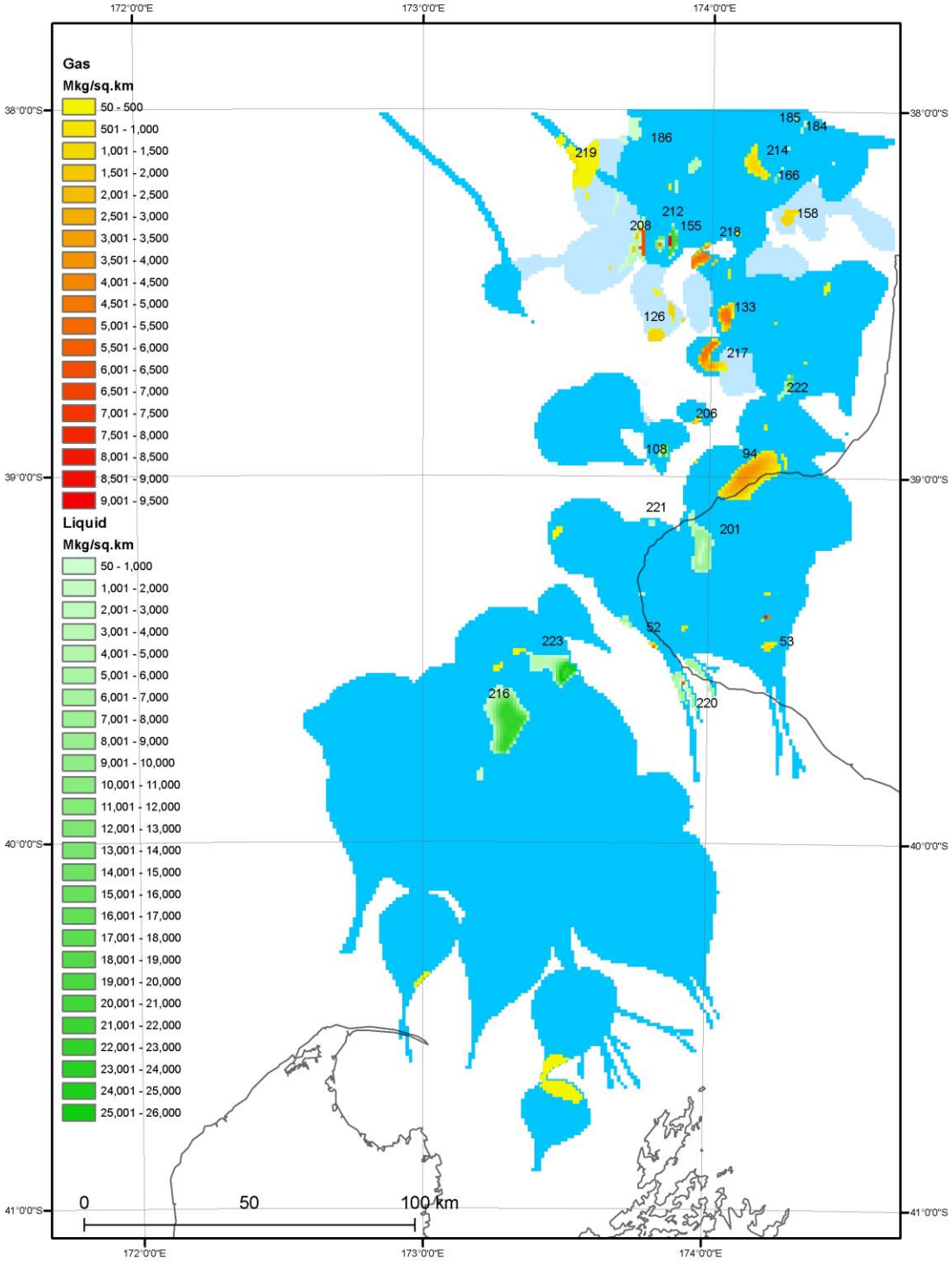

Figure 6.6: Map showing the locations of the basin-modelled oil and gas accumulations for the Miocene play. The numbered accumulations are the evaluated accumulations and accumulation volume is Mkg/km^2 (Appendix 13, Table A1). The dark blue shows the distribution of Mid Miocene Moki Formation and Late Miocene Mount Messenger Formation sandstones. The light blue shows the lateral extent of volcaniclastics.

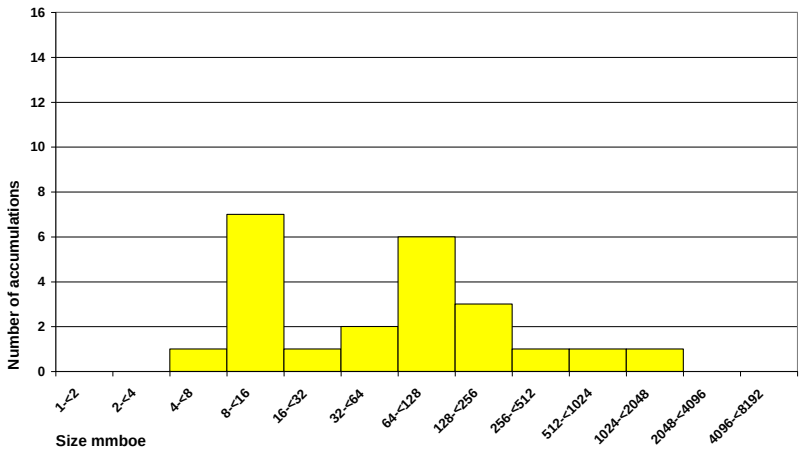

(a)

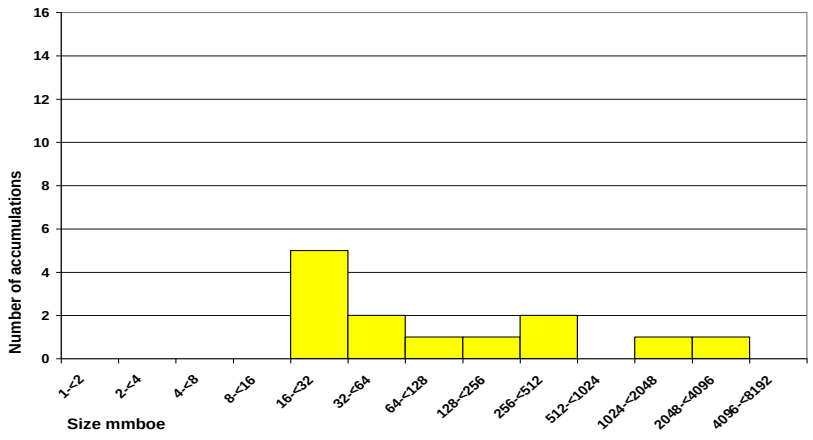

(b)

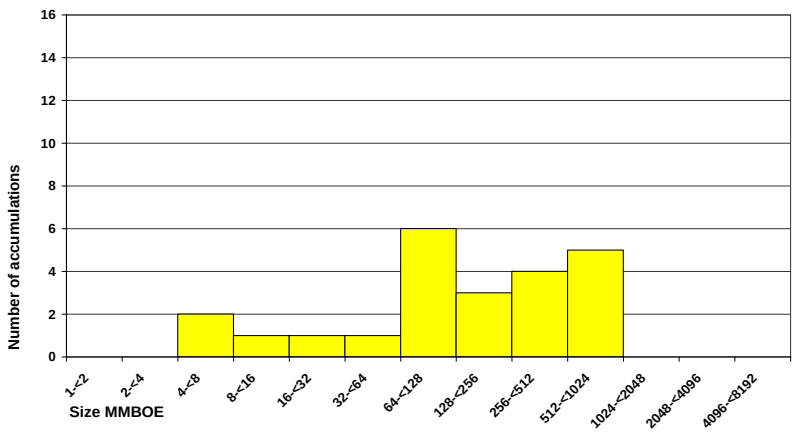

(c)

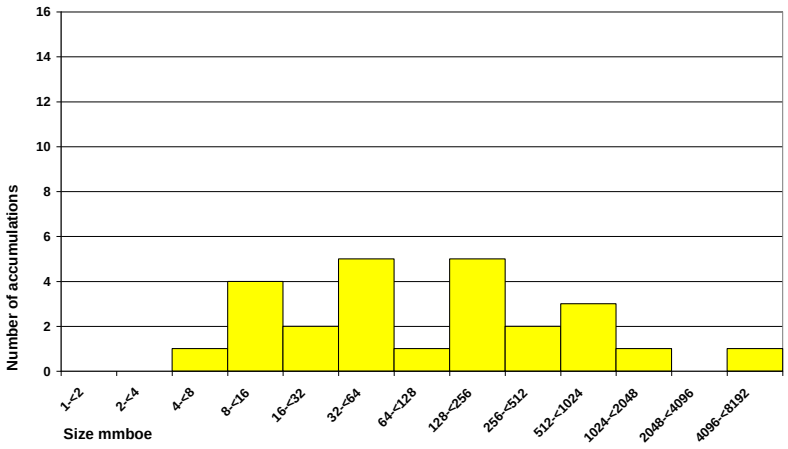

(d)

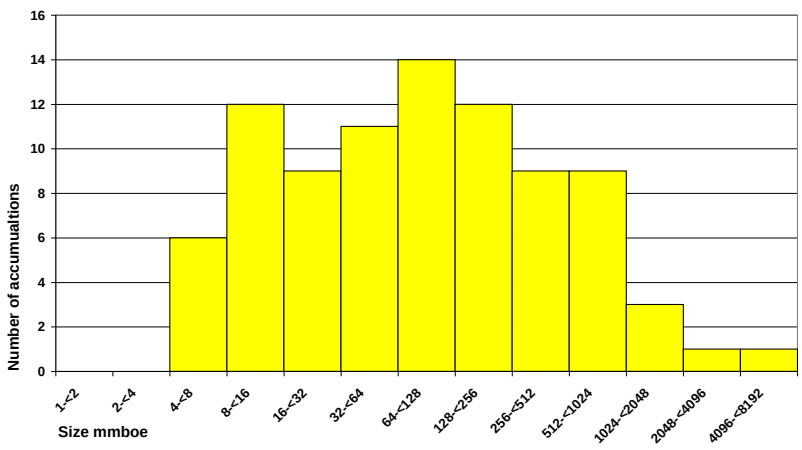

(e)

Figure 6.7: Size-frequency histograms of the sampled populations of basin-modelled accumulations, $S_{2,}$, for each of the plays: (a) Cretaceous; (b) Paleocene; (c) Eocene; (d) Miocene; and (e) the basin.

The 539 unevaluated structural traps that make up the S_{3i} dataset for the basin (Figures 6.8–6.11) are based on the top- Cretaceous, Paleocene, Eocene and Miocene structural surfaces (Appendix 2). The histogram of S_{3i} (Figure 6.12e) has a strong, bell-shaped form and a mode of 32–64 mmboe with 68% of the accumulations within one standard deviation and 95% within two standard deviations of the mean, indicating a statistically stable dataset (Moore and McCabe, 2003). Histograms for each of the plays are less stable and modes vary; 256–512 mmboe for the Cretaceous play, 16–32 mmboe for the Paleocene play, 32–64 mmboe for the Eocene play and 4–8 mmboe for the Miocene play (Figure 6.12b–d). The Eocene play is relatively stable and similar to the basin. Large accumulations are well sampled for the basin and the Cretaceous, Eocene and Miocene plays. The erratic form of the Paleocene histogram is attributed to the paucity of Paleocene-level traps and use of a proxy top Paleocene structure contour surface to identify traps at this level.

The set of evaluated structural traps, S_{3ii} includes traps with the highest probability of containing hydrocarbons and are those that become charged in the basin model (Section 3.1). All histograms of S_{3ii} exhibit a strong, bell-shaped form and are unimodal (Figure 6.13a–d). Although the S_{3i} sample for the basin has the greatest number of accumulations and is the most statistically stable (Figure 6.14) the S_{3ii} sample is used to model the parent for the basin and each play because it too is statistically stable, however includes traps that are expected to contain oil and gas.

Input parameters (NS, a_{mean}, a_0, a_1, NP) used in the discovery-sequence simulation to draw a sample of discoveries with a size distribution similar to S_{3ii} in order to define the most representative parent population (as described in Section 4.2.2) are shown in Table 6.2. They are the result of an iterative try–and–test process and correspond to a mean parent population. An exponential (γ) of 2 +/- 0.5 was used in all simulations because sensitivity tests showed that $\gamma > 1.5$ and < 2.5 produced stable results. The multiple trials resulted in a range of parent population distributions, however only the mean parents are presented in this chapter. Output graphs of the mean drawn sample and the associated mean parent are presented as frequency histograms and the amount of undiscovered oil and gas is shown on a cumulative size-probability distribution plot (Section 3.4.5).

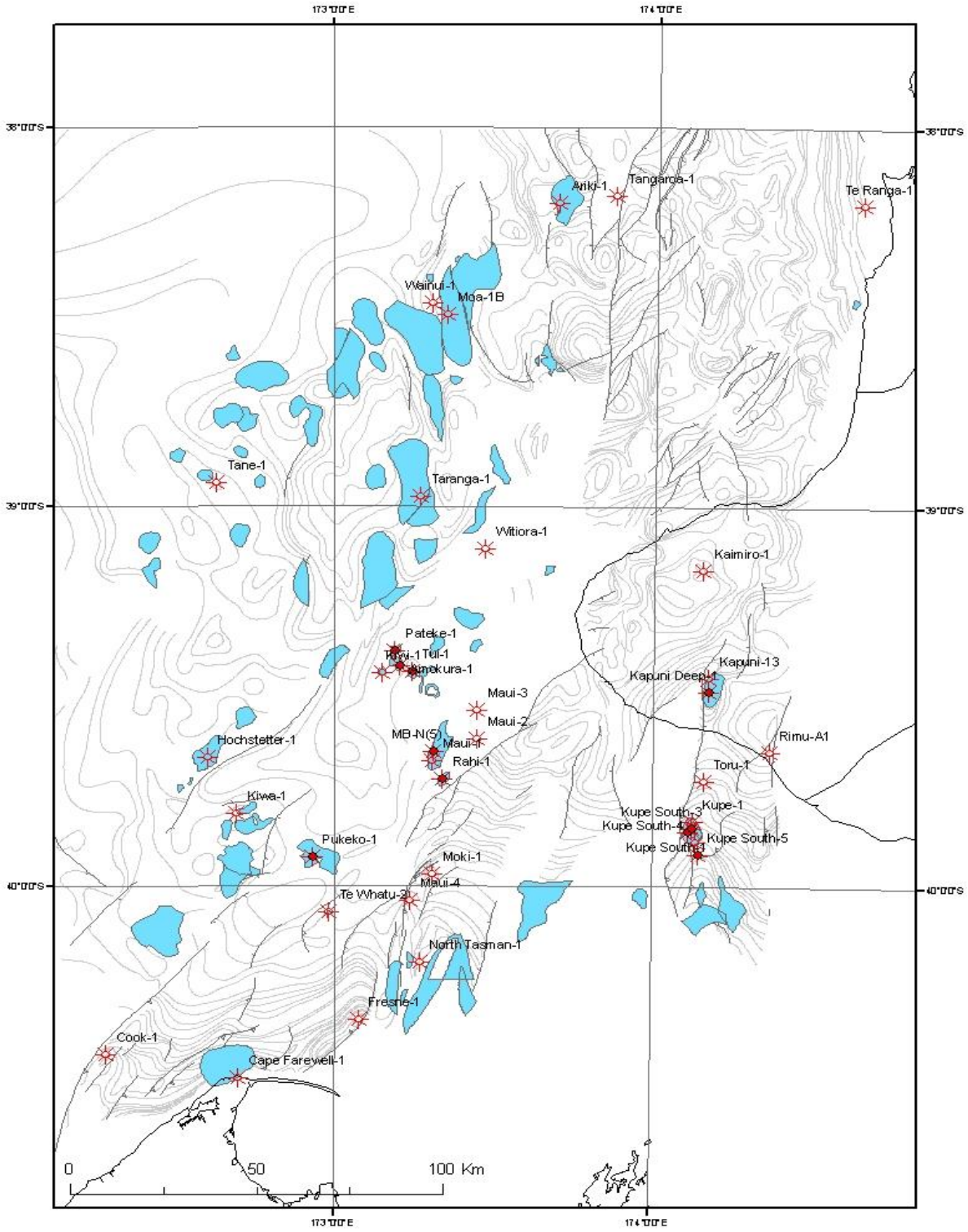

Figure 6.8: Map showing the structural traps used in the sampled population of unevaluated mapped traps (S3i), for the Cretaceous play. The traps are shown on the top Cretaceous structural contour depth surface and with regional-scale top Cretaceous faults. Wells shown have encountered Late Cretaceous age reservoir lithologies.

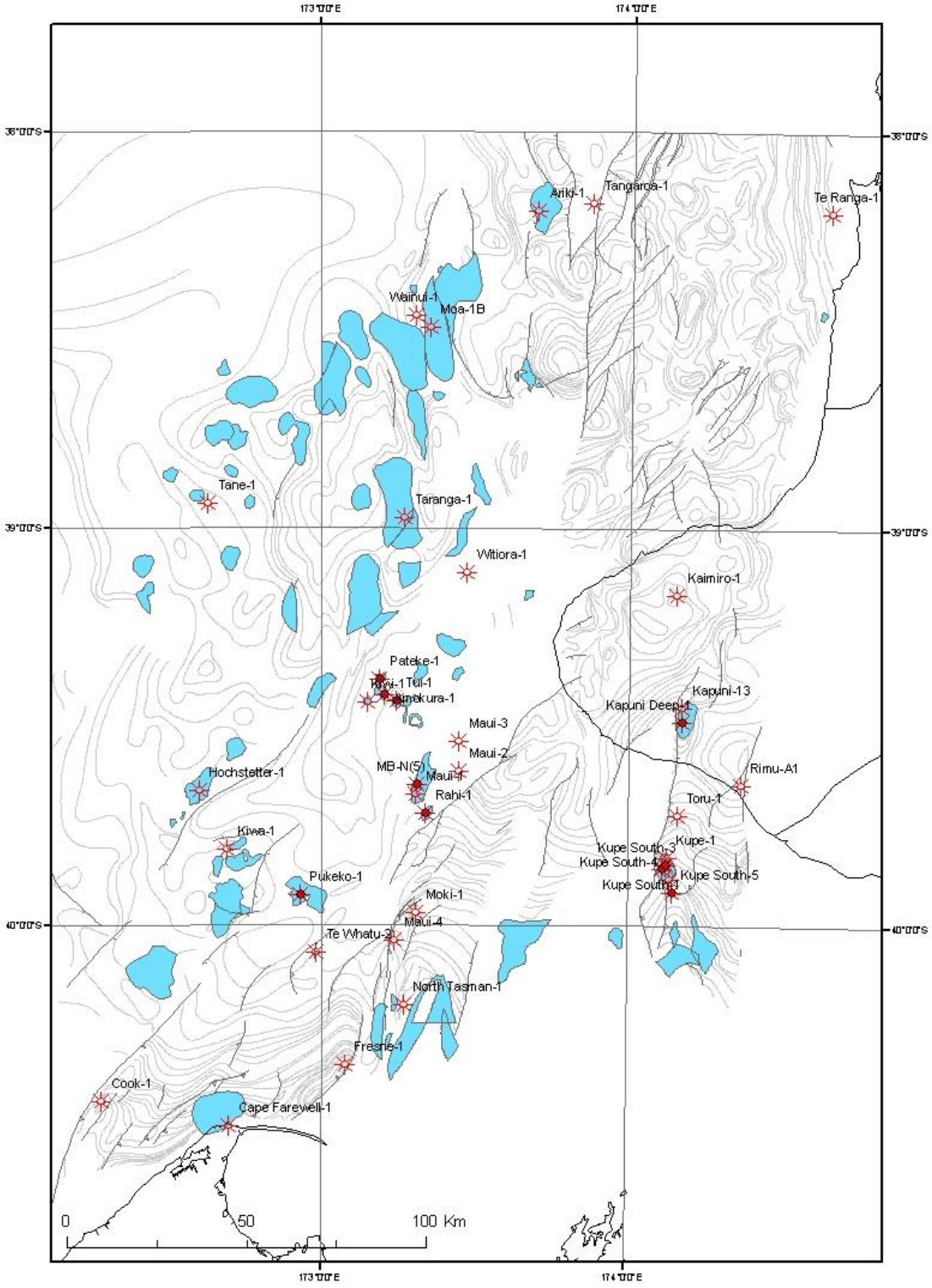

Figure 6.9: Map showing the structural traps used in the sampled population of unevaluated mapped traps (S_{3i}) for the top Paleocene play shown on the top Cretaceous structure contour depth surface with regional-scale Cretaceous faults. Wells shown have encountered Paleocene age reservoir lithologies.

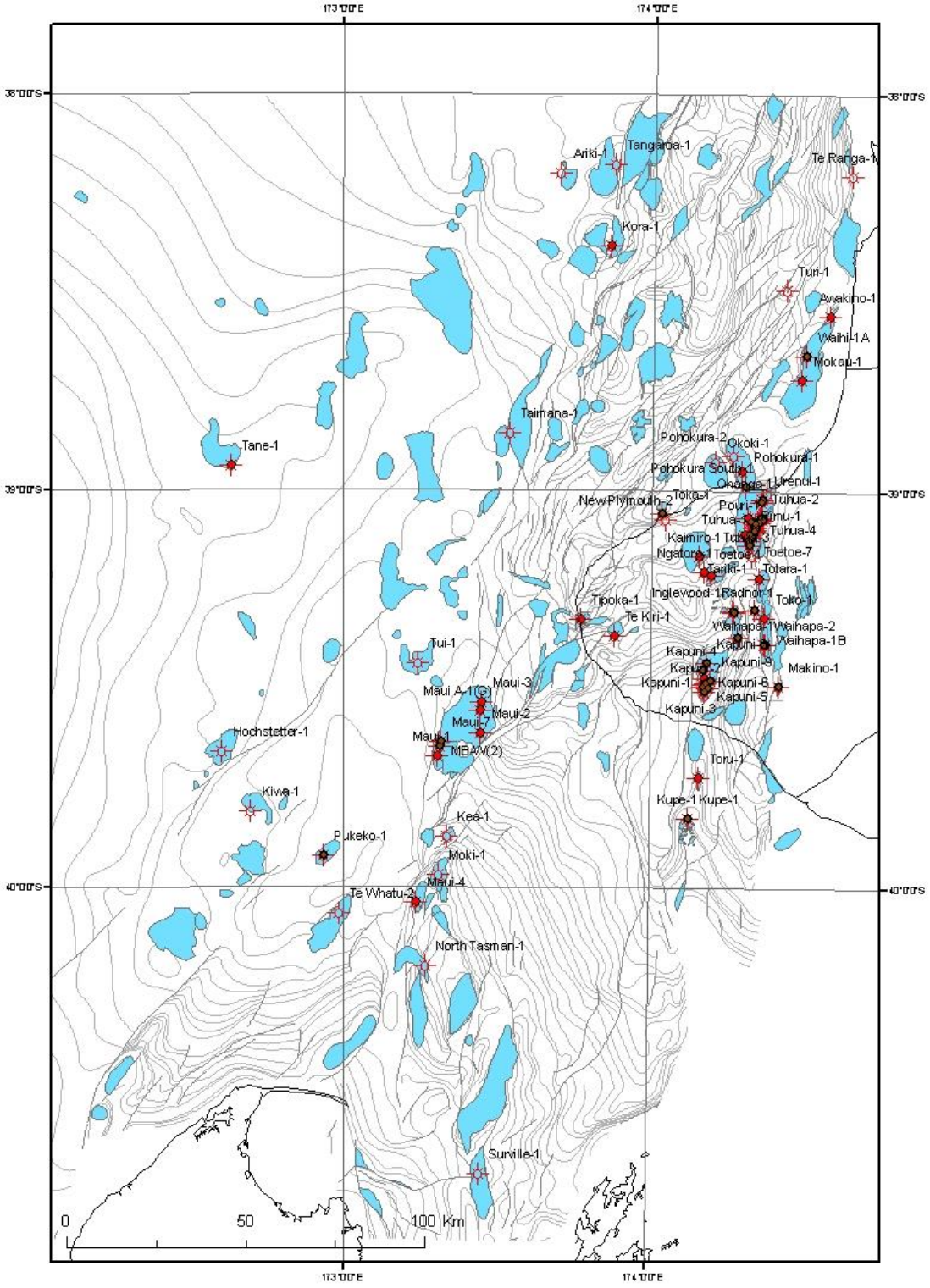

Figure 6.10: Map showing the structural traps used in the sampled population of unevaluated traps (S_{3i}) for the Eocene play. The traps are shown on the top Eocene structural contour depth surface and shown with regional-scale top Eocene surface faults. Wells shown have encountered Eocene age reservoir lithologies.

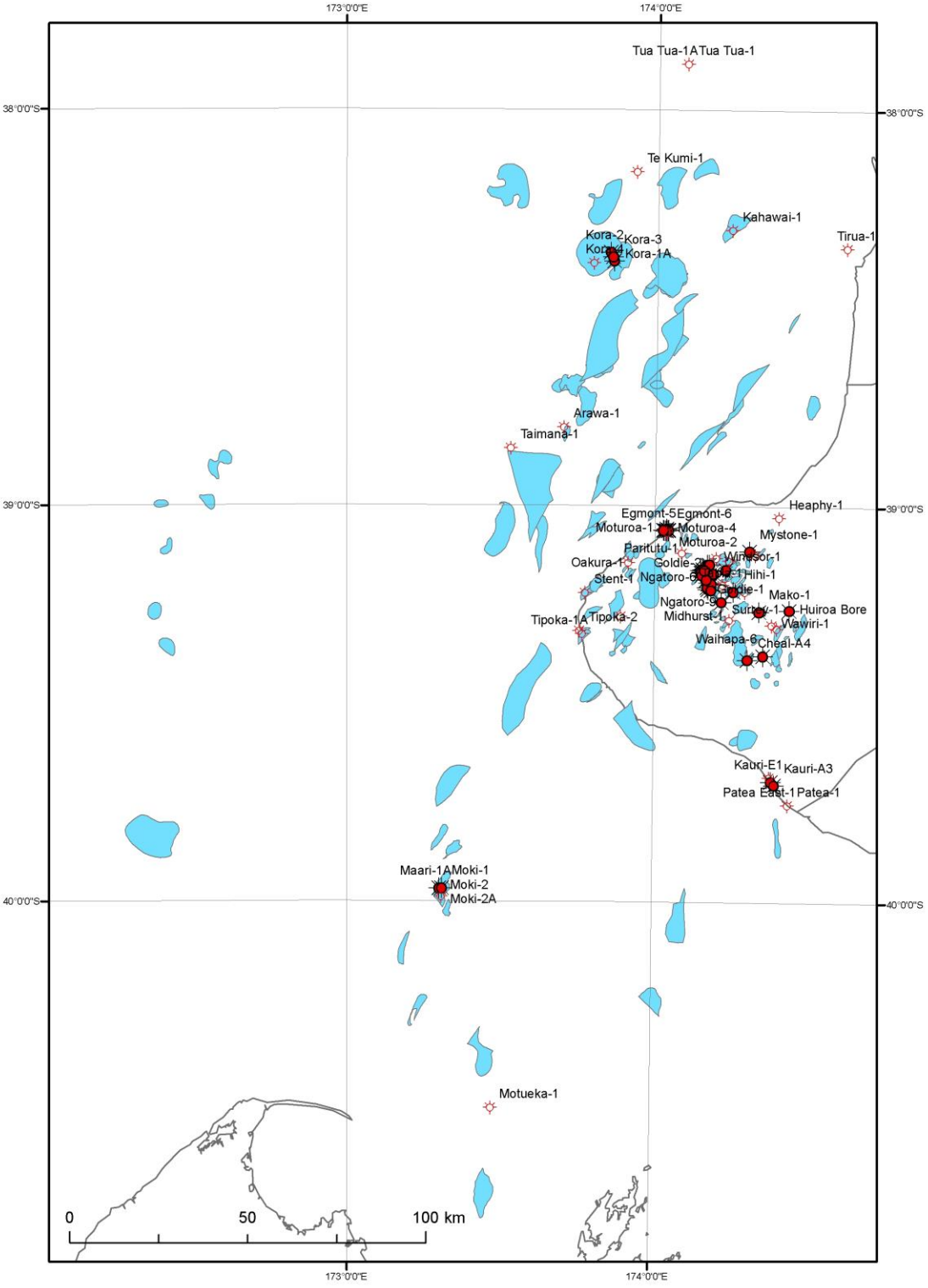

Figure 6.11: Map showing the structural traps used in the sampled population of unevaluated mapped traps (S_{3i}) for the Miocene play. The traps are shown on the top Miocene surface and with regional-scale top Miocene surface faults. Wells shown have encountered Middle to Late Miocene age reservoir lithologies.

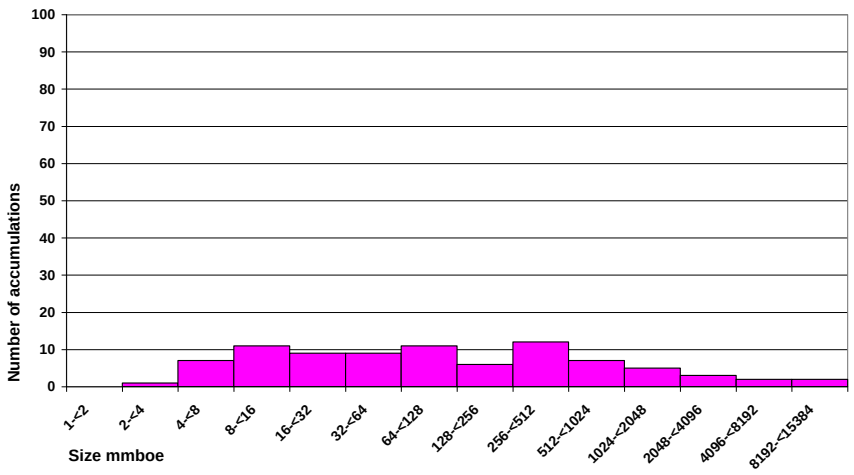

(a)

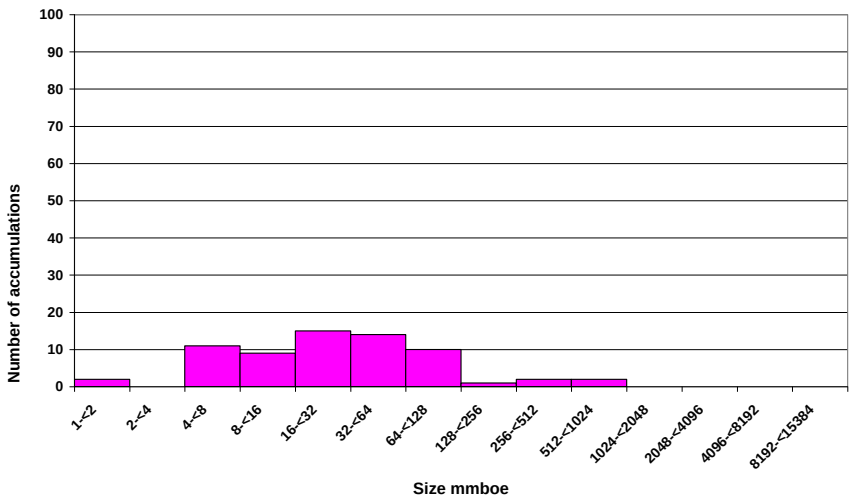

(b)

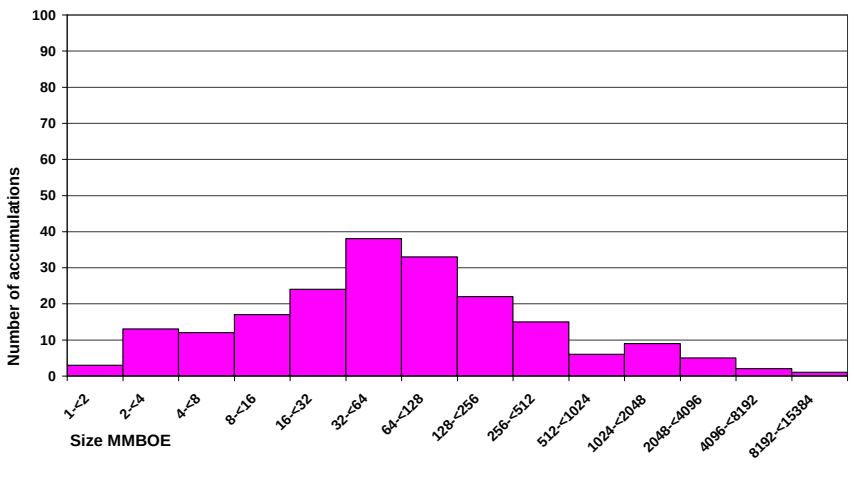

(c)

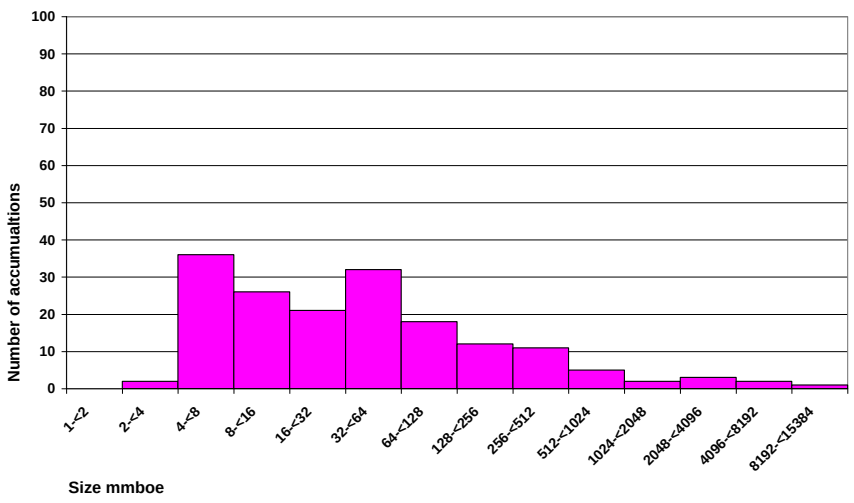

(d)

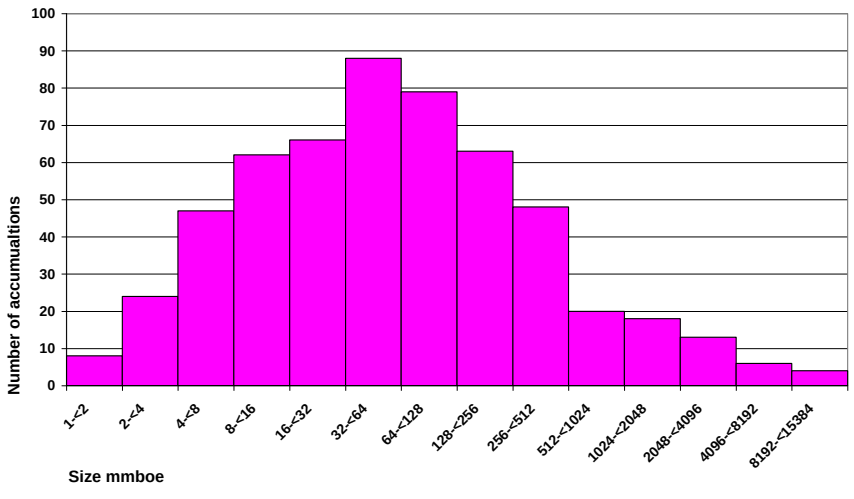

(e)

Figure 6.12: Size-frequency histograms of the sampled populations of unevaluated mapped traps, S_{3i}, for each of the plays: (a) Cretaceous; (b) Paleocene; (c) Eocene; (d) Miocene; and the basin (e).

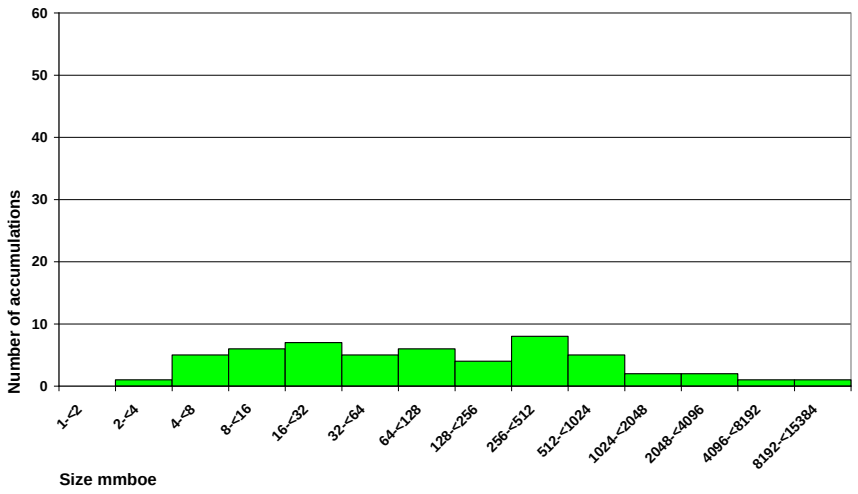

(a)

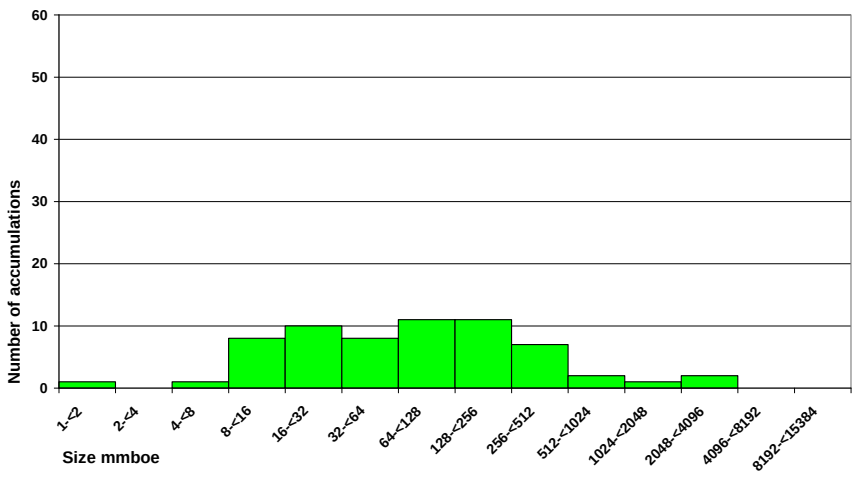

(b)

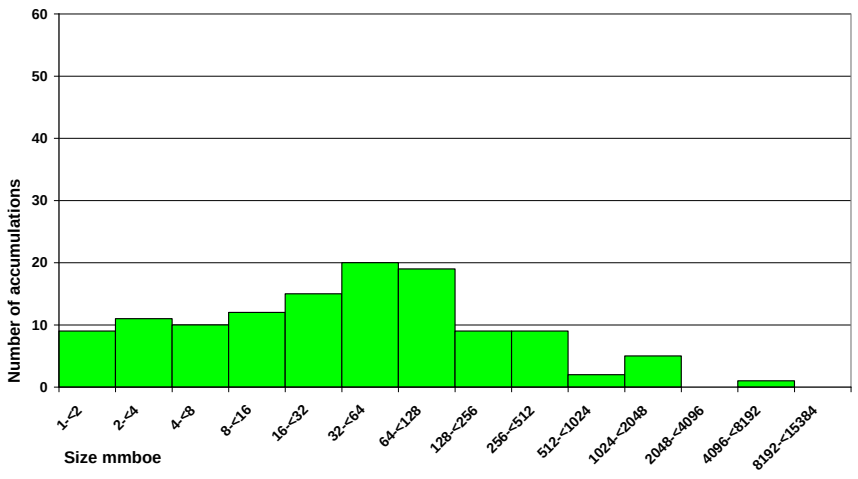

(c)

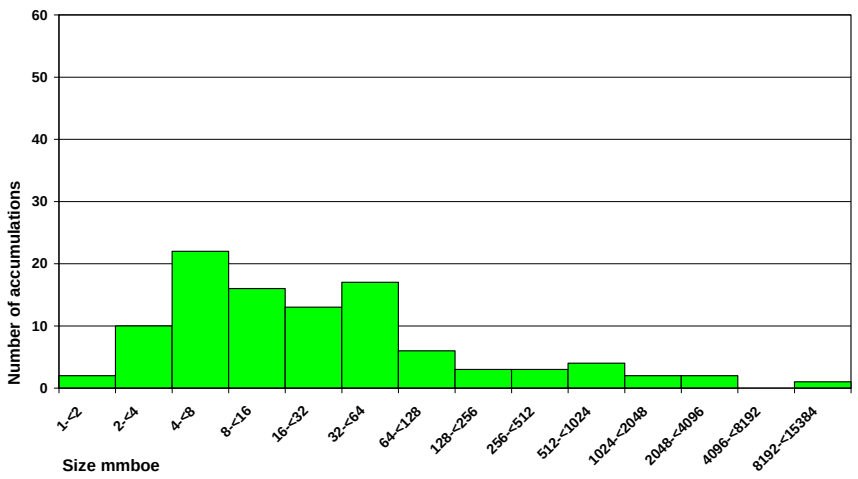

(d)

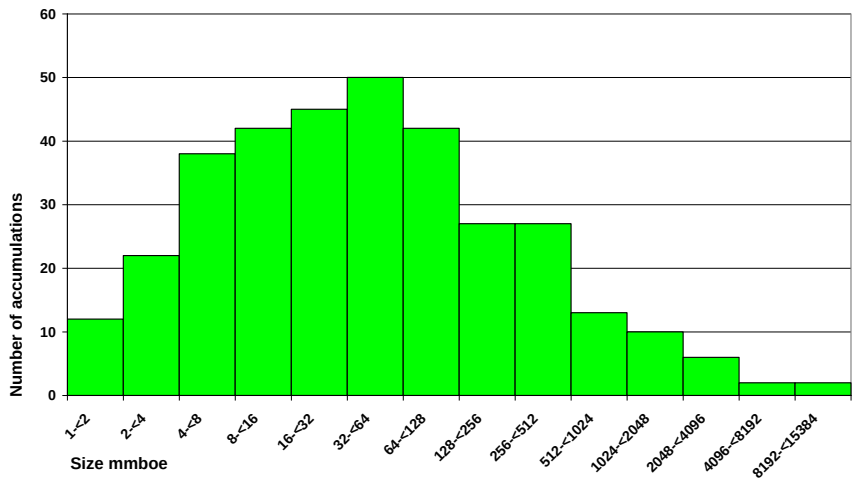

(e)

Figure 6.13: Size-frequency histograms of the sampled populations of evaluated mapped traps, S_{3ii}, for each of the plays: (a) Cretaceous; (b) Paleocene; (c) Eocene (d) Miocene; and (e) for the basin.

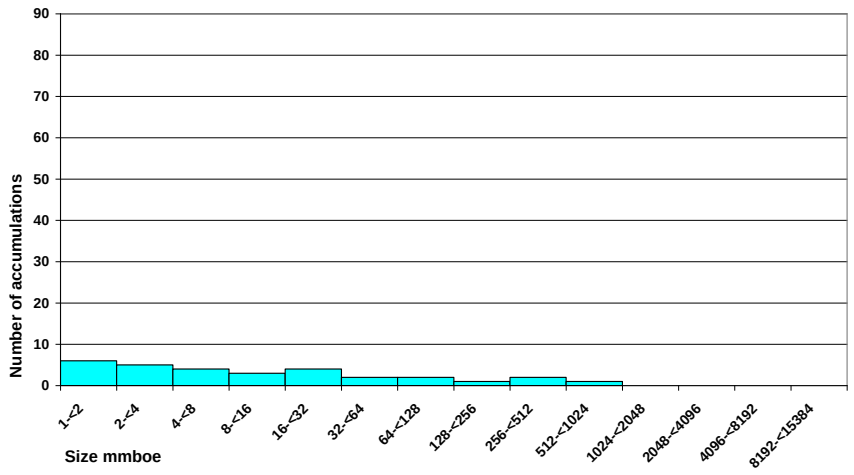

(a)

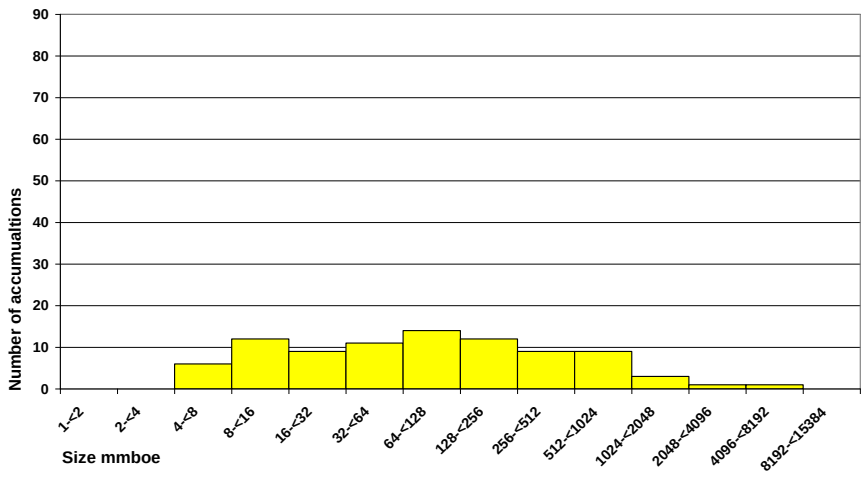

(b)

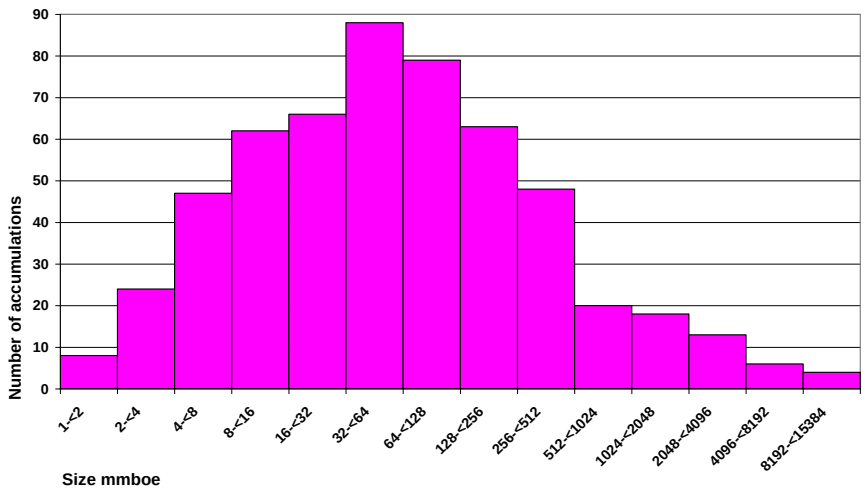

(c)

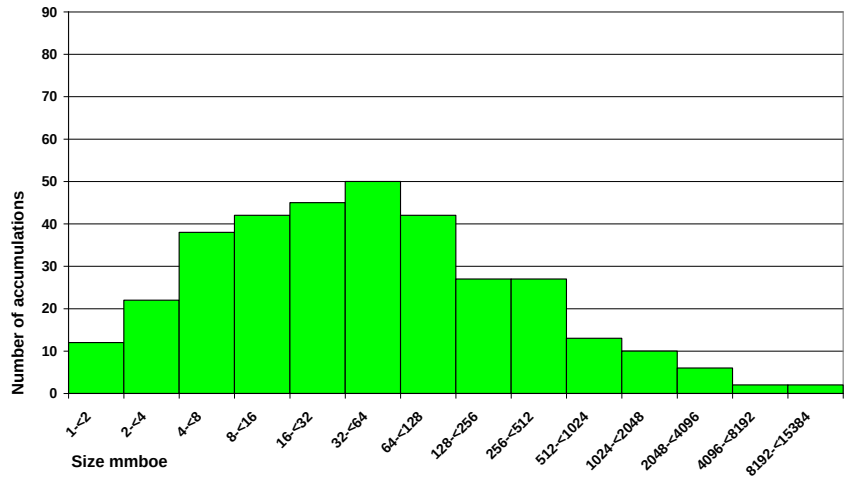

(d)

Figure 6.14: Size-frequency histograms of the sampled populations of oil and gas accumulations for the Taranaki Basin: (a) discoveries, S_1; (b) basin-modelled accumulations, S_2; (c) accumulations based on the unevaluated structural traps S_{3i}; and (d) accumulations based on the evaluated structural traps S_{3ii}.

Play	NS	a_1 km^2	a_0 km^2	a_{mean} km^2	γ	Pareto NP	Lognormal NP
Cretaceous	53	615	1	61.35	2	2000	2000
Paleocene	62	197	1	36.33	2	200–1000	200–1000
Eocene	122	136	1	18.65	2	100–1000	100–1000
Miocene	101	197	1	11.48	2	100–1000	100–1000
Basin	338	197	1	31.95	2	300–10000	300–10000
Size-probability distribution of modelled population of undiscovered oil and gas							
Play	LN P10 mmboe	LN P90 mmboe	LN Pmean mmboe	P P10 mmboe	P P90 mmboe	P Pmean mmboe	Pmean LN/P
Cretaceous	450	35	189.5	600	67	242.1	0.78
Paleocene	490	38	200.4	450	45	190.5	1.05
Eocene	500	38	197.4	220	30	119	1.66
Miocene	800	70	301.8	310	40	151	2.00
Basin	900	45	363.5	550	55	328.7	1.11

Table 6.2: Input parameters used in the discovery-sequence simulation and corresponding calculated undiscovered oil and gas volumes for the Taranaki Basin. The volumes are based on a cumulative probability of discovery and are minimum values. P10 and P90 = 10% and 90% probability of discovery. Pmean is a Swanson's derived mean (Section 3.4.5). NS = number of accumulations in the drawn sample. NP = number of accumulations in the parent population. LN = lognormal, P = Pareto. a_0 = minimum accumulation size, a_1 = maximum accumulation size, a_{mean} = mean accumulation size. γ = exponential gradient. For example LN P10 for the basin of 900 means there is a 10% probability that the next discovery will be equal to or greater than 900 mmboe. mmboe = millions of barrels of oil equivalent.

Areas of undiscovered oil and gas in the Cretaceous play were not modelled because there are no significant hydrocarbon-encountering wells to train a spatial model for this play.

6.2 Taranaki Basin

6.2.1 Amount of undiscovered oil and gas

There is an estimated amount of 8210–10800 mmboe of undiscovered oil and gas in the basin. This estimate is for a 100,000 km^2 study area and includes Cretaceous, Palaeocene, Eocene and Miocene reservoir intervals. The total volumes are based on the estimated Pareto population shown in Figure 6.15 and

the assumption that there is one maximum-sized accumulation in the basin, typical of all petroleum provinces in the world (Drew, 1997).

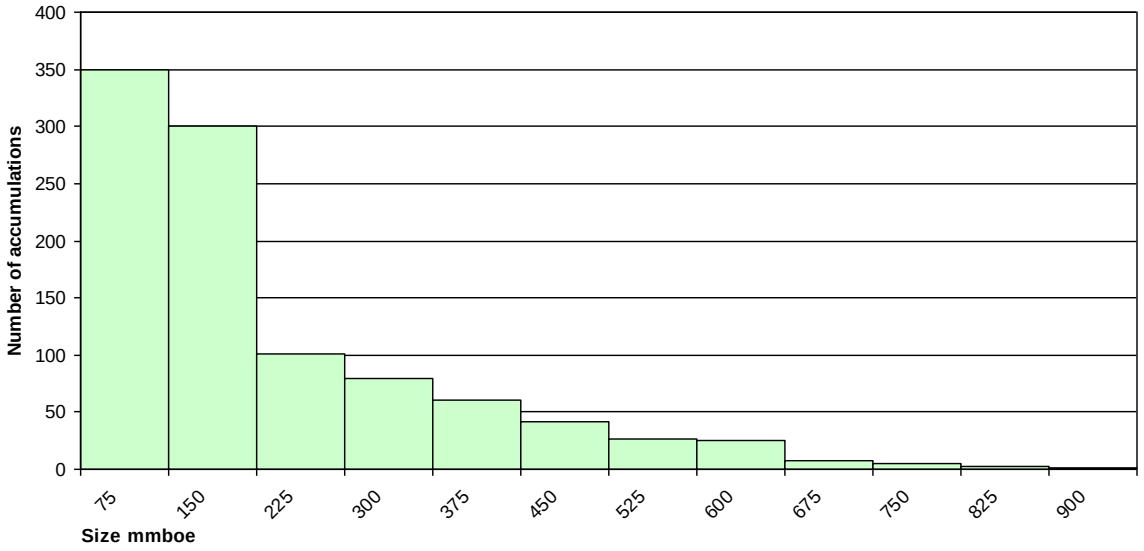

Figure 6.15: Histogram of undiscovered oil and gas for the Taranaki Basin that was modelled from a truncated Pareto parent population. Bin size denotes the maximum accumulation size for a bin, for example, 73 is bin size 1–73 mmboe.

However, if the Maui A accumulation of 533 mmboe is the largest accumulation in the Taranaki Basin the estimated total volume of undiscovered oil and gas is 5432–7800 mmboe based on the same Pareto parent population and shown in Figure 6.15.

The next discovery in the basin, from the estimated volumes, is most likely to be equal to or greater than 55 mmboe (with a 90% probability) (Figure 6.16) which is slightly bigger than the Tui Field discovered in 2003 and approximately a third of the significant Pohokura Field discovered in 2000. It may, however, be much larger and be equal to or greater than 550 mmboe (with a 10% probability). The mean accumulation size is 327.9 mmboe.

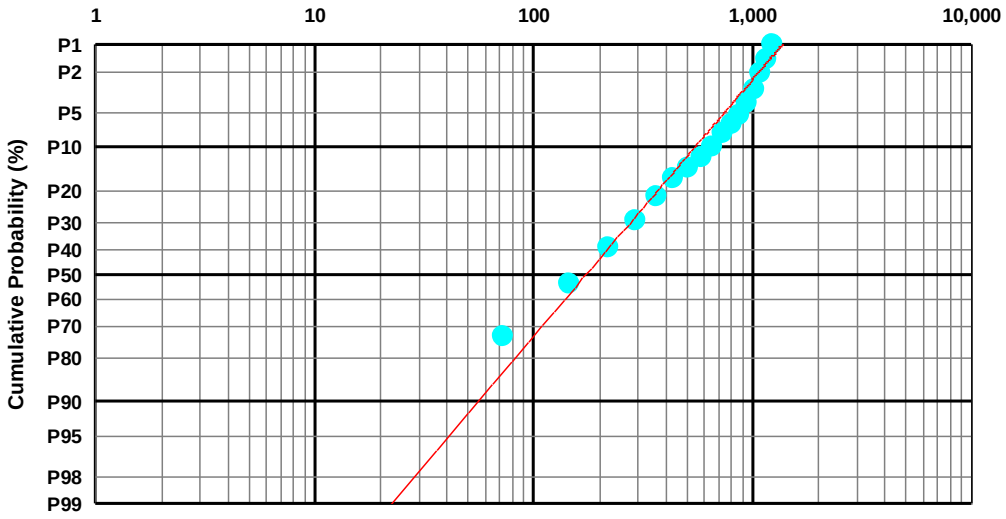

Figure 6.16: Cumulative probability distribution plot based on a Pareto parent population, which is used to estimate undiscovered oil and gas in the Taranaki Basin. The horizontal axis is size, mmboe. The blue dots represent modelled discoveries. The red line is a best-fit regression curve and represents the parent population that is used to estimate the probability that the next discovery in the basin is a certain size.

These results are based on an undiscovered population (Figure 6.15) calculated from a Pareto parent population of 1000 accumulations (Figure 6.17a). The mean drawn sample that statistically matched S_{3ii} (Figure 6.14c) and was used to define the parent has 332 accumulations (Figure 6.17b).

6.2.2 Likely location of undiscovered oil and gas

The most probable areas expected to contain undiscovered oil and gas in the basin are located in the onshore Taranaki peninsular and offshore in the Northern Graben, Western Platform and Central Graben areas (Figure 6.18). In particular the most likely undiscovered resource is predicted to be located in the Manaia Anticline area between the Kapuni Field and Toru-1 well area, which is dominated by a series of large anticlines that were formed by reverse-fault movement on basement faults during the latest-Miocene (Thrasher et al., 1995a, 1995b). Undiscovered oil and gas is also predicted onshore, along the eastern margin of the basin and Central Graben, where the Eocene coastal plain and detached shoreline sandstone fairway (King & Thrasher 1992; Flores et al., 1993; Thrasher et al., 1995d) is mapped and inferred (Figure A4, Appendix 14).

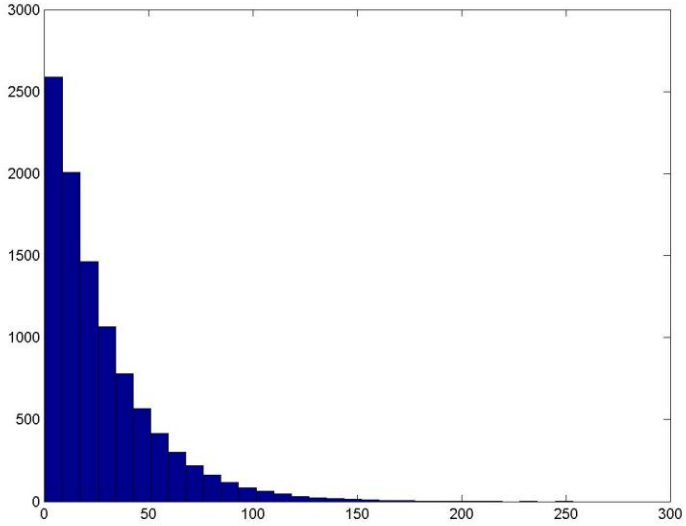

(a)

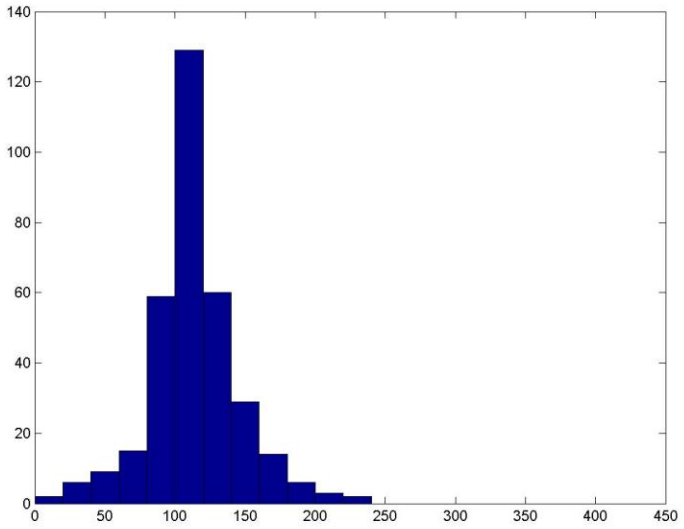

(b)

Figure 6.17: (a) Binned histogram of the Pareto parent population, from which sample (b) was drawn. The x-axis is size (km^2) and y-axis is the number of accumulations. (b) Binned histogram of the simulated mean drawn sample of 332 oil and gas accumulations drawn from a Pareto parent population of 10,000 accumulations for the Taranaki Basin. These two histograms have different bin sizes.

These areas (large grey-coloured dots in Figure 6.18) result from integrating the spatial modelling results for the probable scenario for the Paleocene, Eocene and Miocene reservoir plays shown in Figures 6.19–6.21. The most favourable areas of hydrocarbon accumulation are represented by the highest relative conditional probabilities, which are shown in red in these maps. These areas are predicted to be prospective based on spatial correlations between mapped working petroleum systems and discoveries in the basin.

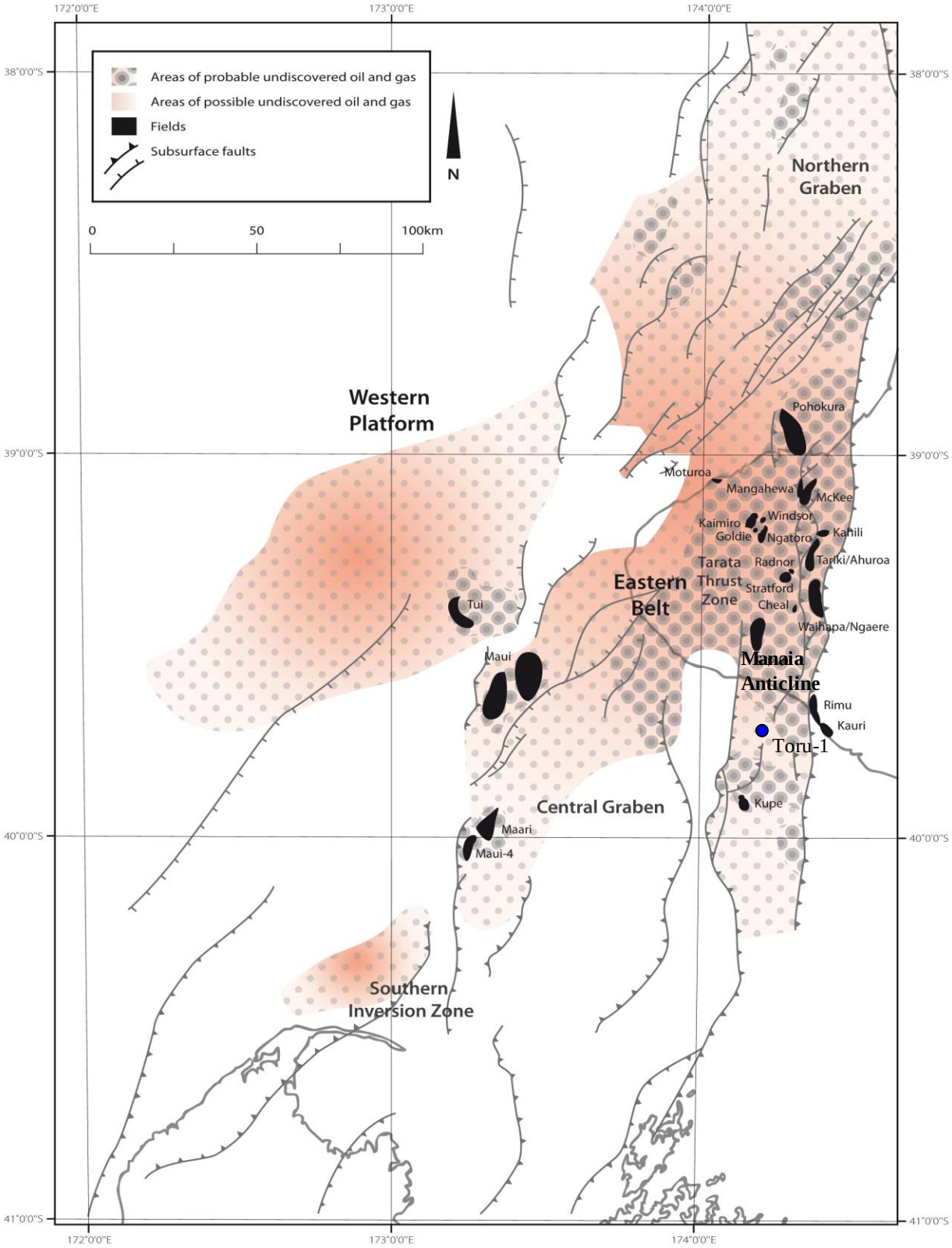

Figure 6.18: Estimation of areas most likely to contain undiscovered oil and gas in the Taranaki Basin, as a result of the integration of the relative posterior probabilities for the Paleocene, Eocene and Miocene reservoir plays. The graded colour ramp and a range in dot size are used to represent the rolled-up, calculated, absolute, posterior probabilities, which are a series of values instead of three ranked classes. The dot matrix is for the probable scenario. The red-brown colour ramp is for the possible scenario.

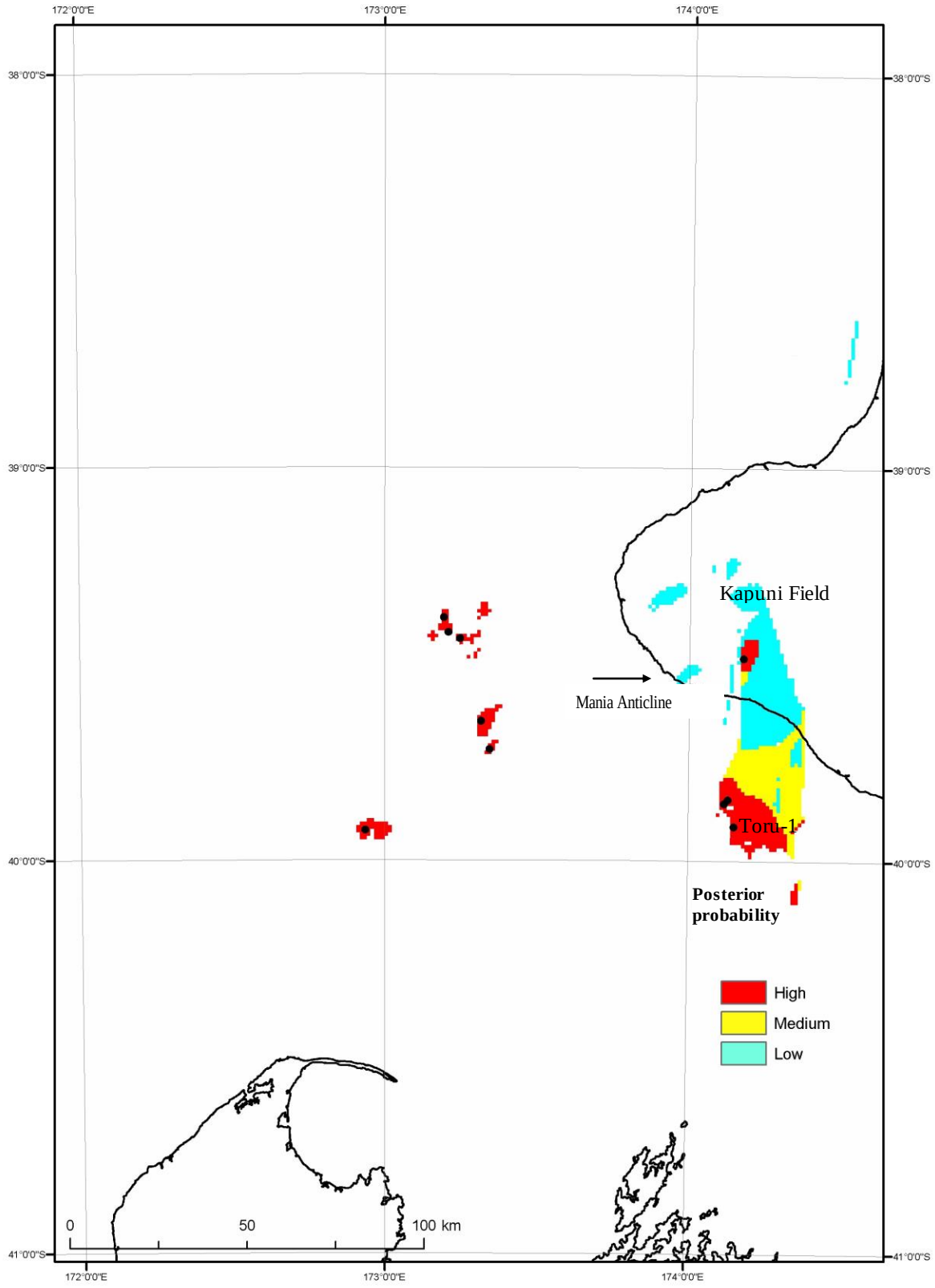

Figure 6.19: Relative posterior probability map for the Paleocene reservoir play based on the absolute probabilities of preferential hydrocarbon occurrence that were calculated for the probable scenario using the points of success that are based on discoveries.

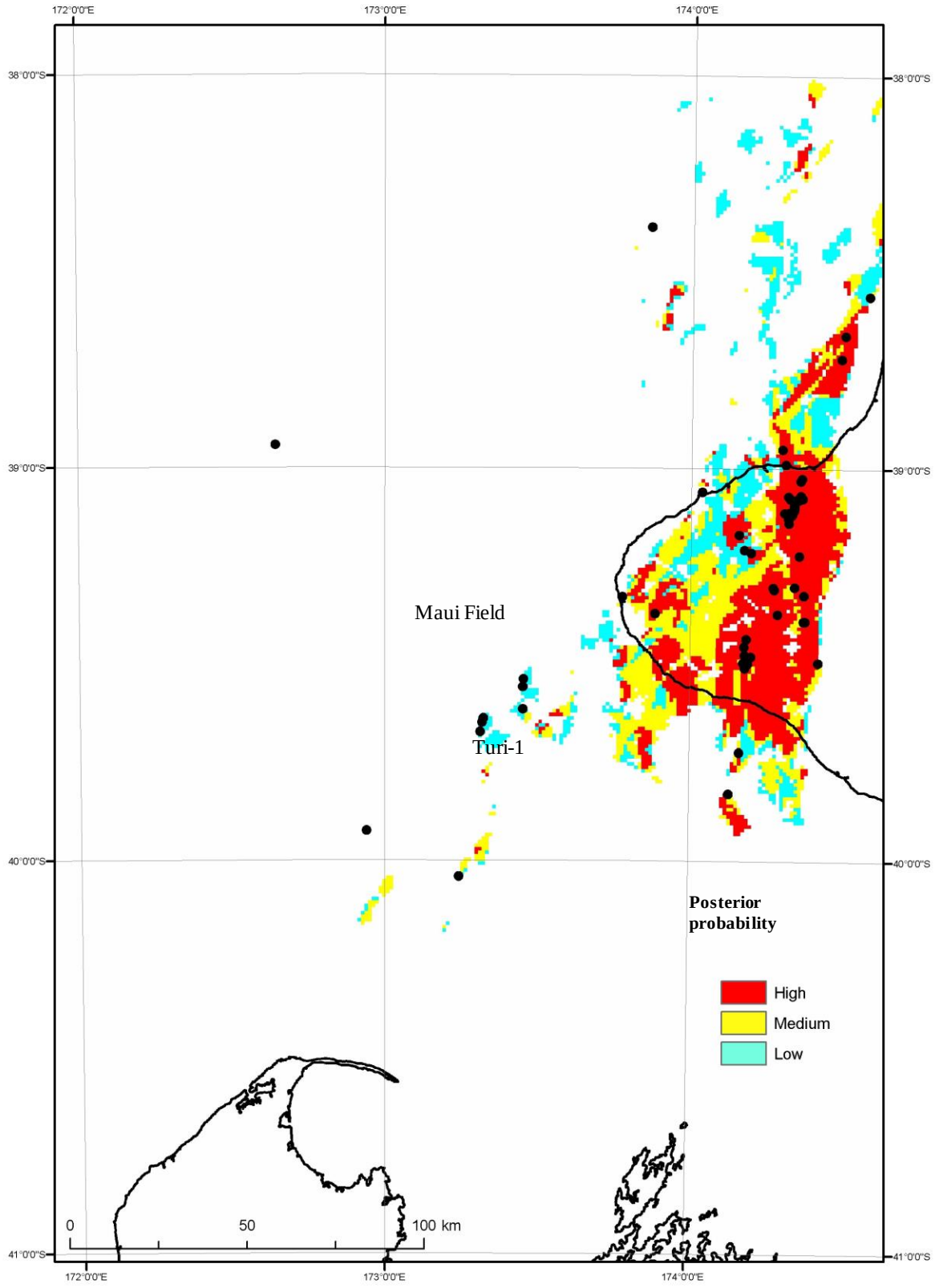

Figure 6.20: Relative posterior probability map for the Eocene reservoir play based on the absolute probabilities of preferential hydrocarbon accumulation that were calculated for the probable scenario using the points of success that are based on discoveries.

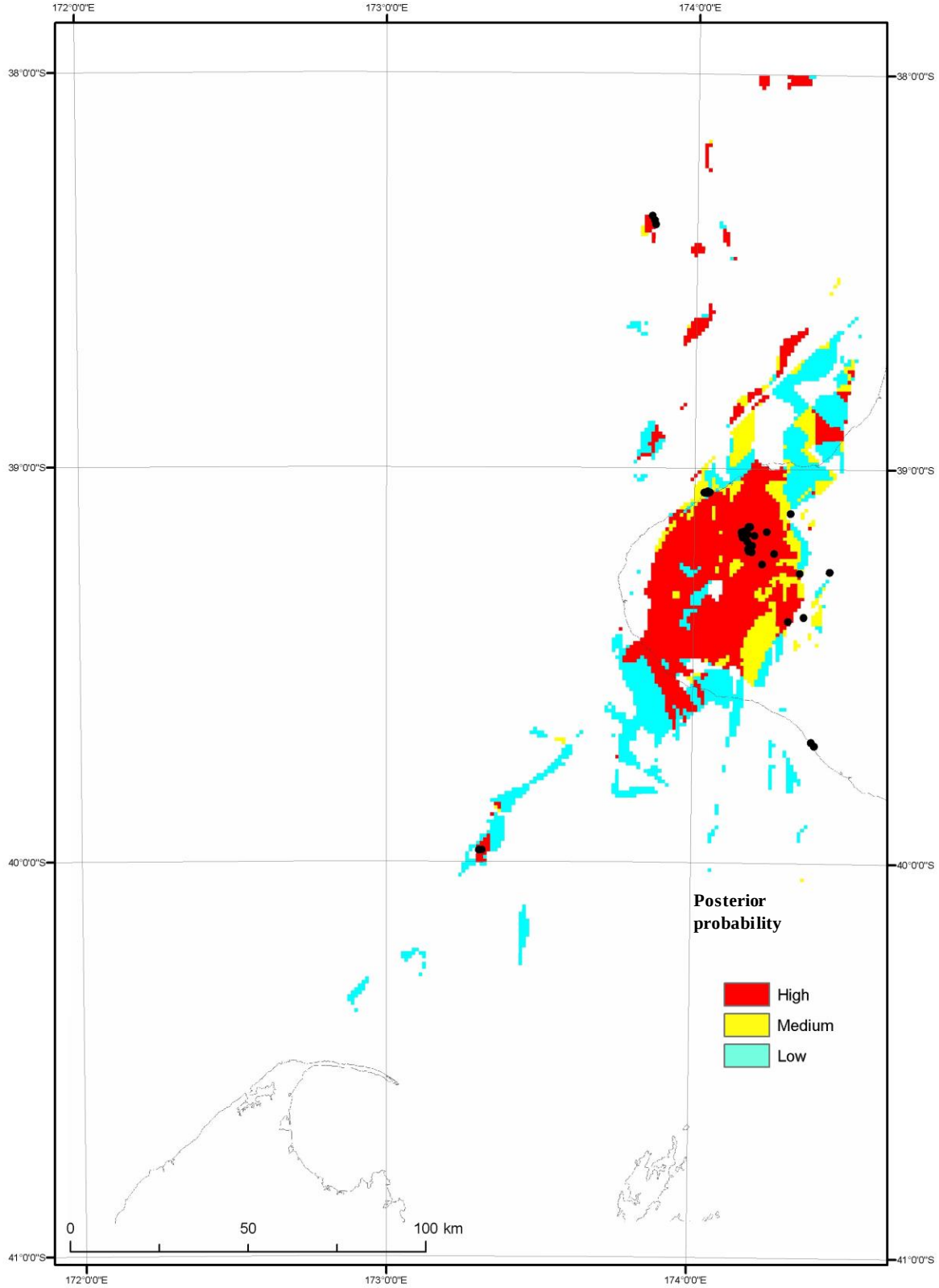

Figure 6.21: Relative posterior probability map for the Miocene reservoir play based on the absolute probabilities of preferential hydrocarbon occurrence that were calculated for the probable scenario using the discoveries success points.

Offshore, the high-probability localities, in the southwestern extent of the Central Graben, are on the flanks of the Maui Field structure and where a number of high-resolution structural traps (E2, Otakeho, and Motumate, refer to Figures 6.8-11) have been mapped east of the Maui Field. In the Northern Graben, the areas with the highest probability of hydrocarbon accumulation are located where there are many reverse faults and multiple fault-blocks (Thrasher et al., 1995a and Thrasher et al, 2002) and where Moki and Mount Messenger submarine fan systems are mapped extensively (King & Thrasher, 1996).

The most prospective areas correspond to areas which exhibited the strongest spatial correlations. The areas of highest posterior probability are influenced by a number of different petroleum systems maps, which is indicated by the high contrast values, C, in Table 6.3. The maps of reservoir distribution, structural traps, and amounts of gas generated and expelled have had the greatest influence on the estimation results.

Maps of the spatial modelling results for the possible scenarios (Section 4.3.1) which have also influenced the rolled-up estimation for the basin (Figure 6.18) are presented in Appendix 14. Two different possible scenarios were modelled; one is based on the sampled population of basin-modelled accumulations, S_2, and the other is based on the sampled population of trap-based accumulations, S_3. The number of accumulations in the S_2 and S_3 datasets, used in these scenarios, is shown in Table 6.4.

Evidential theme map	Wells-based points of success C	W+	s(C.)	Wells-based points of success C	W+	s(C.)	Wells-based points of success C	W+	s(C.)
Carrier bed distribution	1.85	1.57	2.68	0.99	0.89	3.13	1.96	0.24	3.86
Carrier bed porosity	1.44	0.23	1.37	1.43	0.28	3.83	1.05	0.64	2.52
Amounts of oil generated				0.53	0.45	1.83	2.43	1.61	5.67
Amounts of gas generated				0.53	0.45	1.83	2.43	1.61	5.67
Structural traps	5.35	3.09	5.08				2.71	2.26	6.33
Faults	0.5	0.28	0.79	0.33	0.11	1.36	1.13	0.55	2.57
Structural zones	1.61	1.22	2.5	0.73	0.29	3.02	2.47	1.65	5.76
Top seal lithology	2.62	2.16	4.05	0.84	0.79	2.25	2.2	1.89	4.84
Seal integrity	1.31	0.24	1.24	2.77	0.32	3.89	0.73	1.89	4.84
Migration flowpaths	0.17	0.09	0.27	0.04	0.02	0.21	1.21	0.48	2.56
Carrier bed distribution	3.55	1.28	7.62	0.94	0.6	6.06	3.03	1.23	8.5
Carrier bed porosity	1.73	1.42	6.46	1.05	0.91	5.34	1.63	1.34	6.32
Amounts of oil generated	3.27	2.21	12.23	1.25	1.05	7	2.94	2.1	12.2
Amounts of gas generated	3.44	2.54	13.36	1.32	1.17	6.62	3.17	2.42	13.29
Structural traps	4.95	2.64	11.53				4.64	2.61	12.96
Faults	2.21	0.81	6.43	1.23	0.59	7.53	4.4	1.17	6.14
Structural zones	3.43	1.94	11.04	1.54	1.2	9.6	3.03	1.85	11.42
Top seal lithology	3.31	0.97	6.42	0.91	0.48	5.82	2.68	0.91	7.15
Seal integrity	2.13	1.41	8.44	0.94	0.74	5.57	2.04	1.37	8.6
Migration flowpaths	4.28	1.16	5.96	1.43	0.76	8.87	4.4	1.17	6.14
Carrier bed distribution	3.71	1.05	5.13	1.77	0.81	9.18	3.44	1.04	6.67
Carrier bed porosity				0.72	0.69	1.85	0.18	0.17	0.25
Amounts of oil generated	3.1	1.75	8.64	1.48	1.05	8.78	2.8	1.67	10.34
Amounts of gas generated	3.26	1.7	8.34	1.93	1.21	11.24	2.76	1.59	9.99
Structural traps	4.63	3.16	12.82				4.21	3.07	15.8
Faults	0.7	0.49	2.27	1.28	0.76	7.54	1.26	0.8	5.18
Structural zones	4.1	1.04	8.61	2.43	1.66	14.2	2.62	1.72	10.25
Top seal lithology	1.94	1.08	5.95	1.32	0.83	7.84	1.21	0.78	4.9
Seal integrity	0.32	0.08	0.85	1.12	0.21	4.09	0.42	0.1	1.35
Migration flowpaths	3.32	0.78	4.59	2.28	0.71	8.89	3.33	0.78	5.64

Table 6.3: Summary of the derivative correlation values used to measure the strength and validity of the spatial correlations resulting from the spatial data-modelling analysis for the Paleocene, Eocene and Miocene plays. C is the contrast value, W+ is the positive weight, and s(C) is the Studentised contrast value. Where a value is not shown, no correlation was contrasted because all the points of success for that analysis were located within a single class. Red values are the strongest spatial correlation values, showing the three most influential evidential theme maps, for each play, used in the spatial analyses.

Points of success			
Area	S_1	S_2	S_3
Paleocene reservoir play	10	72	13
Eocene reservoir play	46	184	8
Miocene reservoir play	21	141	22
Taranaki Basin	77	397	43

Table 6.4: Number of points of success in each of the sampled populations S_1, (discoveries) S_2, (basin modelled-accumulations) and S_3, (trap-based accumulations) used in the spatial model.

The spatial modelling results were based on the following petroleum systems maps:

- main regional structural domains;
- distribution of regional fault-traces;

- amounts of oil that have been generated and expelled and are available for migration;
- amounts of gas that have been generated and expelled and are available for migration;
- distribution of reservoir rock;
- reservoir rock quality using predicted porosity;
- distribution of top-seal rock;
- maximum burial depth of seal rock;
- distribution of main migration flowpaths; and
- distribution of mapped structural traps.

The reclassified versions of each of these maps (Section 4.3.4) and the points of success that were used in the probable and possible scenarios are shown in Appendix 10.

An evidential theme map of the main structural domains in the basin is used to highlight the Western Platform, Southern Inversion Zone, Central Graben, Northern Graben, and Tarata Thrust Zone (Figure A1, Appendix 10). It was initially reclassified by treating the structural areas as five different categorical classes: where 1 = the Western Platform, 2 = the Southern Inversion Zone, 3 = the Northern Graben, 4 = the Tarata Thrust Zone and 5 = the Central Graben and correlating them with points of success that are based on known discoveries.

The Tarata Thrust Zone structural domain showed the strongest spatial correlation with the points of success producing a contrast value, C, = 4.43, positive weight, W+, = 3.67, and a Studentised contrast, s(C), = 23.7. The Central Graben domain also showed a good correlation with the points of success; C = 1.41, W+ = 1.14, and s(C) = 7.98. The Northern Graben domain showed a relatively mild correlation with C = 0.29, W+ = 0.23, and s(C) = 1.41. The very strong spatial correlation for the Tarata Thrust Zone was caused predominantly by its relatively small area and because of this, it was combined with the Central Graben. The combined class also has a strong spatial correlation, with C = 2.433, W+, = 1.22, and s(C) = 12.46 and this correlation is distributed over a larger area, which is

similar in size to the other domains. The resulting categorical classification for the structural domains evidential theme map is shown in Appendix 10.

Maps showing the amounts of oil and gas generated and expelled (Appendix 4) were reclassified into evidential theme maps (Appendix 10) where Class 1 represents <1000 mkg/km^2 and >4000 mkg/km^2 of oil and has been generated and expelled. Class 2 represents areas where 2000–4000 mkg/km^2 of oil gas has been generated and expelled. Class 3 represents areas where oil generation and expulsion has not been modelled.

Reservoir maps were prepared using the methods described in Section 3.2.3. They were classified into evidential theme maps to highlight probable, possible and limited reservoir potential (Appendix 10).

Seal rock distribution and maximum burial depth to seal maps were prepared using the methods described in Section 3.2.3. They were reclassified into evidential theme maps to highlight probable, possible and limited seal rock potential (Appendix 10).

PCE® was used to generate maps showing the distribution of hydrocarbon migration flowpaths in the Taranaki Basin (Section 3.2.3). This study reclassified the PCE® flowpath maps into evidential theme maps to optimise the correlation between the location of oil and gas accumulations and the distribution of the flowpaths

A 5 km buffer zone around the flowpaths was divided into 1 km intervals to determine a spatial correlation between the locations of discoveries and their proximity to a migration flowpath. A spatial correlation out to each 1 km interval was calculated using the reclassification method described in Section 4.3.6. The strongest correlation was within 1 km distance from the flowpath traces, with C = 3.15, W+ = 1.25, and s(C) = 12.21. A much weaker correlation resulted within 4 km from the flowpaths, with C = 0.65, W+ = 0.62, and s(C) = 1.76. Results suggest the flowpaths are narrow and localised, and the optimal buffer distance should be no more than 1 km. Hydrocarbon accumulations in the basin are in close proximity to mature source (King & Thrasher, 1996) suggesting migration

flowpaths extend predominantly vertically and not far beyond where hydrocarbons were generated. As a consequence of the correlation results the reclassified flowpaths maps are reclassified so that 1 = a flowpath (which includes the flowpath trace plus a 1 km wide buffer) and 2 = no flowpath (Appendix 10).

Maps of structural traps for each play were prepared from structure contour maps using the method described in Section 3.3. They were reclassified to show the presence of a structural trap, where 1 = a structural trap and 2 = the surrounding area of the traps.

Maps of regional faults for each top reservoir surface were reclassified using the method described in Section 4.3.6. Results show there is a strong correlation between the distribution of faults and the location of oil and gas accumulations in the basin and most accumulations are located within 5 km of a major fault (Section 4.3.6).

A strong spatial correlation within 1 km of a major fault may suggest that a discrete movement of a fault may influence the entrapment of hydrocarbons, such as the structural control at the crest of the anticline. However, a spatial correlation out to 5 km suggests a different fault-associated control may be influencing the accumulation of oil and gas. Faults influence the accumulation of hydrocarbons in various ways, depending on characteristics such as fault dip and fault throw, the thickness of the lithology that is offset and whether the trapping structure is controlled by the fault or not (Carstens, 1995; Nicol et al., 2004). However, the fault-associated impact may extend into the adjacent rock as a zone of deformation around a fault system and influence the entrapment of hydrocarbons (Carstens, 2005). This may explain the strong correlation out to 5 km in the Taranaki Basin and one way to test this would be to map fault facies to see if petrophysical properties of the reservoir and the behaviour of fluid flow change as a function of strain during fault movement, as suggested by Carstens (2005).

Three evidential theme maps displayed high Chi-squared (χ^2) values, suggesting they may be conditionally dependent (Chapter 3). These maps are: amount of oil generated and expelled; amount of gas generated and expelled; and distribution of migration flowpaths. However, these maps were not removed from the model to

minimise a possible conditional independence violation because each theme is a direct indicator of hydrocarbon charge (Section 4.3.8). Areas of generated and expelled oil and gas amounts coincide because they are likely to have originated from the same source rocks. However the distribution of trapped oil and gas-condensate in the basin may be indicative of different source rock facies and generation and expulsion conditions in the basin, therefore the gas and oil maps are conditionally independent. The flowpaths map coincides with the oil and gas maps because trapped accumulations are located in close proximity to mature source rock and flowpaths are predominantly vertical and relatively short (Armstrong et al., 1996; Killops et al., 1998; Wood et al., 1998; Funnell et al., 2004) and are conditionally independent.

6.3 Cretaceous play

6.3.1 Amount of undiscovered oil and gas

The next discovery in the Cretaceous play is likely to be (with a 90% probability) equal to or greater than 67 mmboe (Figure 6.22). It may, however, be much larger (with a 10% probability) and be equal to or greater than 600 mmboe. The mean accumulation size is 242.1 mmboe. The Pareto results are based on an undiscovered population (Figure 6.23) that was calculated from a Pareto parent population containing 400 accumulations (Figure 6.24a). The mean drawn sample that statistically matched S_{3ii} (Figure 6.25c) and was used to define the parent has 53 accumulations (Figure 6.24b).

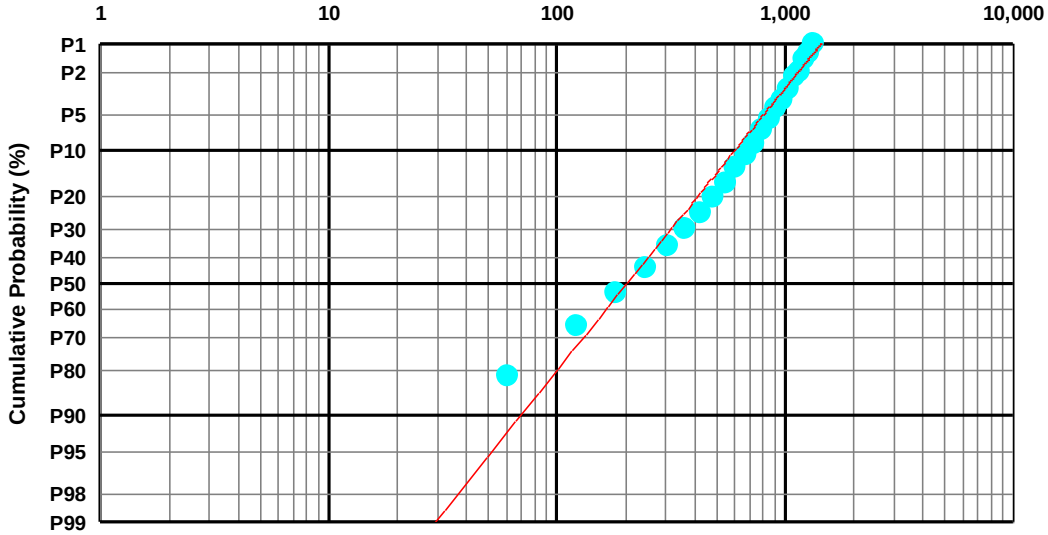

Figure 6.22: Cumulative probability distribution plot based on a Pareto parent population, which is used to estimate undiscovered oil and gas in the Cretaceous play. The horizontal axis is size, mmboe. The blue dots represent modelled discoveries. The red line is a best-fit regression curve and represents the parent population that is used to estimate the probability that the next discovery in this play is a certain size.

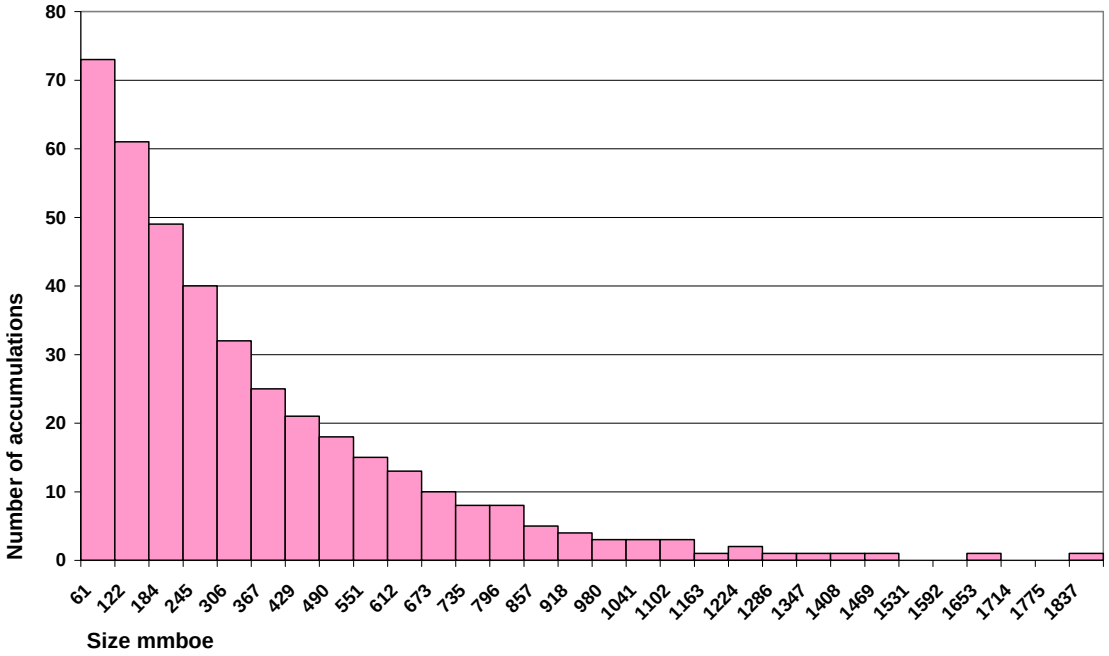

Figure 6.23: Size-frequency histogram of the mean parent population based on a Pareto probability distribution function, which was modelled for the Cretaceous play. Bin size denotes the maximum accumulation size for a bin, for example 61 is bin size 0-61 mmboe

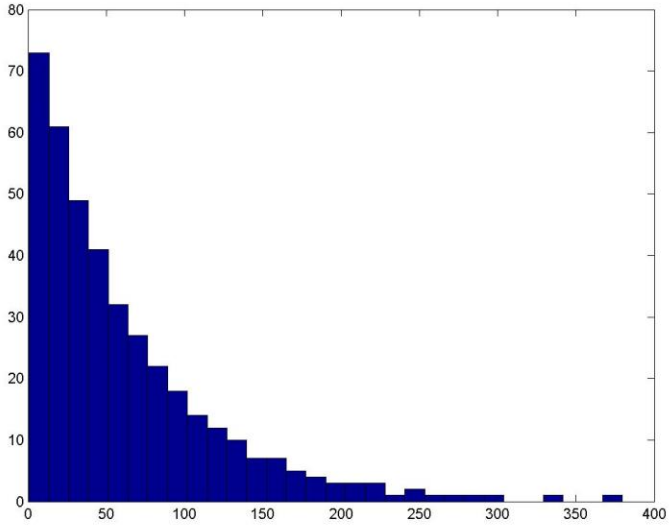

(a)

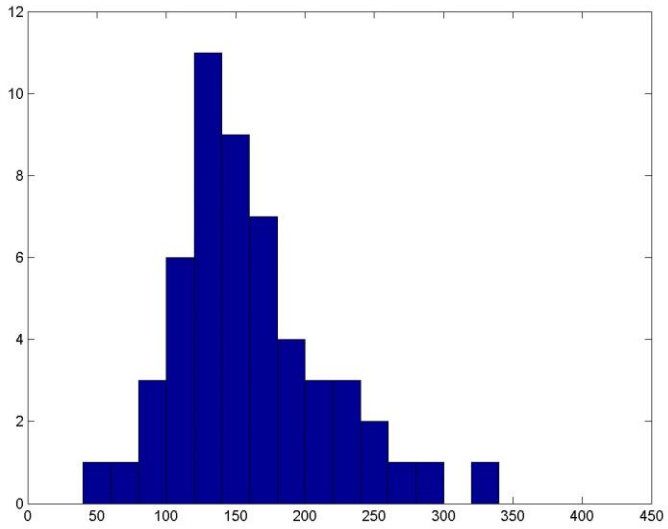

(b)

Figure 6.24: (a) This is the size distribution of the parent population, from which sample (b) was drawn. The x-axis is size (km^2) y-axis is the number of accumulations. (b) This is the simulated mean sample of 53 oil and gas accumulations drawn from a Pareto parent population of NP = 400 accumulations for the Cretaceous play. These two histograms have different bin sizes.

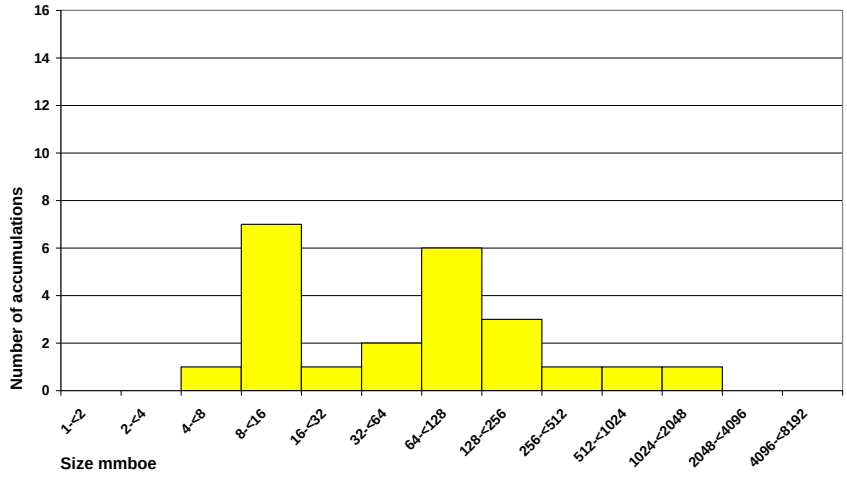

(a)

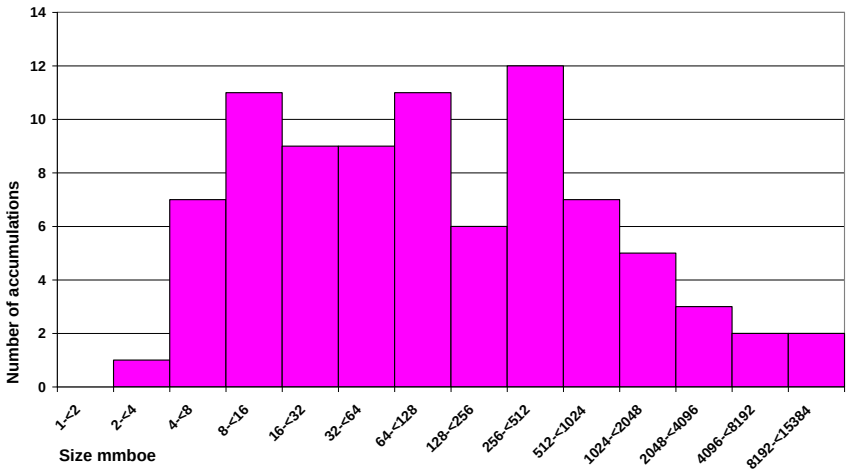

(b)

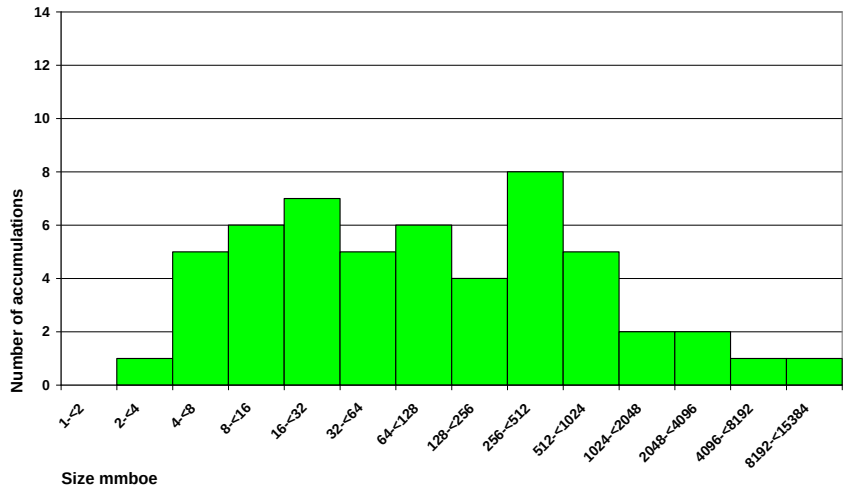

(c)

Figure 6.25: Size-frequency histograms of the sampled populations for the Cretaceous play including: (a) basin-modelled accumulations, S_2; (b) accumulations based on the unevaluated structural traps S_{3i}; and (c) accumulations based on the evaluated structural traps S_{3ii}.

6.4 Paleocene play

6.4.1 Amount of undiscovered oil and gas

The next discovery in the Paleocene play is likely to be (with a 90% probability) equal to or greater than 45 mmboe (Figure 6.26). It may, however, be much larger (with a 10% probability) and be equal to or greater than 450 mmboe. The mean accumulation size is 190.5 mmboe. These results are based on an undiscovered population (Figure 6.27) that was calculated from a Pareto parent population containing 400 accumulations (Figure 6.28a). The mean drawn sample that statistically matched S_{3ii} (Figure 6.29d) and was used to define the parent has 62 accumulations (Figure 6.28b).

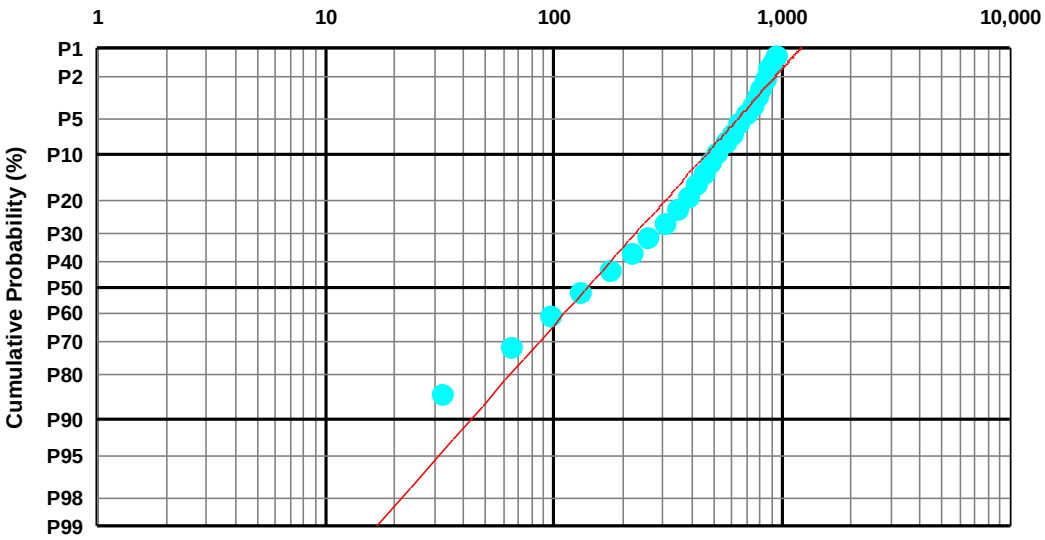

Figure 6.26: Cumulative probability distribution plot based on a Pareto parent population, which is used to estimate undiscovered oil and gas in the Paleocene play. The horizontal axis is size, mmboe. The blue dots represent modelled discoveries. The red line is a best-fit regression curve and represents the parent population that is used to estimate the probability that the next discovery in this play is a certain size.

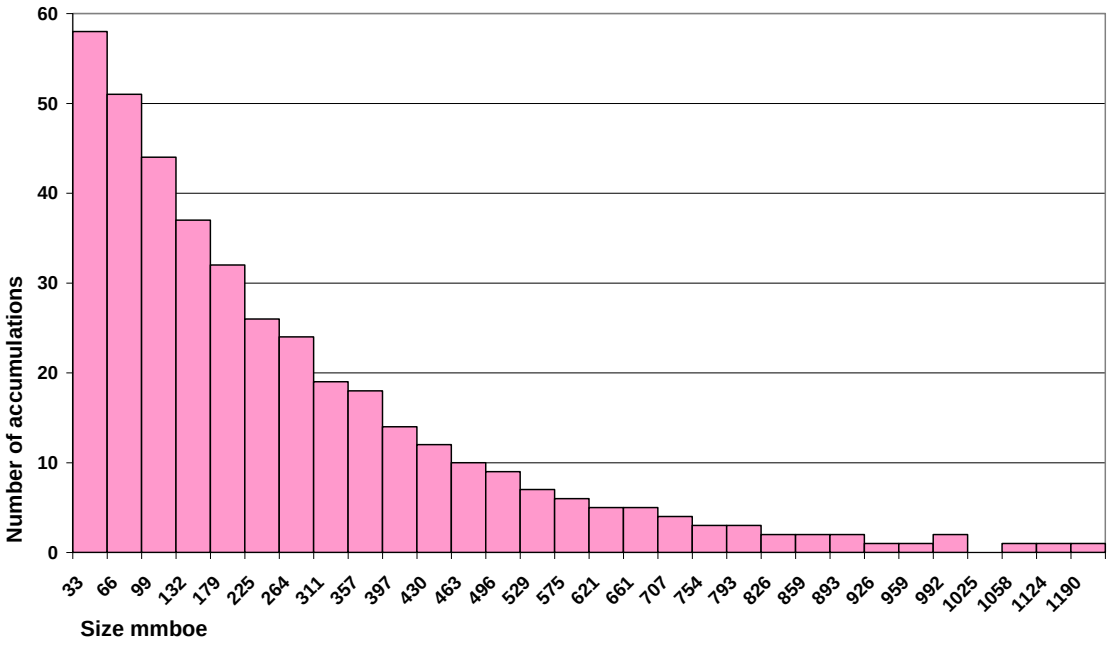

Figure 6.27: Size-frequency histogram of the mean parent population based on a Pareto probability distribution function, which was modelled for the Paleocene play. The volume size for a bin denotes the maximum accumulation size in a bin, for example 33 is bin size 0–33 mmboe.

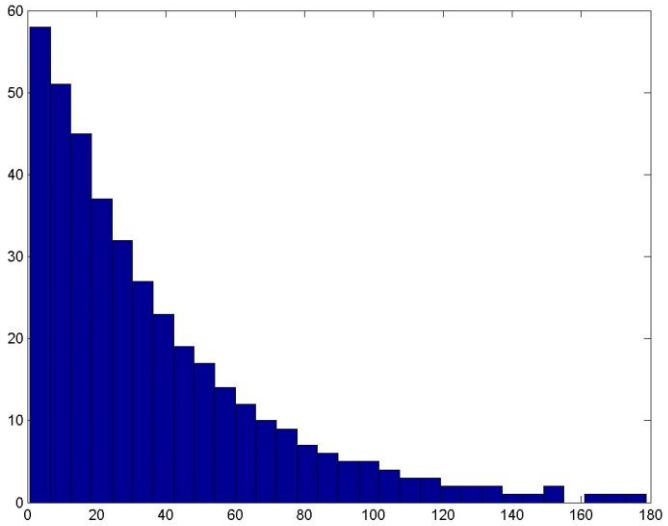

(a)

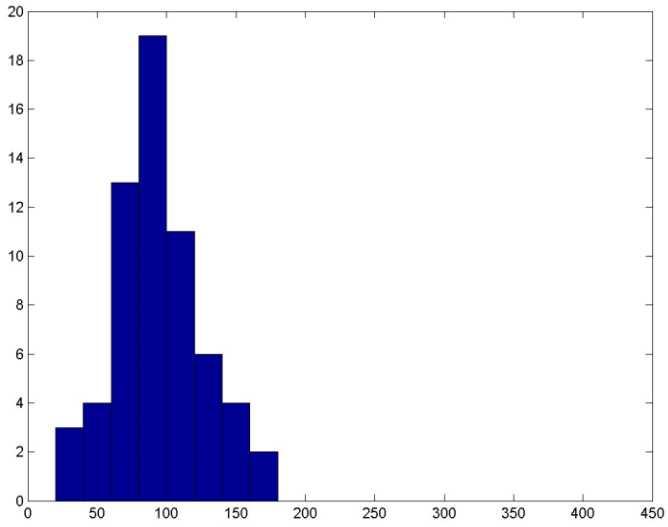

(b)

Figure 6.28: (a) This is the size distribution of the parent population, from which sample (a) was drawn. The x-axis is size (km^2) y-axis is the number of accumulations. (b) This is the simulated mean sample of 62 oil and gas accumulations drawn from a Pareto parent population of NP = 400 accumulations for the Paleocene play. These two histograms have different bin sizes.

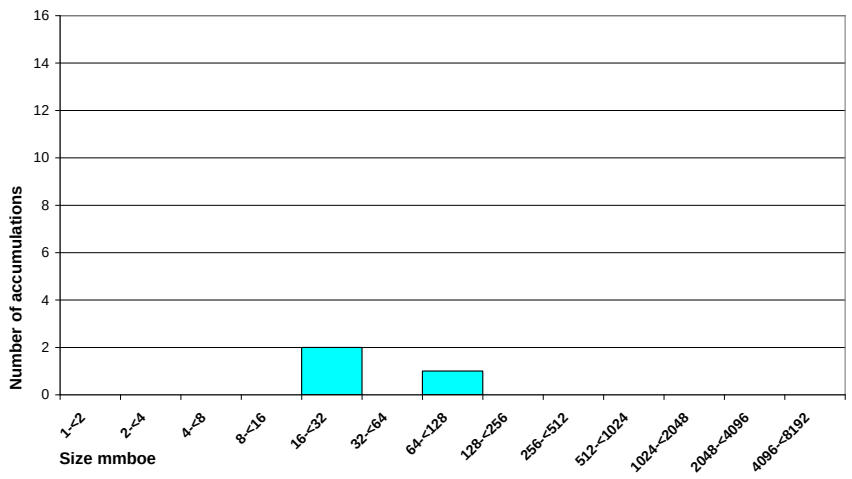

(a)

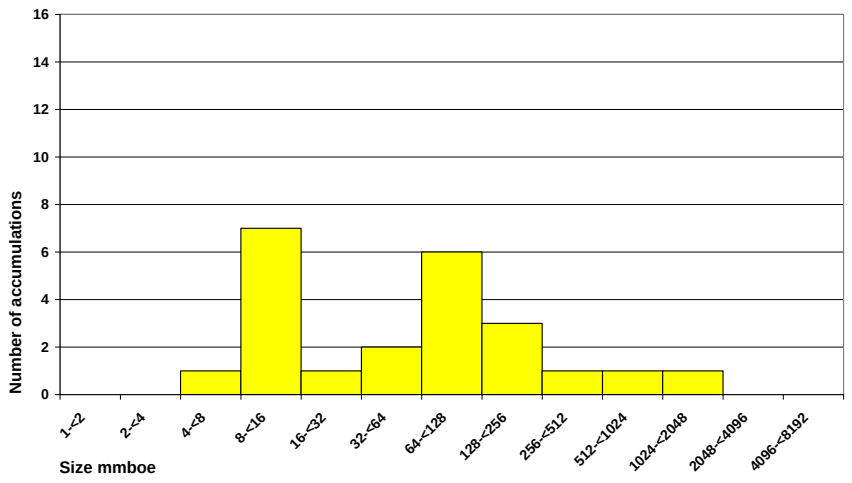

(b)

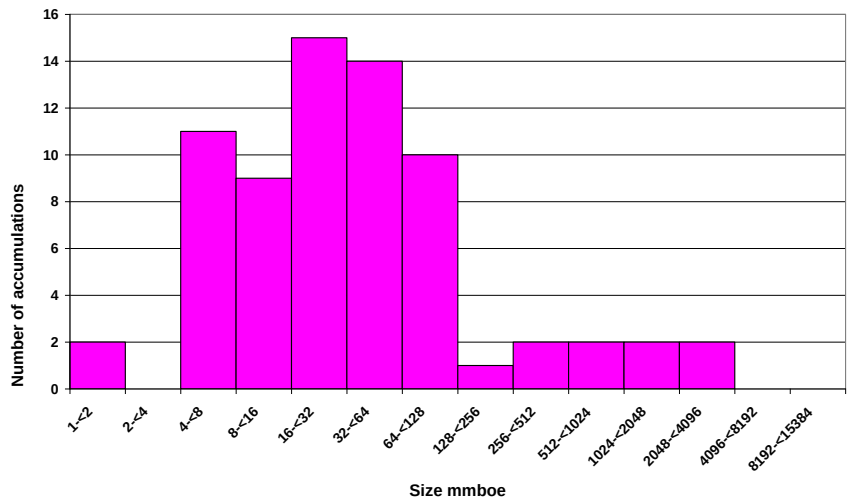

(c)

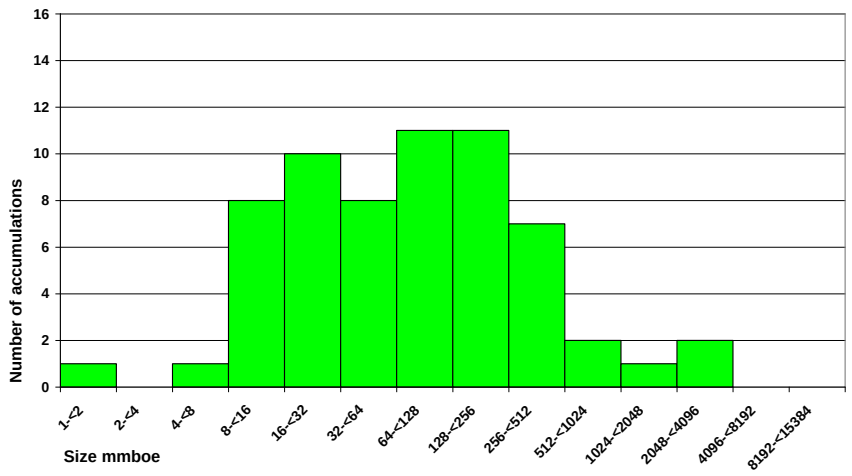

(d)

Figure 6.29: Size-frequency histograms of the sampled populations for the Paleocene play: (a) discoveries, S_1; (b) basin-modelled accumulations, S_2; (c) accumulations based on the unevaluated structural traps S_{3i}; and (d) accumulations based on the evaluated structural traps $S_{3ii.}$

6.4.2 Likely locations of undiscovered oil and gas

The most prospective areas in the Paleocene play are located immediately surrounding areas where Paleocene wells have already been drilled (Figure 6.30) based on the probable scenario using locations of discoveries and wells that have had strong indications of encountering hydrocarbons (Section 3.1).

There is, however, a large undrilled area that has a medium to low probability of hydrocarbon accumulation in the Manaia Anticline area. These results are most influenced by the structural traps, top-seal lithology and reservoir distribution input maps, based on the contrast values presented in Table 6.3.

The highest probability of hydrocarbon accumulation in the Paleocene play for the possible scenario, using the basin-modelled points of success, is along the eastern margin of the basin (Figure A2, Appendix 14). This area stretches from the Manaia Anticline area in the south and along most of the onshore eastern margin towards the north. Known as the Paleocene Taranaki Fault sub-play (IGNS, 1995) only one well, Te-Ranga-1, has tested the northern extent of this prospective area. The sandstone content of the reservoir increases toward the south (IGNS, 1995) and although no structural traps were identified on the regional maps, used in this study, there may be some structural closure against the Taranaki Fault (IGNS, 1995). An area of medium to low probability of hydrocarbon accumulation is predicted in a northeast-southwest striking band that begins just east of the Maui Field, heads eastward across the onshore peninsula and up into the offshore, southeastern extent of the Northern Graben. No wells have been drilled in this area, at this reservoir level. These results are most influenced by the structural traps, structural domains and gas generation and expulsion input maps, based on the contrast values presented in Table 6.3.

The only area with a high probability of hydrocarbon accumulation in the Paleocene play for the possible scenario using the evaluated traps points of success is around the Kupe and Toru fields (Figure A3, Appendix 14).

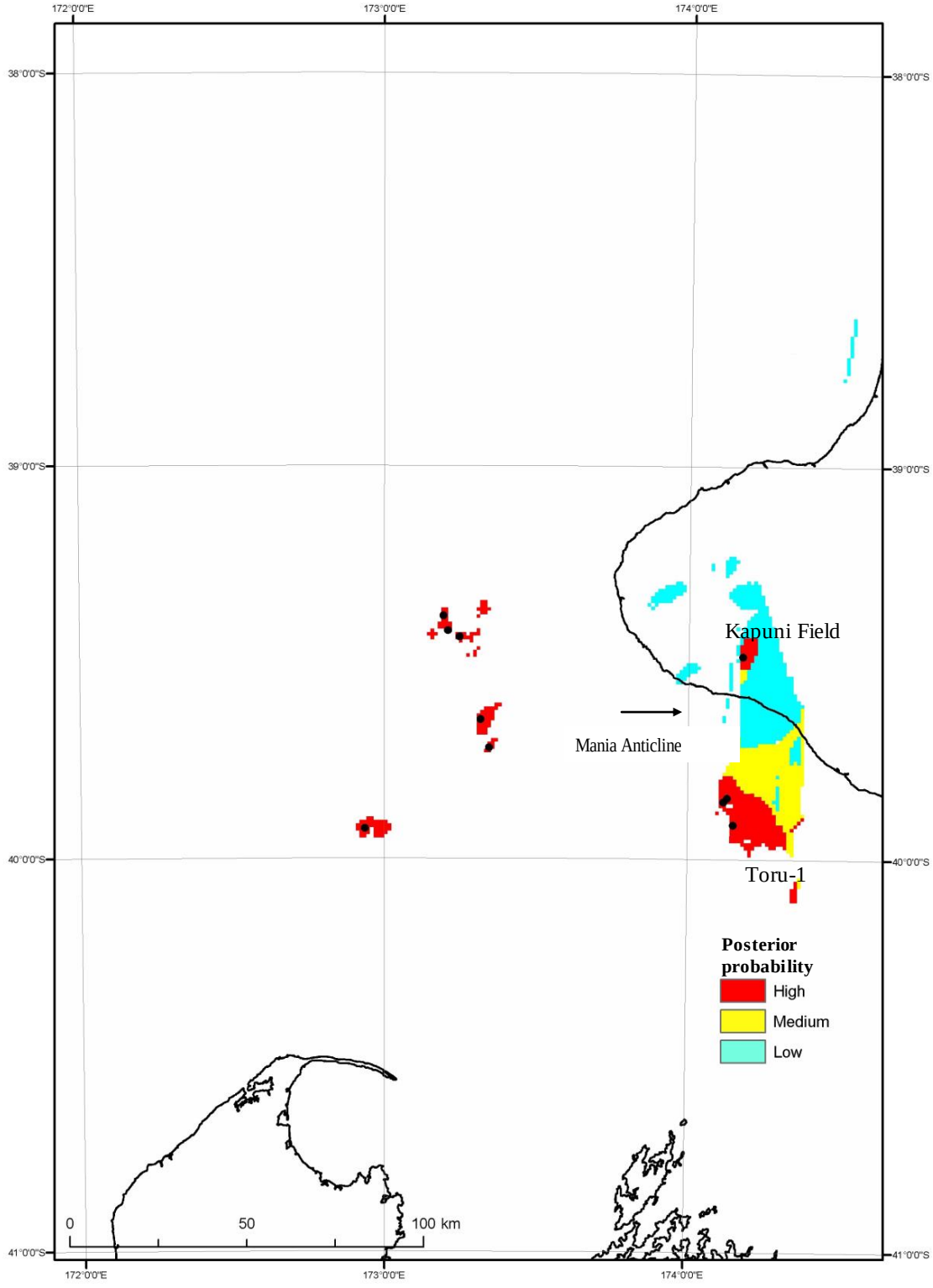

Figure 6.30: Relative posterior probability map for the Paleocene reservoir play based on the absolute probabilities of preferential hydrocarbon occurrence that were calculated for the probable scenario using success points based on discoveries and wells that encountered hydrocarbons (but were not discoveries).

Reverse faulting and subsequent uplift in the latest-Miocene has created large anticlines in this area (Thrasher et al., 1995a, 1995b) and these structures may be ideal traps, if not at the crest of the structure then possibly on the flanks of these anticlines (IGNS, 1995). These results are most influenced by the reservoir distribution and porosity, and seal integrity input maps, based on the contrast values presented in Table 6.3.

6.5 Eocene play

6.5.1 Amount of undiscovered oil and gas

The next discovery in the Eocene play is likely to be (with a 90% probability) equal to or greater than 30 mmboe (Figure 6.31). It may, however, be much larger (with a 10% probability) and be equal to or greater than 220 mmboe. The mean accumulation size is 119 mmboe. The Pareto results are based on an undiscovered population (Figure 6.32) that was calculated from a Pareto parent population containing 500 accumulations (Figure 6.33a). The mean drawn sample that statistically matched S_{3ii} (Figure 6.34d) and was used to define the parent has 121 accumulations (Figure 6.33b).

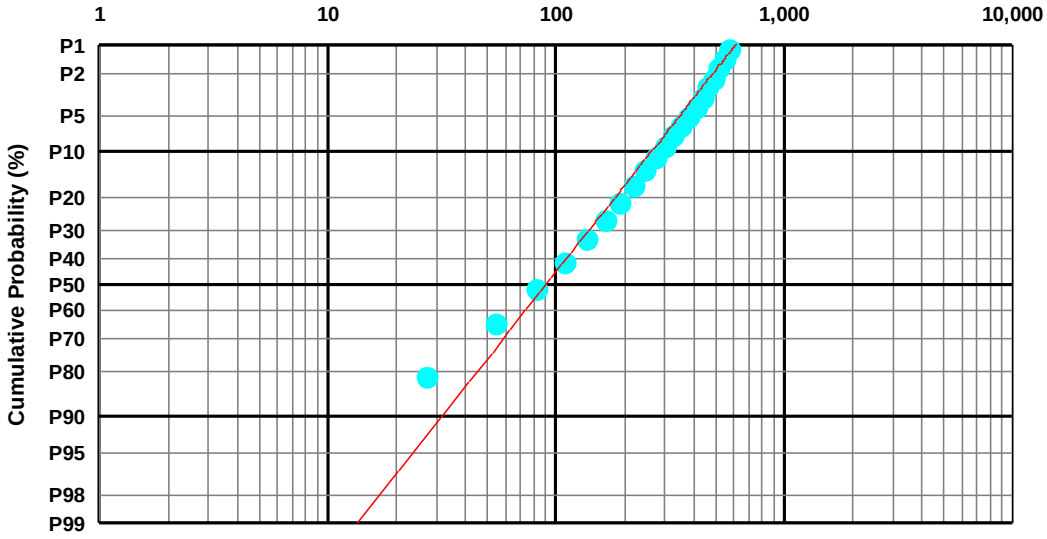

Figure 6.31: Cumulative probability distribution plot based on a Pareto parent population, which is used to estimate undiscovered oil and gas in the Eocene play. The horizontal axis is size, mmboe. The blue dots represent modelled discoveries. The red line is a best-fit regression curve and represents the parent population that is used to estimate the probability that the next discovery in this play is a certain size.

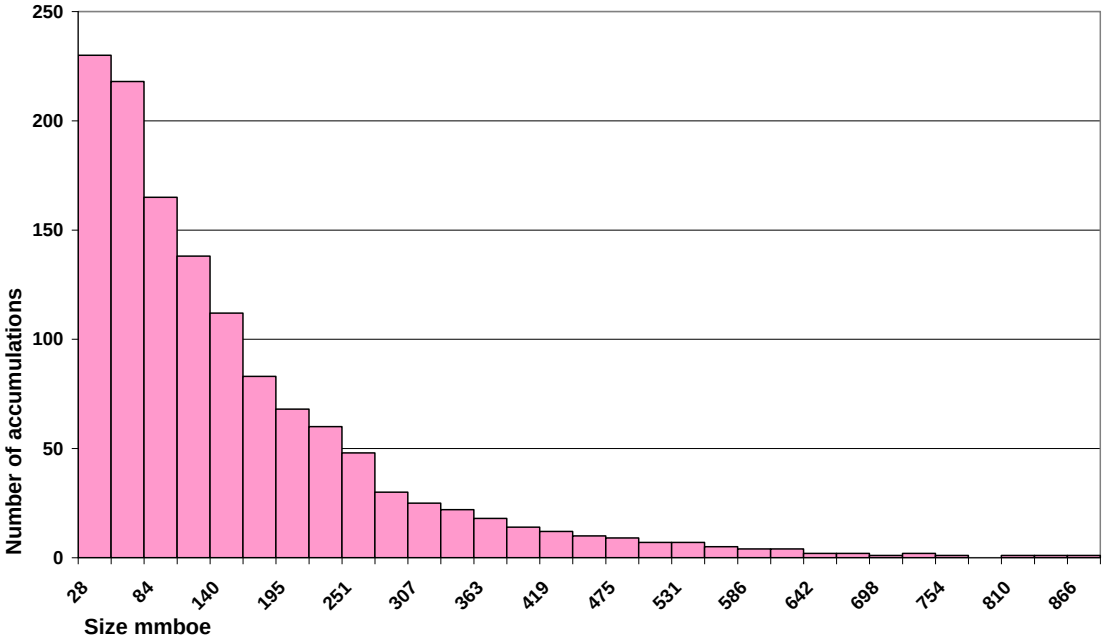

Figure 6.32: Size-frequency histogram of the mean parent population based on a Pareto probability distribution function, which was modelled for the Eocene play. Bin size denotes the maximum accumulation size for a bin, for example 28 is bin size 1–28 mmboe.

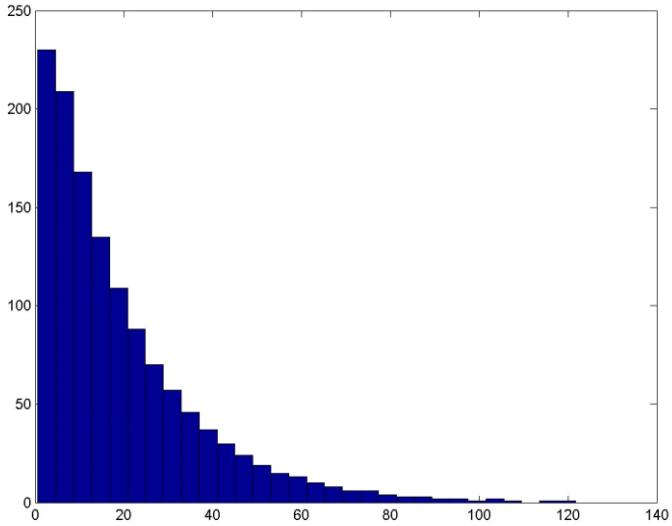

(a)

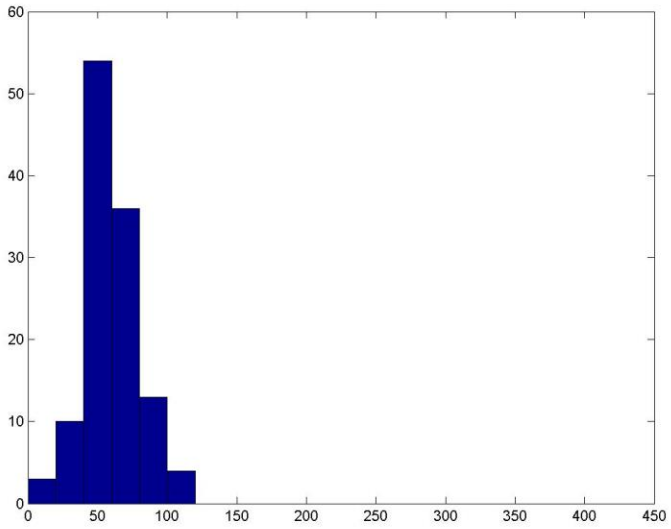

(b)

Figure 6.33: (a) This is the size distribution of the parent population from which sample (b) was drawn. The x-axis is size (km^2) y-axis is the number of accumulations. (b) This is the simulated mean sample of 120 oil and gas accumulations drawn from a Pareto parent population of NP = 1300 accumulations for the Eocene play. These two histograms have different bin sizes.

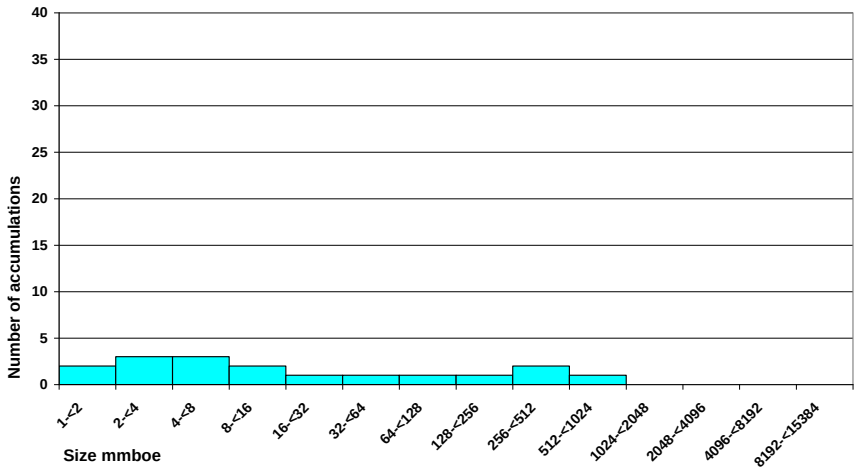

(a)

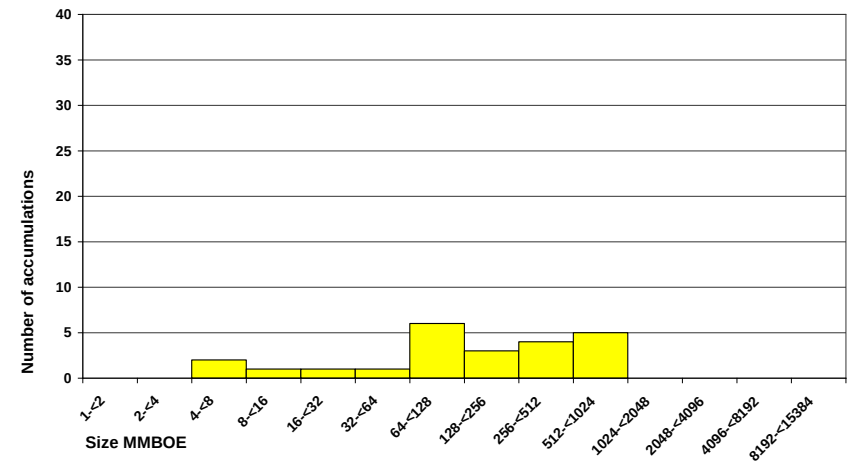

(b)

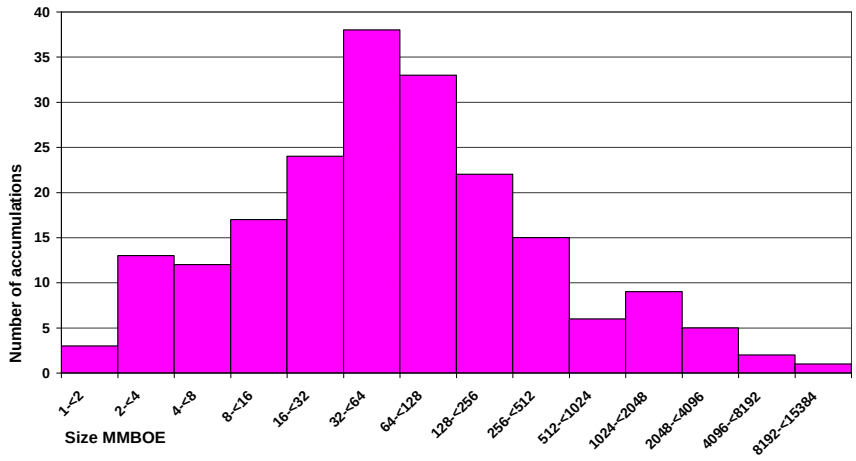

(c)

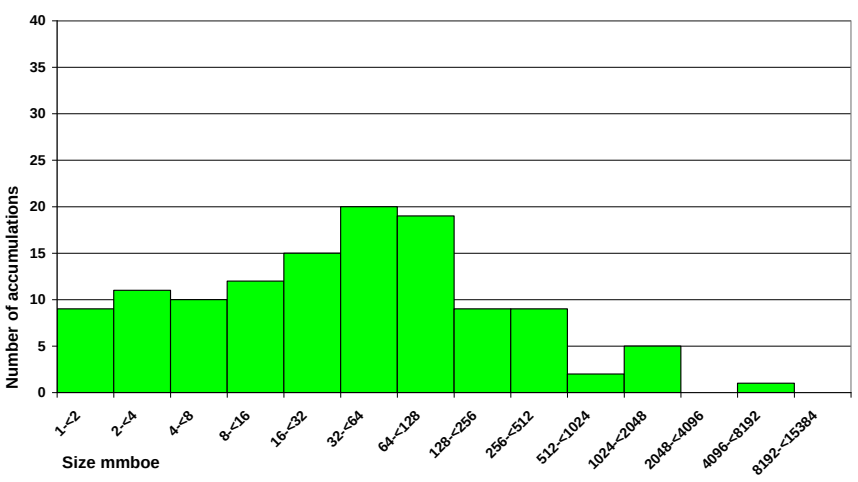

(d)

Figure 6.34: Size-frequency histograms of the sampled populations for the Eocene play: (a) discoveries, S_1; (b) basin-modelled accumulations, S_2; (c) accumulations based on the unevaluated structural traps S_{3i}; and (d) accumulations based on the evaluated structural traps S_{3ii}.

6.5.2 Likely locations of undiscovered oil and gas

The most prospective areas in the Eocene play are located predominantly onshore, along the eastern margin of the basin and Central Graben, where the Eocene coastal plain and detached shoreline sandstone fairway (King & Thrasher 1992; Flores et al., 1993; Thrasher et al., 1995d) is mapped and inferred (Figure 6.35). This result is based on the probable scenario using locations of discoveries and wells that have had strong indications of encountering hydrocarbons (section 3.1).

There are a number of other high-probability localities (Figure 6.35) that have not been drilled within the southwestern extent of the Central and Northern grabens, which are described in the basin assessment in section 5.2.2. There are no structural traps mapped in the two areas which have a high probability of hydrocarbon accumulation, straddling the southwestern edge of the basin coastline and offshore in the southern extent of the eastern margin. Suitable traps may exist, but without further information these areas are assigned with a relatively higher risk of containing undiscovered oil and gas, compared to areas where traps are identified. The probable scenario results have been mainly influenced by the maps of structural traps, migration pathways and reservoir distribution based on the contrast values in Table 6.3.

The estimation of undiscovered oil and gas in the Eocene play for the possible scenario, which is based on the basin-modelled points of success (Figure A5, Appendix 14) is similar to the probable scenario because there are only eight additional points of success in this scenario. The main difference is there are more areas of medium probability in the Northern Graben and Toru-1 well areas.

In contrast, the possible scenario, which is based on the evaluated traps (Figure A6, Appendix 14) has resulted in a probability map that is quite different from the probable scenario. In comparison, there is a slightly larger area of high probability over the Central Graben area. There is also a much greater coverage of medium and low probability in the Northern Graben, parts of the southwestern Central Graben and west of the Southern Inversion Zone. The increased areas of hydrocarbon prospectivity result in this scenario because of the greater number of structural traps that are included.

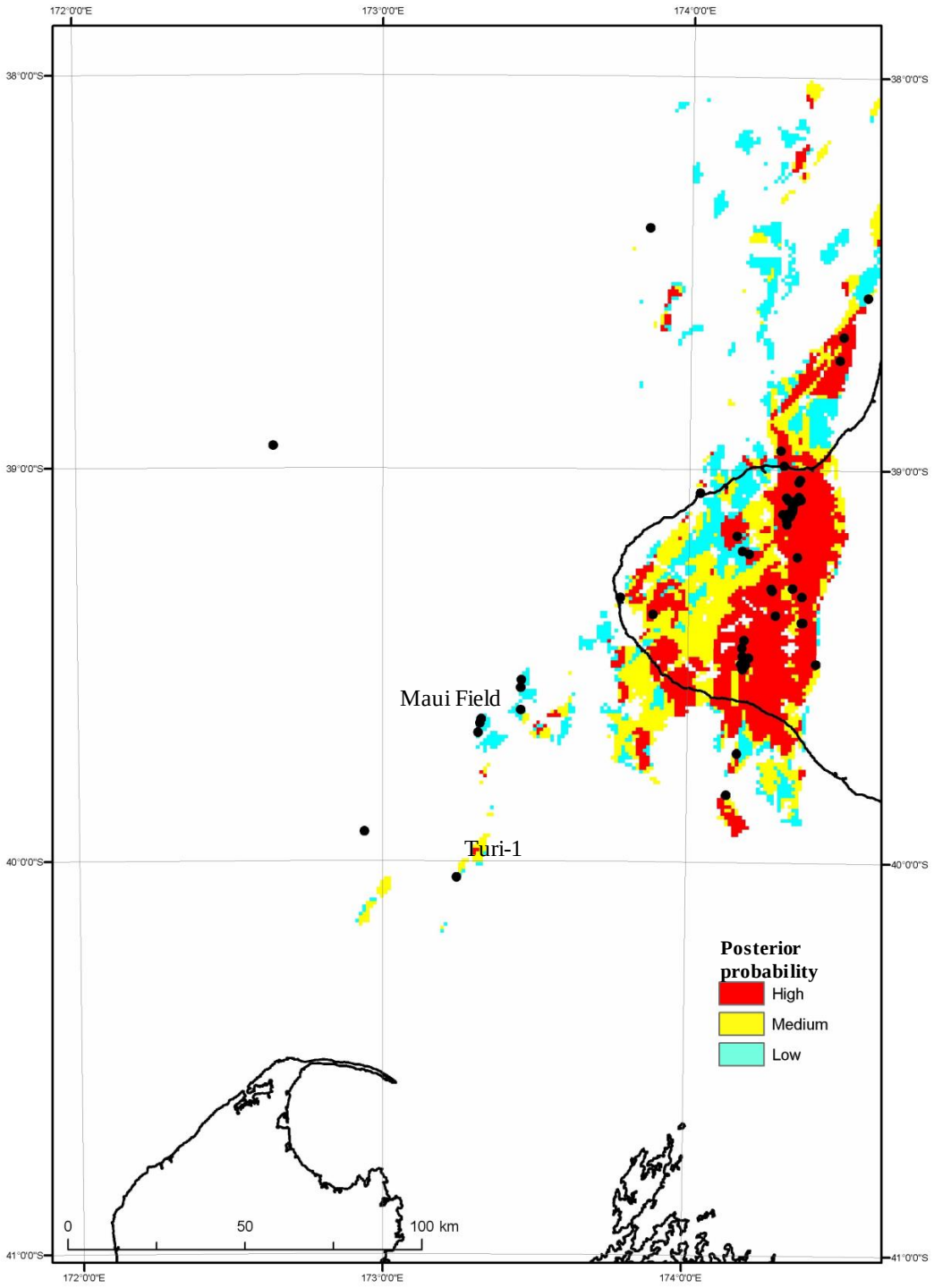

Figure 6.35: Relative posterior probability map for the Eocene reservoir play based on the absolute probabilities of preferential hydrocarbon occurrence that were calculated for the probable scenario using the discoveries success points.

Although there are a large number of structural traps further offshore towards the Western Platform, the posterior probability is not high in this area because other geological data, such as the distribution of mature source rock, are not mapped sufficiently in this area to generate higher probabilities.

6.6 Miocene play

6.6.1 Amount of undiscovered oil and gas

The next discovery in the Miocene play is likely to be (with a 90% probability) equal to or greater than 40 mmboe (Figure 6.36). It may, however, be much larger (with a 10% probability) and be equal to or greater than 310 mmboe. The mean accumulation size is 301.8 mmboe. The Pareto results are based on an undiscovered population (Figure 6.37) that was calculated from a Pareto parent population containing 300 accumulations (Figure 6.38a). The mean drawn sample that statistically matched S_{3ii} (Figure 6.39d) and was used to define the parent has 101 accumulations (Figure 6.38b).

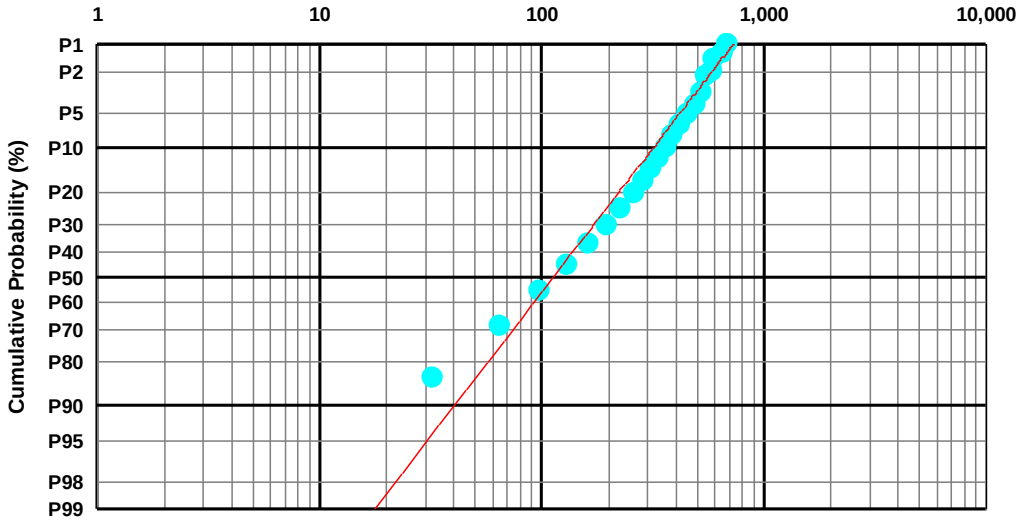

Figure 6.36: Cumulative probability distribution plot based on a Pareto parent population, which is used to estimate undiscovered oil and gas in the Miocene play. The horizontal axis is size, mmboe. The blue dots represent modelled discoveries. The red line is a best-fit regression curve and represents the parent population that is used to estimate the probability that the next discovery in this play is a certain size.

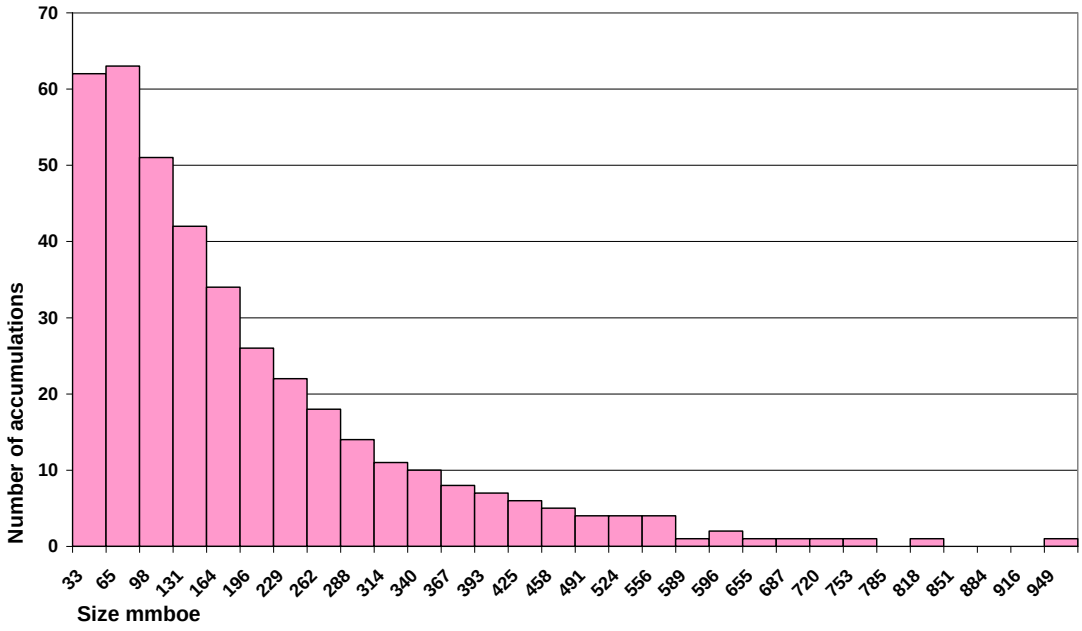

Figure 6.37: Size-frequency histogram of the mean parent population based on a Pareto probability distribution function, which was modelled for the Miocene play. Bin size denotes the maximum accumulation size for a bin, for example 33 is bin size 1–33 mmboe.

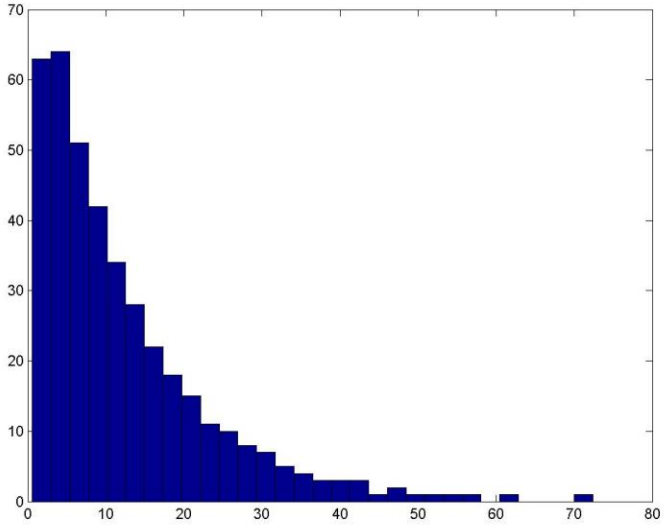

(a)

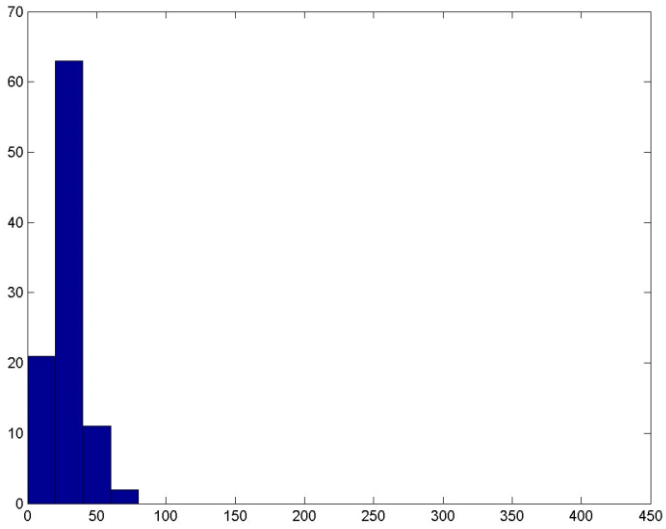

(b)

Figure 6.38: (a) This is the size distribution of the parent population from which sample (b) was drawn. The x-axis is size (km^2) y-axis is the number of accumulations. (b) This is the simulated mean sample of 97 oil and gas accumulations drawn from a Pareto parent population of NP = 300 accumulations for the Miocene play. These two histograms have different bin sizes.

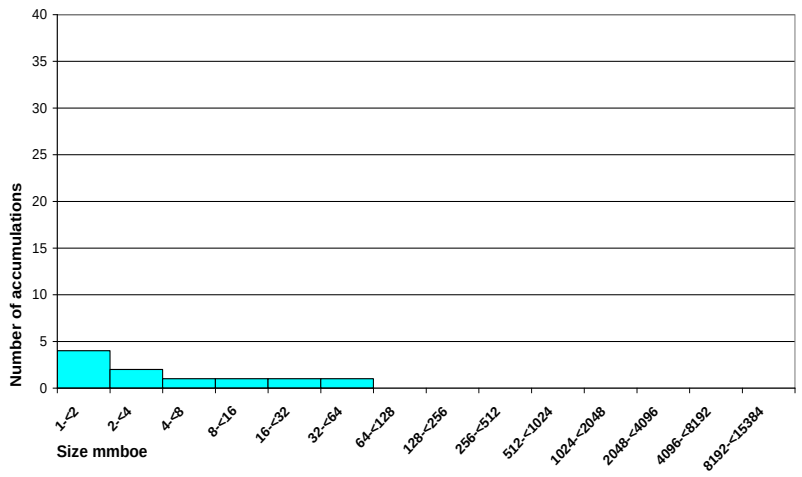

(a)

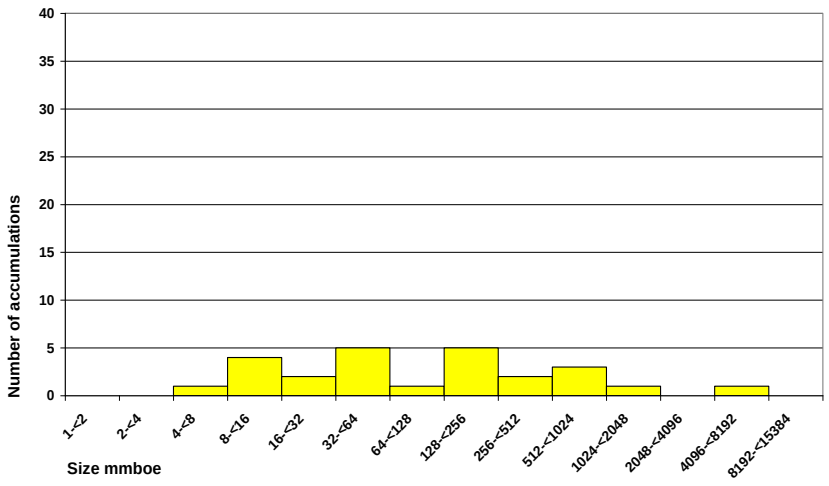

(b)

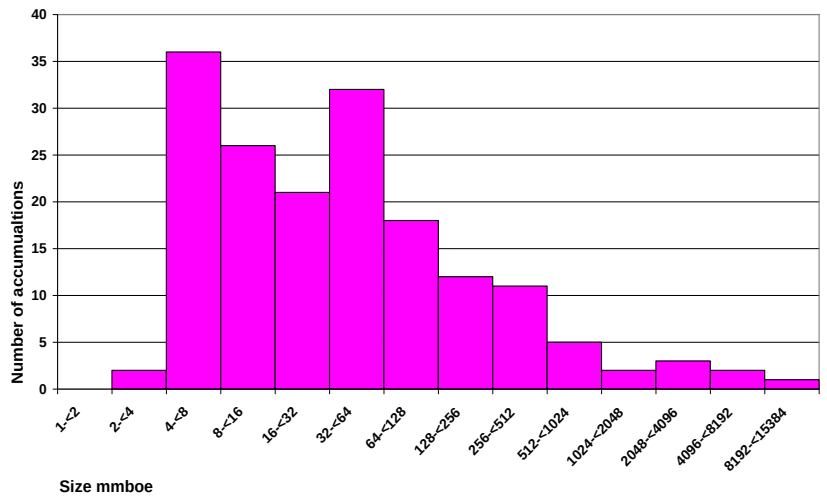

(c)

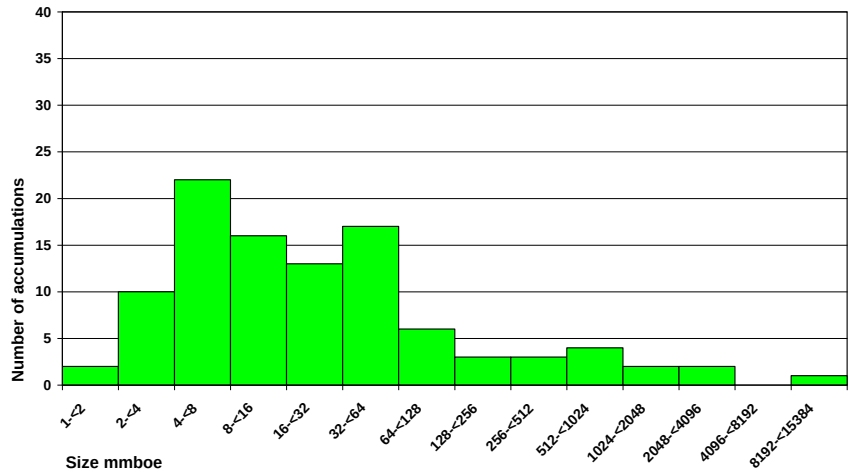

(d)

Figure 6.39: Size-frequency histograms of the sampled populations for the Miocene play: (a) discoveries, S_1; (b) basin-modelled accumulations, S_2; (c) accumulations based on the unevaluated structural traps S_{3i}; and (d) accumulations based on the evaluated structural traps S_{3ii}.

6.6.2 Likely locations of undiscovered oil and gas

The most prospective areas in the Miocene play are located in the onshore part of the basin and areas within the Northern Graben based on the probable scenario (Figure 6.40) and the possible scenario using the basin-modelled points of success (Figure A8, Appendix 14). These are as discussed in the basin assessment in Section 6.2.2.

The possible scenario estimation is most influenced by the input maps which show the main structural domains, distribution of migration pathways and gas generation and expulsion. Nearly the entire Northern Graben has a medium to low probability of hydrocarbon accumulation. An offshore area immediately northeast of the Maui Field, which is assigned with a medium to high probability, was not generated by the probable scenario. No wells have been drilled here but the high probabilities are where the Moki sandstones sub-play (IGNS, 1995) and Neogene created fault blocks (Thrasher et al., 1995) are mapped.

The estimation of undiscovered oil and gas in the Miocene play for the possible scenario using the evaluated traps (Figure A9, Appendix 14) is similar to that of the possible scenario using the basin-modelled points of success. The greatest difference is the reduced area of high probability in the onshore peninsula area. Another difference is in the Northern Graben area, where areas are assigned with a medium to low probability of hydrocarbon accumulation. There are no areas assigned with a high probability of hydrocarbon accumulation, as in the possible scenario. An area that was assigned a low probability of hydrocarbon accumulation that was not generated using the basin-modelled data is located in the Kupe and Toru fields' area. This locality coincides with the Manaia and Tarata flank play (IGNS, 1995) where Moki Formation sandstones may onlap inverted anticlines, creating prospective stratigraphic traps (King & Thrasher, 1996). These results are most influenced by the evidential theme maps of structural traps, migration pathways and reservoir distribution, based on the contrast values in Table 6.3.

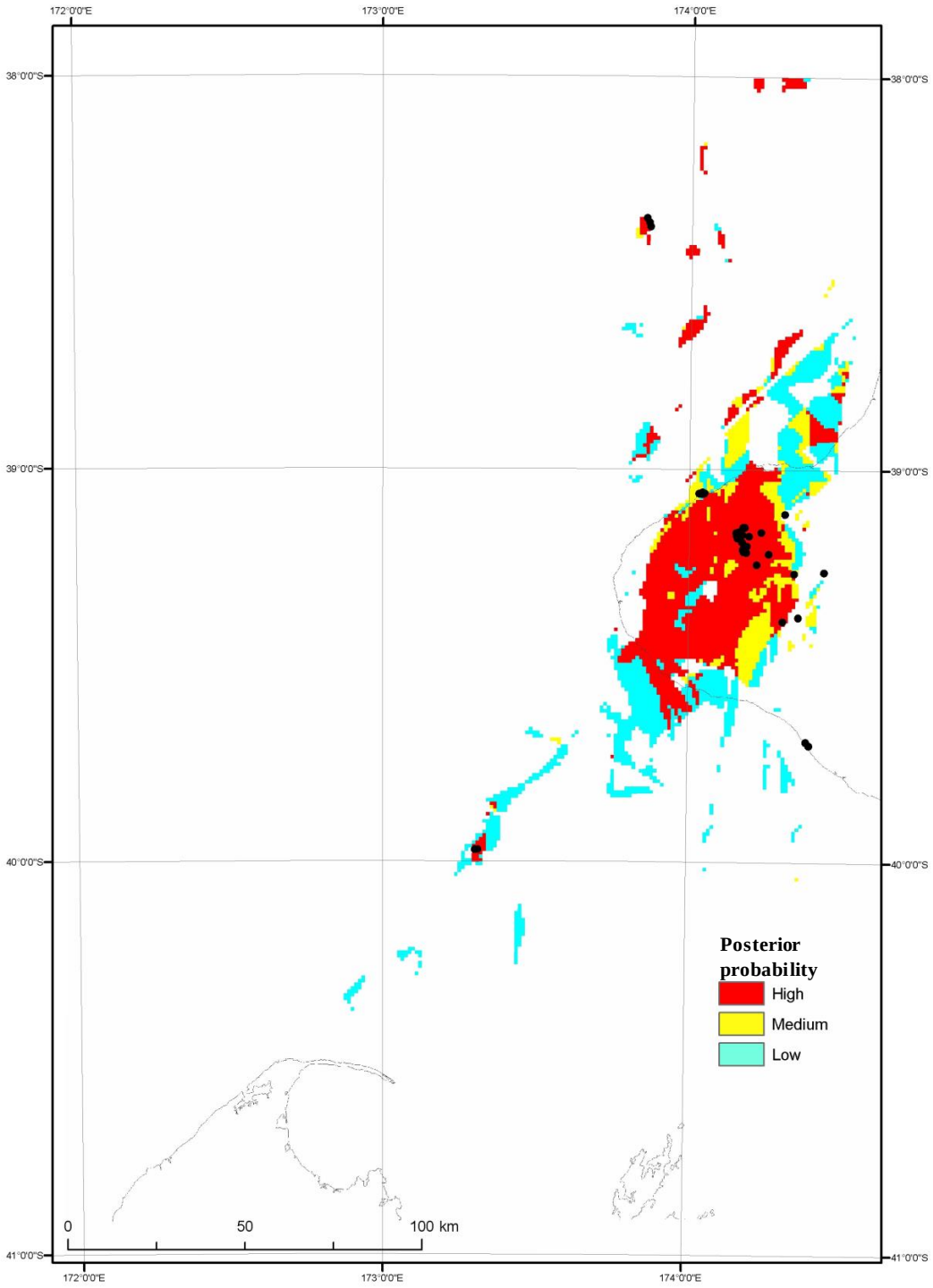

Figure 6.40: Relative posterior probability map for the Miocene reservoir play based on the absolute probabilities of preferential hydrocarbon occurrence that were calculated for the probable scenario using the discoveries success points.

6.7 Discussion

6.7.1 Volumetric estimation

6.7.1.1 Number and size of accumulations in a sampled population

The S_{3ii} dataset of evaluated traps for the basin has a significantly larger number of accumulations (338) than the S_1 dataset of discoveries (33) (Table 6.1). The number and size of the accumulations in the sampled population, which is used in the discovery-sequence simulation to define the parent population, has significant impact on the size distribution of the modelled parent. For example, Figure 6.41 shows a cumulative probability plot of undiscovered oil and gas that is modelled using the S_1 sample and Figure 6.42 shows a cumulative probability plot of undiscovered oil and gas that is modelled using the S_{3ii} sample. The regression curve through the S_{3ii}-derived parent population is much steeper, which means it has a larger P50 of 160 mmboe, compared to 10 mmboe of the S_1 parent.

The largest accumulation in a S_1-based parent is very similar to the largest accumulation in most of the parent populations that were modelled using S_{3ii} for the Pareto and lognormal distributions. However the S_{3ii} dataset has a tendency to produce a parent that contains a greater number of large accumulations and less small accumulations than the S_1 dataset. For example, the size-probability trend of discoveries shown in Figure 6.41 predicts a P90 of ~1 mmboe, P10 of 180 mmboe and mean of 58 mmboe. In comparison, the regression curves that are based on the evaluated traps are much steeper (e.g. Figure 6.42). This figure shows a P90 of 55 mmboe, P10 of 510 mmboe and mean of 234 mmboe. This outcome is attributed to the greater number of large accumulations in the S_{3ii} population.

6.7.1.2 Fitting a parent population regression curve

Predicting the size of the next discovery on a cumulative probability plot is sensitive to the gradient of the regression curve. For example, the regression curve of Figure 6.43 has been refitted in Figure 6.44 by forcing the regression through the smallest accumulations, which results in a less steep curve. As a result the estimation results, and in this example

the refitted curve, predicts a lower P90 (17 versus 30 mmboe) a higher P10 (450 versus 220 mmboe) and higher mean (172.1 versus 132.3 mmboe).

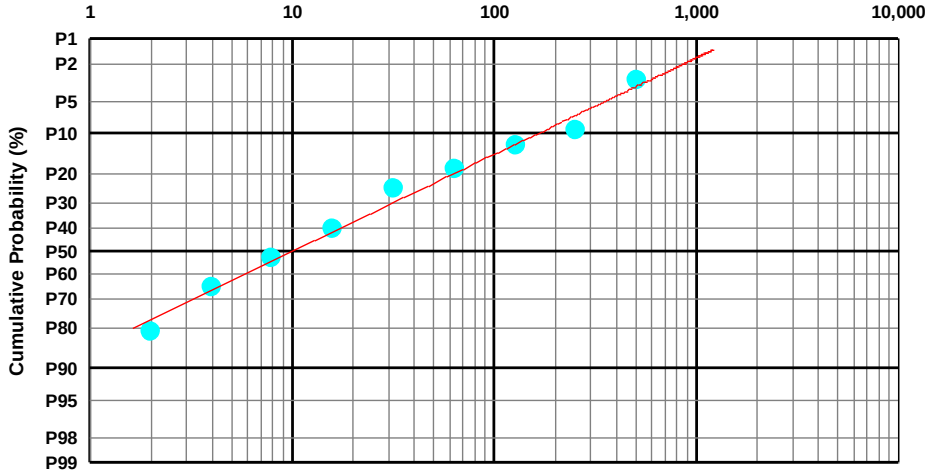

Figure 6.41: Cumulative size-probability distribution plot based on a Pareto parent population probability distribution function and used to estimate undiscovered oil and gas accumulations in the Taranaki Basin. The parent population was modelled using the S_1 sampled population of discoveries. The red line is the best-fit regression curve through the discoveries (blue dots). The horizontal axis is size, mmboe.

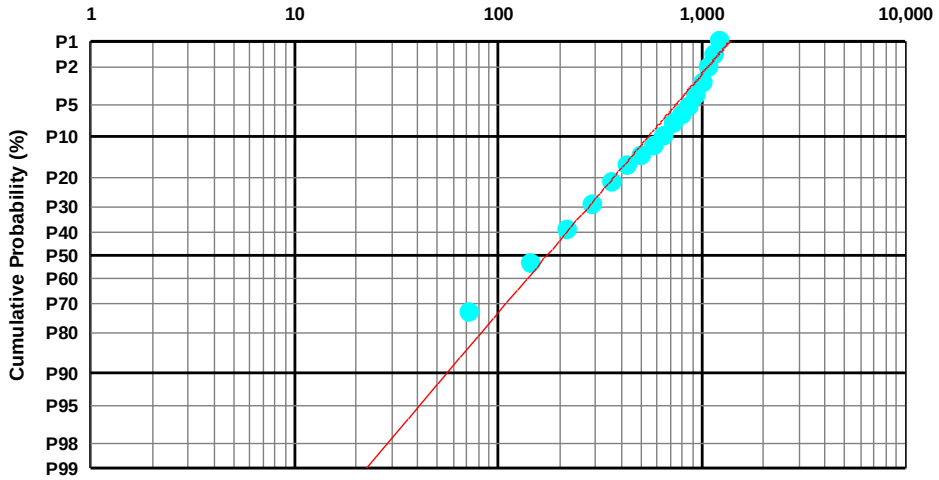

Figure 6.42: Cumulative size-probability distribution plot based on a Pareto parent population probability distribution function, and used to estimate undiscovered oil and gas accumulations in the Taranaki Basin. This parent population was modelled using S3ii, the sampled population of evaluated traps. The red line is the best-fit regression curve through the trap-based accumulations. The horizontal axis is size, mmboe.

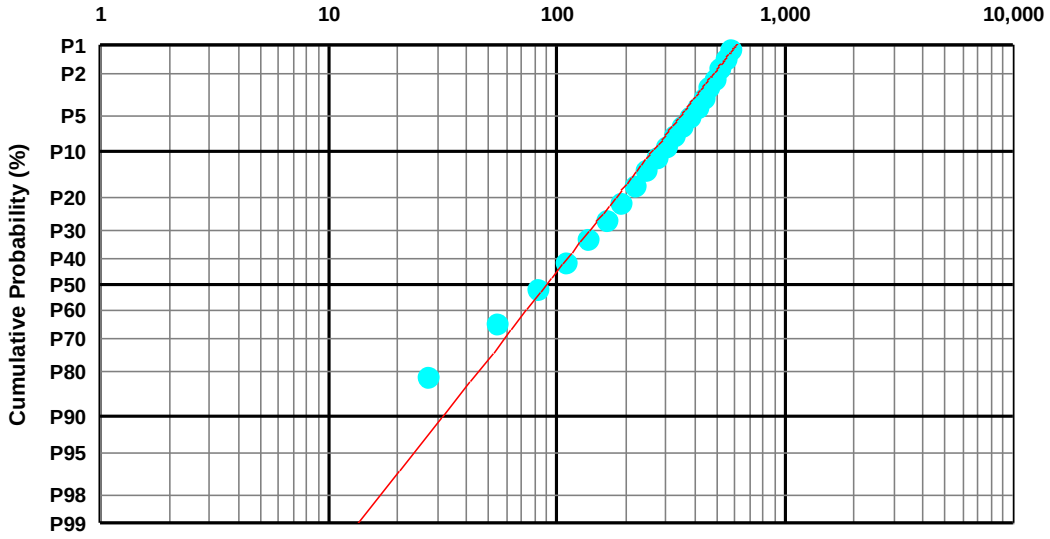

Figure 6.43: Cumulative size-probability distribution plot for the Eocene play, based on a Pareto parent population probability distribution function, which is used to estimate undiscovered oil and gas accumulations for this play in the Taranaki Basin.

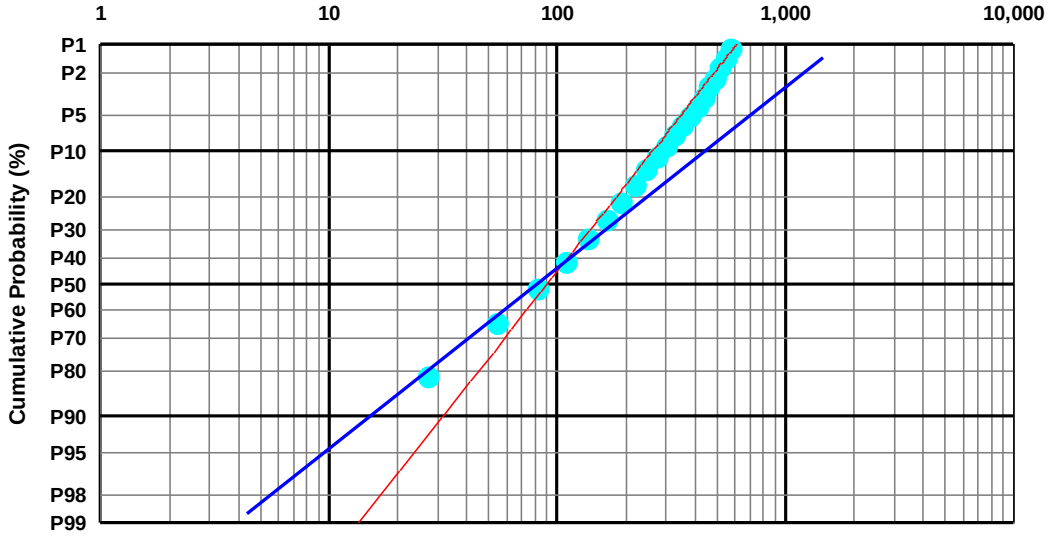

Figure 6.44: Revised cumulative size-probability distribution plot for the Eocene play, based on a Pareto parent population probability distribution function which is used to estimate undiscovered oil and gas accumulations for this play in the Taranaki Basin. The red line is the original best-fit regression curve through the accumulations. The dark-

blue line is a best-fit curve that has been refitted to include the smallest accumulations. The horizontal axis is size, mmboe.

6.7.1.3 Approximating the parent population

The Pareto and lognormal distributions are graphically similar and have long right-hand-side tails of probability space, which indicates most of the accumulations are approximately mean size and smaller, and very few are large (Laherrere, 2000; Downey, 2005). However, they are different numerically; which causes differences in estimation results.

The number of accumulations modelled in a parent population differs for a Pareto and lognormal probability distribution functions. For example, for the basin assessment the Pareto parent produced an undiscovered population of 1,000 accumulations and the lognormal parent produced an undiscovered population of 10,000 accumulations. This difference may be due to the way they are numerically truncated and the subsequent ability of each distribution to simulate proportional size ranges (Attanasi & Charpentier, 2002).

The greatest impact of this difference is the lognormal distribution is weighted more towards predicting a greater number of large oil and gas accumulations whereas the Pareto probability distribution tends to produce a greater number of small accumulations. This difference in the number of accumulations in the modelled undiscovered population has a minimal impact on the mean accumulation size for the basin assessment; it is 328.7 mmboe for the Pareto distribution and 363.5 mmboe for the lognormal distribution.

However the difference in the number of accumulations in the undiscovered population has a significant impact on the probability of discovering a large accumulation, such as the P10 volume. The differences in the probability-size estimates (P10, P90, Pmean) are shown in Table 6.2. For the basin and all plays, except the Cretaceous, the lognormal distribution predicts larger P10 values than the Pareto. This outcome has a direct impact on the number of large accumulations that are modelled in the undiscovered population

and total resource volumes estimated; it is 8210–10800 mmboe using the Pareto probability distribution function and 30727–38275 mmboe using the lognormal probability distribution function.

6.7.2 Spatial estimation

The probable and possible scenarios predict that the onshore part of the basin is the most prospective even though there are more structural traps mapped offshore for all plays. Therefore, other evidential theme maps must have had a greater influence on the probability predictions. A greater amount of exploration has occurred in the Eastern Belt compared to the Western Platform and as a result, more wells have been drilled onshore and there is greater understanding of the petroleum systems in this part of the basin. The spatial data modelling results are most influenced by the variation in the amount of data across the basin (Ganguli & Dandopadhyay, 2003) and this may explain why more favourable areas of hydrocarbon accumulation are predicted in the onshore part of the basin.

Evidential theme maps with the greatest contrast have the greatest control on the spatial predictions and Table 6.3 shows the results were influenced by a variety of evidential theme maps, for all modelling scenarios and all plays. For example, the structural domains and oil and gas generation and expulsion maps had the greatest influence on the results of the Paleocene and Eocene plays. The reservoir distribution and migration flowpath maps had the greatest influence on the results for the Miocene play.

However, the reservoir distribution and structural trap maps had the greatest influence on the spatial predictions for all three plays, in both scenarios. This outcome suggests new discoveries are most likely where reservoir and structural traps are mapped, as expected, and is a reminder that future research and exploration may be best focused on acquiring improved data and knowledge about reservoir and structural traps in the basin. For example, there are a number of thrust fault zones in the Taranaki Basin and imaging these faults on seismic data is a challenge (Percher et al., 2004). However, with improved seismic acquisition and processing and better resolved thrust faults, more structural traps

may become obvious in these potentially prospective areas. Similarly, improved seismic imaging of reservoir intervals and more detailed facies mapping and modelling would improve the interpretation of reservoir features such as reservoir seal pairs and basin floor sands within the Miocene sequences.

6.8 Conclusion

The estimated undiscovered resource in the Taranaki Basin is 8,210-10,800 mmboe across some 1,500 accumulations. This volume is approximately 4.5 times greater than what has already been discovered and expresses the hydrocarbon potential of the underexplored parts of the basin, which represent ~70% of the study area. Current working petroleum systems are expected in areas of the basin that are most likely to contain the undiscovered resource, suggesting the basin is geologically favourable for future exploration.

Based on the locations of existing discoveries in the basin, new discoveries are most likely in the onshore Taranaki Peninsula, along the eastern margin of the basin, in the Northern Graben, and the Western Platform and Central Graben areas; especially where the Eocene reservoir play is mapped. The Manaia anticline area and two offshore areas immediately east of the Maui Field and proximal to the Toru-1 discoveries are particularly prospective. New discoveries may be located also in more extensive areas of the Northern Graben, Western Platform and Central Graben, as well as the Southern Inversion Zone, based on the spatial modelling possible scenario and potential discoveries produced by identifying structural traps and basin-modelling.

A Pareto and lognormal probability distribution function were used to approximate the original population of all oil and gas accumulations and derive populations of undiscovered oil and gas. The Pareto function is preferred because the lognormal function generated a large number of accumulations >1,000 mmboe which was considered geologically unrealistic. As a result of its tendency to generate many large accumulations the lognormal population estimates an undiscovered resource of ~10,000 accumulations, totalling 30,727–38,275 for the basin. Although the estimation is based

on a large study area of 100,000 km^2 and a 9–11 km-thick sedimentary sequence of multiple reservoirs these results are considered excessive.

Chapter 7

Conclusions and recommendations for future work

Estimates of the amount and likely location of undiscovered oil and gas are presented for the Taranaki Basin. The Dual Component Estimation (DCE) approach combines a modified size-distribution-based, discovery-sequence sampling model (e.g. Arps & Roberts, 1958; Barouch & Kaufman, 1977; Forman & Hinde, 1986) with a spatial model (Bonham-Carter, 1994) to revise previous estimations for the Taranaki Basin (Cook, 1985; Beggs & Cook, 1993; King & Thrasher, 1996; Beggs, 1998; O'Connor, 2002; Mare-Jones, 2004) leading to a number of conclusions.

7.1 Resource potential and prospectivity

It is estimated that ~1500 oil and gas accumulations remain undiscovered, totalling a resource potential of 8210–10800 mmboe (Appendix 16). However, if the Maui A accumulation (Table 1.1) is the biggest accumulation in the Taranaki Basin the resource potential is 4962–5850.

All four plays have potential to yield new discoveries including the Cretaceous play, which remains unproven and the Paleocene and Eocene plays that have produced the greatest volumes to date. New discovery sizes are likely to be at least 50 mmboe (with a 90% probability) which is a significant commercial size and the mean discovery size is 328.7 mmboe. However, there is potential for a much greater and the next discovery could be at least 550-900 mmboe (with a 10 % probability).

New discoveries are estimated both onshore and offshore and are most likely to be found in the onshore Taranaki Peninsula along the eastern margin, especially in the Manaia anticline area (Section 6.3) and offshore in the Northern Graben, Western Platform and Central Graben where Eocene reservoirs are deposited (Figures A4-A6, Appendix 14). In

particular, a new discovery is likely immediately east of the Maui Field and proximal to the Toru-1 discovery in an area which is currently undrilled.

The basin has good potential to yield further significant discoveries based on the basin-wide extent of the mapped working petroleum systems (King & Thrasher, 1996) and unproven play concepts (Thrasher et al., 1995a–e). In particular, hydrocarbon charge is likely to be from a number of mature source rocks, which are located throughout most of the basin. Spatial modelling shows that most of the discoveries are located within five kilometres of a major fault, suggesting faults are probably effective migration pathways in the Taranaki Basin. Based on this and the amount of faulting migration pathways are expected throughout most of the basin.

Most potential accumulations modelled in this study are located offshore and are yet to be tested (Figures A1–A4, Appendix 14). Most of the structural traps that were identified in this study also remain untested. Some of the mapped traps were not charged in the basin model and further work is needed to explain this outcome.

The predominantly onshore-based discoveries in the basin probably reflect explorers' preferences to drill shallow and easily accessible wells, more than the prospectivity of the basin. The few offshore fields, such as Kupe, Tui and Maui (Figure 1.3) and discoveries, such as Moki-1, Karewa-1 and Kora-1 (Figure 1.3) confirm there are working petroleum systems in deeper-water parts of the offshore basin.

7.2 Advantages of the inverse discovery-sequence simulation

A traditional discovery-sequence sampling method, which makes well-known assumptions about the probability of discovery, was modified in this study (Chapter 4) to derive a parent population of oil and gas accumulations that is suitable to estimate undiscovered oil and gas in an underexplored basin. The sampling method was used to simulate a mean sample of potential discoveries in order to estimate a mean parent population. As a result many possible parent populations were simulated ensuing a good probabilistic model is used to estimate the undiscovered portion.

The inverse nature of the sampling method means that the size distribution of the parent population was defined first using quantitative analysis and was not based on a direct extrapolation of a sample of discoveries, typical of forward-modelled discovery-sequence methods. This resulted in the derivation of a parent population unconstrained by the size distribution of few discoveries, typical of an underexplored basin.

The parent population was then redefined using potential discoveries, which were based on basin modelling and structural traps. This means the hydrocarbon potential of unexplored areas were included in the assessment and the number of accumulations to base the parent population on increased from 33 to 338 (Table 6.1). As a result the estimated parent has a more representative size distribution and is geologically based; for example, the maximum size of the parent is based on the largest possible trap and not the largest discovery to date.

7.3 Usefulness of the assessment

The assessment presented here is an invaluable addition to our understanding of the hydrocarbon potential of the Taranaki Basin and will assist any review of New Zealand's future energy supply. It is better than previous assessments of the hydrocarbon potential of the Taranaki Basin because it uses a methodology that is specifically suitable for the basin, given a large part of it is underexplored and geologically prospective. In particular, the estimates are calculated from a mean parent population that is geologically defined and has been determined from a large number of possible outcomes resulting in an original population of all oil and gas accumulations that is representative of the basin's prospectivity. The estimates are also presented probabilistically to acknowledge the many sources of uncertainty that are involved with assessing undiscovered oil and gas in such a large underexplored area that has experienced a variable tectonic and depositional history.

This is the first time the combined volumetric and spatial models have been applied to estimate undiscovered oil and gas in Taranaki Basin and the first available maps showing where the undiscovered oil and gas is likely to be located are presented. The estimation

results are particularly suitable to guide exploration risk profiles and inform investors interested in exploring in the basin.

The estimation results presented indicate that the basin is more prospective than the ~1000 mmboe undiscovered oil and gas suggested by previous resource assessments (Table 1.2). The estimates in this study are greater than those previously published primarily because they take account the entire basin, onshore and offshore, are for both oil and gas, and include the four most productive and prospective reservoir intervals in the basin. Previous estimates are also probably underestimates because a small number of discoveries were used to approximate the parent population using non-quantitative analyses (Chapter 2).

The estimated volumes are credible because a number of discoveries in the Taranaki Basin are of a similar size and basin and spatial modelling indicate there is potential for new accumulations of oil and gas in all reservoirs that were studied. Many structural traps were identified in these prospective areas, including some that are larger than the largest discovery, Maui-A, which has 533 mmboe.

In contrast to other statistical estimation methods, the estimation here builds in a substantial amount of geological data. Understanding hydrocarbon generation, charge and entrapment is fundamentally necessary to be able to understand the potential for undiscovered oil and gas in a basin.

7.4 Recommendations for future work

Several aspects of this study should be reinvestigated to improve the approach and estimates, and minimise the associated uncertainties.

7.4.1 Improved data quality

Chapter 6 shows that a discovery equal to or greater than 550 mmboe has only a 10% probability; however, the estimation presented may also be an underestimation, given the geological potential and hydrocarbon prospectivity of the basin (Sections 2.3 and 3.4).

The estimation primarily depends on the semi-synthetic datasets of oil and gas accumulations and they depend primarily on the resolution of the data that were used to build the inputs of the basin model and identify the structural traps. As a consequence, more detailed data should result in a greater number of semi-synthetic accumulations and improve the validity of them (in the basin model) which would improve the quality of the estimation.

7.4.2 3D basin model

Some of the basin modelling limitations discussed in Chapter 6 may have been reduced by applying a fully integrated 3D basin model. However, the scope of this research, which was focused on developing a method to estimate undiscovered oil and gas in an underexplored basin, did not allow for the time required to build a 3D basin model for the Taranaki Basin.

An integrated 3D basin model, which combines hydrocarbon generation and expulsion with migration and entrapment, would result in a better examination of the accumulation of oil and gas in the Taranaki Basin. A full basin evolution approach would mean the impacts of major geological processes that affect the thermal regime and sediment compaction, such as uplift and erosion, volcanism and overpressures, and process that affect trap volumes, such as tectonic tilting, would be included in the model. For example, the models used here do not predict reservoir temperature, which impacts on the quality of trapped hydrocarbons and reservoir. More detailed input maps, such as reservoir distribution, would have a significant impact on the size, number and location of simulated accumulations. A 3D model would also enable detailed sensitivity studies by modelling processes such as top seal fracturing and hydrocarbon leakage, and physical conditions, such as stacked reservoirs and pore pressure build-up.

7.4.3 Variable exponential of discovery

The discovery coefficient, γ, (Arps & Roberts, 1958; Attanasi, 1980; Power, 1990), which is used in the discovery-sequence simulation to model the probability of discovery

(Section 4.2.2.6) is fixed. In reality it is variable in order for it to properly reflect impacts such as advances in technology and increased geological knowledge (Forman & Hinde, 1986). The potential discoveries that were simulated in this study are essentially time-less because a series is simulated instantaneously. They were used to produce a sample of discoveries representative of the overall exploration effort in a basin, therefore the fixed exponential was suitable. However, if a variable exponent were to be used, series of discoveries through time could be used to generate projected series of discoveries until the parent population of all accumulations was exhausted. This approach could be used to ground truth the statistical pattern of the size-frequency histogram of each series of simulated discoveries with the modelled progression of discovery.

7.4.4 Automated statistical comparison

The statistical comparison between the drawn sample of discoveries and a sampled population of accumulations, such as S_3, could be improved by automating the statistical comparison within the simulation. This would increase the accuracy and objectivity of the comparison and the simulation would run automatically until a statistical match was found.

References cited

Adams, S. (1998). Formation evaluation of wells in and adjacent to PEP38462, Offshore Taranaki Basin, New Zealand. Open file petroleum report: PR2433, Spectrum Exploration Limited: 26.

Allen, J.R (1990). The petroleum play. Basin Analysis. Blackwell Science Ltd: 309–396.

Agterberg, F. P., G. F. Bonham-Carter, Q. Chen and D. F. Wright (1993). Weights-of-evidence modelling and weighted logistic regression for mineral potential mapping. Computers in Geology, 25 years of progress (Eds: J.C Davis and U.C Herzfield). (Oxford University Press, Oxford): 13-32.

Aitchison, J. and J. A. C. Brown (1957). The lognormal distribution, Cambridge University Press, Cambridge.

Allis, R. G., P. A. Armstrong and R. H. Funnell (1995). Implications of a high heat flow anomaly around New Plymouth, North Island, New Zealand. New Zealand Journal of Geology and Geophysics 38: 121-130.

ARCO Petroleum (1985). Final well report Kora-4, PPL38447. Open-file petroleum report PR1443, Ministry of Economic Development, Wellington, New Zealand.: 243.

ARCO Petroleum (1988). Final well report Kora-1, Kora-1A, PPL38447. Open-file petroleum report PR1374, Ministry of Economic Development: 781.

Armstrong, P. A. (1996). Thermal History of the Taranaki Basin. Department of Geology and Geophysics. Utah, University of Utah: 245.

Armstrong, P. A., R. G. Allis, R. H. Funnell and D. S. Chapman (1998). Late Neogene exhumation patterns in Taranaki Basin (New Zealand). Evidence from offset porosity-depth trends. Journal of Geophysical Research 103(B12): 30,269-30,282.

Armstrong, P. A., D. S. Chapman, R. H. Funnell, R. G. Allis and P. J. J. Kamp (1996). Thermal modelling and hydrocarbon generation in an active-margin basin: Taranaki Basin, New Zealand. American Association of Petroleum Geology Bulletin 80: 1216-1241.

Armstrong, P. A., D. S. Chapman, R. H. Funnell, R. J. Allis and P. J. J. Kamp (1994). Thermal state, thermal modelling, and hydrocarbon generation in the Taranaki Basin, New Zealand. 1994 New Zealand Petroleum Conference Proceedings, New Zealand, Ministry of Commerce, Wellington.

Arnold, B. C. (1983). Pareto distributions, International Cooperative Publishing House, Fairland MD.

Arps, J. J. and T. G. Roberts (1958). Economics of Drilling for Cretaceous Oil on East Flank of Denver-Julesburg Basin. Bulletin of the American Association of Petroleum Geologists 42(11): 2549 - 2566.

Athy, L. F. (1930). Density, Porosity, and Compaction of Sedimentary Rocks. American Association of Petroleum Geologists Bulletin 14(1): 1-24.

Attanasi, E. D. (1980). Petroleum resource appraisal and discovery rate forecasting in partially explored regions. An application to supply modelling. US Geological Survey Professional Paper: 1138.

Attanasi, E. D. and R. R. Charpentier (2002). Comparison of Two Probability Distributions Used to Model Sizes of Undiscovered Oil and Gas Accumulations: Does the Tail Wag the Assessment? Mathematical Geology 34(6): 767-777.

Attanasi, E. D. and D. H. Root (1988). Small field oil and gas resource estimation for the National Assessment, in Carter, L.M.H., ed., USGS research on energy resources, Program and abstracts: U.S. Geological Survey Circular 1025: 1.

Baillie, P. and C. Uruski (2004). Reassessment of the prospectivity of the New Zealand Cretaceous: Navigating with an Astrolabe. 2004 New Zealand Petroleum Conference Proceedings, Auckland, New Zealand, Ministry of Economic Development.

Baker, R. A., H. M. Gehman, W. R. James and D. A. White (1984). Geologic field number and size assessments of oil and gas plays. American Association of Petroleum Geologists Bulletin 68.4: 426-437.

Bardossy, G. and V. e. Pawlowsky-Glahn (1997). Some fields of geomathematics as seen by a geologist (is there a bridge between geologists and mathematician? Third annual conference of the International Association for Mathematical Geology (IAMG) 1997, Barcelona, Spain.

Barouch, E. and G. M. Kaufman (1974). Sampling without replacement and proportional to random size. Unpublished manuscript.

Barouch, E. and G. M. Kaufman (1976a). Probabilistic modelling of oil and gas discovery. Energy - Mathematics and Models: Society Industrial and Applied Mathematics, Roberts, F. S: 248-260.

Barouch, E. and G. M. Kaufman (1976b). Oil and gas discovery modelled as sampling proportional to random size. Cambridge Mass., Massachusetts Institute of Technology, Alfred P Sloan School of Management Working Paper 888-76: 64.

Barouch, E. and G. M. Kaufman (1977). Estimation of Undiscovered Oil and Gas. Proceedings of Symposia in Applied Mathematics: American Mathematical Society 21: 77-91.

Barrett, A. G., A. L. Hinde and J. M. Kennard (2003). Undiscovered resource assessment methodologies and application to the Bonaparte Basin. Timor Sea Symposium.

Barton, C. C. and P. R. La Pointe (1995). Fractals in Petroleum Geology and Earth Processes. New York, Plenum Press.

Baskin, D.K. (1997). Atomic H/C ratio of kerogen as an estimate of thermal maturity and organic matter conversion. AAPG Bulletin, v.81, p. 1473-1470

Bear, J. (1972). Dynamics of Fluids in Porous Media. Dover Publications. 764.

Beggs, J. (1996). New Zealand's Prospectivity - A geological perspective with international comparisons. 1996 New Zealand Petroleum Conference Proceedings Volume 2: 22 - 26.

Beggs, J. M. and R. A. Cook (1993). Prospects for significant undiscovered gas resources in Taranaki Basin. IGNS client report 1993/56. Lower Hutt, New Zealand, Institute of Geological and Nuclear Sciences Limited: 36.

Benchilla, L., V. Stagpoole and R. H. Funnell (2006). Petroleum system analysis in an inverted basin, a case study within the Taranaki Basin (New Zealand). 2006 New Zealand Petroleum Conference Proceedings, Auckland.

Bergman, S. C., J. P. Talbot and P. R. Thompson (1992). The Kora Miocene submarine andesite stratovolcano hydrocarbon reservoir, Northern Taranaki Basin, New Zealand. 1991 New Zealand Oil Exploration Conference proceedings, Ministry of Commerce, Wellington.

Berryman, K, Beanland, S. 1988. Ongoing deformation of New Zealand: rates of tectonic movement from geological evidence. Transactions of the Institution of Professional Engineers New Zealand. General Section 15:25-35.

Bettini, C. (1987). Forecasting populations of undiscovered oil fields with the log-Pareto distribution. Applied Earth Sciences. Stanford, Stanford University: 221.

Bird, K. J. (1999). Assessment overview, in The Oil and Gas Resource Potential of the 1002 Area, Arctic National Wildlife Refuge, Alaska, U.S Geological Survey.

Bloomer, A. J. (1990). Porosity study of wells in the Southern Taranaki Basin, New Zealand. Open-file petroleum report: PR1600, Stirling Petroleum NL: 21.

Bonham-Carter, G. F. (1994). Geographic information systems for geoscientists; modelling with GIS. Computer Methods in the Geosciences 13: 398.

Bonham-Carter, G. F., F. P. Agterberg and D. F. Wright (1988). Integration of geological datasets for gold exploration in Nova Scotia, American Society for photogrammetry and remote sensing 54: 171-183.

Bostrom, N. W., D. D. Griffin, R. L. Kleinberg and K. K. Liang (2005). Ultrasonic bubble point sensor for petroleum fluids in remote and hostile environments. Institute of Physics Publishing. Measurement Science and Technology 16: 2336-2343.

BP Research (1995). Petroleum migration. Geological Society Special Publication Classics. Edited by England, W.A and Fleet, A.J. The Geological Society, London: 280.

Bradshaw, J Boreham, C and La Pedalina (2004). Storage retention time of Co2 in sedimentary basins, examples from petroleum systems. Greenhouse Gas Technologies Cooperative Research Centre (Co2CRC) & Geoscience Australia. Proceedings of the 7th International Conference on Greenhouse Gas Control Technologies, Vol. 1 (4): 541-550.

Brophy, F. and A. Falloon (1979). North Tasman-1 well completion report. Petroleum report PR736, Ministry of Economic Development: 153.

Brown, W., T. D. Gedeon, D. I. Groves and R. G. Barnes (2000). Mineral prospectivity mapping; a comparison of MLP neural network, fuzzy logic and weights-of-evidence methods, In: Understanding planet Earth, Searching for a sustainable future on the starting blocks of the third Millennium, Skilbeck,C.G Hubble, T.C.T (eds.) Abstract volume. Geological Society of Australia 59: 63.

Brown, W. M., D. I. Groves and T. D. Gedeon (2003). Use of Noise to Augment Training Data: A Neural Network Method of Mineral-Potential Mapping in Regions of Limited Known Deposit Examples. Natural Resources Research 12(2): 141-151.

Bussell, M. R. (1994). Seismic interpretation of the Moki Formation on the Maui 3D survey, Taranaki Basin. Ministry of Commerce, Wellington. 1994 New Zealand Petroleum Conference Proceedings,

Carranza, E.J (2004). Weights of Evidence Modeling of Mineral Potential: A Case Study Using Small Number of Prospects, Abra, Philippines. Natural Resources Research 13 (3):173-187

California Department of Conservation (2007). Oil and Gas Statistics: 2007 Annual Report. Division of oil, gas and geothermal resources.

Capen, E. C. (1984). The lognormal distribution, exploration plays: risk analysis and economic assessment [short course], American Association petroleum Geologists: 63.

Carstens, H. (2005). Understanding fault facies improves reservoir modelling. Geo ExPro. 2: 27 - 30.

Carter, M. and E. R. L. Kintanar (1987). Cape Farewell-1 well completion report PPL38119. Petroleum report PR1234, Ministry of Economic Development: 458.

Charpentier, R. R. (2005). Estimating undiscovered resources and reserve growth: contrasting approaches. Petroleum Geology: North-West Europe and Global Perspectives

- Proceedings of the 6th Petroleum Geology Conference, London, Petroleum Geology Conferences Ltd. Geological Society, London.

Charpentier, R. R., G. L. Dolton and G. F. Ulmishek (2000). Annotated Bibliography of Methodology for Assessment of Undiscovered oil and gas resources, United States Geological Survey.

Chen, Z., K. G. Osadetz, F. E. Ashton and P. Hannigan (2001a). Geological favourability mapping of hydrocarbon potential using a fuzzy integration method, Western Sverdrup Basin of Canadian Arctic Archipelago. Rock the Foundation Convention, Canadian Society of Petroleum Geologists.

Chen, Z., K. G. Osadetz, A. F. Embry, H. Gao and P. K. Hannigan (2000a). Petroleum potential in western Sverdrup Basin, Canadian Artic Archipelago. Bulletin of Canadian Petroleum Geology 48: 323-338.

Chen, Z., K. G. Osadetz, A. F. Embry, H. Gao and P. K. Hannigan (2002a). Hydrocarbon favourability mapping using fuzzy integration: western Sverdrup Basin, Canada. Bulletin of Canadian Petroleum Geology 50(4): 492-506.

Chen, Z., K. G. Osadetz, H. Gao, P. Hannigan and C. Watson (1999). Mapping Undiscovered Petroleum Resources in a Play. International Association of Mathematical Geology, Trondheim, Norway.

Chen, Z., K. G. Osadetz, H. Gao, P. Hannigan and C. Watson (2000). Characterising spatial distribution of undiscovered hydrocarbon resource with application to the Rainbow Gas Play, Western Canada Sedimentary Basin. Bulletin of Canadian Petroleum Geology 48: 150-163.

Chen, Z., K. G. Osadetz, H. Gao, P. Hannigan and C. Watson (2001). Improving exploration success through uncertainty mapping, Keg River Reef Play, Western Canada Sedimentary Basin. Bulletin of Canadian Petroleum Geology 49(3): 367-375.

Chen, Z., K. G. Osadetz and P. Hannigan (2002). An Improved Fractal Model for Characterizing Spatial Distribution of Undiscovered Petroleum Accumulations. Annual Conference of the International Association for Mathematical Geology Proceedings, Cancun, Mexico, IAMG.

Chung, C. F. and F. P. Arterberg (1980). Regression models for estimating mineral resources from geological map data. Mathematical Geology 15(5) (473-488).

Chung, C. F. and A. G. Fabbri (1993). The representation of geoscience information for data integration. Non-renewable Resources 2(2): 122-139.

Chungcharoen, E. (1994). Approximating the distributions of the total amount of hydrocarbons discovered by a family of beta distributions. MSc thesis. University of Waterloo: 149.

Chungcharoen, E. (1997). Economic analysis of hydrocarbon exploration by simulation with geological uncertainties. PhD thesis, University of Waterloo, Waterloo, ON, Canada.

Clark, R. M. and S. J. D. Cox (1996). A modern regression approach to determining fault displacement-length scaling relationships. Journal of structural geology 18: 147-152.

Clark, R. M., S. J. D. Cox and G. M. Laslett (1997). Generalizations of power-law distributions applicable to sampled fault-trace lengths: model choice, parameter estimation and caveats. Journal of international geophysics 136: 357-372.

Cook, R. A. (1985). Trends in New Zealand Hydrocarbon Exploration and Discovery, 1950 - 1985. Wellington, New Zealand Geological Survey: 21.

Cook, R. A. (1987). The geology and geochemistry of the crude oils and source rocks of Western New Zealand, Victoria University of Wellington.

Cook, R. A. (1987). The geology and geochemistry of the crude oils and source rocks of western New Zealand. Open file petroleum report PR1250, Ministry of Commerce, Wellington.

Cooles, G. P., A. S. Mackenzie and T. M. Quigley (1986). Calculation of petroleum masses generated and expelled from source rocks. Advances in Organic Chemistry 10: 235-245.

Crovelli, R. A. (1985). An analytic probabilistic methodology for resource appraisal of undiscovered oil and gas resources in play analysis. U.S. Geological Survey Open-File Report 85-657: 51.

Crovelli, R. A. and R. H. Balay (1986). FASP, an analytic resource appraisal program for petroleum play analysis. Computers & Geosciences 12: 423-475.

Crovelli, R. A. and C. C. Barton (1995). Estimation of Undiscovered Hydrocarbon Potential through Fractal Geometry. Fractals in Petroleum Geology and Earth Processes. C. C. Barton, and La Pointe, P.R. New York, Plenum Press: 59-71.

Crown Minerals (2004). New Zealand's Petroleum Basins, Crown Minerals, Ministry of Economic Development.

Crown Minerals (2006). Website, Ministry of Economic Development. www.crownminerals.govt.nz.

Darby, D. and S. Ellis (2002). Seal properties, overpressure and stress in the Taranaki and East Coast basins. 2002 New Zealand Petroleum Conference Proceedings 1: 363 - 372.

Davy, P. (1993). On the frequency-length distribution of the San Andreas fault system. Journal of Geophysical Research 98: 12141-12151.

de Bock, J. F., S. Perry, D. Webby and B. Goodin (1991). Appraisal of the Maui-4 and Moki-1 oil discoveries PML38144 PML38145. Petroleum report PR1800, Ministry of Economic Development: 121.

De Mets, C., R. G. Gordon, D. F. Argus and S. Stein (1994). Effect of recent revisions to the geomagnetic reversal timescale on estimates of current plate motions. Geophysical Research Letters 21: 2191-2194.

De Mets, C., R, G. Gordon, D. F. Argus and S. Stein (1990). Current plate motions. Geophysics Journal International 101: 425-478.

Downey, A. B. (2005). Lognormal and Pareto distributions in the internet. Elsevier Science.

Drew, L. J. (1990). Oil and Gas Forecasting: reflections of a petroleum geologist. New York, Oxford University Press.

Drew, L. J. (1997). Undiscovered petroleum and mineral resources; assessment and controversy. 210.

Drew, L. J., E. D. Attanasi and J. H. Schuenemeyer (1988). Observed oil and gas field size-distributions; a consequence of the discovery process and prices of oil and gas. Mathematical Geology 20(8): 939-953.

Drew, L. J. and J. H. Schuenemeyer (1992). A petroleum discovery-rate forecast revisited; the problem of field growth. Non-renewable Resources 1(1): 51-60.

Drew, L. J., J. H. Schuenemeyer and R. F. Mast (1995). Application of the Modified Arps-Roberts Discovery Process Model to the 1995 U.S National Oil and Gas Assessment. Non-renewable Resources 4(3): 242-252.

Drew, L. J., J. H. Schuenemeyer and V. e. Pawlowsky-Glahn (1997). Composition of oil gas field discovery rates and its bearing on resource assessment; the North Sea Proceedings of IAMG '97, the Third annual conference of the International Association for Mathematical Geology. Third annual conference of the International Association for Mathematical Geology 3: 427-432.

Eckbo, P. L., H. D. Jacoby and J. L. Smith (1978). Oil supply forecasting: a disaggregated process approach. The Bell Journal of Economics 2: 218-235.

EIA (2006). Energy Information Advisory. www.eis.doe.gov.

Franchi, J. R. (2000). Integrated flow modelling, Developments in Petroleum Science 49. Elsevier.

Feller, W. (1966). An introduction to probability theory and its application, John Wiley & Sons, Inc.

Flores, R. M., J. M. Beggs and P. R. King (1993). Sedimentology of tide-dominated reservoir sandstones in the Eocene Kapuni Group, Taranaki Basin, New Zealand. American Association of Petroleum Geologists 1993 annual convention abstracts 102.

Folinsbee, R. E. (1977). World's view - from Alph to Zipf. Geological Society of American Bulletin 88: 897 - 907.

Forman, D. J. and A. L. Hinde (1985). Improved statistical method for assessment of undiscovered petroleum resources. AAPG Bulletin 69(1): 106-118.

Forman, D. J. and A. L. Hinde (1986). Examination of the Creaming Methods of Assessment Applied to the Gippsland Basin, Offshore Australia. Oil and Gas Assessment - Methods and Applications: American Association of Petroleum Geologists Studies in Geology 21.

Franchi, J. (2006). Principles of applied reservoir simulation. Gulf Professional Publishing. 520.

Frechet, M. (1941). Sur la loi de repartition de certaines grandeurs geographiques. J.Soc Statistique de Paris 82: 114-122.

Fuller, J. D., P. C. Wang and M. Power (1991). On a rapid approximation of the first and second moments of a simulation model of hydrocarbon exploration. Working paper. Department of Management Sciences, University of Waterloo, Waterloo, Ontario, Canada.

Funnell, R. H. (2005). GNS Science. Personal communication.

Funnell, R. H., D. Chapman, R. Allis and P. Armstrong (1996). Thermal state of the Taranaki Basin, New Zealand. Journal of Geophysical Research 101: 25,197-25,215.

Funnell, R. H., P. King and D. Darby (2002). Prospects for New Zealand's undiscovered gas reserves. Institute of Geological & Nuclear Sciences Limited Client Report 2002/136, Institute of Geological & Nuclear Sciences Limited, Lower Hutt, New Zealand: 39.

Funnell, R. H., V. Stagpoole, A. Nicol, S. D. Killops, A. G. Reyes and D. Darby (2001). Migration of oil and gas into the Maui Field, Taranaki Basin, New Zealand. Eastern

Australian Basins Symposium Proceedings, Melbourne, Australia, Petroleum Exploration Society of Australia.

Funnell, R. H., V. M. Stagpoole, A. Nicol, N. McCormack and A. G. Reyes (2004). Petroleum generation and implications for migration: a Maui Field charge study, Taranaki Basin. 2004 New Zealand Petroleum Conference Proceedings, Auckland, New Zealand, Ministry of Economic Development.

Ganguli, R. and S. Dandopadhyay (2003). Dealing with Sparse Data Issues in a Mineral Industry Neural Network Application. Computer Applications in the Mineral Industry (CAMI), Calgary, Alberta, Canada.

Gao, H., Z. Chen, K. G. Osadetz, P. Hannigan and C. Watson (2000). A Pool-Based Model of the Spatial Distribution of Undiscovered Petroleum Resources. Mathematical Geology 32(4): 725-748.

Geotechnical Services Pty Ltd (2005). Hydrocarbon characterisation study Tangaroa play. Petroleum Report PR3259, Ministry of Economic Development.

GNS Science (2006). Petroleum wells shape file.

Gordon, L. (1981). Successive sampling in large finite populations. The Annals of Statistics 11: 702-706.

Gresko, M. J., D. W. Jordon and P. R. Thompson (1992). Sequence stratigraphic analysis of the Tangaroa Sandstone, northern Taranaki Basin, New Zealand. 1991 New Zealand Oil Exploration Conference Proceedings, Christchurch, New Zealand, Ministry of Commerce.

Halliburton Australia Pty Ltd (1999). Maari-1 & 1A well completion report, PPL38413. Petroleum exploration report, PR 1572, Ministry of Economic Development, Wellington, New Zealand.

Hamilton, E. (1976). Variations of Density and Porosity with Depth in Deepsea Sediments. Journal of Sedimentary Petrology 46(2): 280-300.

Harbaugh, J. W. and J. C. e. Davis (1977). Integrated oil exploration decision systems, Quantitative strategy for exploration. 25th International geological congress; Symposium 116.3; Quantitative strategy for exploration 9(4): 441-449.

Harbaugh, J. W. and M. Ducastaing (1981). Historical changes in oil field populations as a method for forecasting field sizes of undiscovered populations - A comparison of Kansas, Wyoming and California. Kansas Geological Survey, Subsurface Geological Series 5: 56.

Harding, T. P. (1985). Seismic characteristics and identification of negative flower structures, positive flower structures, and positive structural inversion. American Association of Petroleum Geologists Bulletin 69: 582-600.

Harris, D. P. (1990). Mineral exploration decisions; a guide to economic analysis and modelling. 436.

Haskell, T. (1991). An analysis of Taranaki Basin hydrocarbon migration paths: some questions answered. Petroleum Exploration in New Zealand News, January 1991.

Hayward, B. W. (1987). Paleobathymetry and structural tectonic history of Cenozoic drillhole sequences in Taranaki Basin, New Zealand Geological Survey report: PAL122.

Hayward, B. W. (1990). Use of foraminiferal data in analysis of Taranaki Basin, New Zealand. Journal of foraminiferal research 20: 71-83.

Hayward, B. W. and R. A. Wood (1989). Computer generated geohistory plots for Taranaki Basin drillhole sequences, New Zealand Geological Survey report: PAL147.

Heinemann Publishers (1980). Eton statistical and math tables, Heinemann Publishers (NZ) Ltd.

Hendricks, T. A. (1965). Resource of oil, gas and natural gas liquids in the United States and the world. US Geological Survey Circular 522: 20.

Hendricks, T. A. (1974). Estimating resources of crude oil and natural gas in inadequately explored areas. In Crandall, K.H., and Harbaugh, J.W., convenors, Methods of estimating the undiscovered oil and gas resources. American Association of Petroleum Geologists Research Symposium, Stanford California University: 47-57.

Henry, J. D. (1911). Oil fields of New Zealand, J.D Henry (London) and T Avery (NZ).

Hermanrud, C. (1993). Basin-modelling techniques - an overview. Basin-modelling: advances and applications. Norwegian Petroleum Society (NPF) special publication No.3. A. G. Dore, J. H. Auguston, C. Hermanrud, D. J. Stewart and O. Sylta, Elsevier Science Publishers B.V: 675.

Hill, P.J and Collen, J.D (1978). The Kapuni Sandstones from Inglewood-1 well, Taranaki - petrology and the effects of digenesis on reservoir characteristics. New Zealand Journal of Geology and Geophysics 21: 215 - 228

Hillyer, M. G. (1989). The Tariki and Ahuroa gas-condensate fields. Volumetric hydrocarbons in place and reserves update. PML38138 and PML38139. Petroleum Report PR1727, Petroleum Corporation of NZ Exploration Ltd: 54.

Hirner, A. V. and G. L. Lyon (1989). Stable isotope geochemistry of crude oils and of possible source rocks from New Zealand. 1, Carbon. Applied geochemistry 4: 109 - 120.

Hirner, A. V. and B. W. Robinson (1989). Stable isotope geochemistry of crude oils and of possible source rocks from New Zealand. 2, Sulphur. Applied geochemistry 4: 121 - 130.

Holt, W. E. and T. A. Stern (1994). Subduction, platform subsidence, and foreland thrust loading: the late Tertiary development of the Taranaki Basin, New Zealand. Tectonics 13: 1068-1092.

Hood, S. D., C. S. Nelson and P. J. J. Kamp (2003). Depositional and diagenetic characteristics and origin of the Tikorangi Formation fractured reservoir, Taranaki Basin, New Zealand. Open-file petroleum report: PR2864. Ministry of Economic Development: 363.

Horvitz, D. G. and D. J. Thompson (1951). A generalisation of sampling without replacement from a finite universe. Iowa Agricultural Experiment Station, Ames, Iowa, Project 1005: 663-706.

Houghton, J. C. (1988). Use of the truncated shifted Pareto distribution in assessing size-distribution of oil and gas fields. Mathematical Geology 20(8): 907-937.

Howarth, R. J., C. M. White and G. S. Koch, Jr. (1980). On Zipf's Law applied to resource prediction. Institution of Mining and Metallurgy, Transactions, sec. B, Applied Earth Science 89: B182-190.

Hunter, R. L., C. J. Mann, W. J. Conover, R. J. Budnitz, R. L. e. Hunter and C. J. e. Mann (1992). Introduction of techniques for determining probabilities of geologic events and processes. Studies in Mathematical Geology 4: 3-21.

IES (2000). IES PetroMod reference manual. Release 3.0. Part 7: theoretical aspects, Integrated Exploration Systems (IES) GmbH: 118.

IGNS (1995). Taranaki Basin Petroleum Atlas: Map 47, Eocene Kaimiro and Mangahewa formations, exploration potential and play concepts. Wellington, Institute of Geological and Nuclear Sciences Limited.

IGNS (1995). Taranaki Basin Petroleum Atlas: Map 49, Late Neogene exploration potential and play concepts. Wellington, Institute of Geological and Nuclear Sciences Limited.

Ilg, B. (2006). GNS Science. Personal communication.

Ivanhoe, L. F. (1986). Limitation of geological consensus estimates of undiscovered petroleum resources. Rice, D.D., (Ed). Oil and gas assessment - Methods and applications. American Association of Petroleum Geologists Studies in Geology 21: 77-83.

Johnson, J. (1990). Tikorangi Limestone study report PPL38706 and adjacent areas. Petroleum report PR1586, Ministry of Economic Development: 281.

Johnston, J. H., R. J. Collier and J. D. Collen (1990). What is the source to Taranaki Basin oils?: geochemical biomarkers suggest it is the very deep coals and shales. 1989 New Zealand Oil Exploration Conference Proceedings, Ministry of Commerce, Wellington.

Jones, R. W. (1975). A quantitative geologic approach to prediction of petroleum resources. In Haun, J.D., (Ed). Methods of estimating the volume of undiscovered oil and gas resources: American Association of Petroleum Geologists Studies in Geology 1: 186-195.

Jones, R.R, K.J.W McCaffrey, R.W. Wilson and R.E Holdsworth (2004). Digital field data acquisition: towards increased quantification of uncertainty during geological mapping. The Geological Society of London. Special Publications 2004, v. 239, p. 43-56.

Kaufman, G. M. (1963). Statistical decision and related techniques in oil and gas exploration. 307.

Kaufman, G. M. (1986). Finite population sampling methods for oil and gas resource estimation. Oil and gas assessment, methods and applications. Edited by Dudley D. Rice. AAPG Studied in Geology 21(AAPG Studies in Geology #21): 43-53.

Kaufman, G. M. (1993). Statistical issues in the assessment of undiscovered oil and gas resources. Energy Journal 14(1): 183--215.

Kaufman, G. M. (1996). Risk analysis: from prospect to exploration portfolio and back. Quantification and Prediction of Petroleum Resources, Dore, A. G
Sinding-Larsen, R: 135-151.

Kaufman, G. M., Y. Balcer and D. Kruyt (1975). A probabilistic model of oil and gas discovery; in J.D. Haun, ed., Methods of Estimating the Volume of Undiscovered Oil and gas Resources. AAPG Bulletin 1(1): 113-142.

Kemp, L. D., G. F. Bonham-Carter, G. L. Raines and C. G. Looney (2001). Arc-SDM: ArcView extension for spatial data modelling using weights-of-evidence, logistic regression, fuzzy logic and neural network analysis. http//ntserv.gis.nrcan.gc.ca/sdm/.

Killops, S. (1996). A geochemical perspective of oil generation in New Zealand basins. 1996 New Zealand Petroleum Conference Proceedings, Ministry of Commerce. Wellington.

Killops, S., R. H. Funnell, R. P. Suggate, R. Sykes, R. A. Cook, K. E. Peters, C. Walters, A. D. Woolhouse, R. J. Weston and J. P. Boudou (1998). Assessing oil generation and

expulsion from New Zealand coals. 1998 New Zealand Petroleum Conference, New Zealand, Ministry of Commerce.

Killops, S., A. D. Woolhouse, R. J. Weston and R. A. Cook (1994). A geochemical appraisal of oil generation in the Taranaki Basin, New Zealand. American Association of Petroleum Geology Bulletin 78: 1560-1585.

Killops, S. D., R. H. Funnell, R. P. Suggate, R. Sykes, K. E. Peters, C. Walters, A. D. Woolhouse, R. J. Weston and J. P. Boudou (1998). Predicting generation and expulsion of paraffinic oil from vitrinite-rich coals. Organic geochemistry 29(1-3): 1-21.

King, P. R. (2000). New Zealand's changing configuration in the last 100 million years: plate tectonics, basin development and depositional setting. 2000 New Zealand Petroleum Conference Proceedings.

King, P. R. and G. P. Thrasher (1992). Post-Eocene development of the Taranaki Basin, New Zealand: convergent overprint of a passive margin. In Watkins, J.S, Zhiqiang, F., McMillen, K.J (eds) Geology and geophysics of continental margins. American Association of Petroleum Geologists memoir 53: 93-118.

King, P. R. and G. P. Thrasher (1996). Cretaceous-Cenozoic Geology and Petroleum Systems of the Taranaki Basin, New Zealand. Lower Hutt, New Zealand, Institute of Geological & Nuclear Sciences Limited.

Klemme, H. D. (1971). The Giants and the Supergiants. Part I. Oil and Gas Journal. 69: 85-90.

Klemme, H. D. (1971). The Giants and the Supergiants. Part II. Oil and Gas Journal. 69: 103-110.

Klemme, H. D. (1971). The Giants and the Supergiants. Part III. Oil and Gas Journal. 69: 96-100.

Klemme, H. D. (1983). Field Size-distribution Related to Basin Characteristics. Oil and Gas Journal. 81: 168-176.

Kontorvich, A. E. and V. I. Dyomin (1979). A method for assessing the amount and distribution of oil and gas reserves in large oil and gas basins. International Geological Review 22(3): 361-367.

Kosko, B. (1992). Neural networks and fuzzy systems. Englewood Cliffs, New Jersey, Prentice Hall.

Laherrere, J. (1997). Distribution and evolution of recovery factor. Oil reserves conference proceedings, Paris, International Energy Agency.

Laherrere, J. (1999). Parabolic fractal, creaming curve improvement estimate of US Gulf reserves. Offshore Magazine. May: 113-114, 177.

Laherrere, J. (2000). Distribution of field sizes in a petroleum system: parabolic fractal, lognormal or stretched exponential? Marine and Petroleum Geology 17: 539-546.

Laherrere, J. (2003). Modelling future oil production, population and the economy. ASPO second International workshop on oil and gas, Paris.

Laherrere, J. (2003). Personal communication.

Laherrere, J. and D. Sornette (1998). Stretched Exponential Distributions in Nature and Economy. European Physical Journal B2 (April II): 525-539.

Lander, R. H. and O. Walderhaug (1999). Predicting porosity through simulating sandstone compaction and quartz cementation. AAPG Bulletin 83(3): 433-339.

Lee, P. J. and P. C. Wang (1983). Probabilistic formulation of a method for the evaluation of petroleum resources. Mathematical Geology 15(1): 163-181.

Lee, P. J. and P. C. C. Wang (1985). Prediction of oil or gas pool sizes when discovery record is available. Journal of the International Association for Mathematical Geology 17(2): 95-113.

Lee, P. J. and P. C. C. Wang (1990). An introduction to petroleum resource evaluation methods (3rd edition), Geological Survey Canada: 108.

Lee, P. J., P. C. C. Wang and T. A. Jones (1983). Conditional analysis for petroleum resource evaluations, geostatistics, geomathematics, and computer applications. First MGUS conference on the management, analysis and display of geoscience data; Geostatistics, geomathematics, and computer applications 15(2): 349-361.

Lerche, I. (1991). Theoretical aspects of problems in basin-modelling, Basin-modelling: Advances and Applications. Norwegian Petroleum Society (NPF) special publication No.3. A. G. Dore, J. H. Auguston, C. Hermanrud, D. J. Stewart and O. Sylta. Stavanger, Norway, Elsevier Science Publishers B.V: 35-65.

Long, K. R. (1988). Estimating the number and sizes of undiscovered oil and gas pools. Department of Mining and Geological Engineering. Arizona, University of Arizona: 159.

Macdonald, D. G. (1992). A differential equation based approach to estimating future hydrocarbon discoveries. MSc thesis, University of Waterloo, Canada.

MacDonald, D. G., M. Power and J. D. Fuller (1994). A new discovery process approach to forecasting hydrocarbon discoveries. Resource and Energy Economics 16(2): 147-166.

Mackenzie, A. S. and T. M. Quigley (1988). Principles of geochemical prospect appraisal. AAPG Bulletin 72: 399-415.

Magara, K. (1976). Porosity-depth relationship during compaction in hydrostatic and non-hydrostatic cases.

Magara, K. (1980). Agents for primary hydrocarbon migration. *Problems of petroleum migration*. American Association of Petroleum Geologists Studies in Geology 10: 33-45.

Magoon, L. B. and W. G. Dow (1984). The petroleum system - from source to trap. American Association of Petroleum Geologists Memoir 60: 655.

Magoon, L.B, and Z.C Valin (1994). Overview of Petroleum Systems case Studies; The petroleum system – from source to trap. AAPG Memoir 60, The American Association of Petroleum Geologists, Tulsa, USA: 329-338.

Mallory, W. W. (1975). Accelerated national oil and gas resource appraisal (ANOGRE). in Haun, J.D., ed. Methods of estimating the volume of undiscovered oil and gas resources: American Association of Petroleum Geologists Studies in Geology 1: 23-30.

Mandelbrot, B. B. (1995). Statistics of Natural Resources and the Law of Pareto. Fractals in Petroleum Geology and Earth Processes. C. C. Barton, and La Pointe, P.R. New York, Plenum Press: 1-12.

Mann, C. J., J. C. e. Davis and U. C. e. Herzfeld (1993). Uncertainty in geology Computers in geology; 25 years of progress. Studies in Mathematical Geology 5: 241-254.

Manzano-Kareah, B. K. (2004). Energy & Geoscience Institute (EGI) University of Utah. Personal communication.

Mare-Jones, B. (2004). Quantifying undiscovered oil and gas in the Taranaki Basin. 2004 New Zealand Petroleum Conference Proceedings, Ministry of Economic Development.

Martin, K. R. (1989). Petrography of the Tikorangi limestone and Moki Formation in the Northern Taranaki Basin. Petroleum report PR1513, Ministry of Economic Development: 59.

Marjoribanks, R. (1997). Geological methods in mineral exploration and mining. Chapman & Hall, London, 238 p.

Matheron (1962). Traite de geostatistique appliquee, Editions Technip, France.

Mathews, E. R. and D. J. Bennett (1987). Kupe South-1 well completion report PPL38116. Petroleum exploration report PR1284. Ministry of Economic Development.

McAlpine, A. (2005). Maximum burial seal plot for some Taranaki Basin seals. Personal communication.

McAlpine, A. and S. J. O'Connor (1998). An Engineering Analysis of Taranaki Petroleum Systems: A 4-Dimensional Multi-Disciplinary Approach to Reduce Exploration Risk. 1998 New Zealand Petroleum Conference Proceedings, Queenstown, New Zealand, Crown Minerals, Ministry of Commerce.

McCray, A. W. (1975). Petroleum Evaluations and economic decisions. Englewood Cliffs, New Jersey, Prentice-Hall Inc.

McCrossan, R. G. (1969). An analysis of size frequency distribution of oil and gas reserves of western Canada. Canadian Journal of Earth Sciences 6(2): 201-211.

McGill, R. E. (1995). Estimating Prospect Size. The Business of Petroleum Exploration. N. H. Foster and E. A. Beaumont. Tulsa, The American Association of Petroleum Geologists.

MED. (2005). New Zealand Energy Outlook to 2025, Ministry of Economic Development.

MED. (2006). Cheal and Cardiff Field: Petroleum Mining Permit 38156, Ministry of Economic Development, Wellington, New Zealand.

MED. (2007). Crown Minerals Report 2006-2007, Ministry of Economic Development.

MED. (2010). Crown Minerals Report 2009-2010, Ministry of Economic Development.

Megill, R. (1992). Estimating prospect size. The Business of Petroleum Exploration. Treatise of petroleum geology, handbook of petroleum geology. R. Steinmetz, American Association of Petroleum Geologists.

Meisner, J. and F. Demirmen (1981). The creaming method - A Bayesian procedure to forecast future oil and gas discoveries in mature exploration provinces. Journal of the Royal Statistical Society 144(Part 1): 1-31.

Miller, B. M., H. L. Thomsen, G. L. Dolton, A. B. Coury, T. A. Hendricks, F. E. Lennartz, R. B. Powers, E. G. Sable and K. L. Varnes (1975). Geological estimates of undiscovered recoverable oil and gas resources in the United States. US Geological Survey Circular: 725-78.

Mills, K. (2000). Hochstetter-1 well completion report, PEP38460, offshore Taranaki Basin., New Zealand Oil & Gas (NZOG). PR2524: 517.

Moore, D. S. and G. P. McCabe (2003). Introduction to the Practice of Statistics. New York, W.H Freeman and Company.

Morris, B. D. (1995). The geology of the Matemateaonga Formation, central Taranaki, New Zealand. PhD thesis. Victoria University of Wellington.

Nicol, A., V. Stagpoole and G. Maslen (2004). Structure and petroleum potential of the Taranaki Fault play. 2004 New Zealand Petroleum Conference, Auckland, Ministry of Economic Development, Wellington.

Nicol, A (2005). GNS Science. Personal communication.

Ninpong, R., M. Power and J. D. Fuller (1992). A rapid approximation for predicting the hydrocarbon discovery rate: Part 1 - assessing the accuracy. Natural Resources Modelling 6(3): 285-303.

North, F. K. (1985). Petroleum Geology, George Allen and Unwin. 671.

NZ Aquitaine Petroleum Ltd (1976). Well completion report Fresne-1. Petroleum report 674, Ministry of Economic Development.

NZOG. (1995). Cheal-1 completion report, PPL38707, New Zealand Oil & gas Ltd. Petroleum exploration report, PR2179, Ministry of Economic Development, Wellington, New Zealand: 743.

NZOG. (2006). New Zealand Oil & Gas Ltd company website: www.nzog.net.

O'Carroll, F. M. and J. L. Smith (1980). Probabilistic methods for estimating undiscovered petroleum resources. Advance in the Economics of Energy and Resources 3: 31-63.

O'Connor, (2004). Personal communication.

OMV (2006). OMV company website www.omv.com.

Osadetz, K. G., Z. Chen and H. Gao (2003). Mapping undiscovered resources - basin analysis and models for petroleum resource assessment. Mathematical Geology, Vol. 38, No. 1.

Pacheco, J. F., C. H. Scholtz and L. R. Sykes (1992). Changes in frequency-size relationship from small to large earthquakes. Nature 355: 71-73.

Palmer, J. and G. Bulte (1991). Taranaki Basin, New Zealand. Active Margin Basins. K. T. Biddle, The American Association of Petroleum Geologists. AAPG Memoir 52: 261-282.

Partington, G. A. (1999). Database management and GIS: practical considerations and use in the exploration industry. Fourth national forum on information management and GIS in the Geosciences (AGSO record 1999/24): 177-187.

Pepper, A. S. (1995). Estimating the petroleum expulsion behaviour of source rocks: a novel quantitative approach. Petroleum Migration. Geological Society Special Publication Classics. W. A. England and A. J. Fleet, The Geological Society, London: 9-31.

Pepper, A. S. and P. J. Corvi (1995). Simple kinetic models of petroleum formation. Part I: oil and gas generation from kerogen. Marine Petroleum Geology 12: 291-319.

Pepper, A. S. and P. J. Corvi (1995). Simple kinetic models of petroleum formation. Part III: modelling an Open System. Marine Petroleum Geology 12: 417-452.

Percher, I. A., G. Maslen, V. Stagpoole and A. R. Gorman (2004). Wide-angle seismic surveys - the solution for imaging beneath the Taranaki Fault. 2004 New Zealand Petroleum Conference proceedings, Auckland, Ministry of Economic Development.

Perrodon, A. (1983). Dynamics of Oil and Gas Accumulations. Pau, Elf Aquitaine, Documentation Centre Micoulau.

Power, M. (1990). Modelling natural gas exploration and development on the Scotia Shelf. Waterloo, Ontario, University of Waterloo, Canada.

Procter, R., G. C. Taylor and J. A. Wade (1984). Oil and natural gas resource of Canada. Department of Energy, Mines, and Resources, Geological Survey of Canada. Paper 83-31: 59.

Proffett, J M (2004). Geologic mapping and its use in mineral exploration. In: Muhling J, Goldfarb N,Vielreicher N, Bierlin E, Stumpfl E, Groves DI, Kenworthy S (eds) Predictive mineral discovery under cover. SEG 2004 extended abstracts, vol 33. University of Western Australia, Centre for Global Metallogeny, Nedlands, WA, 153–157

Quirk, D. G. and R. Ruthrauff (2006). Analysis of reserves discovered in petroleum exploration. Journal of Petroleum Geology 29(2): 125-146.

Raines, G. L. (1999). Evaluation of weights-of-evidence to predict epithermal deposits in the Great Basin of the Western United States. Natural Resource Research 8(4): 257-276.

Rattenbury, M. and G. A. Partington (2003). Prospectivity models and GIS data for the exploration of epithermal gold mineralisation. Epithermal Gold in New Zealand GIS Data Package and Prospectivity Modelling, Crown Minerals, Ministry of Commerce, New Zealand: 68.

Reed, J. D. (1992). Exploration geochemistry of the Taranaki Basin with emphasis on Kora, Ministry of Commerce, Wellington.

Riesz, E. J. (1978). Can rank-size laws be used for undiscovered petroleum and mineral assessments? BMR Journal of Australian Geology and Geophysics 3(3): 253-256.

Roadifer, R. E. (1975). A probability approach to estimate volumes of undiscovered oil and gas. Methods and models for assessing energy resources, First IIASA Conference on Energy Resources. 5: 279-290.

Rose, P. (2001). Risk Analysis and Management of Petroleum Exploration Ventures, The American Association of Petroleum Geologists.

Rose, P. (2006). An overview of exploration risk analysis. Workshop: Selected topics from an overview of exploration risk analysis, Wellington, New Zealand.

Rose, P. and D. Cook (2006). Rose and Associates L.L.P website www.roseassoc.com.

Rostirolla, S. P., A. C. Mattana and M. K. Bartoszeck (2003). Bayesian assessment of favourability for oil and gas prospects over the Reconcavo Basin, Brazil. AAPG Bulletin 87(No 4): 647-666.

Roy, K. J. (1979). Hydrocarbon assessment using subjective probability and Monte Carlo method: First IIASA Conference on Energy Resources. Methods and Models for Assessing Energy Resources, Grenon, M. 5: 279-290.

Rudenno, V. (1981). The probability of economic success in exploring for tin deposits. Canadian Institute of Mineral Metallurgy Bulletin April: 99-101.

Sawatzky, D. L., G. L. Raines, G. F. Bonham-Carter and C. G. Looney (2004). ARCSDM3: ArcMAP extension for spatial data modelling using weights-of-evidence,

logistic regression, fuzzy logic and neural network analysis, US Geological Survey and Geological Survey of Canada.

SBPT (1986). Well resume Te Ranga-1, PPL38107 Taranaki New Plymouth. Open-file petroleum report: PR1197, Shell BP & Todd Oil Services Ltd: 747.

Scholtz, C. H. (1995). Fractal transitions on geological surfaces. Fractals in the earth sciences. C. C. Barton and P. R. La Pointe, Plenum, New York: 131-140.

Scholtz, C. H. and B. B. Mandelbrot (1989). Fractals in Geophysics. Basal, Birkhauser, Basal.

Schowalter, T. T. (1979). Mechanics of secondary hydrocarbon migration and entrapment. American Association of Petroleum Geologists Bulletin 63: 723-760.

Schroeder, F. W. and O. Sylta (1991). Modelling the hydrocarbon system of the North Viking Graben: a case study, in Basin-modelling: Advances and Applications. Norwegian Petroleum Society (NPF), Special Publication No.3. Norwegian Petroleum Society Conference, Stavanger, Norway, Elsevier Science Publishers B.V.

Schuenemeyer, J. H. and L. H. Drew (1983). A procedure to estimate the parent population of the size of oil and gas fields as revealed by a study of economic truncation. Mathematical Geology 15(1): 145-161.

Schuenemeyer, J. H., L. J. Drew, D. H. Root, E. D. Attanasi, J. C. Davis and T. Chang (1990). Estimating potential for small fields in mature petroleum province; discussion and reply. AAPG Bulletin 74(11): 1761-1765.

Shell BP & Todd Oil Services Ltd (1973). Reserves of the Maui Field. Petroleum Report PR707, Ministry of Economic Development.

Shell BP & Todd Oil Services Ltd (1975). Well resume Turi-1. Petroleum Report. PR659, Ministry of Economic Development, New Zealand.

Shell BP and Todd Oil Services Ltd (1979). Maui Field maps generated during early exploration. Petroleum exploration report, PR811, Ministry of Economic Development, Wellington, New Zealand.

Sills, S. R. (1992). Drive mechanisms and recovery. Development geology reference manual, AAPG methods in exploration series, No.10. D. Morton-Thompson and A. Woods, AAPG: 518-522.

Sinding-Larsen, R. (2004). UTNO. Personal communication. Denver.

Sinding-Larsen, R. and K. B. Brandsegg (2005). Characteristic analysis - GIS and petroleum exploration risk. International Association of Mathematical Geology 2005, Toronto, Canada.

Singer, D. A. and R. Kouda (1997). Classification of mineral deposits into types using mineralogy with a probabilistic neural network. Nonrenewable Resources 6(1): 27-32.

Singer, D. A. and R. Kouda (1997). Use of a neural network to integrate geoscience information in the classification of mineral deposits and occurrences. Exploration 97: Fourth Decennial International Conference Minerals Exploration Proceedings.

Singer, D. A. and R. Kouda (1999). A comparison of the weights-of-evidence method and probabilistic neural networks. Natural Resources Research (International Association for Mathematical Geology) 8(4): 287-298.

Smith, J. L. (1980). A probabilistic model of oil discovery. Review of Economics and Statistics 62(4): 587-594.

Smith, J. L., G. L. Ward and T. A. e. Jones (1981). Maximum likelihood estimates of the size-distribution of North Sea oil fields. Special issue on statistics and the Earth sciences. American Statistical Association annual meeting; session on geometrical probability and statistical problems in the geosciences 13(5): 399-413.

Sphere Consulting Limited (2001). Technical summary of maturation modelling, PEP38468, North Taranaki Basin, New Zealand. EEX New Zealand Limited. Petroleum Report PR2643.

Stern, T. A. and F. A. Davey (1989). Crustal structure and origin of basins formed behind the Hikurangi subduction zone, New Zealand. In Price, R.A (ed) Origin and evolution of sedimentary basins and their energy and mineral resources. Geophysical monograph, American Geophysical Union, Washington, DC 48: 73-85.

Stern, T. A. and F. A. Davey (1990). Deep seismic expression of a foreland basin: Taranaki Basin, New Zealand. Geology 18: 979-982.

Suggate, R. P. (2002). Application of Rank (Sr), a maturity index based on chemical analyses of coals. Marine and Petroleum Geology 19(8): 929 - 950.

Suggate, R. P. and J. P. Boudou (1993). Coal rank and type variation in Rock-Eval assessment of New Zealand coals. Journal of Petroleum Geology 16: 73-88.

Sustakoski, R. J. and D. Morton-Thompson (1992). Reserves estimation. Development geology reference manual, AAPG methods in exploration series, No.10. D. Morton-Thompson and A. Woods, AAPG: 513-517.

Sykes, R. (2001). Depositional and rank controls on the petroleum potential of coaly source rocks. Eastern Australasian Basins Symposium, a refocused energy perspective for the future. Petroleum Exploration Society of Australia Special Publication, Melbourne, Australia, Petroleum Exploration Society of Australia.

Sykes, R. and M. G. Dow (2000). Petroleum source rock potential of North Cape Formation (Late-Cretaceous) coaly sediments, Taranaki Basin. 2000 New Zealand Petroleum Conference Proceedings, Christchurch, New Zealand.

Sykes, R., M. J. Dow and J. I. Raine (2004). Petroleum source rock potential of Late-Cretaceous coaly sediments, Taranaki Basin, New Zealand: depositional controls and rank effects. Marine and Petroleum Geology.

Sykes, R., R. H. Funnell, S. D. Killops and M. J. Dow (2001). Synsedimentary marine influence of coaly source rocks and its effects on petroleum potential and kinetic parameters. 20th International Meeting on Organic Geochemistry Proceedings, Nancy, France, Vandoeuvre, France: Universite Henri Poincare.

Sykes, R., L. R. Snowdon and P. E. Johansen (2004). Leaf biomass - a new paradigm for sourcing the terrestrial oils of Taranaki Basin. PESA Eastern Australian Basins Symposium II Proceedings, Adelaide, Petroleum Exploration Society of Australia (PESA).

Sykes, R., R. P. Suggate and P. R. King (1991). Timing and depth of maturation in southern Taranaki Basin from reflectance and rank(s). New Zealand Oil Exploration Conference Proceedings, New Zealand, Ministry of Commerce, Wellington, New Zealand.

Thompson, J. G. (1982). Hydrocarbon source rock analysis of Pakawau Group and Kapuni Formation sediments, northwest Nelson and offshore South Taranaki, New Zealand. New Zealand Journal of Geology and Geophysics 25: 141-148.

Thomson, R. O. (1998). Aspects of applied basin-modelling: sensitivity analysis and scientific risk. Basin-modelling: practice and progress. S. J. Duppenbecker and J. E. Iliffe, Geological Society Special Publication No.141. The Geological Society, London: 209-221.

Thrasher, G. P. (1992). Late-Cretaceous geology of Taranaki Basin, New Zealand. PhD thesis, Victoria University of Wellington.

Thrasher, G. P. (1992). Late-Cretaceous source rocks of Taranaki Basin, New Zealand. 1991 New Zealand Oil Exploration Conference Proceedings, Ministry of Commerce, Wellington.

Thrasher, G. P. and J. P. Cahill (1990a). Structural contours on seismic basement. Subsurface maps of the Taranaki Basin. Report G142. Sheet 12. Wellington, New Zealand Geological Survey.

Thrasher, G. P. and J. P. Cahill (1990b). Structural Contours on Top Cretaceous. Subsurface maps of the Taranaki Basin, New Zealand. Report G142. Sheet 11. Wellington, Department of Scientific and Industrial Research.

Thrasher, G. P., P. King and R. Cook (1995a). Taranaki Basin Petroleum Atlas: Map 44, Late-Cretaceous Rakopi Formation, exploration potential and play concepts. Wellington, Institute of Geological and Nuclear Sciences Limited.

Thrasher, G. P., P. King and R. Cook (1995b). Taranaki Basin Petroleum Atlas: Map 45, Late-Cretaceous North Cape Formation, exploration potential and play concepts. Wellington, Institute of Geological and Nuclear Sciences Limited.

Thrasher, G. P., P. King and R. Cook (1995c). Taranaki Basin Petroleum Atlas: Map 46, Paleocene Farewell Formation, exploration potential and play concepts. Wellington, Institute of Geological and Nuclear Sciences Limited.

Thrasher, G. P., P. King and R. Cook (1995d). Taranaki Basin Petroleum Atlas: Map 47, Eocene Kaimiro and Mangahewa formations, exploration potential and play concepts. Wellington, Institute of Geological and Nuclear Sciences Limited.

Thrasher, G. P., P. King and R. Cook (1995e). Taranaki Basin Petroleum Atlas: Map 49, Late Neogene exploration potential and play concepts. Wellington, Institute of Geological and Nuclear Sciences Limited.

Thrasher, G. P., P. R. King and R. A. Cook (1995f). Structural Contours on Top Cretaceous; Taranaki Basin petroleum atlas, 6. Wellington, Institute of Geological and Nuclear Sciences Limited.

Thrasher, G. P., P. R. King and R. A. Cook (1995g). Structural Contours on Top Eocene, Taranaki Basin petroleum atlas, 7. Wellington, Institute of Geological and Nuclear Sciences Limited.

Thrasher, G. P., P. R. King and R. A. Cook (1995h). Structural Contours on Top Miocene; Taranaki Basin petroleum atlas, 8. Wellington, Institute of Geological and Nuclear Sciences Limited.

Thrasher, G. P., B. Leitner and A. W. Hart (2002). Petroleum system of the Northern Taranaki Basin. 2002 New Zealand Petroleum Conference Proceedings, Auckland, New Zealand, Ministry of Economic Development, New Zealand.

Tissot, B. P., R. Pelet and P. Ungerer (1987). Thermal history of sedimentary basins, maturation indices, and kinetics of oil and gas generation. American Association of Petroleum Geologists Bulletin 71: 1445-1466.

Tissot, B. P. and D. H. Welte (1984). Petroleum formation and occurrence, Springer, Heidelberg.

Titheridge, D. G. (1977). Stratigraphy and sedimentology of the upper Pakawau and lower Westhaven groups (upper Cretaceous-Oligocene), northwest Nelson, MSc thesis, University of Canterbury, University of Canterbury.

Trotter, H. F. (1959). An elementary proof of the central limit theorem. Archiv der Mathematik 10: 226-234.

Turcotte, D. L. (1989). Fractals in Geology and Geophysics. Pure Applied Geophysics 131: 171-96.

Turcotte, D. L. (1997). Fractals and Chaos in Geology and Geophysics, Cambridge University Press.

Uruski, C. (2006). Sedimentary systems of northwest New Zealand. 2006 New Zealand Petroleum Conference Proceedings, Auckland, Ministry of Economics.

Uruski, C. and P. Baillie (2002). Petroleum systems of the deepwater Taranaki Basin, New Zealand. 2002 New Zealand Petroleum Conference Proceedings 1: 402 - 407.

Uruski, C., P. Baillie and V. Stagpoole (2003). Development of the Taranaki Basin and comparisons with the Gippsland Basin: implications for deepwater exploration. APPEA: 185-196.

Uruski, C., V. Stagpoole, M. J. Isaac, P. R. King and G. Maslen (2002). Seismic interpretation report Astrolabe survey Taranaki Basin, New Zealand. Wellington, Institute of Geological & Nuclear Sciences Limited: 51.

USGS (1995). 1995 National Assessment of USA Oil and Gas Resources. USGS Report.

USGS (2000). Petroleum system of the Gippsland Basin, Australia. Open-File Report 99-50-Q, United States Geological Survey.

USGS (2000). U.S Geological Survey World Petroleum Assessment 2000; Description and Results, United States Geological Survey.

van der Lingen, G. J. and D. Smale (1990). Porosity evaluation of an upper-Cretaceous marine sandstone, Tane-1 offshore oil exploration well, Taranaki Basin, New Zealand. 1989 New Zealand oil exploration conference proceedings.

van der Lingen, G. J. and D. Smale (1992). High primary porosity preserved in deep (3.5 km) upper-Cretaceous marine sandstone, offshore Taranaki Basin, New Zealand, New Zealand Geological Survey record 44: 7-35.

van Oyen, F. H. and J. Branger (1970). Cook-1 well completion report PPL693. Petroleum report, PR513, Ministry of Economic Development.

Voggenreiter, W. R. (1993). Structure and evolution of the Kapuni anticline, New Zealand: evidence from the Kapuni 3D seismic survey. New Zealand Journal of Geology and Geophysics 36: 77-94.

Walcott, R. I. (1984). Reconstructions of the New Zealand region for the Neogene. Paleogeography, paleoclimatology, paleoecology 46: 217-231.

Walcott, R. I. (1987). Geodetic strain and the deformation history of the North Island of New Zealand during the late Cainozoic. Philosophical transactions of the Royal Society of London A321: 163-181.

Watson, G. P., A. N. Rencz and G. F. Bonham-Carter (1989). Computers assist prospecting. Geos 18(1): 8-15.

Westaway, R. (1994). Quantitative analysis of populations of small faults. Journal of structural geology 16: 1259-1273.

Weston, R. J., R. P. Philip, C. M. Sheppard and A. D. Woolhouse (1989). Sesquiterpanes, diterpanes and other higher terpanes in oils from the Taranaki Basin of New Zealand. Organic geochemistry 14: 405-421.

White, C. M. (1986). Oil and Gas Assessment - Methods and Applications: American Association of Petroleum Geologists Studies in Geology.

White, D. A. and H. M. Gehman (1979). Methods of Estimating Oil and Gas Resources. The American Association of Petroleum Geologists Bulletin 63(12): 2183-2192.

White, L. P. (1981). A play approach to hydrocarbon resource assessment and evaluation. In Rice, D.D., (ed). Oil and gas assessment - Methods and applications. American Association of Petroleum Geologists Studies in Geology 21: 125-132.

Wikipedia (2005). Pareto Principle, A Wikipedia Project powered by MediaWiki.http://en.wikipedia.org/wiki/Pareto_principle.

Wood, R. A., R. H. Funnell and S. Killops (1996). Maturity Modelling in the South Taranaki Basin. Wellington, Ministry of Economic Development: 24.

Wood, R. A., R. H. Funnell, P. R. King, E. R. Matthews, G. P. Thrasher, S. D. Killops and P. G. Scadden (1998). Evolution of the Taranaki Basin - Hydrocarbon maturation and migration with time. 1998 New Zealand Petroleum Conference Proceedings, Queenstown, New Zealand, Ministry of Commerce, New Zealand.

www.answers.com (2005). Answers.com website, GuruNet. 2005.

Zipf, G. K. (1949). Human behaviour and the principle of least effort, Hafner Publishing, New York, 573.